Geosynthetic-Reinforced Retaining Walls-Deterministic And Probabilistic Approaches

Hicham Alhajj Chehade

THÈSE

Pour obtenir le grade de

DOCTEUR DE L'UNIVERSITE GRENOBLE ALPES

préparée dans le cadre d'une cotutelle *entre la Communauté Université Grenoble Alpes* et l'Université Libanaise

Spécialité : **Matériaux, Mécanique, Génie Civil, Électrochimie**

Arrêté ministériel : le 6 janvier 2005 – 25 mai 2016

Présentée par

Hicham ALHAJJ CHEHADE

Thèse dirigée par **Daniel DIAS** et **Marwan SADEK**
codirigée par **Orianne JENCK et Fadi HAGE CHEHADE**

préparée au sein des **Laboratoires « Sols, Solides, Structures, Risques » (3SR) et « Centre de Modélisation en Génie Civil »**

dans **les Écoles Doctorales « Ingénierie - Matériaux Mécanique Énergétique Environnement Procédés Production » (I-MEP2) et « l'Ecole Doctorale des Sciences et des Technologies » (EDST)**

Geosynthetic-reinforced retaining walls - Deterministic and Probabilistic Approaches

Thèse soutenue publiquement le **09 février 2021**
devant le jury composé de :

M. Dashnor HOXHA
Professeur à l'Université d'Orléans (Rapporteur)
M. Isam SHAHROUR
Professeur à l'Université de Lille (Rapporteur)
M. Pascal VILLARD
Professeur à l'Université Grenoble-Alpes (Examinateur ; Président de jury)
Mme Farimah MASROURI
Professeur à l'Université de Lorraine (Examinateur)
M. Yasin FAHJAN
Professeur à Istanbul Technical University (Examinateur)
M. Daniel DIAS
Professeur à l'Université Grenoble-Alpes (Directeur de thèse)
M. Marwan SADEK
Professeur à l'Université Libanaise (Directeur de thèse)

Abstract

The aim of this thesis is to assess the seismic internal stability of geosynthetic reinforced soil retaining walls. The work first deals with deterministic analyses and then focus on probabilistic ones. In the first part of this thesis, a deterministic model, based on the upper bound theorem of limit analysis, is proposed for assessing the reinforced soil wall safety factor or the required reinforcement strength to stabilize the structure. A spatial discretization technique is used to generate the rotational failure surface and give the possibility of considering heterogeneous backfills and/or to represent the seismic loading by the pseudo-dynamic approach. The cases of dry, unsaturated and saturated soils are investigated. Additionally, the crack presence in the backfill soils is considered. This deterministic model gives rigorous results and is validated by confrontation with existing results from the literature. Then, in the second part of the thesis, this deterministic model is used in a probabilistic framework. First, the uncertain input parameters are modeled using random variables. The considered uncertainties involve the soil shear strength parameters, seismic loading and reinforcement strength parameters. The Sparse Polynomial Chaos Expansion that consists of replacing the time expensive deterministic model by a meta-model, combined with Monte Carlo Simulations is considered as the reliability method to carry out the probabilistic analysis. Random variables approach neglects the soil spatial variability since the soil properties and the other uncertain input parameters, are considered constant in each deterministic simulation. Therefore, in the last part of the manuscript, the soil spatial variability is considered using the random field theory. The SIR/A-bSPCE method, a combination between the dimension reduction technique, Sliced Inverse Regression (SIR) and an active learning sparse polynomial chaos expansion (A-bSPCE), is implemented to carry out the probabilistic analysis. The total computational time of the probabilistic analysis, performed using SIR-SPCE, is significantly reduced compared to directly running classical probabilistic methods. Only the soil strength parameters are modeled using random fields, in order to focus on the effect of the spatial variability on the reliability results.

Keywords: Reinforced soil retaining wall, limit analysis, discretization, pseudo-dynamic approach, probabilistic analysis, polynomial chaos expansion, spatial variability.

Résumé

L'objectif de cette thèse est de développer, dans le cadre de la mécanique des sols, des méthodes d'analyse de la stabilité interne des murs de soutènement renforcés par géosynthétiques sous chargement sismique. Le travail porte d'abord sur des analyses déterministes, puis est étendu à des analyses probabilistes. Dans la première partie de cette thèse, un modèle déterministe, basé sur le théorème cinématique de l'analyse limite, est proposé pour évaluer le facteur de sécurité d'un mur en sol renforcé ou la résistance nécessaire du renforcement pour stabiliser la structure. Une technique de discrétisation spatiale est utilisée pour générer une surface de rupture rotationnelle, afin de pouvoir considérer des remblais hétérogènes et/ou de représenter le chargement sismique par une approche de type pseudo-dynamique. Les cas de sols secs, non saturés et saturés sont étudiés. La présence de fissures dans le sol est également prise en compte. Ce modèle déterministe permet d'obtenir des résultats rigoureux et est validé par confrontation avec des résultats existants dans la littérature. Dans la deuxième partie du mémoire de thèse, ce modèle déterministe est utilisé dans un cadre probabiliste. Tout d'abord, l'approche en variables aléatoires est utilisée. Les incertitudes considérées concernent les paramètres de résistance au cisaillement du sol, la charge sismique et la résistance des renforcements. L'expansion du chaos polynomial qui consiste à remplacer le modèle déterministe coûteux par un modèle analytique, combinée avec la technique de simulation de Monte Carlo est la méthode fiabiliste considérée pour effectuer l'analyse probabiliste. L'approche en variables aléatoires néglige la variabilité spatiale du sol puisque les propriétés du sol et les autres paramètres modélisés par des variables aléatoires, sont considérés comme constants dans chaque simulation déterministe. Pour cette raison, dans la dernière partie du manuscrit, la variabilité spatiale du sol est considérée en utilisant la théorie des champs aléatoires. La méthode SIR/A-bSPCE, une combinaison entre la technique de réduction dimensionnelle SIR (Sliced Inverse Regression) et une expansion de chaos polynomial adaptative (A-bSPCE), est la méthode fiabiliste considérée pour effectuer l'analyse probabiliste. Le temps de calcul total de l'analyse probabiliste, effectuée à l'aide de la méthode SIR-SPCE, est considérablement réduit par rapport à l'exécution directe des méthode probabilistes classiques. Seuls les paramètres de résistance du sol sont modélisés à l'aide de champs aléatoires, afin de se concentrer sur l'effet de la variabilité spatiale sur les résultats fiabilistes.

Mots-clés : Mur de soutènement en sol renforcé, analyse limite, discrétisation, pseudo-dynamique, analyse probabiliste, Chaos Polynomiaux, variabilité spatiale.

Acknowledgements

I would like to express my sincerest gratitude to my supervisor at Grenoble-Alpes University, Prof. Daniel Dias, as well as, my supervisor at Lebanese University, Prof. Marwan Sadek for placing trust and confidence in my abilities, for having guided me in this research work with their masterful intellect and openness to innovative ideas. They have been very helpful, always available with their constructive suggestions. Besides the academic guidance, they have always been next to me as friends.

I would also thank my co-supervisors Dr. Orianne Jenck, and Prof. Fadi Hage Chehade for their insightful guidance, their support, their helpful advices, their fruitful discussions and their careful reviews of my manuscripts for journal papers and for this thesis.

I would like to thank all the members of my dissertation committee: Prof. Dashnor Hoxha, Prof. Isam Shahrour, Dr. Julien Baroth, Prof. Fatima Masrouri and Prof. Yasim Fahjan. Special thanks to Prof. Dashnor Hoxha and Prof. Isam Shahrour for their valuable time spent to review the manuscript and for their insightful comments and advices. My thanks also go to Dr. Julien Baroth, Prof. Fatima Masrouri and Prof. Yasim Fahjan for their precious time to participate in the PhD defense and to examine my work.

I would like to acknowledge the support of my friends and colleagues at 3SR laboratory for providing a great environment to work in during these three years of thesis. I also thank all my friends in Grenoble, outside of civil engineering, who made me realize how the collectivity make us feel at home where ever we are.

Above all, I am deeply grateful to my parents for their unconditional support, patience and love. I thank them for everything you have done and for being always next to me in both good and difficult times.

The present work was supported by Grant from the Lebanese University. This funding is greatly appreciated.

Table of contents

GENERAL INTRODUCTION

Reinforced soil retaining walls are geotechnical structures based on the association of compacted backfill soil and reinforcement elements. The reinforcements improve significantly the soil mass shear strength due to the soil-reinforcement interaction. Metallic or geosynthetic (non-corrodible) reinforcements could be used. These later are often used in aggressive environments and are considered in this work. The geosynthetic reinforced soil retaining walls are greatly appreciated thanks to their effective performance, high resistance to dynamic loading and economic benefit compared to the conventional retaining walls (Masini et al., 2015; Latha and Santhanakumar, 2015; Gaudio et al., 2018). They are used for transportation construction like in roads, highways, bridges and railway structures, as well as for industrial and protective structures, for dams, mining structures, in addition to their use for commercial and public structures. The vital role of geosynthetic reinforced soil walls, can be explained by their multiple applications. Safety constitutes the great challenge of the urban development space. The failures of these structures could lead to huge human and economic losses. Many challenging issues must be addressed when dealing with these structures such as very large structural loads, water presence and crack-formation in the backfill. In addition, the seismic behavior is not clearly identified and the seismic codes provide only simple rules based on pseudo-static approaches. According to Koerner and Koerner (2018), around 200 000 geosynthetic reinforced soil walls are constructed worldwide. However, these authors reported also, that 1 to 3% among them suffer from failures. This study aims to investigate the seismic internal stability of geosynthetic reinforced soil retaining walls in the context of deterministic and probabilistic analyses, in order to improve the understanding of their behavior.

The analysis and design of the reinforced soil structures is generally conducted using deterministic approaches. In these approaches, the model input parameters and the system responses are considered as deterministic. These approaches could be grouped into three categories: numerical approaches (finite elements and finite differences), experimental methods and, analytical methods such as the limit equilibrium and the limit analysis methods. The use of numerical techniques usually induces computational time costs. The physical model studies on reinforced soil-retaining structures are highly expensive and time-consuming. The upper bound theorem of the limit analysis theory is an effective manner to assess the stability of reinforced soil retaining walls at the ultimate limit state. In this work, the developed deterministic model is based on this latter. The kinematic approach based on the spatial discretization technique, developed by Mollon et al. (2011) to generate a log-spiral failure mechanism in the stability analysis of tunnels, is extended to the case of reinforced soil retaining walls. The discretization technique allows to overcome the limitations of the conventional limit analysis method, which can only be applied to a homogeneous backfill soil and which can only use the pseudo static approach to consider the seismic loading.

On the other hand, it has been well recognized that all the input data are associated with some degree of uncertainty in the stability analysis of these structures (Low and Phoon, 2015; Ferreira et al., 2016; Javankhoshdel and Bathurst, 2017). Despite being familiar to geotechnical engineers, the deterministic models are based on the global factor of safety. They cannot accurately reflect all the uncertainties and often result in an overdesigns or instabilities when uncertainties are considered as respectively smaller or greater than anticipated (Chalermyanont and Benson, 2004-2005). In addition, the deterministic approach suffers from limitations regarding the difficulties in linking the global factor of safety to the considered system level of reliability and in assessing the uncertainties effects on the model results (Ferreira et al., 2016). An alternative strategy for the design and analysis of reinforced soil retaining walls, are the probabilistic methods. These approaches have gained increased attention recently, as they are able to consider the uncertainties of input parameters in a rational way. The system reliability can be computed in a logical manner (Low and Phoon, 2015; Phoon, 2017; Bathurst et al., 2019b). Many attempts have been made to assess the reinforced soil structures stability with these probabilistic methods (Chalermyanont and Benson, 2004-2005; Sayed et al., 2008; Basha and Sivakumar Babu, 2009-2010-2011-2012; Sivakumar Babu and Singh, 2011; Bathurst and Miyata, 2015; Luo et al., 2016; Ferreira et al., 2016; Zevgolis and Bourdeau, 2017; Javankhoshdel and Bathurst, 2017; Yu and Bathurst, 2017; Bathurst et al., 2019b). Most of these studies modelled the different uncertain input parameters as random variables. However, both laboratory investigations and field observations show that the soil parameters vary spatially even within homogeneous layers in both directions as a result of depositional and post-depositional processes (Cho, 2010; Pan and Dias, 2015). Hence it increases the importance of modelling the soil parameters by random fields. Several methods were proposed in the literature to perform reliability analyses. Recently, the metamodeling techniques have been widely adopted in order to overcome the shortcomings of the traditional approaches regarding the time computational cost or the difficulty to converge when dealing with highly nonlinear limit-state functions (Pan et al., 2017). Among these metamodeling techniques, the Sparse Polynomial Chaos Expansion (SPCE) which is an extension of the Polynomial Chaos Expansion (PCE) is used for probabilistic analysis in this study.

This thesis aims to develop a rigorous deterministic model to assess the seismic internal stability of geosynthetic reinforced soil retaining walls using the pseudo-dynamic approach. It allows to reduce the computational time required by numerical approaches. Then, this deterministic model is used to perform a reliability-based analysis of the internal seismic stability of reinforced soil retaining walls considering the soil spatial variability. This thesis is organized in four chapters as follows:

The first chapter presents a literature review on respectively three topics. It presents an overview on the concept of reinforced soil retaining walls, their historical development, the elements of these structures and their application fields. In addition, the state of the art in terms of reinforced soil retaining wall stability analysis and design, the different deterministic investigation methods including the theoretical, experimental and numerical methods used in the literature are presented. This chapter ends up with a

presentation of the probabilistic analysis of reinforced soil retaining walls. The sources of uncertainties are presented, in addition to the reliability concept and the methods commonly used in geotechnical engineering.

The second chapter focuses on the seismic internal stability of reinforced soil retaining walls assessment. A deterministic model based on the kinematical approach of limit analysis and the spatial discretization technique is developed and validated with the results of Michalowski (1998a) obtained using the conventional limit analysis method. This deterministic model is then used to assess the seismic internal stability of geosynthetic reinforced soil retaining walls in cases of dry, unsaturated and saturated soils. The influence of cracks on the seismic internal stability of reinforced soil retaining walls is also investigated.

In the third chapter, the Sparse Polynomial Chaos Expansion (SPCE) combined with Monte Carlo Simulations is used to perform a reliability-based analysis of the internal seismic stability of geosynthetic reinforced soil retaining walls. The uncertainty and variability of the soil shear strength parameters, reinforcement strength and characteristics of seismic loading are considered using random variables. The deterministic computation of the structure safety factor is based on the developed deterministic model to ensure rigorous results and to represent the seismic loading by the pseudo-dynamic approach. The strength reduction method is employed to calculate the safety factor.

In the last chapter, the effect of the soil spatial variability, ignored in the third chapter, on the seismic internal stability analysis of geosynthetic reinforced soil retaining wall is investigated. A random fields approach is adopted to model the spatial variability of the soil strength parameters. A combination between an active learning sparse polynomial chaos expansion (A-bSPCE) and a dimension reduction technique, the sliced inverse regression SIR, is used to deal with the high dimensional considered problem.

The manuscript ends by a general conclusion of the principal results obtained from the analyses.

The results presented in the second chapter were published in three papers (Alhajj Chehade et al., 2019b-2020-2021). A fourth article is submitted and presents the content of the third chapter. Finally, a paper is under preparation about the results of the last chapter.

1 Chapter 1 Literature view

1.1 Introduction

Reinforced soil retaining walls are structures composed of structural (retaining walls) and geotechnical (soil reinforcement) elements. This construction technique has become popular since its invention by the French architect and engineer Henri Vidal in the early 1960s (Leshchinsky and Han, 2004). The construction method is based on the association of a compacted backfill and strip reinforcement elements connected to the wall facing. The reinforcements improve significantly the soil mass shear strength due to the soil-reinforcement interaction. The reinforcements generally used in these structures are made of steel (inextensible materials). However, in aggressive environments, these metal reinforcements are replaced by non-corrodible geosynthetic reinforcements, which have a higher extensibility than the metal ones. Reinforced soil walls constructed with geosynthetic reinforcements are considered in this dissertation. Traditionally, the analysis of reinforced soil retaining walls are based on deterministic approaches. However, all the input data are associated with some degree of uncertainty in geotechnical engineering problems.

This chapter aims to present an overview of the reinforced soil retaining walls, their concept, historical development, research related works and, the used elements in their construction in addition to their possible application fields. The second part of this chapter focuses on the stability of the reinforced soil retaining walls. Then, the deterministic investigation methods are presented, including theoretical, experimental and numerical methods developed in the literature. In addition, an overview of the previous studies employing these methods in the framework of reinforced soil retaining walls stability analysis is provided. This chapter ends up with a presentation of the probabilistic analysis of reinforced soil retaining walls. The sources of uncertainties are discussed, in addition to the reliability concept and the methods commonly used in geotechnical engineering. A detailed description of the Polynomial Chaos Expansion (PCE) meta-modeling method and its extension the Sparse Polynomial Chaos Expansion (SPCE) methodology are given, as they are implemented to perform the probabilistic analysis of reinforced soil retaining walls in the framework of this dissertation.

1.2 Reinforced soil retaining walls

1.2.1 Definition and historical background

Reinforced soil retaining wall is a cost-effective soil-retaining structure, based on the association of compacted backfill and reinforcement (metallic or geosynthetic) elements connected to a wall facing (Figure 1-1). It is a composite structure formed by a frictional backfill set up by horizontal successive compacted layers between which are arranged the reinforcing elements. Reinforced soil retaining walls,

by behaving like coherent flexible blocks, can support larger loads and deformations than conventional reinforced concrete retaining structures. This significant technical advantage allows their applications in areas where foundation soils are poor. In such cases, the foundation improvements to support conventional structures are not required which result in important cost savings. The reinforcements improve significantly the apparent soil shear strength due to the soil-reinforcement interaction by friction, and passive resistance depending on reinforcement geometry. The reinforcement's most common resisting mode is tension while some reinforcement types can also resist in bending and shear, providing additional stability to the reinforced soil structures. The wall facing, relatively thin, prevents the erosion of the backfill soil. The internal behavior of this type of structure depends on several parameters related to the soil, the reinforcing elements and the soil/reinforcement interaction.

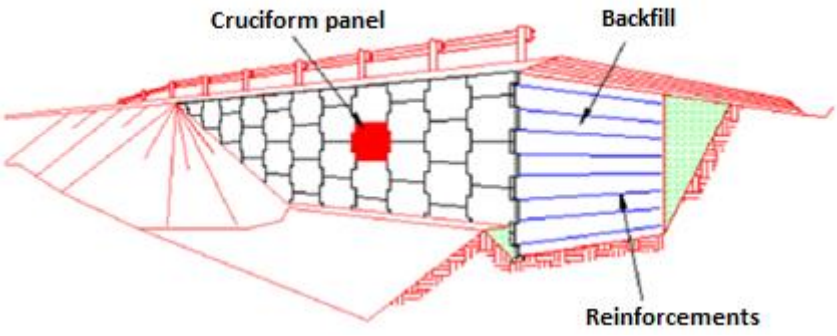

Figure 1-1 Reinforced Soil Retaining Wall (Alhajj Chehade et al., 2019d)

Inclusions have been used since ancient times to improve soil by using sticks, earth dikes, tree branches, wooden pegs among other natural materials. The modern methods of soil reinforcement for retaining wall construction was invented by the French architect and engineer Henri Vidal in 1963 and has become popular (Leshchinsky and Han, 2004). Henri Vidal marks, by this invention, a very important date in the design of retaining structures and more generally, in the soil strengthening by fully involving the soil in the stability of structures. The concept of the reinforced soil retaining wall was first experimented using sands and pine needles. His research work led to the development of the Reinforced Earth, a system in which steel strip reinforcement is adopted. The first Reinforced Earth retaining structure by metallic elements was established in 1965-1966, with the realization of the first reinforced soil wall in Pragnières (Pyrénées -France) (Figure 1-2). In the United States, the first one, which is still in use today, was constructed in California using this technology in 1972. Since the introduction of the Reinforced Earth, several other systems with synthetic reinforcements have been developed and used. The use of geotextiles in reinforced soil retaining walls started after their beneficial effect, noticed in highway embankments constructed over weak subgrades. The first geotextile-reinforced wall was constructed in France in 1971 (FHWA, 2009). In addition, the use of geogrids for soil reinforcement were developed around 1980 (FHWA, 2009). The success of the reinforced soil retaining walls is mainly due to their advantages compared to conventional retaining walls, due to their flexibility to settlements and by

providing higher resistance to seismic loading in seismically active zones (Ling et al., 2004-2005a-2005b; Koseki et al., 2006; El-Emam and Bathurst, 2007; Latha and Santhanakumar, 2015). Nowadays, these walls types are a mature technology and are used extensively worldwide. They constitute the first choice solution for retaining walls and highway structures construction (Alhajj Chehade et al., 2019b).

Figure 1-2 First reinforced soil retaining wall constructed in 1965 by EDF (Chéret, 2015)

1.2.2 Components of Reinforced Soil Walls

The construction of reinforced soil retaining walls requires a good knowledge of their components as they have a direct influence on its performance. They are three major components: reinforcing elements, facing system, and soil backfill.

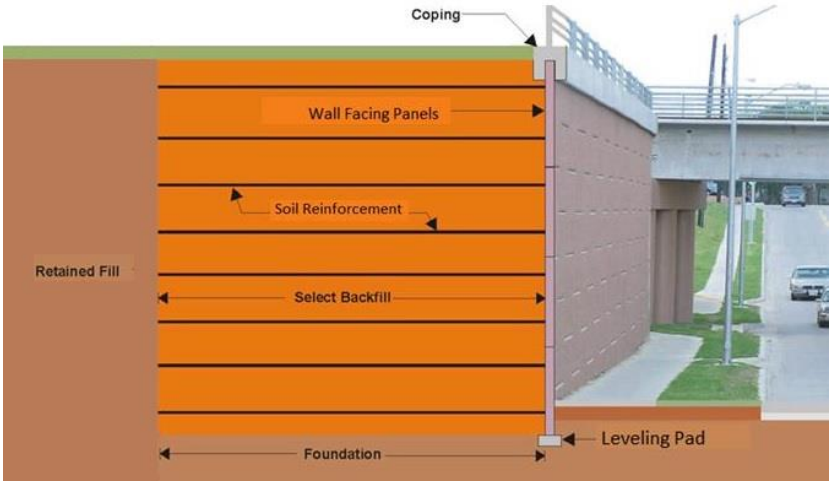

Figure 1-3 Reinforced soil retaining wall elements (Passe, 2000)

1.2.2.1 Reinforcement elements

The reinforcing elements are incorporated in the soil in horizontal layers to improve its behavior. They are available in a variety of types, configurations, and sizes. They could be described or classified according to the material type, the extensibility and the geometry.

The reinforced soil retaining wall are reinforced by metallic reinforcements or by non-corrodible synthetic reinforcements. The metallic reinforcements are typically formed of mild steel galvanized, while the synthetic reinforcement are products with at least one of their constituents is based on synthetic or natural polymer (Polyester PET, Polyvinyl-Alcohol PVA, Polyethylene PE or Polypropylene PP). When using the metallic reinforcements, they should be hot dip galvanized and the galvanization coating thickness depends on the material type being galvanized. In addition, it is important to add a waterproofing membrane in the upper portion of the reinforced system. The geosynthetic reinforcements present certain advantages compared to metallic reinforcements because of their lightness, their flexibility, and especially their resistance to corrosion. However, the behavior of this type of reinforcement is more complex due to its extensibility and therefore requires a deep understanding of the soil-reinforcement interaction mechanisms.

In terms of stress-strain behavior, there are two classes of reinforcement extensibility with respect to the soil stiffness. The reinforcing elements may be considered inextensible or extensible. For the former, the reinforcement's deformation at failure is much less compared to the soil deformation, such as steel strips and bar mat reinforcements. It is worth noting that some ultra-high modulus polymers and newer glass-fiber reinforced composites have modulus that approach that of mild steel. For the latter, the reinforcement's deformation at failure is comparable to the soil deformability and even greater. This includes geogrids and geotextiles. In addition, the woven steel wire mesh reinforcements deform more than the soil at failure and are thus classified extensible.

Based on their geometric shapes, three categories of reinforcements can be considered. The first category is linear unidirectional metallic or geosynthetic strips, smooth or ribbed for high adhesion. The second one is composed from the composite unidirectional reinforcements, which includes grids or bar mats. The grid spacing must be greater than 150 mm (FHWA, 2009). The last one is composed from the planar bidirectional reinforcements, which contains continuous geosynthetics sheets, welded and woven wire meshes. The mesh element spacing is smaller than 150 mm.

1.2.2.2 Facing systems

The facing elements are the only visible parts of the completed reinforced soil retaining walls. In addition to the mechanical role, they thus control the structures aesthetics. Moreover, the choice of the structure facing type should also consider the application field, the acceptable differential settlement and the wall service life. The main function of the facing is to provide local stability and protection against reinforced backfill erosion. Facing elements, when employed, can be precast concrete panels or modular blocks, gabions, welded wire mesh, cast-in-place concrete, timber, shotcrete, vegetation, or geosynthetic material. The most used facing systems are:

Steel facing panels: The first type of facing panels used for reinforced soil retaining walls was the metal facing made of very deformable semi-elliptical galvanized steel panels. It is used since 1968 and presents unique characteristics such as lightness, structural resistance properties and continuity, which make it appropriate in structures where difficult access or difficult handling requires lighter facing elements.

Precast concrete panels: The precast concrete panels are of a cruciform, square, rectangular, diamond, or hexagonal geometry. Each panel shape has benefits related to differential settlement and aesthetics. The panel dimensions and thicknesses are manufactured based on the project needs even if the commonly used panels are the cruciform ones of 1.5m in width and height. To prevent the contact between the concrete panels, joints are placed between them to provide some movement between panels during elastic compression and reinforced backfill settlement. In addition, a geotextile is installed on the back face, to provide adequate drainage of the reinforced soil retaining wall. The segmental precast concrete facing is the most used facing system for reinforced soil retaining walls. The galvanized steel reinforcements are generally used with segmental panel. However, the geosynthetic straps and High Density Polyethylene (HDPE) geogrids have also been used with segmental panel facing.

Dry cast modular block wall units: The wall facing is constructed using small concrete units specially produced for retaining wall applications. The prefabricated elements can be solid or hollowed and filled by aggregate during erection. The concrete units are arranged in a running bond configuration where the adjacent vertical ones are connected with shear pins or keys. This facing type are now used worldwide thanks to its lower cost. The grid reinforcements are generally used with this wall facing. Most Dry cast modular block walls use geosynthetic reinforcement, predominantly geogrids. The steel grids with two longitudinal wires have been used in some structures.

In addition to these facing types, there is various facing systems less used than the precast panels and dry cast modular blocks. The Gabion Facing combined with metallic welded wire mesh and welded bar-mats, or with geogrids and geotextiles connected to the rock-filled wire baskets. This facing type gives the possibility of vegetation that can grow through the gabion basket. Another facing type is the welded wire grid where the grids are bent up at wall front to form the wall facing. In the same manner, geosynthetic grid used as reinforcing elements in the backfill can be looped around to form the exposed retaining wall facing. Geotextile reinforcements can also be looped around to form the wall facing. This facing type gives also the possibility of vegetation that can grow through the grid structure to provide a pleasing appearance. It is worth noting that for the last three facing systems (welded wire mesh, geogrids and geotextile), it is possible to cover the wrapped facing by shotcrete, installing cast-in-place concrete or prefabricated facing panels.

(a) Precast concrete panels

(b) Dry cast modular block wall units

(c) Gabion facing

(d) Steel facing panels

Figure 1-4 Different wall-facing types

The reinforcement-panel connection is an essential characteristic of reinforced soil retaining walls. When precast concrete panels are used for wall facing, the connection is sealed in the concrete facing panel during its prefabrication. A classic connection is used with steel strips that are connected to galvanized primers incorporated in the facing panels and fixed using a high strength nut/bolt/washer assembly. The high adherence ladders use the same bolted connection to facing panels as for reinforcing strips through the hole in the flat connection plate at the end of the ladder.

The use of galvanized metallic elements in reinforced soil structures imposes, due to corrosion, limitations on the backfill soil (electrochemical characteristics) and on the environment. For this reason, a wall system known as GeoMega (Soletanche Freyssinet, 2013) is developed in 2004 involving a fully synthetic connection, composed of a blow molded, polyolefin, omega shaped sleeve embedded in the facing panels during its production (Figure 1-5b). The synthetic connection shape allows optimal anchoring resistance. Associated with geosynthetic straps, it allows retaining structures to be constructed in chemically aggressive environments such as marine environments, corrosive backfilling materials, pollution risks, etc.

(a) Metallic connection

(b) Synthetic connection

Figure 1-5 Reinforcement-facing connection types (Soletanche Freyssinet, 2013)

1.2.2.3 Backfill material

The backfill material plays a vital role in the reinforced soil retaining walls stability. It can be divided into two parts as shown in Figure 1-3: the retained soil and the reinforced soil.

Reinforced backfill constitutes the part of soil material placed within the reinforced zone. It is the most important element that influences the structure performance. The use of an appropriate material is therefore of particular importance. The soil can be taken on site or it can be imported. In addition, it can be from natural or industrial origin. Good-quality granular soil is the required backfill for reinforced soil walls construction. It must meet geotechnical requirements (gradation, plasticity, corrosion, density, internal friction angle, organic content and others), in addition to the placement and electro-chemical properties. These specifications provide good drainage, better durability - especially for metallic reinforcements, constructability (handling, placement and compaction advantages), and good soil-reinforcement interaction through high friction characteristics and avoiding soils with high clay contents. Tests conducted prior to construction and periodically during construction, are performed to ensure the soil quality.

On the other hand, the retained backfill constitutes the part of soil material without reinforcement, placed or in situ, directly adjacent to the reinforced backfill zone. It forms the back of the wall and constitutes the earth pressure source that the reinforced massif must resist against sliding, overturning and bearing.

A drainage system between the two zones and below the reinforced zone must be implemented to prevent the development of pore water pressure within the reinforced backfill zone.

1.2.3 Construction sequence

The construction process has an effect on the reinforced soil retaining wall performance. Any mistake or inaccuracy in the construction could have a detrimental effect on the wall performance. The construction of different reinforced soil wall types is almost similar with some small differences. The example of the reinforced earth retaining systems construction with precast panels is presented and it includes the following steps:

- Foundation preparation for the area to be occupied by the retaining structure (wall facing zone, soil reinforcement and reinforced soil wall select backfill). This area shall be graded level and compacted and the unsuitable loose or soft materials must be removed.
- The correct placement of the first panel row is very crucial. A leveling pad, which in general is an unreinforced concrete pad, is placed for this reason. This leveling pad is just a guide for facing panel erection and it is not playing any role as a structural foundation support. After that, the first row of panels is placed on the leveling pad and braced to maintain stability and alignment.
- Placement and compaction of the first backfill lift on the subgrade to the first layer of reinforcement. The thickness of every lift should not be greater than $30\ cm$. The select lift should be placed starting approximately $1\ m$ from the wall panels. The fill is then leveled by machinery that windrows the material toward the reinforcement rear ends. It is then placed within $1\ m$ behind the wall panels by windrowing the soil. Reinforced wall fill material should be compacted at 95% of the optimum moisture content dry density value, recommended for these structures. For too dry moisture contents, significant settlement occurs during precipitation periods. Moisture content wet of optimum makes it more difficult to maintain an acceptable facing alignment, especially if the fines content is important. The backfill moisture content shall be uniformly distributed throughout each material lift during compaction. A vibratory roller or plate weighing less than 450 kilograms should be used for the compaction of the zone extended $1\ m$ from the wall facing. The rest of the backfill could be compacted by a roller, smooth wheeled or a rubber-tired roller weighting up to 8 tons.
- Placement of the first layer of reinforcements in the horizontal direction and connected to the concrete panels by an appropriate connection system. It is restricted for any construction equipment to be in direct contact with the reinforcements to prevent the damage of protective coatings and reinforcements.
- Placement and compaction of the second layer of backfill with the same thickness of the first layer.
- These steps are repeated until reaching the desired wall height. Noting that only the first row of concrete panels will be braced, and the remaining rows are simply wedged and clamped to adjacent panels.

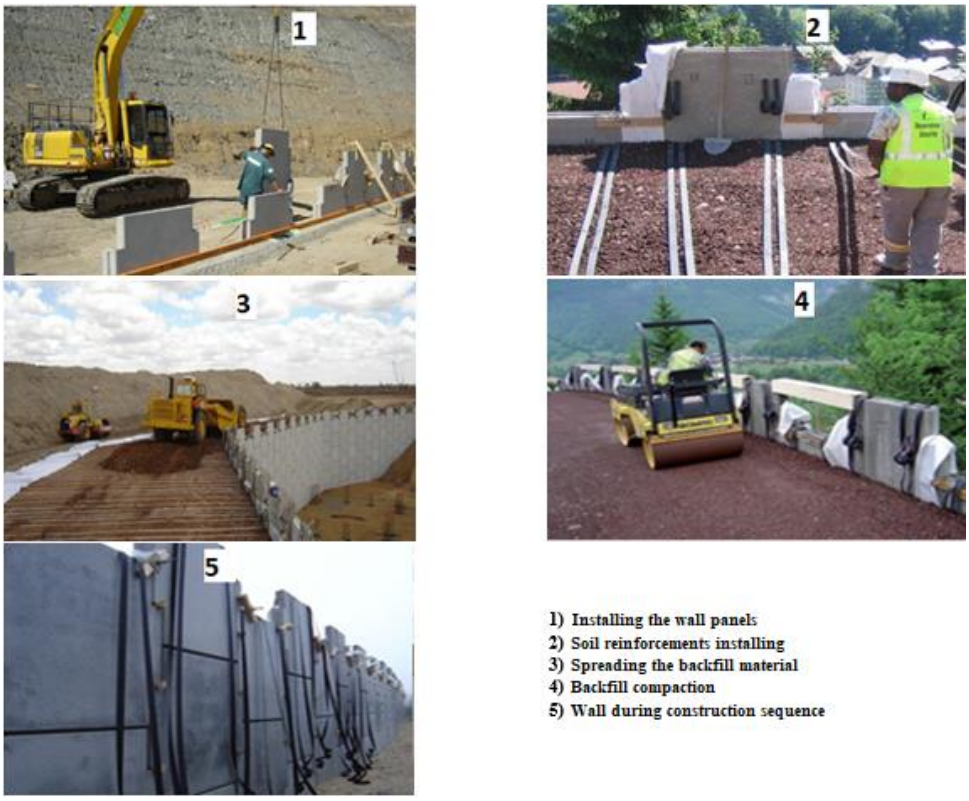

Figure 1-6 Construction sequence for retaining wall with unidirectional strips

1.2.4 Advantages and fields of application of Reinforced Soil walls

The reinforced soil technique constitutes one of the most important developments in civil engineering in the last five decades. This success is explained by the unique advantages offered by this technique due to their intrinsic characteristics:

- The great flexibility of the system.
- A relatively low cost.
- Technically feasible to height greater than 30m.
- The systematic use of prefabricated elements (Reinforcements, precast concrete panels) which will accelerate the construction and do not require special skills for construction.
- Require less site preparation than other alternatives and less space in front of the structure for construction operations.
- By their variety, the facing panels can meet all the architectural requirements.
- The reinforced soil walls technique reduces the construction impact on the environment: fewer materials needed and less CO2 generated than the conventional solutions.
- The interaction between the backfill and the reinforcements permits an effective absorption of the vibrations, such that generated by the heavy trains, high speed trains (TGV), the industrial equipment's or the explosions, and offer an exceptional resistance against earthquakes.

All these advantages have led to a wide use of reinforced soil structures for different functions. They can be used as solutions for all retaining projects, bridge abutments and tunnels constructions, and to reduce the vulnerability of people and infrastructures to natural and industrial hazards.

1.2.4.1 Highways and roads

The most common use of reinforced soil retaining structures concerns the highway and roads grade separations when there is a desired change in ground elevation that exceeds the angle of repose of the soil. These retaining walls are needed to prevent landslides along highways and between highways and adjacent properties. Reinforced soil walls along highways and roads frequently include integrated traffic barriers and a customized architectural finish, giving beauty to the structure.

1.2.4.2 Railway structures

Reinforced soil structures associated with railways can be divided into categories: those adjacent to the rails tracks and those that support them. Those that are adjacent to the tracks do not require any specific foundations and do not have significant influence on the rail traffic. On the other hand, the construction of these structures to support railways and light rail systems should meet the strict requirements related to heavy loads and the associated decelerations and vibrations induced by the passage of trains.

1.2.4.3 Bridges

Bridge abutment is a persistent need for urban transportation system. However, this structure type is very critical since it should support the earth pressures behind it as well as the heavy surcharge loads imposed by the bridge superstructure and traffic loading. Reinforced soil structures present the most efficient solution, economically and structurally, to deal with this structure type thanks to their unique strength and load distribution capabilities. Two bridge abutment types exist: the first is the case without piles when the bridge seat is supported directly on the reinforced soil. On the other hand, the second case is when piles are necessary to support the bridge seat. The piles can be placed easily between the reinforcing elements. In both cases, the typical reinforced soil structures shallow foundation depth and the use of prefabricated elements lead to a significant reduction in the project time and cost.

1.2.4.4 Hydraulic structures

Reinforced soil structures are widely used to build port, sea walls, dams and coastal structures that withstand marine environments and resist to very severe stresses such as floods, strong tides, floating debris, storms, ice forces and various shocks (boats, wrecks, etc.). It can be also combined with a waterproofing system to build drinking water reservoirs. They offer a speed of execution especially on

narrow coastal region where reclamation is necessary and in the tidal zones. The wall panels through the open facing joints and the appropriate free draining backfill ensure an efficient drainage of marine structures. These panels can move slightly relative to each other, giving flexibility and resiliency to the wall system. In addition, the fully non-corrodible synthetic connections and reinforcements gives the possibility of the construction projects carried out entirely under water and the solution to projects in which the backfill contains chemically corrosive materials.

1.2.4.5 Industrial and protective structures

The Reinforced soil technology is widely used in classic and specific industrial sites and protective structures due to its satisfactory performance and cost-effectiveness. Reinforced soil structures have demonstrated their ability to resist vibrations, to support the extreme dynamic loads generated by heavily loaded mining vehicles and the extremely high loads induced in the other industrial projects such as power plants, unloading docks, storage and manufacturing facilities. In addition, these structures have demonstrated their ability to resist thermal excursions of over 1200℃ and to control explosive blasts so they are used currently on the military equipment storages.

(a) Highway structure

(b) Railway structure

(c) Bridge abutment

(d) Hydraulic structure

(e) Industrial structure

(f) Protective structure

Figure 1-7 Different applications of reinforced soil structures (Soletanche Freyssinet, 2014; Vivas and Calatrava, 2016)

1.3 Stability of Reinforced Soil Walls

The reinforced soil retaining walls design is carried out by checking the external stability that deals with the global composite structures, the internal stability that deals with soil reinforcements, in addition to the global and compound stability of the wall system.

For many decades, the design of retaining walls including reinforced soil ones was done using allowable stress design (ASD). The experience-calibrated factor of safety is used in this framework to compensate for all the uncertainties in applied loads and material resistance as well as the inadequacies in the calculation models (Low and Phoon, 2015; Ferreira et al., 2016). Recently, the design procedure of these structures was modified and updated from ASD basis to load and resistance factor design (LRFD) basis that presents many advantages compared to the former one in most current standard codes (Eurocode 7, 2004, FHWA, 2011). In LRFD, uncertainty in load and material resistance are accounted for separately through the characteristic values and partial safety factors. The calibrated load factors and the resistance factors account respectively for the uncertainties in load and material resistance. The model uncertainty is also included by changing the resistance factor according to the method used to estimate the resistance. This approach provides safety levels in the reinforced soil retaining walls design in terms of reliability index when the load and resistance factors are properly calibrated.

1.3.1 External stability

The external stability of reinforced soil retaining structures is carried out like any retaining wall stability. First, the reinforcement elements length is fixed in the design procedure. Then, the external stability is checked for the reinforced zone against sliding, overturning and bearing. The reinforced soil is assumed to act as a coherent rigid block with lateral earth pressures acting on the back side of the block, at the reinforcement's rear ends and parallel to the facing. The calculations are carried out to check sliding on the base of the wall, bearing capacity of the foundation soil as well as the overturning of the block. The

weight and dimensions of the wall facing elements are typically ignored for external stability calculations.

1.3.2 Internal stability

The internal stability is verified to ensure that the layout of reinforcement (grade/strength and vertical spacing) is sufficient to meet the design requirements. It depends on three fundamental characteristics, the soil-reinforcement interaction, the reinforcement tensile resistance including their durability. The internal stability analysis is evaluated at each reinforcement layer. The reinforcement load should be determined at two critical locations of each layer, the zone of maximum tension forces and the connection to the wall facing elements. The internal failure can occur generally in three different modes:

- the reinforcement failure that occurs when the tensile forces become so large that the inclusions break, leading to large movements and possible structure collapse,
- and the pullout reinforcement failure that occurs when the tensile forces in the reinforcements become larger than the pullout resistance, i.e. the force required to pull the reinforcement out of the soil mass. This, in turn, leads to excessive movements and possible structure collapse.
- The connection failure that occurs when the developed tension at the reinforcement connection to the wall facing become larger than the reinforcement/wall facing connection strength.

Preventing the internal failure requires, therefore, the determination of the maximum developed tension forces along the reinforcements that must be lower than the reinforcements' pullout capacity and tensile strength and the determination of the tension at the reinforcement connection to the wall facing that must be lower than the reinforcement/wall facing connection strength.

The maximum tension line formed by the locus of the maximum tensile force in each reinforcement layer is assumed to coincide with the most critical failure surface in a simple reinforced soil retaining wall (FHWA, 2009; NF P 94-270, 2009). This surface divides the reinforced backfill into the active zone and the resistant zone. The locus of the maximum tension forces is far from the facing at the top of the wall and close to the facing in depth (Figure 1-8). The active zone is located between the wall facing and the failure surface where the shear stress exerted by the ground on the reinforcement are directed outwards and the soils tends to slide down under its self-weight tends to slip out of the structure. On the other hand, the resistant zone is located behind this failure surface where the shear stresses are directed inwards toward the free end of the reinforcements mobilized to prevent the sliding of the reinforcements. The active zone soils tend to slip out of the structure, while the reinforcement anchored in the stable zone provide tensile resistance to maintain the active zone stability. The experimental results show that the tension in the reinforcements, that presents a maximum at the potential failure surface, decreases in the resistant zone and becomes zero at the reinforcement rear end. It decreases also

from the potential failure surface in the active zone toward the back of the wall facing where it is equal to T_o (Han and Leshchinsky, 2006).

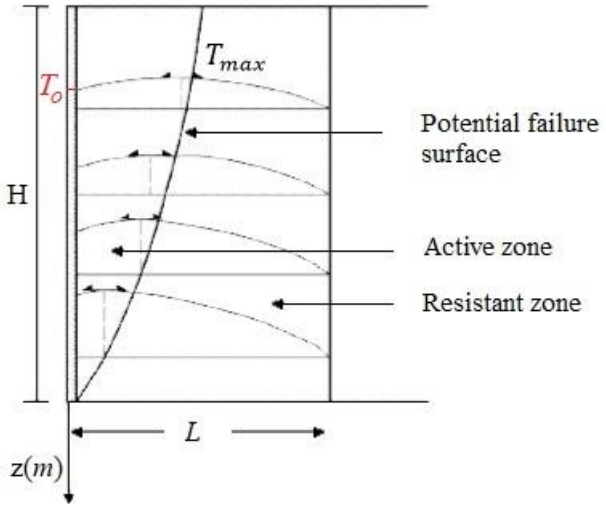

Figure 1-8 Line of maximum tension forces for internal stability design of reinforced soil retaining walls

The shape and location of the slip surface (line of maximum tension forces) depends on various features such as reinforcing elements stiffness, the wall facing inclination and applied loads. Metallic reinforcements have higher stiffness that minimizes the wall movement compared to the geosynthetic reinforcements that have lower tensile stiffness. As a result, the potential slip surface is closer to the wall facing for inextensible reinforcements. Certain design codes (Ex. (FHWA, 2009)) assume two different slip surface shapes for extensible and inextensible reinforcements. The maximum tension line was reported to define a bilinear failure surface for metallic reinforcements (Figure 1-9a) based upon instrumented structures and theoretical studies, and a Rankine linear failure surface for geosynthetic reinforcements, because these extensible reinforcements can elongate more than the soil, before failure, and therefore do not significantly affect the failure surface shape in the soil mass. This failure surface is oriented at an angle of $45 + \varphi/2$ from the horizontal, for the case of vertical wall facing (Figure 1-9b). The potential failure surface is assumed to pass through the wall toe in both cases. However, the French standard NF P 94-270 (based on Eurocode 7) suggested the same slip surface for both reinforcement's types since the hypothesis of Rankine failure surface is not suitable for all types of geosynthetic reinforcements as shown by Schlosser et al. (1993). The slip surface has been assumed bilinear as shown in Figure 1-10.

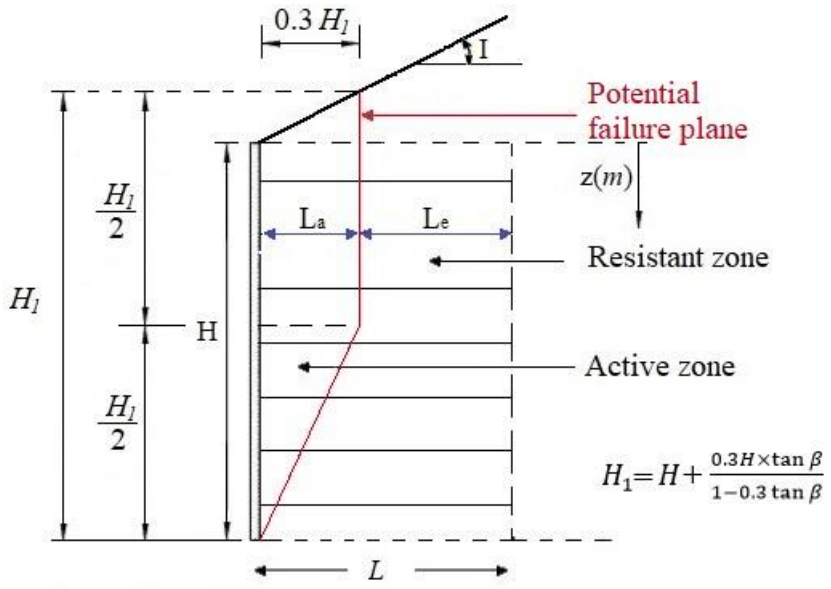

(a)

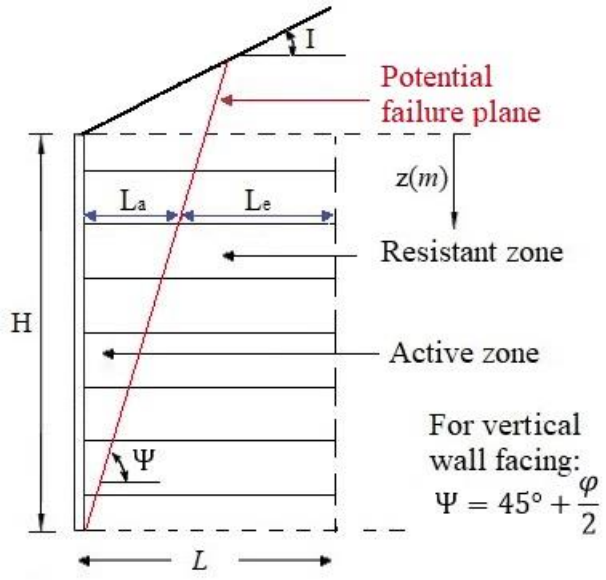

(b)

Figure 1-9 Location of potential failure surface for internal stability design of reinforced soil retaining walls (FHWA, 2009)

(a) Inextensible reinforcements and (b) extensible reinforcements

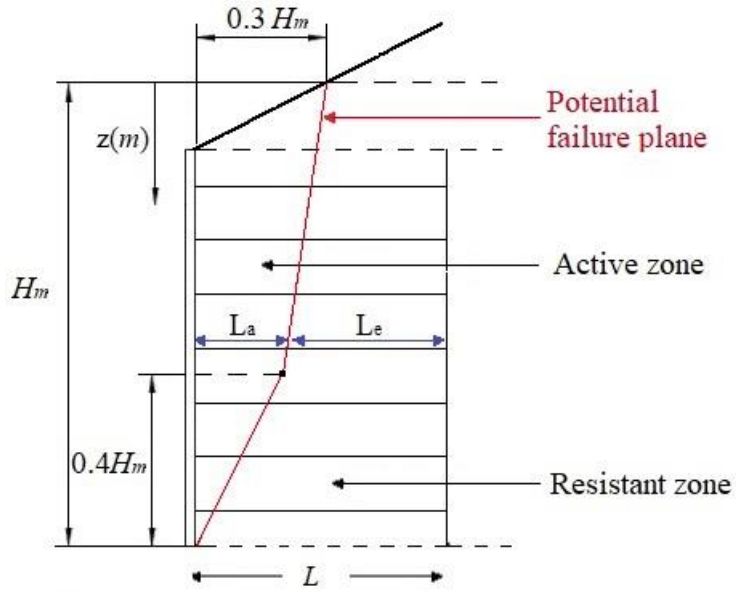

Figure 1-10 Location of potential failure surface for internal stability design of reinforced soil retaining walls (NF P 94-270, 2009)

1.3.2.1 Maximum tension forces

Most design methods determine the reinforcement load based on calculated lateral earth pressures. The maximum tension force T_m per unit width of wall at the potential slip surface of each reinforcement layer can be determined as follows: $T_m = \sigma_h \times S_v$.

S_v denotes for the vertical spacing of reinforcement and σ_h is the total horizontal soil stress at the reinforcement level determined as $\sigma_h = k_r \sigma_v + \Delta\sigma_h$.

σ_v is the vertical soil stress at the reinforcement level, $\Delta\sigma_h$ is the additional horizontal stress at reinforcement level that could result from a variety of sources such as traffic load, roadway fill or any fill type above the reinforced soil zone, the normal and shear pressures at the bottom of a spread footing on top of the reinforced soil wall. k_r is the lateral earth pressure coefficient determined empirically based on experimental results.

In NF P 94-270, this coefficient is equal to:

$$\begin{cases} k_r(z) = \Omega_1 k_a \left[1.6\left(1 - \frac{z}{z_0}\right) + \frac{z}{z_0}\right] & \text{if } z < z_0 = 6\ m \\ k_r(z) = \Omega_1 k_a & \text{if } z > z_0 = 6\ m \end{cases} \quad (1\text{-}1)$$

where z is the depth below the top of the wall facing in case of level backfill or the depth starting from the intersection of the slip surface with the ground surface in case of level backfill as shown in Figure 1-10, Ω_1 is a coefficient that depends on the reinforcement type since the maximum tensile force depends on the modulus, extensibility and density of reinforcement in the reinforced soil retaining wall, as shown in several research studies (Christopher et al., 1990; Allen et al., 2001). k_a is the active earth pressure

calculated using the Rankine formula ($k_a = tan^2(45° - \varphi/2)$), with φ the reinforced soil internal friction angle.

In the design code of FHWA (2009), the simplified method (Allen et al., 2001) is used to determine the horizontal earth pressure coefficient k_r. Figure 1-11 gives the ratio k_r/k_a depending on the reinforcement type (geotextile, geogrids, metal strip or metal grid), and depth, where the active earth pressure coefficient k_a is computed using the Rankine formula i.e. independent of backfill slope and interface friction. This method was developed based on empirical available data and constitutes an improvement of the coherent gravity method (AASHTO, 1996) and the structural stiffness method (Christopher et al., 1989). Figure 1-11 shows the ratios k_r/k_a for different reinforcement types. For geosynthetic reinforcements, this ratio is constant and equal to one. However, for the metallic reinforcement, the ratio k_r/k_a on the top of the reinforced soil wall depends on the reinforcement type with the metallic strips having the smallest ratio. This ratio decreases for all metallic reinforcements starting from the wall top to a ratio equal to 1.2 at a depth $z_0 = 6\,m$ and remains constant below this depth. It is worth noting here, that the depth z is computed starting from the top of the wall facing, as shown in Figure 1-9, in both cases of level or slopping backfill.

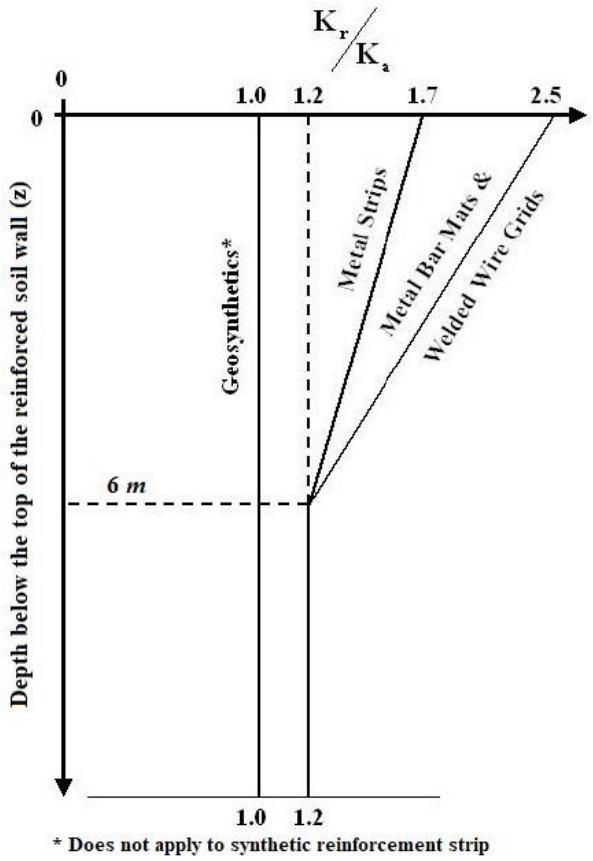

Figure 1-11 Variation of the lateral stress ratio coefficient k_r/k_a with depth in a reinforced soil retaining wall (FHWA, 2009)

1.3.2.2 Tension at the reinforcement/wall face connection

The tension force T_o per unit width of wall at the connection with the wall face can be determined as follows: $T_o = \alpha_i \times T_m$.

In the design code of FHWA (2009), the reinforcements connection to the wall face should be designated for T_m, i.e. α_i=1. On the other hand, in NF P 94-270, the coefficient α_i depends on the flexibility of the wall face and the depth of the reinforcement layer. For precast concrete panels for example, α_i is equal to 0.85 for a depth z between 0 and $0.6H_m$ and increases linearly from 0.85 to 1 between $0.6H_m$ and H_m where this latter is the total wall height (Figure 1-10).

1.3.2.3 Reinforcement strength

The maximum tension forces along the reinforcements should be smaller than the reinforcement strength at every level within the reinforced zone. The reinforcement durability in the environment in which they are placed represents a major concern for reinforced soil structures design. The metallic and synthetic reinforcements must be considered separately.

For metallic reinforcements, the potential corrosion losses must be considered to identify the long-term tensile strength of the reinforcements. The corrosion is a natural process where the metallic reinforcement rusts due to chemical or electrochemical reaction with the environment. To limit this phenomenon, the backfill used in the reinforced zone should meet the electro-chemical properties requirements (soluble salts concentration, pH ...). Poorly draining backfill (clay, silt) are generally more corrosive than granular soils such as sand and gravel that are characterized by good drainage and greater air circulation. In addition, the corrosion can be reduced using coatings. The metallic reinforcements are galvanized with zinc coating to protect the underlying steel. Neglecting the corrosion of the reinforcements could cause sudden and catastrophic failure of reinforced soil retaining structures (Armour et al., 2004; Gladstone et al., 2006).

The long-term tensile strength of the reinforcement T_r is obtained for metallic reinforcement using the anticipated cross-sectional area of the reinforcement at the end of the design life. This anticipated cross-sectional area is calculated by reducing the initial cross-sectional area of the reinforcement by the anticipated corrosion losses over the design life period as follows:

$$T_r = A_c f_y \tag{1-2}$$

Where A_c is the cross-sectional area of the reinforcement at the end of the service life of the structure and f_y the steel yield stress.

For synthetic reinforcements, the cross-sectional area is not needed, since their strength is expressed by a tensile force per unit width. However, even if they are not susceptible to corrosion, these reinforcing elements strengths could be affected by environmental factors such as creep, installation damage, aging, temperature, and confining stress. Potential degradation of synthetic reinforcements depends on the polymer type, reinforcements configuration used in addition to the environment, the temperature, and the stress level to which they are subjected. To consider the long-term degradation strength losses and the installation damages, the reinforcement nominal strength T_r is obtained as follows:

$$T_r = \frac{T_u}{RF} \tag{1-3}$$

Where T_u is the geosynthetic ultimate tensile strength, and RF is the combined reduction factor to account for potential long-term degradation due to installation damage, creep and chemical aging. This reduction factor is the product of the applicable three reduction factors, RF_{ID}, RF_{cr} and RF_D that represent, respectively, the installation damage reduction factor, the creep reduction factor and the chemical and biological degradation reduction factor.

1.3.2.4 Reinforcement pullout

The maximum tension forces along the reinforcements should be smaller than the reinforcement pullout capacity at every level within the reinforced zone. The stress transfer mechanism between the soil and reinforcement occurs by friction in addition to the passive resistance provided through the development of bearing type stresses on transverse reinforcement surfaces when ribbed reinforcement strips, bar mat, wire mesh reinforcements, and geogrids with relatively stiff cross machine direction ribs are used. The reinforcement pullout resistance is defined by the required amount of mobilized tensile load to cause the outward movement of the reinforcement through the reinforced soil mass. The pullout force for a single layer of reinforcement is given by:

$$T_p = C\gamma z^* L_e f^* \tag{1-4}$$

Where C is the overall reinforcement surface area geometry factor based on the reinforcement gross perimeter (equal to 2 for strip, grid, and sheet-type reinforcements), z^* is the overburden depth, L_e is the effective length i.e. the reinforcement length in the resistant zone (Figures 1-9; 1-10), $f^* = F^*\alpha$ where F^* is the pullout resistance factor and α is the correction factor that accounts for a nonlinear stress reduction over the embedded length of highly extensible reinforcement. The factor F^* considers both stress transfer mechanisms to pullout resistance simultaneously. It is always more reliable to estimate its value by conducting pullout tests of reinforcement in backfill material used in the reinforced zone of the project. However, in the absence of site-specific pullout testing data, most design codes (NF P 94-

270, FHWA…), suggest empirical or theoretical relationships for each reinforcement type to provide a conservative evaluation of pullout resistance.

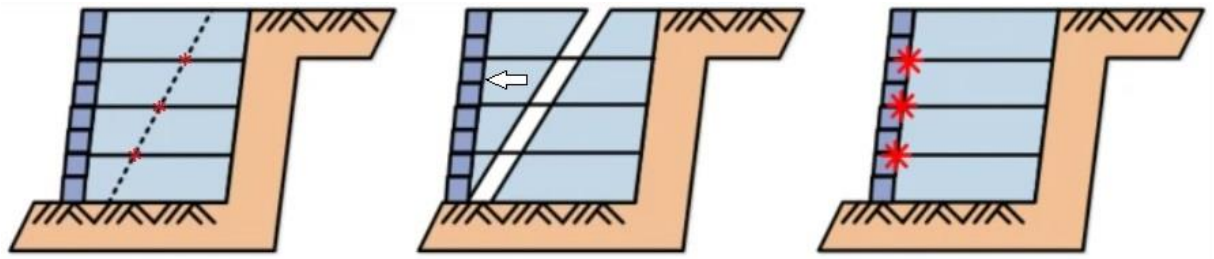

(a) (b) (c)

Figure 1-12 Internal failure mechanisms (Kong et al., 2018): (a) Tensile over-stress; (b) Pullout; (c) Connection failure

1.3.3 Overall and compound stability

The global and compound stability analysis should also be checked for reinforced soil retaining walls. The global or overall stability of the site is investigated as a classical slope stability problem using one of the slope stability computer programs. The overall stability concerns the potential failure surfaces behind and under the reinforced zone, i.e. the slip surfaces completely outside this zone.

On the other hand, the compound stability analysis concerns all the potential slip surfaces passing through a portion of the reinforced zone and should be investigated. Contrary to the overall stability check, where the reinforced zone is considered a rigid body, the compound stability is performed using computers programs that directly incorporate reinforcement elements in the analysis as discrete elements. The compound stability is generally not critical for simple reinforced soil structures. However, it must be considered carefully in complex structures supporting high surcharge loads, seismic conditions, tiered walls, variable reinforcement type or vertical spacing… In these complex structures, to satisfy the compound stability, the reinforcement strength or reinforcement length may be increased. Reducing the reinforcement vertical spacing also enhanced the structure stability.

1.3.4 Seismic design of Reinforced Soil Walls

The reinforced soil walls suffer from vulnerability to natural hazards such as earthquakes. Safety constitutes the great challenge of this space. The earthquake events tend to affect the external and internal stability of these structures.

1.3.4.1 Pseudo static approach

The most common approach used to represent the ground shaking in design codes (FHWA, 2009; NF P 94-270, 2009) is the pseudo-static method. The seismic influence is substituted by inertial forces with constant horizontal and/or vertical acceleration. First, an initial design of the reinforced soil wall is established based on static loading i.e. without any consideration of the seismic loading. Then, the reinforcements' distribution and strength obtained based on static loading, are verified under seismic conditions. Regarding the external stability, the seismic verification involves in addition to the static forces, the total (static and dynamic) thrust and the inertia forces. On the other hand, with respect to the internal stability verification, it involves in addition to the static forces, the internal dynamic forces. The seismic coefficients used in the seismic design within the framework of pseudo-static approach, are determined based on the seismic hazard and the site effects that include the site peak ground acceleration, spectral acceleration, Site Class and Site Factors (Topographic amplification). For the design code FHWA, based on these parameters, the maximum acceleration k_{max} and the average peak ground acceleration k_{av} can be determined. Alternatively, in Eurocode 8 (EC8), these parameters are used to determine the horizontal and vertical seismic coefficients k_h and k_v. k_h is generally equal to $0.5\frac{a_g}{g}S$, where a_g is the reference maximum acceleration of the zone where the reinforced soil wall is constructed, g is the acceleration due to gravity and S is a parameter that depends on the type of the spectral response and the soil class.

The value of the total thrust P_d can be calculated through a generalized Limit Equilibrium slope stability analysis or the Mononobe-Okabe formulation. The former can be conducted using an appropriate slope stability analysis method while the latter can be applied in the case of homogeneous cohesionless backfill as follows:

$$P_d = 0.5\gamma(1 \pm k_v)KH^2 \tag{1-5}$$

With

$$K = \frac{cos^2(\varphi_b - \xi + 90 - \beta)}{cos\xi cos^2\beta \cos(\delta - 90 + \beta + \xi)\left[1 + \sqrt{\frac{\sin(\varphi_b + \delta)\sin(\varphi_b - \xi - I)}{\cos(\delta - 90 + \beta + \xi)\cos(I + 90 - \beta)}}\right]^2} \tag{1-6}$$

$$\xi = \tan^{-1}\left(\frac{k_h}{1 - k_v}\right) \tag{1-7}$$

Where φ_b is the retained soil friction angle, β the angle between the horizontal and the wall direction (90° in case of vertical wall), δ is the angle of wall friction, I is the backfill slope angle as shown in Figure 1-13, k_h and k_v are respectively the horizontal and vertical seismic coefficients. For the design code FHWA, the vertical seismic coefficient k_v is assumed to be zero and the horizontal seismic one k_h

is taken equal to k_{max}. On the other hand, in EC8, the vertical seismic coefficient is assumed equal to $0.33k_h$ or $0.5k_h$ depending on the zone where the reinforced soil wall is located.

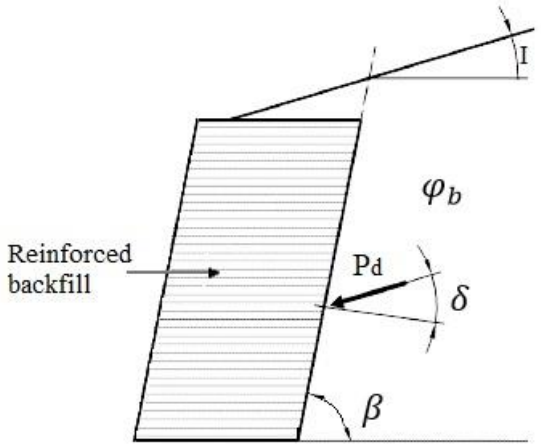

Figure 1-13 Total thrust under seismic loading

With regard to the inertia forces, the design code FHWA considers only the horizontal component since the seismic vertical acceleration is neglected and the value of this force is calculated as follows:

$$P_{IR} = 0.5(k_{av})(W) \tag{1-8}$$

where W is the reinforced soil full weight.

Alternatively, the values of the horizontal and vertical seismic inertia forces within the framework of the NF P 94-270 are determined as follows:

$$\begin{cases} F_H = k_h W = 0.5\frac{a_g}{g} S(W) \\ F_V = k_v W \end{cases} \tag{1-9}$$

For internal stability, an internal dynamic force is assumed to act within the active zone (Figure 1-9 and 1-10). Therefore, the reinforcements must withstand the total horizontal forces generated by these dynamic forces and the static forces. In the design code FHWA, the internal dynamic force acts in the horizontal direction and it is equal to:

$$P_i = (k_{av})(W_a) \tag{1-10}$$

Where W_a is the area of the active zone (Figures 1-9 and 1-10).

In NF P 94-270, the seismic consideration in the internal stability is considered by the horizontal internal dynamic force obtained by Eq. 1-10 using the coefficient k_h instead of k_{av} and by the increment of the vertical forces due to the vertical pseudo-static force.

1.3.4.2 Pseudo dynamic approach

The pseudo-static method considers the dynamic behavior of seismic loading in an approximate manner without considering the time and depth effects of the ground shaking.

The pseudo-dynamic method, originally proposed by Steedman and Zeng [1990], considers these effects such as the motion amplification, earthquake duration and frequency (Nimbalkar et al., 2006; Choudhury and Nimbalkar, 2007; Basha and Babu, 2011; Qin and Chian, 2017), which is more realistic compared to the pseudo-static one. The pseudo-dynamic approach has been applied to determine the seismic stability of geosynthetic reinforced homogeneous soil retaining walls with considering the time effects and phase change effects due to body waves propagating trough the reinforced backfill (Nimbalkar et al., 2006; Basha and Babu, 2011).

1.4 Deterministic design and investigation methods for reinforced soil wall stability analysis

The seismic stability assessment of reinforced soil walls could be grouped into three categories: experimental studies, theoretical and analytical methods and numerical approaches (finite elements and finite differences).

1.4.1 Experimental studies

An important amount of experimental studies on the response of reinforced soil retaining walls has been reported in the literature for a better understanding of these structure performances under static and seismic loadings. These experimental investigations include studies of both full-scale and reduced scale models. A sample of these studies are presented here.

Richardson et al. (1977) performed the first seismic full-scale model test on the 6 m-high steel-strip reinforced soil retaining wall. They compared the measured dynamic forces of the strips with the forces predicted by the recommended methods for the seismic design and showed that the former are much smaller. The results showed also that increasing the reinforcements' length could reduce greatly the induced dynamic forces of strip.

Ling et al. (2005b) presented the results of three full-scale shaking table tests conducted using Kobe-earthquake motions on modular-block reinforced-soil retaining walls, constructed with sand backfill and polymeric reinforcements. The results showed that the reinforced wall would be more stable with the reduction of the reinforcement spacing and the increase of the upper reinforcement layer length. The wall stability is enhanced by grouting the top blocks, which ensure a strong connection between the wall facing and the geogrids reinforcement. In addition, Ling et al. (2005b) observed that the reinforced soil walls performed well under earthquake loading and the small acceleration amplification of the

reinforced wall equal 1.35 indicates that it exhibits better earthquake performance than the conventional walls.

El-Emam and Bathurst (2007) examined the influence of reinforcement parameters on the seismic response of reinforced soil retaining walls by carrying five shaking table tests on 1/6-scale model walls using a stepped-amplitude harmonic base acceleration record. They concluded that increasing the reinforcements length, decreased the wall lateral displacement, the total reinforcement connection loads, the normalized horizontal toe load, the total seismic-induced earth forces acting at the back of the facing and the magnitude of acceleration amplification factors. Increasing the reinforcement stiffness increased the total reinforcement connection loads, the normalized horizontal toe load and the total seismic-induced earth forces acting at the back of the facing. However, it decreased the wall lateral displacement. Finally, reducing the reinforcement's vertical spacing decreased the wall lateral displacement and the magnitude of acceleration amplification factors. However, the total reinforcement connection loads decreased with the reinforcements vertical spacing increasing.

Latha and Krishna (2008) investigated the influence of backfill relative density on the seismic response of reinforced soil retaining wall models by conducting shaking table tests on 24 model walls. Two types of wall facings were considered: wrap-faced walls and rigid-faced walls. They found that the relative density was insignificant at smaller base excitation. However, at higher base excitation, they observed that increasing the relative density decreased the wall displacement and increased slightly the acceleration amplification. These results showed that an appropriate backfill compaction could limit the damage of reinforced soil retaining walls in case of strong seismic events. The results showed also that displacements in wrap-faced walls are much higher compared to rigid-faced walls.

Latha and Santhanakumar (2015) carried out 1 g shaking table tests on reduced models of modular block and rigid faced reinforced soil retaining walls. Two types of geogrids were used in their study. They found that the seismic performances of modular block and rigid faced reinforced soil walls depend on the type and quantity of reinforcement and that their influence is more pronounced in the case of modular-block reinforced soil walls.

Ahmadi and Bezuijen (2018) presented the results of two large-scale model tests on geogrids reinforced walls under a strip footing. The wall facing type was the only difference between the two models. One of them was constructed with rigid wall face while the second with a flexible one. They found that the tensile force on reinforcement's layers and the maximum wall deflection for flexible facing were higher than the rigid facing.

El-Emam (2018) compared the responses from a series of reinforced soil wall models, tested on shaking table with the responses predicted using two limit equilibrium design approaches (NCMA, and AASHTO/FHWA). The comparison showed that the soil slip surface found analytically under predicted

the soil failure wedge size obtained experimentally. Figure 1-14 shows the physical reinforced soil model wall and the instrumentation layout of the reduced scale model.

Ren et al. (2020) carried out five reduced-scale shaking table tests to investigate the deformation evolution mechanism of reinforced soil retaining wall subjected to the rainfall-earthquake combined effects using five different saturation degrees. They showed a good performance of reinforced soil retaining walls even when subjected to the rainfall and earthquake combined effects. In addition, they found that the soil suction enhanced the seismic performance of these walls in terms of reinforcement strain and wall displacement and therefore, the dry and saturated backfill soil states were the most critical states.

The full-scale experimental tests are the most appropriate options. However, they are highly expensive and time-consuming. In the case of reduced-scale models that requires less experimental time and budget, it is important to apply appropriate scaling rules to extrapolate the results to the real dimensions.

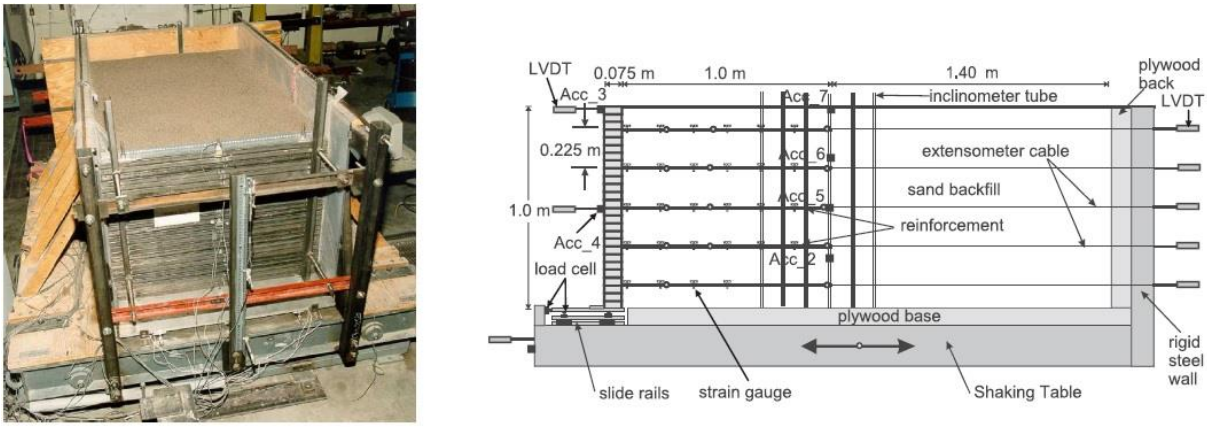

Figure 1-14 Reduced scale reinforced soil model wall and instrumentation layout (El-Emam, 2018)

1.4.2 Theoretical and analytical methods

1.4.2.1 Limit Equilibrium

The Limit equilibrium (LE) method is one of the several analysis methods used to assess the limit state of a system. The limit equilibrium method is frequently used to obtain approximate solutions for the problems of instability in soil mechanics. The method consists in estimating a planar, circular or log-spiral failure surface. With the assumption of the shape of the rupture surface, the stability problem is reduced then to determine the most "dangerous" slip surface position.

To calculate the factor of safety, it is necessary to assume a slip surface shape, and at least one of the equations of equilibrium is used to calculate the stresses. Then, the safety factor for each slip surface is assumed. Three conditions for the static equilibrium are available: the equilibrium of the forces in the

vertical and horizontal directions and the equilibrium of the moments relative to any point. The limit equilibrium approach incorporates the reinforcement's force into limit equilibrium equations (Zhang et al., 2014). All limit equilibrium methods use at least one of these equations to calculate the factor of safety. Regardless of the procedure considered for the equilibrium, there will be a number of unknowns (forces, locations of forces, factor of safety, etc.) larger than the number of equilibrium equations; the problem of the determination of the safety factor will be statically indeterminate. Thus, it is necessary to make assumptions in order to balance the number of unknowns with the number of equations and makes the problem therefore statically determinate.

There are two different approaches used in the limit-equilibrium analysis procedures. A part of the procedures considered the equilibrium of the total mass of the soil block limited between the slip surface and the ground surface. Among these approaches, there is the procedure of the infinite slope and the method of Swedish Circle (Swedish circle method). For the second part of procedures known as the methods of slices, the soil mass is divided into several horizontal, vertical or inclined slices, hence the nomenclature. The number of slices depends on the geometry of the slope and the profile of the soil. Some of the procedures assume a circular slip surface and others assume arbitrary shapes of slip surfaces. The assumptions are made on inter-slices forces instead of the global normal stress distribution. These procedures, known as the methods of slices, include several methods such as the ordinary method of slices, the method of Bishop, the method of Spencer.

The limit equilibrium method, being easily understood and popular, is the technique commonly used to design and analyze the seismic stability of reinforced soil retaining walls. Nouri et al. (2006) investigated the seismic stability of reinforced soil slopes and walls a limit equilibrium method known as the Horizontal Slice Method (HSM) where the sliding soil block is divided into horizontal slices, in such a way that the reinforcements do not have a direct effect on inter-slice forces (Figure 1-15). The proposed method HSM was verified by comparison with three published studies which were based on limit analysis method and another limit equilibrium method proposed by Ling et al. (1997) since no experimental data were available for direct comparison. Using HSM and limit equilibrium method, a new design methodology, for unreinforced and reinforced c-φ soil retaining walls, was proposed by Ahmadabadi and Ghanbari (2009). A planar failure surface is assumed. The analytical results of the proposed methodology were compared with those of previous works. This comparison shows the efficiency of the proposed method in determining the active lateral earth pressure distribution, reinforcement’s tensile forces and the critical failure surface for both unreinforced and reinforced cases. Pain et al. (2017) investigated the seismic internal stability of reinforced soil retaining structures using the limit equilibrium method. A rotational log-spiral failure mechanism was assumed in their study. The soil was modeled as a viscoelastic Kelvin-Voigt (KV) homogeneous medium. The seismic loading is considered in a rational way so that the amplitude and phase of seismic accelerations vary with depth and the accelerations amplification at the ground surface depends on the dynamic soil properties and

input excitation frequency content. In addition, the amplifications of accelerations obtained analytically were compared with the results of DEEPSOIL, a unified 1D equivalent linear and 1D nonlinear site response analysis program, for both linear and equivalent linear analysis cases and showed a good agreement. The results of this method in terms of required reinforcement strength and length are compared with the results obtained by Ling et al. (1997). In addition, the limit equilibrium method was widely used for deterministic model in reliability analysis of reinforced soil retaining walls (Basha and Sivakumar Babu, 2009-2010-2011-2012; Luo et al., 2016).

A weak point of the limit equilibrium method is that the results cannot be regarded as rigorous due to the arbitrary assumptions of the forces between the slices. Two different methods satisfying the same equilibrium conditions but using different assumptions produce different values of factor of safety. In addition, it does not consider the stress-strain relation of soils which is must be satisfied for a complete solution according to the solids mechanics (Patra and Basudhar, 2005; Nouri et al., 2006).

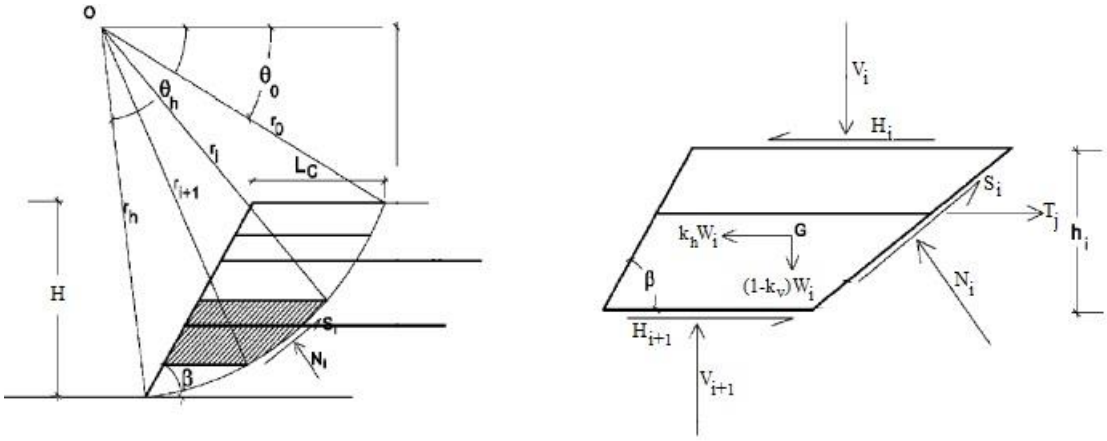

(a) (b)

Figure 1-15 (a) Log-spiral failure surface and Horizontal Slice Method; (b) Forces acting on a slice (Nouri et al., 2006)

1.4.2.2 Limit Analysis

Limit analysis offers an effective tool, widely used to perform stability analysis for a wide variety of practical problems in geotechnical engineering (slopes, retaining walls, foundations, dams and tunnels). Through the concept of a yield criterion and its associated flow rule, limit analysis permits to consider the stress-strain relationship neglected through limit equilibrium methods. The limit analysis theorems give upper and lower bounds on the collapse load. The kinematic approach of limit analysis, which is based on the plasticity upper bound theory, has increasingly grown for the reinforced soil retaining structures stability design. Applicability of the theorem requires that the soil mass behavior is considered as ideally rigid, perfectly plastic according to an associated normality rule based on the Coulomb yield condition. The kinematic approach deals with the construction of a kinematically admissible failure

mechanism. Hence, when it is used to calculate driving forces such as the collapse load or slope critical height, the solution obtained is an upper bound of the real solution. On the other hand, when it is used to seek resisting forces, the solution obtained is a lower bound of the real solution. Consequently, the upper bound theorem is used to find a lower bound to the reinforcement forces required to prevent failure of reinforced soil systems. For any assumed kinematically admissible failure surface, the reinforced structure will collapse if the rate of external work exceeds the internal energy dissipation rate:

$$\int_V \sigma_{ij}^* \dot{\varepsilon}_{ij}^* dV \geq \int_S T_i v_i dS + \int_V X_i v_i^* dV \quad (1\text{-}11)$$

Where $\dot{\varepsilon}_{ij}^*$ is the strain rate in a kinematically admissible velocity field, σ_{ij}^* is the associated stress tensor, S and V are the loaded boundary and the volume, respectively, $v_i^*=v_i$ is the velocity on boundary S, X_i is body forces vector and T_i is the stress vector on the boundary S. Examples of the application of limit analysis in reinforced soil can be found in many papers.

Michalowski (1997-1998a-1998b) investigated the seismic internal stability of reinforced soil slopes using the pseudo-static approach to represent the seismic loading. Figure 1-16 shows the rotational log-spiral failure surface considered in these studies. This surface can be fully described using two parameters: θ_0 and θ_h (see Figure 1-16). The kinematical admissibility condition requires that the angle between the velocity vector [v] and the failure surface must be equal to the soil internal friction angle φ. The expressions of the energy dissipation (left-hand side of Eq. 1-11) and the work rates of the external forces (right-hand side of Eq. 1-11) are determined as functions of the parameters θ_0 and θ_h. Readers can refer to Michalowski (1997-1998a-1998b) for the expressions of the work rates and a more comprehensive description of the method. The required reinforcement strength is determined to ensure the reinforced soil slopes stability considering only the tension or rupture failure of reinforcement through an optimization process with angles θ_0 and θ_h being variables. The optimization process gives a lower bound to the reinforcement strength required to ensure the wall stability and the associated failure surface (θ_0 and θ_h that give the maximum required reinforcement strength). Then, the reinforcement length was also calculated considering the tension and the pullout failure of reinforcements.

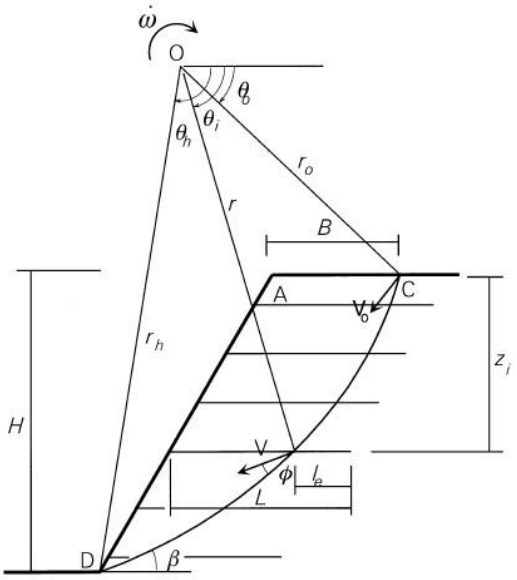

Figure 1-16 Rotational collapse failure surface of the reinforced slope (Michalowski, 1998a)

Ausilio et al. (2000) performed a seismic internal stability analysis of geosynthetic-reinforced soil slopes within the framework of the pseudo-static approach. Translational and rotational failure mechanism were considered. The reinforcement force required to prevent failure and the yield acceleration of slopes subjected to earthquake loading were determined and the comparison between the planar and rotational failure surface assumption is presented.

Abd and Utili (2017a-2017b) investigated the seismic internal stability of reinforced soil slopes with consideration of the cracks. The lower bound to the required reinforcement strength and the reinforcement length are determined using the kinematic analytical approach. The influence of water pore pressures was investigated.

It is worth noting, that numerical limit analysis approaches were developed in which, it is not necessary to assume arbitrarily a failure mechanism, which is an advantage when complex problems are considered. Numerical LA can deal with layered soil, complex geometries, water, seismicity etc… For instance, Camargo et al. (2016) developed a numerical limit analysis for assessing slope stability problems. They obtained almost the same safety factor obtained as with the limit equilibrium methods.

1.4.2.3 K-Stiffness Method

K-Stiffness Method is a relatively new method, which used either the Load and Resistance Factor Design (LRFD) procedure or the Allowable Stress Design (ASD) procedure. This method was developed by Allen et al. (2003) for geosynthetic reinforced soil retaining walls and was calibrated by measurement of the loads and the deformations from a large database of retaining walls reinforced by geosynthetics. The method aims to predict the reinforcement loads and strains for internal stability design of geosynthetic reinforced soil walls under static conditions. A main objective of this method is

to design the wall reinforcements so that the soil in backfill is prevented from reaching the failure, in accordance with the concept of allowable stresses. The concept presents a new approach for checking the internal stability of geosynthetic reinforced soil retaining walls, since the prevention of soil failure at limit state is considered in addition to the current practice of the prevention of reinforcement rupture. This method defined a new limit state which was not considered in the other design codes; the soil failure limit-state. This is important, especially for the geosynthetic reinforced retaining walls, as this type of reinforcement continues to deform and acquire tension loads after that the soil has reached its resistance limit. Consequently, if the soil deformation is limited to prevent it from going toward the Residual State, the failure by excessive deformation or rupture is prevented and the equilibrium is maintained. This represents the design method philosophy.

Allen et al. (2003) observed that the distribution of tension forces along the reinforcements according to the depth of the wall is generally trapezoidal in shape and not linear as proposed in the simplified methods. The method starts with the prediction of the total lateral force that must be resisted by the reinforcements, which is consistent with the simplified method approach.

The K-Stiffness method takes this force and adapts it empirically based on the effects of the global reinforcement stiffness, the local reinforcement stiffness, the facing stiffness/the lateral restraint of the wall facing at the wall toe and the wall batter, the shear strength of the soil, and the distribution of the total lateral force with depth based on the observations of a large set of real instrumented walls in the literature. The formulation of the global reinforcement stiffness is consistent with that one used in the 'FHWA Structure Stiffness Method' (Christopher et al., 1990; Christopher, 1993). The methods used in practice, (e.g. the simplified method) calculates the vertical stress due to sol weight with depth, which contributes to a linear increase of the gravity force and a distribution of lateral stress that increase linearly with depth, while the K-Stiffness method calculates the maximum vertical stresses due to soil weights in the reinforced backfill, and that for determination of the maximal reinforcement loads in the reinforced backfill, T_{mxmx}, and consequently, this method adapt this maximal load with the depth for every layer of reinforcement using a distribution factor, $D_{t\ max}$, to calculate T_{max}.

The maximal load in the layer i is as follows:

$$T_{max}^{i} = 0.5K\Upsilon(H+S)S_v^i D_{t\ max}\Phi_g\Phi_{local}\Phi_{fs}\Phi_{fb} \quad (1\text{-}12)$$

where:

K : the lateral earth pressure coefficient calculated using the Jacky equation $K = 1 - \sin\varphi$. It must be greater than 0.3 when metallic reinforcements are used in the system;

γ : the unit weight of the soil;

H : the height of the wall;

S : the equivalent height of uniform surcharge pressure q ($S = q/\gamma$);

S_v^i : the tributary area (equivalent to vertical spacing of the reinforcements);

$D_{t\,max}$: the load distribution factor that modifies the reinforcement load based on the layer depth;

The other parameters Φ_g ; Φ_{local} ; $\Phi_{fs}\ et\ \Phi_{fb}$ are the influence factors that take into account respectively, the effect of the global stiffness, local stiffness, the facing stiffness/the toe restraint condition and the facing batter of the facing.

The parameters of this empirical method are calibrated using a database of geosynthetic reinforced soil walls reinforcement strain and load data (Allen et al., 2003). The database used to calibrate the method was extended by adding additional data of field and laboratory case studies (Bathurst et al., 2008b). The obtained values of deformations are converted into stresses knowing the geosynthetic reinforcement stiffness value. The latter is determined by the authors considering several parameters: the confinement pressure, the deformation level, potential loading, the time and the temperature. These parameters are supposed to be constant along the reinforcement. Accordingly, the stresses deducted along the reinforcements are the averages stresses.

It is important to note that the K-stiffness method has been improved to consider a greater number of walls of the literature, in addition to consider the effect of the cohesion of the backfill (Bathurst et al., 2008b). Although the consideration of the soil cohesion helps to improve the precision of the prediction of the method K-stiffness for the walls with a soil containing a significant component of the cohesion contributing in its shear resistance, in general, it is not recommended to consider the cohesion of the soil in the backfill in the design of the reinforced soil walls because of the blurring on the effect of moisture in the long term in the soil and the possibility of soil creep.

A comparison of the values predicted by the K-Stiffness method with measurements of real instrumented walls, indicates that this method is the most accurate for the estimation of the reinforcements efforts among all the method available in the design-codes and therefore reduces the required amount of reinforcements and improves the economy of the reinforced soil walls (Allen et al., 2003). The same authors extend this methodology for metallic reinforced soil retaining walls based on a large database of walls reinforced by steel reinforcements (Allen et al., 2004). The economic improvement obtained is significant for both the metallic and geosynthetics reinforcements, but it is more pronounced in the second case. Two geosynthetic reinforced soil walls have been designed based on this method. They were constructed and instrumented by the Washington State Department of Transportation (WSDOT) and completed in 2006. The first instrumented reinforced wall that was the largest with $11\ m$ height, whereas the second wall was $6.3\ m$ in height. Both reinforced soil walls were about $200\ m$ long. The amount of reinforcements in these walls is reduced by 35 to 50% compared to the quantity required by the simplified method. The results are reported by Allen and Bathurst (2014a-2014b). These results

indicate and show that the loads in the reinforcements are well predicted by this new method and that the walls perform well since the time of their constructions.

The K-Stiffness method has been adapted for the LRFD design procedure for different types of reinforced soil retaining walls (Bathurst et al., 2008a-2011-2012-2019a; Huang, 2010; Huang et al., 2012). In addition, the Geotechnical Design Manual of WSDOT presents a detailed guideline of all the steps of the reinforced soil retaining walls design procedure using the K-Stiffness in a load and resistance factors design framework.

1.4.2.4 Homogenized concept

The discrete methods are generally used to model the behavior of the reinforced soil system. In these methods, different mathematical models are separately used to simulate the soil, the reinforcements and the soil-reinforcement interface. Alternatively, the homogenized approach could be used for the reinforced soil retaining walls assessment. This approach considers an anisotropic reinforced soil massive as a homogeneous medium, by using the weighted strength or weighted stiffness concept (Moroto and Hasegawa, 1990; Michalowski and Zhao, 1995). As the reinforcement elements are generally arranged horizontally in the backfill, an orthotropic or transversely isotropic model is often used in the homogeneous method.

Chen et al. (2000) proposed a numerical procedure for the analysis of reinforced soil structures, based on the transversely isotropic homogenized concept and considered, in this model, the linear and non-linear behavior of the reinforced soil and appropriate boundary conditions. The proposed model is programmed in the commercial computer code FLAC for the numerical analysis and it is validated by comparing the results of two models studied with those of the experimental tests on the same models. In this model, the composite material soil/reinforcement, with the transversely isotropic property, is treated as an equivalent homogeneous medium.

Two assumptions are made in order to simplify the considered system:

- The reinforcement elements and the soil are considered both as isotropic materials.
- A perfect adherence is assumed to exist between the soil and the reinforcing elements.

Five parameters, which include the tangent modulus of the reinforced soil in the horizontal and vertical directions, the Poisson's ratio in the anti-plane and in plane directions and the shear modulus, are required to describe the behavior of the equivalent homogenized medium.

Figure 1-17 represents a schematic diagram of a reinforced soil system. In this figure, A^s and S^s are the cross-sectional area and the thickness of the soil, A^r and S^r those of the reinforcement and A^c and S^s

those of the reinforced composite. Using different equilibrium and compatibility equations of the reinforced soil system, the five parameters of the equivalent homogenized medium can be determined.

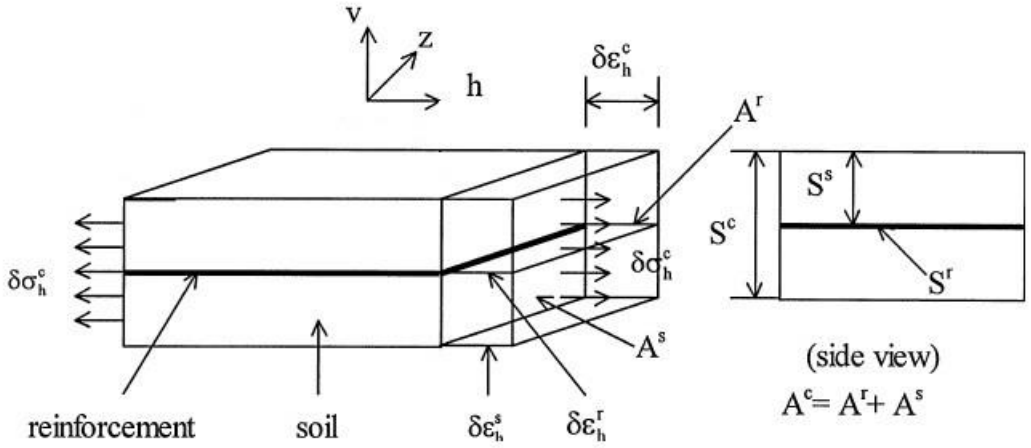

Figure 1-17 Free body diagram of the soil-reinforcement system

The tangent modulus in the horizontal direction is given by:

$$E_h^c = \frac{1}{1+\eta}\left[\frac{(\Omega^r+\Omega^s)^2-(\upsilon^r\Omega^r+\upsilon^s\Omega^s)^2}{(\Omega^r+\Omega^s)}\right] \tag{1-13}$$

where:

$$\Omega^r = \frac{\eta E^r}{1-\upsilon^{r2}} \quad \Omega^s = \frac{E^s}{1-\upsilon^{s2}} \tag{1-14}$$

with:

υ^r : The Poisson's ratio of the reinforcement;

υ^s : The Poisson's ratio of the soil;

η : The ratio of the reinforcement volume defined as the ratio between the reinforcement volume V^r and the soil volume V^s, and expresses as:

$$\eta = \frac{V^r}{V^s} \tag{1-15}$$

$\mathrm{E^r}$, $\mathrm{E^s}$: The tangent modulus of reinforcement element and soil, respectively.

The Poisson's ratio of the transverse strain, due to the horizontal stress on the reinforced soil, known as the Anti-plan Poisson's ratio is given by:

$$\upsilon_{hz}^c = \frac{\upsilon^r\Omega^r+\upsilon^s\Omega^s}{(\Omega^r+\Omega^s)} \tag{1-16}$$

The Poisson's ratio in plane directions, namely the Poisson's ratio of the vertical strain, due to the horizontal stress on the reinforced soil, is given by:

$$\upsilon_{hv}^{c} = \frac{(1-\upsilon^{r})\Omega^{r}+(1-\upsilon^{s})\Omega^{s}}{(1+\eta)(\Omega^{r}+\Omega^{s})}\,(\Psi^{r}+\Psi^{s}) \tag{1-17}$$

where:

$$\begin{cases}\Psi^{r} = \dfrac{\eta\upsilon^{r}}{1-\upsilon^{r}} \\ \Psi^{s} = \dfrac{\eta\upsilon^{s}}{1-\upsilon^{s}}\end{cases} \tag{1-18}$$

The elastic modulus in the vertical direction and the shear modulus are given, respectively, by:

$$\frac{1}{E_{v}^{c}} = \frac{1}{1+\eta}\left\{\left(\frac{\eta^{2}}{\Omega^{r}}+\frac{1}{\Omega^{s}}\right)+\left[\frac{-1}{\Omega^{r}+\Omega^{s}}+\frac{2}{(1+V^{r})\Omega^{r}+(1+V^{s})\Omega^{s}}\right](\Psi^{r}+\Psi^{s})^{2}\right\} \tag{1-19}$$

$$\frac{1}{G_{hv}^{c}} = \frac{1}{1+\eta}\left(\frac{\eta^{2}}{\Omega^{r}}+\frac{1}{\Omega^{s}}\right)+\frac{\left(1+\upsilon_{hv}^{c}\right)^{2}}{E_{h}^{c}} \tag{1-20}$$

Chen et al. (2000) have conducted two numerical examples for the analysis of reinforced soil walls to study the validity and the applicability of the proposed method. The results obtained are compared with experimental work conducted by other researchers (experimental study at the University of Colorado by Wu (1991) of a reinforced soil wall, 3.05 m height 2,08 m wide, and reinforced with 12 layers of non-woven geotextile, and a large-scale wall test conducted by Sampaco (1996). The comparison of the results obtained with the available experimental data shows a reasonable agreement.

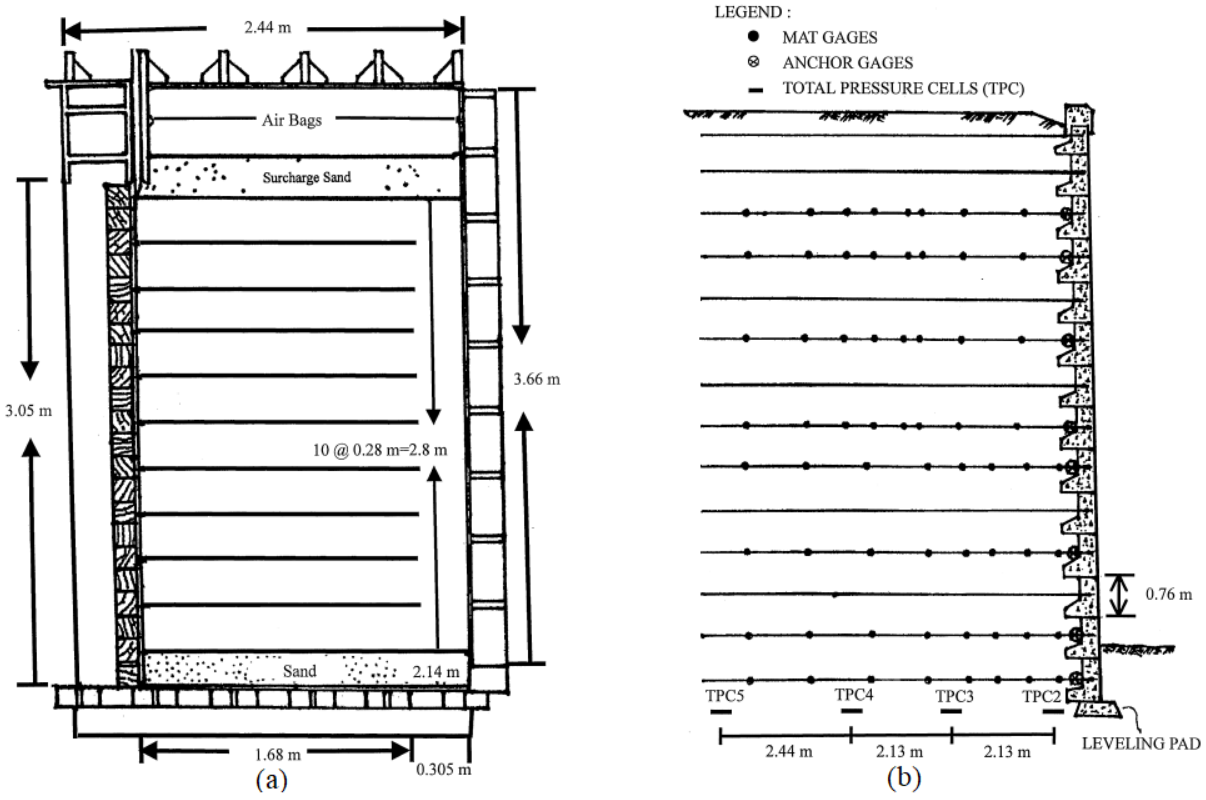

Figure 1-18 (a) University of Colorado wall (Wu, 1991); (b) Large-scale wall test conducted by Sampaco (1996)

Maji et al. (2016) have analyzed the reinforced soil using the equivalent approach by conducting a set of experimental and numerical studies. To study the behavior of the reinforced soil, triaxial tests are carried out in a way to clarify the global behavior of the reinforced soil. Numerical simulations of these triaxial tests are performed with the numerical code FLAC and a reinforced soil model based on the equivalent approach is developed. The parameters of this model are deduced from the triaxial tests. This model uses an elastic-perfectly plastic model and a non-linear hyperbolic model with verification of the results by comparing them to the triaxial tests. The model is also compared with the discrete model where the reinforcements are modeled explicitly. This model can capture the resistance and the behavior of the reinforced soil, and the mechanism of failure. The hyperbolic model is found to be effective in simulating the non-linear stress-strain response of the reinforced soil up to the peak. The model is then applied to two reinforced soil retaining walls from the literature. The effectiveness and the capability of the numerical analysis of the equivalent approach is verified by comparison with the experimental data and with the discrete model where the reinforcements are modeled explicitly.

1.4.3 Numerical approaches

The use of numerical methods, the elasto-plastic finite element analysis and the limit analysis finite element method are the most comprehensive approach to investigate the performance of reinforced soil walls under seismic loading. The use of the numerical limit analysis remains limited in engineering practice. Many studies are conducted in the literature to assess numerically the performance of reinforced soil retaining walls under static and dynamic loading.

Yu et al. (2017) reported the results of numerical modelling of two 3.6 m-high well-instrumented wrapped-face walls using the finite difference program FLAC2D 7.0 (Itasca, 2011). The only difference between the two-instrumented walls were the reinforcement type used. The first was constructed using welded wire mesh reinforcement while the second was constructed using biaxial polypropylene geogrids. A linear elastic-plastic Mohr-Coulomb (MC) and nonlinear elastic-plastic model with MC failure criterion were used to model the backfill soil behavior, while the welded wire mesh and the geogrids reinforcements were modeled using a hyperbolic axial load-strain-time model. Cable elements were used to simulate the reinforcements. The interaction between the soil and the reinforcement were considered through the grout of the FLAC cable element. The two different soil constitutive models used in the numerical simulations give similar results of the wall construction. The comparison between the maximum reinforcement loads obtained from numerical simulations, experimental measurement showed a good agreement for the case of welded wire mesh wrapped-face wall and a poor agreement for the case of polypropylene geogrids wrapped-face wall where the numerical results in terms of reinforcement strains and loads were greater than the measured values.

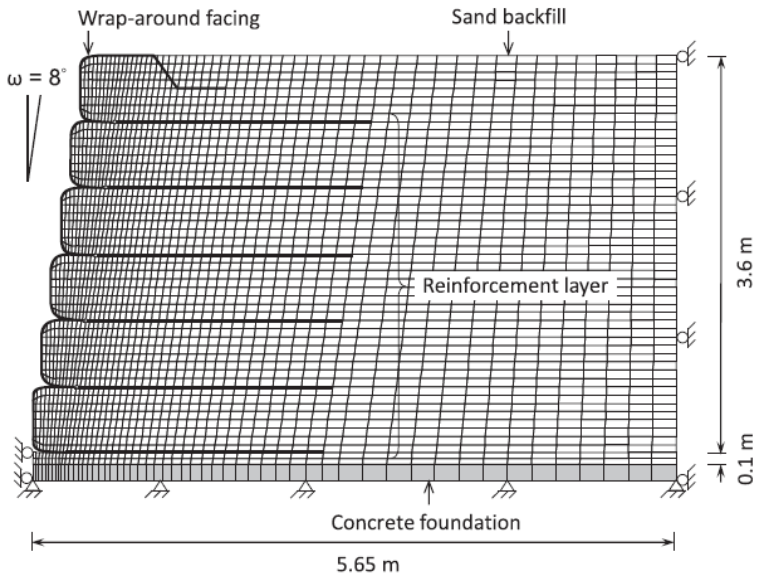

Figure 1-19 Numerical model at the end of construction (Yu et al., 2017)

Gu et al. (2017) developed two numerical models to simulate the behavior of two instrumented reinforced soil retaining walls constructed in Izmir, Turkey. The finite difference program FLAC2D 5.0 (Itasca, 2005) was employed in the simulations. These two walls were constructed with gabion facing and hybrid reinforcement layers. Geogrids were used as primary reinforcements and wire mesh as secondary reinforcements. The only difference between the two walls was the vertical spacing between the primary reinforcements. It was $1m$ in one of them and $2m$ in the second. The comparison between the measured results and the numerical results of construction of the wall showed a good agreement in terms of facing and horizontal fill displacements and tensile forces in the hybrid reinforcements verifying therefore, the developed numerical models. Increasing the vertical spacing induced only an increase in the horizontal forces carried with the primary reinforcements. In addition, the numerical results and the theoretical results were compared in terms of earth pressure distributions and maximum tensile strain line. Good agreements were found between the horizontal earth pressures against the wall facing and the active earth pressures and between the predicted reinforcement maximum tensile line and the Rankine's failure line.

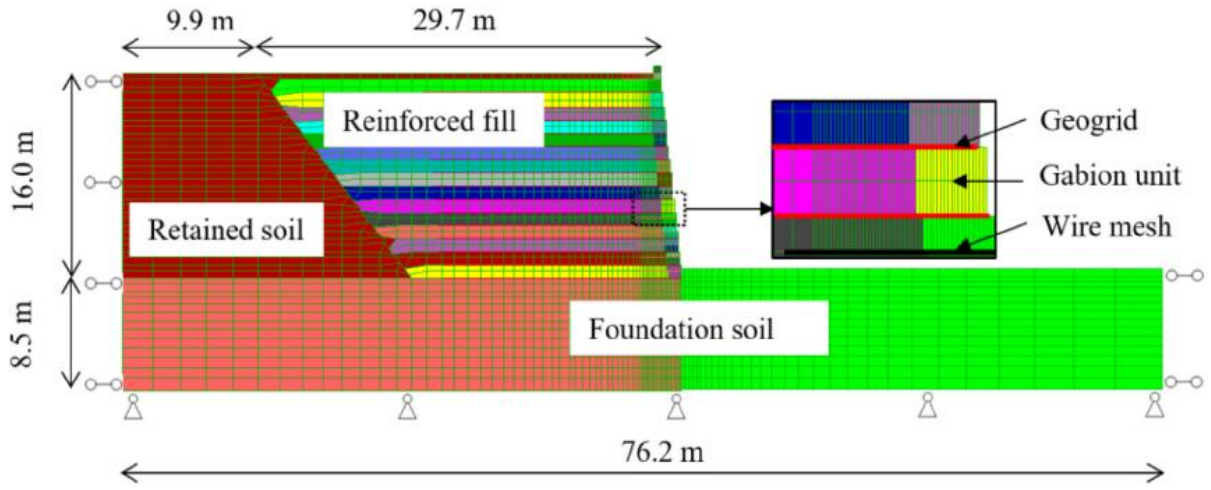

Figure 1-20 Numerical model of the reinforced soil wall with 1m reinforcement spacing (Gu et al., 2017)

The upper-mentioned studies considered static loading. However, many researchers investigated the dynamic response of the reinforced soil walls. Ling et al. (2010) analyze the dynamic behavior of four full-scale geosynthetic reinforced soil walls using an improved version the finite element software Diana-Swandyne-II. A unified generalized plasticity sand model was used to model the backfill soil. The interest readers should refer to Ling et al. (2010) to obtain the details of the model and its parameters. The reinforcements (geogrids) were modeled using three-node one-dimensional bar elements. The thin-layer interface element having elastic perfectly plastic behavior was used to simulate the soil/reinforcement interaction. Figure 1-21 presents the finite element mesh of the walls. The reinforcements length, the reinforcement vertical spacing and the applied accelerations vary from wall to the other. The numerical results are compared with experimental ones obtained with shake table tests and showed a satisfactory agreement, in terms of time accelerations response, as well as wall deformations and reinforcements tensile force.

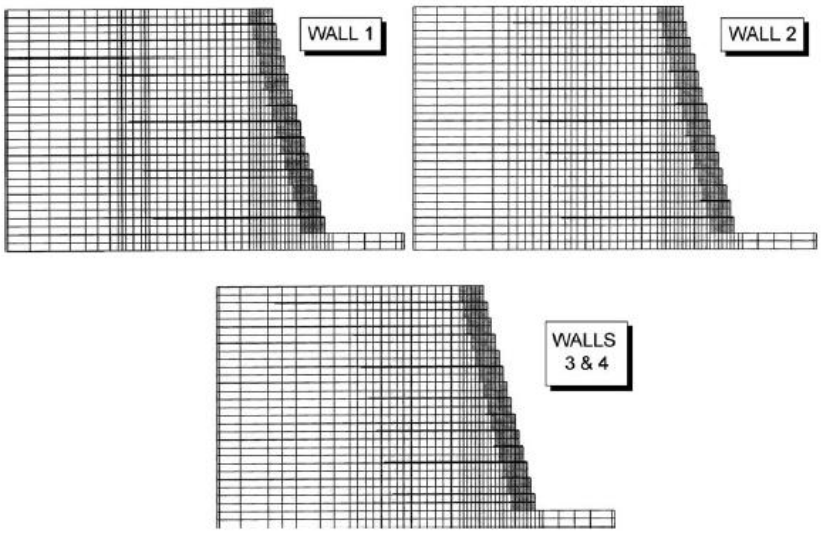

Figure 1-21 Finite elements mesh of the walls

Akhlaghi and Nikkar (2014) investigate the influence of mechanical and geometrical properties of the wall and amplitude and frequency of the source vibration on the dynamic behavior of a geosynthetic-reinforced soil retaining wall using the finite difference program FLAC2D. An elastic perfectly plastic Mohr-Coulomb (MC) was used to model the backfill soil behavior, the reinforcements were modeled using an elastic perfectly plastic cable elements, and the soil/reinforcement interaction were considered through the grout of the FLAC cable element. A parametric study was conducted, and the results show that the type of facing affects the general form of deformation. Also, increasing the reinforcement length and stiffness decreases the wall displacement. Any increase in the acceleration amplitude increase the wall displacement and reinforcement loads. The difference between the frequency of the base excitation and the natural frequency of the model is the most important factor determining the wall dynamic response.

However, the use of numerical techniques under dynamic loading usually induces computational costs. In addition, it requires an accurate knowledge of the soil properties, the reinforcements' properties and the soil/reinforcements interface parameters.

1.5 Probabilistic analysis of Reinforced Soil Retaining Walls

The stability analysis and design of reinforced soil retaining walls and other geotechnical problems (slope stability, tunnel face stability, foundations bearing capacity, foundation settlements, etc.) is conducted generally using deterministic approaches. In these approaches, the model input parameters and the system responses are considered deterministic. Various deterministic computational models to assess the reinforced soil retaining walls stability have been developed by means of the numerical approaches, experimental tests and analytical methods. However, it has been well recognized that all the input data are associated with some degree of uncertainty in the stability analysis of the geotechnical structures (Youssef Abdel Massih and Soubra, 2008; Low and Phoon, 2015; Ferreira et al., 2016; Javankhoshdel and Bathurst, 2017; Pan et al., 2017; Pan and Dias, 2017a; Al-Bittar et al., 2017-2018). Traditionally, the experience-calibrated factor of safety is usually used in reinforced earth retaining wall design within an allowable stress design (ASD) framework to compensate for uncertainties in input parameters, as well as the inadequacies in the calculation models (Sayed et al., 2008; Low and Phoon, 2015; Ferreira et al., 2016; Zevgolis and Bourdeau, 2017). However, this global factor of safety cannot reflect the uncertainty in its real meaning and provides rational results in terms of reliability level: two design solutions can have the same factor of safety although it cannot be expected to have the same failure probability in probabilistic framework (Chalermyanont and Benson, 2004)2005; Griffiths and Fenton, 2004; Cho, 2010; Javankhoshdel and Bathurst, 2014; Luo et al., 2016; Bathurst, 2019). In addition, the deterministic approaches suffer from limitations regarding the difficulties in linking the global factor of safety to the considered system level of reliability (Ferreira et al., 2016). Therefore, it can result in an overdesign or instability when uncertainties are respectively smaller or greater than

anticipated (Chalermyanont and Benson, 2004-2005). Nowadays, the load and resistance factor design approach (LRFD) is used in the limit state design approach in most current standard codes (Eurocode 7, 2004; FHWA, 2011; AASHTO, 2017…). These methods and design codes incorporate the uncertainty concepts through the characteristic values and partial factors. A relation exists between these latter and reliability index. The most important advantage of these semi-probabilistic approaches is the possibility to consider all the parameters uncertainties by calibrating the relevant partial factors and other reliability elements. However, a rigorous calibration has not yet been realized for internal limit states design of reinforced earth wall structures. In addition, the LRFD approach permits to the engineer to choose the load and resistance models to use in a limit state design equation. Consequently, two models with the same load and resistance factors cannot be expected to have the same margins of safety in probabilistic terms (Bathurst, 2019; Bathurst et al., 2019b).

An alternative strategy for the design and analysis of reinforced soil retaining walls, are true reliability or probabilistic methods. These methods have gained increased attention recently, as they are able to consider the uncertainties of input parameters in a more rational way using random variables and random fields approaches and thereafter, the system reliability can be computed in a logical manner (Low and Phoon, 2015; Phoon, 2017; Bathurst et al., 2019b). In addition, they ensure a direct link between the input parameters uncertainty and the reliability index (probability of failure) (Phoon et al., 2003; Sayed et al., 2008). Many attempts have been made to perform reliability analysis of reinforced soil structures (Chalermyanont and Benson, 2004-2005; Sayed et al., 2008; Basha and Sivakumar Babu, 2009-2010-2011-2012; Sivakumar Babu and Singh, 2011; Bathurst and Miyata, 2015; Luo et al., 2016; Ferreira et al., 2016; Zevgolis and Bourdeau, 2017; Javankhoshdel and Bathurst, 2017; Yu and Bathurst, 2017; Bathurst et al., 2019b).

1.5.1 Sources of uncertainties

In the stability analysis of geotechnical structures, all the input data are associated with some degree of uncertainty as indicated previously. The sources of geotechnical uncertainties include the inherent uncertainty related to the geological nature of in-situ soil, lack of data availability, measurement and testing errors, and uncertainties when transforming the experimental measurements into design properties through empirical or correlation models (Phoon and Kulhawy, 1999; Phoon, 2004; Ferreira et al., 2016; Wang et al., 2016). These uncertainties are generally categorized as either aleatory or epistemic (Der Kiureghian and Ditlevsen, 2009). The first category refers to the uncertainties that cannot be reduced as the properties state of knowledge improves (Wang and Cao, 2013; Wang and Aladejare, 2015; Wang et al., 2016). The inherent variability of the soil material known also as soil natural variability is considered as aleatory uncertainty. In addition, in the case of seismic analysis, the earthquake exhibits time variability that results from the fact that the values of the acceleration at the different time steps are random. On the other hand, the second category refers to the uncertainties that

can be reduced gradually as knowledge improves. The lack of data availability, the measurement and testing errors are characterized as epistemic uncertainties. They can be reduced by considering more samples and gathering more data. The transformation uncertainties can be reduced by refining the transformation mathematical or empirical models. In the case of reinforced soil retaining walls the inherent variability in the strength of the material are also involved (Basha and Sivakumar Babu, 2010; Bathurst and Miyata, 2015). When analyzing the seismic internal stability of geosynthetic reinforced soil structures, the uncertainties on the tensile strength of the geosynthetic reinforcements, the interface friction angle between the soil and the reinforcement and the dynamic properties of the seismic loading are also involved.

1.5.2 Reliability analysis: Basic concept and methods

Reliability methods are used to quantify the confidence of a model outcome arising from the uncertainties of the input parameters (Sayed et al., 2008; Mollon et al., 2009a). The reliability of a structure is defined generally by two different measures: the reliability index β and the probability of failure P_f. The reliability index is a safety measure that considers the inherent uncertainties of the input parameters. The probability of failure is defined as the probability that a system will fail during the design working life, for which it has been designed. A limit state is defined in this context and it divides the system state into two domains with the one beyond the limit state being the failure region. This domain classification can be made by the definition of a performance function g that assumes positive values in the safe region (g>0) and negative values in the failure region (g<0). In other words, the limit state surface is defined by g= 0, and it represents the boundary between safe domain where the system operates safely (g>0) and failure domain (g<0). Modeling the uncertain parameters by random variables or random fields and using an appropriate stability model for the calculation, the failure probability is then calculated as the probability of the performance function being negative (i.e. $P_f = P(g < 0)$). Given the input random vector X and its corresponding joint probability density function f_X, the failure probability can be expressed as:

$$P_f = \int_{g(X)\leq 0} f_X(X)dX \tag{1-21}$$

A geotechnical structure will have usually many performance criteria for both the ultimate limit state and serviceability limit state, and a probability of failure is assigned for each of these criteria. Furthermore, these two measures of structure reliability can be related by $P_f = \Phi(-\beta)$, where Φ is the cumulative distribution function of the standard normal distribution. In geotechnical problems, the limit state function is generally implicit and therefore, it is impossible to determine the failure region in order to calculate directly the failure probability. Various strategies can be implemented for calculating the reliability index β or the probability of failure such as classical first-order and second-order reliability

methods (FORM/SORM), the Monte Carlo Simulation (MCS), Importance Sampling (IS), Subset Simulation (SS). They can be divided into three categories: approximation, simulation and meta-modelling-based methods.

1.5.2.1 Approximation methods

Approximation methods, such as the First-Order Reliability Method (FORM) and the Second-Order Reliability Method (SORM), are based on approximating the limit-state function locally at a reference point (design point) by using respectively the first-order or the second-order terms of a Taylor series expansion (Baecher and Christian, 2005). This class of methods can be very efficient with a limited required model evaluation number to estimate the failure probability P_f. However, these approaches, based on linear or quadratic assumptions of limit state, may cause significant errors in case of complex, non-linear limit-state functions.

1.5.2.1.1 First-order reliability method

The first order reliability method (FORM) is widely used to calculate the Hasofer-Lind reliability index in geotechnical engineering. It aims to approximate the probability of failure through consecutives steps. First, an isoprobabilistic transform of the original correlated random variables that define the performance function, is realized into uncorrelated standardized normal variables. The most design failure point in the standard normal space is determined being the point on the limit state surface $g = 0$, closest to the origin of the reduced space. The probability of failure is then approximated as follows:

$$P_f = \Phi(-\beta) \tag{1-22}$$

Where the limit state surface is approximated by a hyperplane tangent to the limit surface at the design point.

1.5.2.1.2 Second-order reliability method

Another approximated method is the second-order reliability method (SORM). The curvature of the nonlinear limit state function is ignored in the FORM approach while the SORM approximates the limit state surface by a second-order Taylor expansion, which is considered as a second-order refinement of the FORM solution. This method is less used comparing to FORM due to its computational complexity even if it could improve the accuracy (Lu and Low, 2011).

1.5.2.2 Simulation methods

In order to overcome the shortcomings of approximation methods, the simulation methods have been developed. These methods consist in generating many random samples of the random variables according to their probability density functions PDF and evaluate the model responses of all these samples. Then, the failure probability and all the probabilistic information are determined using the corresponding model responses of the samples. A large realization number is required so that the solution converges. In the following, the most used simulations methods in geotechnical structures reliability analysis are presented.

1.5.2.2.1 Crude Monte Carlo Simulation

The most straightforward and robust method of computing the probability of failure is the Monte Carlo Simulation (MCS), by sampling the probabilistic input model and by respecting the probability density of each variable. Its application is done through several steps:

- Generation of uniform random numbers and transformation of these numbers to the appropriate distribution of each input parameters.
- Use the deterministic stability model to calculate the performance function.
- Repeat this process for a large number of times. This latter depends on the desired accuracy of the output and the convergence of the method.

An unbiased estimate of failure probability is the fraction of samples that belong to the failure domain N_{fails} over the total number of samples N_{total} as follows:

$$P_f = P_f(g < 0) = \frac{N_{fails}}{N_{total}} \tag{1-23}$$

The coefficient of variation COV of the estimator is an important measure of its convergence. It is defined as:

$$COV(P_f) = \sqrt{\frac{(1-P_f)}{N_{tot} \cdot P_f}} \tag{1-24}$$

The MCS method is simple and robust and is independent of the random variables number. However, it suffers from the low efficiency of the failure probability computation of computationally-expensive deterministic models or from the relatively slow converge rate when considering small failure probability encountered in the practice (Soubra et al., 2019).

1.5.2.2.2 Importance Sampling

As noted previously, the convergence of the MCS method may require a large computation time. Importance sampling (IS) is a more efficient approach than MCS since it reduces the number of sample points and therefore, contributes to a fattest convergence with less computation time (Youssef Abdel Massih et al., 2008). Importance sampling (IS) is an extension of the FORM and MCS methods that combines the fast convergence of FORM with the robustness of MCS. The idea underlying IS is that some values taken by a random variable in a simulation have more effect on the desired estimator than other ones. It is clear intuitively that we must get some samples from the interesting or important region. We do this by sampling from a distribution that over-weights the important region, hence the name importance sampling. The initial sampling density is shifted to the design point in order to concentrate the samples in the failure zone. Consequently, the variance of the estimator is reduced.

The estimator of the failure probability is given by (Melchers, 1999):

$$P_f = \frac{1}{N}\sum_{i=1}^{N} I\left(x^{(k)}\right)\frac{f\left(x^{(k)}\right)}{h\left(x^{(k)}\right)} \tag{1-25}$$

where $h(x)$ is the new sampling density centered at the design point, $\mathcal{X} = \{x^{(k)};\ k = 1, \dots, N\}$ is a given sample values vector with probability density function h, and I is an indicator function of the failure domain, defined as:

$$I(x) = \begin{cases} 1 & if\ g(x) \le 0 \\ 0 & if\ g(x) \ge 0 \end{cases} \tag{1-26}$$

The improved coefficient of variation COV of the estimator is given by (Melchers, 1999):

$$COV\left(P_f\right) = \frac{1}{P_f}\sqrt{\frac{1}{N}\left[\frac{1}{N}\sum_{i=1}^{N}\left(I(v_i)\frac{f(v_i)}{h(v_i)}\right)^2 - \left(P_f\right)^2\right]} \tag{1-27}$$

1.5.2.2.3 Subset Simulation

Subset Simulation is an efficient method to perform the reliability analysis in a progressive manner. It was introduced by Au and Beck (2001) to overcome the main limitation of MCS method which requires a large number of evaluations to converge, especially for small values of failure probability. The idea of this method is to convert the initial reliability problem specified by a small failure probability, into a series of simpler reliability problems specified by larger conditional probabilities that are easier to solve through introducing intermediate failure events (Song et al., 2009).

Given a reliability problem, the performance function g(x) divides the domain into safe region S (g(x)>0) and failure region F (g(x)<0). A sequence of intermediate failures regions $F_i =$

$\{x : g(x) \leq a_i\}$ $(i = 1,2, \dots, n)$ is built with a sequence of decreasing failure thresholds a_i $(a_1 > a_2 > \cdots > a_n = 0)$. The failures regions satisfy therefore, the following relations:

$$F_n = F < F_{n-1} < \cdots < F_2 < F_1 \tag{1-28}$$

$$F_i = \bigcap_{j=1}^{i} F_j \tag{1-29}$$

Consequently, the small failure probability can be expressed as a product of larger conditional failure probabilities by applying the probability theory of conditional probability as follows:

$$P_f = P\left(\bigcap_{j=1}^{n} P(F_j)\right) = P(F_1).\prod_{j=2}^{n} P\left(F_j \middle| F_{j-1}\right) \tag{1-30}$$

The convergence of the reliability problem is much faster than the direct search of single failure probability, since the convergence of each intermediate estimation is much faster.

1.5.2.3 Metamodeling methods

The metamodeling methods are becoming increasingly common in reliability analysis. They have been developed from many different disciplines including statistics, computer science, and engineering and they are found to be an efficient tool to perform reliability analysis of various geotechnical problems. The metamodeling technique aims to reduce the large computation time required by the simulation methods to converge by replacing the expensive deterministic model by a meta-model (also known as surrogate model). This meta-model is obtained with the minimum call number to the original model that gives a target accuracy in catching the original model response behavior. Then, instead of the expensive simulation process, the obtained simple analytical equation is used to calculate the system response. The probability distribution function PDF, statistical moments and failure probability can be easily obtained since the simulation methods are no longer applied on the original expensive deterministic model. Several metamodeling techniques were developed to construct the metamodel in geotechnical engineering problems, such as the Response Surface Methodology (RSM) (Youssef Abdel Massih and Soubra, 2008; Lu and Low, 2011; Li et al., 2015; Hamrouni et al., 2017a-2017b), Kriging models (Echard et al., 2011-2013; Al-Bittar et al., 2018; Soubra et al., 2019; Abdul-Kader et al., 2019), Support Vector Machines (SVM) (Zhao, 2008; Pan and Dias, 2017a) and polynomial chaos expansions (PCE) (Blatman and Sudret, 2008-2010a-2010b-2011; Mao et al., 2012; Al-Bittar and Soubra, 2013-2014a-2014b; Pan and Dias, 2017b-2017c; Pan et al., 2017; Guo et al., 2018-2019a-2019b).

Various investigations have proved the highly efficiency of these techniques in terms of computational time and prediction accuracy. Youssef Abdel Massih and Soubra (2008) used the Response Surface Methodology to perform a reliability-based analysis of strip footings that considers both ultimate and serviceability limit states. Two deterministic models based on numerical simulations using the finite difference code FLAC are considered to determine the ultimate bearing capacity and the vertical

displacement of strip footings. The complex numerical models were approximated by simple second-order polynomials. Soubra et al. (2019) perform a reliability analysis on strip footings using Kriging Metamodeling combined with the Importance sampling. A spatially varying soil is considered and the soil strength properties are modeled by random fields and the deterministic model is based on numerical simulations using the finite difference code FLAC. Pan and Dias (2017a) presented an efficient method combining the Adaptive Support Vector Machine and Monte Carlo Simulations (ASVM-MCS) for reliability analysis. The meta-model is constructed using ASVM with the minimum number of model evaluations. Then, the MCS simulations are performed on the constructed surrogate model, which is very fast. Consequently, limited training samples number minimizes the computation time of the probabilistic analysis. The developed reliability method was validated on four representative examples among which the assessment of a tunnel face stability exists, that represents a practical geotechnical problem. The method has shown a great efficiency for reliability computation to treat high-dimensional problems. Guo et al. (2018) investigated the reliability analysis of an embankment dam sliding stability. The Sparse Polynomial Chaos Expansions (SPCE) is the reliability method used to perform the probabilistic analysis. The soil properties are modeled using the random variables approach and the parameters characterization are determined from in-situ measurements and laboratory tests. Two deterministic models, numerical and analytical, are considered and compared in a probabilistic framework. The PCE methodology is the metamodeling technique employed in this work due to its ability to provide rigorous approximation of highly nonlinear response surfaces with reasonable computation time and it is detailed in the following subsection.

1.5.2.3.1 Polynomial Chaos Expansion

The PCE method is an efficient approach to replace a complex deterministic method with a meta-model. Then, the simple analytical equation is combined with one reliability method (usually MCS) to perform a probabilistic analysis with a significantly reduced computation time compared to the direct MCS. This section describes briefly the PCE methodology:

For a deterministic model *R* with L input parameters modeled by random variables, the model response *Y* can be expressed by a PCE of order p (fixed by the user) as:

$$Y = R(\xi) \cong R_{PCE}(\xi) = \sum_{\beta=0}^{P-1} a_\beta \Psi_\beta(\xi) \tag{1-31}$$

Where ξ is an input vector of L independent random variables, $\Psi_\beta(\xi)$ are the multivariate polynomials, P is the term number retained in the truncation scheme, and a_β the PCE unknown coefficients. The multivariate polynomial $\Psi_\beta(\xi)$ is equal to the tensor product of univariate polynomials of the different random variables:

$$\Psi_\beta(\xi) = \prod_{i=1}^{L} H_{\alpha_i}(\xi_i) \tag{1-32}$$

where $H_{\alpha_i}(\xi_i)$ is a univariate polynomial, α_i denotes the univariate polynomial degree and i indexes the ith variable ξ_i.

The multivariate polynomials are orthogonal with respect to the joint probability densities of the input random vector. Several univariate polynomials types exist, and each type corresponds to a unique type of probability distribution. The univariate Hermite polynomials are orthogonal with respect to the normal distribution. Laguerre and Legendre polynomials correspond to Gamma and Uniform random variables respectively. Other input variables distributions types and their corresponding univariate polynomials can be found in Xiu and Em Karniadakis (2003). The Hermite polynomials are the most common used for the polynomial chaos expansion methodology in geotechnical engineering.

The model response *Y* expressed by Eq. (1-31) is exact when an infinite series is considered. However, for a practical application, the PCE is truncated to a finite number of terms P. According to the common truncation scheme, only the multivariate polynomials of total degree less than the specified PCE order p are retained. It leads to the truncate set $A = \{\alpha \epsilon \mathbb{N}^L : \|\alpha\|_1 = \sum_{i=1}^{L} \alpha_i \leq p\}$. The corresponding terms number retained in the truncation scheme P is equal to:

$$P = \frac{(L+p)!}{L!p!} \tag{1-33}$$

As may be seen from Eq. (1-33), the terms number P of the unknown PCE coefficients increases dramatically with the random variables number L and the PCE order. Consequently, the common truncation scheme is not practically applicable for high-dimensional problems. For this purpose, Blatman and Sudret (2011) developed the hyperbolic truncation strategy in which the multidimensional polynomials Ψ_β with high-order interaction are excluded. This truncation scheme defines a so-called q-quasi-norm that should be smaller than the PCE order p as follows (Blatman and Sudret, 2011):

$$\|\alpha\|_q = \left(\sum_{i=1}^{L} (\alpha_i)^q\right)^{1/q} \leq p \quad (0 < q < 1) \tag{1-34}$$

The smaller the value of q, the less the PCE terms. Blatman and Sudret (2011) have shown that in order to prevent the risk of rejecting some significant terms, a value of $q \geq 0.5$ must be considered. In addition, for a good balance between the sparsity and accuracy, a value of q between 0.7 and 0.9 is recommended (Blatman and Sudret, 2011; Al-Bittar and Soubra, 2013).

1.5.2.3.2 Calculation of coefficients by the regression approach

Once the truncation scheme is applied, the unknown coefficients a_β are determined using the regression method. A set of N realizations called Experimental Design (ED): $\mathcal{X} = \{x^{(1)}, \ldots, x^{(N)}\}$ is selected

randomly by using a sampling scheme (e.g. MC simulations, Latin Hypercube sampling or Sobol set). In this PhD work, the Latin Hypercube sampling will be used. For each sample in the ED, the corresponding response is calculated using the deterministic model. Based on the least-square minimization method, the computation of the PCE unknown coefficients a_β is performed by solving a linear system of equations obtained (Blatman and Sudret, 2011):

$$\hat{k} = (\Phi^T \Phi)^{-1} \Phi^T \hat{Y} \tag{1-35}$$

Where $\hat{k}$ represents the column vector of the PCE unknown coefficients, $\hat{Y}$ is the model response of the of the N realizations of the ED, Φ is a space-independent matrix of dimension $N \times P$, defined by:

$$\Phi_{ij} = \Psi_{\alpha_j}\left(x^{(i)}\right), \; i = 1, \dots, N, \; j = 0, \dots, P-1 \tag{1-36}$$

The size N of the ED must be selected to ensure a well-posed regression problem (Blatman and Sudret, 2011; Al-Bittar and Soubra, 2013).

1.5.2.3.3 Error estimates

The accuracy of the metamodel of the PCE depends on its order p. The greater the PCE order, the more accurate the metamodel, i.e. a better fit exists between the meta-model and the computational deterministic model. In order to achieve a prescribed accuracy in a reasonable computation time, one should increase the PCE order successively until obtaining the target accuracy with the minimum possible PCE order.

In least-squares analysis, the generalization error of a PCE is defined as:

$$err = E[(R(\xi) - R_{PCE}(\xi))^2] \tag{1-37}$$

However, the computation of the generalization error is not possible since it requires the knowledge of the model response. Consequently, in order to measure the meta-model accuracy, two estimate measure of the generalization error are used in this dissertation: the empirical mean-square residual error and the leave-one-out error and their coefficients of determination R^2 and Q^2 (Blatman and Sudret, 2010a). These two estimators do not require more additional model evaluation than the N ED realizations.

1.5.2.3.3.1 Empirical error

The empirical error err_E is a generalization error estimator of the fit quality calculated using the experimental design $\mathcal{X}$ and the corresponding model responses $\hat{Y}$. It is given by:

$$err_E = \frac{1}{N}\sum_{i=1}^{N}\left(R\left(x^{(i)}\right) - R_{PCE}\left(x^{(i)}\right)\right)^2 = \frac{1}{N}\sum_{i=1}^{N}\left(\hat{y}_i - \sum_{\alpha \in A} k_\alpha \Psi_\alpha\left(x^{(i)}\right)\right)^2 \tag{1-38}$$

The well-known related coefficient of determination R^2 is expressed as:

$$R^2 = 1 - \frac{err_E}{Var(Y)} \tag{1-39}$$

where $Var(Y)$ represents the empirical variance of the model responses $\hat{Y}$,

$$Var(Y) = \frac{1}{N-1}\sum_{i=1}^{N}(\hat{y}_i - \bar{Y})^2 \tag{1-40}$$

$$\bar{Y} = \frac{1}{N}\sum_{i=1}^{N}\hat{y}_i \tag{1-41}$$

An empirical error $err_E = 0$ or the coefficient of determination $R^2 = 1$ corresponds to a perfect fit between the meta-model and the true model response. However, although being the simplest error estimator, R^2 is a poor estimator of the PCE accuracy when there is overfitting. It is highly biased since it does not consider the meta-model capability in predicting the model response outside the ED and therefore it underestimates the generalization error.

1.5.2.3.3.2 Leave-one-out cross-validation

To overcome the limitation of the empirical error estimator in over-fitting the meta-model, a more reliable estimator of the generalization error could be used, the leave-one-out error err_{LOO} which is a special case of the cross-validation techniques (Blatman and Sudret, 2010a). Molinaro et al. (2005) compared the cross-validation-based error estimates and showed that leave-one-out error is the most rigorous in terms of estimation bias and mean-square error.

The leave-one-out cross-validation consists in building N meta-models $R_{PCE\setminus i}$, where $R_{PCE\setminus i}$ is the one built from the reduced ED $\mathcal{X}\setminus x^{(i)} = \{x^{(j)}, j = 1, \dots, N, j \neq i\}$ obtained by removing sequentially a point from the ED. Each meta-model performance is assessed by comparing its prediction and to the model evaluation on the excluded point $x^{(i)}$ (G. Blatman and Sudret, 2010a-2011).

The leave-one-out cross-validation error can be obtained as:

$$err_{LOO} = \frac{1}{N}\sum_{i=1}^{N}\left(R\left(x^{(i)}\right) - R_{PCE\setminus i}\left(x^{(i)}\right)\right)^2 \tag{1-42}$$

In practice, it is possible to calculate the leave-one-out cross-validation error analytically without the need to build the N meta-models from the N reduced ED. The expression of err_{LOO} could be determined as follows:

$$err_{LOO} = \frac{1}{N}\sum_{i=1}^{N}\left(\frac{R\left(x^{(i)}\right) - R_{PCE}\left(x^{(i)}\right)}{1-h_i}\right)^2 \tag{1-43}$$

Where h_i is the is the ith diagonal term of matrix $\Phi(\Phi^T\Phi)^{-1}\Phi^T$.

The corresponding coefficient of determination of the leave-one-out error estimate Q^2 is then expressed as:

$$Q^2 = 1 - \frac{err_{LOO}}{Var(Y)} \tag{1-44}$$

1.5.2.3.4 Sparse Polynomial Chaos Expansions (SPCE)

The Sparse Polynomial Chaos Expansions (SPCE) is an extension of the PCE. Blatman and Sudret (2011) suggested an iterative procedure known as the stepwise regression technique for building up a SPCE for the purpose of retaining fewer terms of the involved multivariate polynomials. In fact, although the high-order interaction terms are rejected through the hyperbolic truncation scheme, the retained terms may have different contribution to the model response. The stepwise regression technique is then used to identify significant terms of the PCE. The iterative algorithm to build the SPCE is described as follows:

- Select an initial experimental design randomly and compute the model response for each sample using the deterministic model,
- Select the five specified parameters for the algorithm: the target accuracy Q^2_{tgt}, the maximal SPCE order p_{max}, the so-called q-quasi-norm for the hyperbolic truncation scheme, the cutoff values ε_1 and ε_2,
- For each PCE order increasing from 1 to p_{max}, the algorithm consists of two steps as follows:
  - The forward step aimed to retain the significant candidate terms which lead to a significant increase in the coefficient of determination R^2, i.e. greater than ε_1 fixed by the user.,
  - The subsequent backward step, the algorithm consists to reject the insignificant candidate terms from the PCE basis retained at the end of the first step which lead to an insignificant decrease of R^2, i.e. less than ε_2 fixed by the user,
  - After each iteration, the SPCE accuracy Q^2 is calculated. If the target accuracy Q^2_{tgt} is reached, the iterative procedure is stopped. Otherwise, the PCE order is increased.

1.5.2.3.5 Global Sensitivity Analysis (GSA)

The Global Sensitivity Analysis (GSA) allows quantifying the effects of each random variable or their possible combinations on the model response (Sudret, 2008). GSA is useful to identify unimportant input variables, help reduce the dimension of the problem and therefore reduces the number of model evaluations as much as possible. In this dissertation, two sensitivity indices are used: The Sobol and the Kucherenko indices.

1.5.2.3.5.1 Sobol sensitivity indices

The Sobol index is the most widely and commonly used to perform the GSA. Once the SPCE coefficients are determined. The first order Sobol index is widely used to perform the GSA. It can be calculated by:

$$S(\xi_i) = \frac{Var\left[E(\Gamma_{\xi_i})\right]}{Var(\Gamma)} \tag{1-45}$$

Where Var denotes variance, Γ is the model response given by the SPCE and $E(\Gamma_{\xi_i})$ is the expectation of Γ conditional on a fixed value ξ_i. Once the SPCE coefficients are determined, the first order Sobol index can be easily computed using these coefficients (Sudret, 2008; Blatman and Sudret, 2010b):

$$S(\xi_i) = \frac{\sum_{\alpha \epsilon A_i} (a_\beta)^2 E\left[(\Psi_\beta)^2\right]}{\sum_{\alpha \epsilon A} (a_\beta)^2 E\left[(\Psi_\beta)^2\right]} \tag{1-46}$$

Where a_β are the SPCE coefficients, Ψ_β are the multivariate polynomials, A is the obtained truncation set, A_i is a subset of A in which the multivariate polynomials Ψ_β are only functions of the random variable ξ_i, $E[.]$ is the expectation operator defined as (Sudret, 2008):

$$E\left[(\Psi_\beta)^2\right] = \prod_{i=1}^{L} \alpha_i! \tag{1-47}$$

In addition, the high-order and total Sobol indices are easy to compute analytically using the PCE coefficients with almost no additional cost (Sudret, 2008). Higher order Sobol indices evaluate the effect of the interactions of multiple input variables. The total Sobol index of a variable ξ_i quantifies its effect alone and the effect of all its interactions with other variables and are obtained by summation of all the Sobol indices involving this variable.

1.5.2.3.5.2 Kucherenko sensitivity indices

The Sobol sensitivity indices are only applicable in the case of independent input variables. Many sensitivity methods were proposed to overcome this limitation. Kucherenko et al. (2012) generalized the Sobol indices to the case of dependent input variables. They proposed to define the Kucherenko sensitivity indices using a direct decomposition of the output variance with the law of total variance. In this dissertation, in the presence of correlation between input variables, Kucherenko indices are used to perform sensitivity analysis.

1.6 Conclusion

This chapter mainly included a literature review on the reinforced soil walls stability and on their analysis. The technology and the historical development of these structures were firstly described, in addition to the elements used in their construction and their different applications. It showed the

worldwide heavy use of these structures and therefore, the importance of clarifying their response and performance especially in seismic regions. This represents the main objective of this dissertation with a focus on the structures reinforced by geosynthetics. The stability and design of these structures were then highlighted. Four stability modes should be checked including the internal, external, compound and global stability. Among the various deterministic investigation approaches used in the literature, the efficiency of the limit analysis method is demonstrated. It will be used to investigate the seismic internal stability of geosynthetic reinforced soil retaining walls. In the final part of this chapter, a literature review on the reliability analysis of reinforced soil retaining walls was presented. The sources of uncertainty in geotechnical engineering were discussed. Then, the commonly used reliability analysis methods were reviewed. Probabilistic methods are divided into three different categories:

- Approximation methods that include FORM and SORM,
- Simulation methods that include Monte Carlo simulations, Subset simulations and Importance sampling,
- Metamodeling techniques among which the sparse polynomial chaos expansion is described in detail. This latter is adopted, in the present study, in the framework of the probabilistic analysis of reinforced soil retaining walls.

2 Chapter 2: Deterministic model for the internal seismic stability of Reinforced Soil Walls

2.1 Introduction

This chapter focuses on the seismic internal stability of reinforced soil retaining walls based on the limit analysis kinematical approach. The discretization technique developed by Mollon et al. (2011) to analyze the face stability of a pressurized tunnel under active and passive cases, is extended to the case of reinforced soil retaining walls. It permits to generate the potential failure surface of reinforced structures point by point. This technique allows the consideration of heterogeneous backfill soils in the analysis. This was not possible when using traditional limit analysis. In addition, it allows to use the pseudo-dynamic approach instead of the pseudo-static approach to represent the seismic loading. First, the methods used are described including the upper bound theorem of limit analysis and the discretization technique. The validation of the discretization technique is presented using results from literature. The results for the case of dry soils are presented. The results include homogeneous and heterogeneous soil cases. In addition, the influence of cracks on the seismic internal stability of reinforced soil retaining walls is investigated. Knowing that most of the failure cases encountered in the literature were caused by the water presence, the case of saturated soils including the pore water effect within the backfill soil is analyzed. This chapter ends up with the case of unsaturated soils since most soils are unsaturated in nature and the matric suction plays an important role in the wall's stability. The groundwater level can be located at any reinforced backfill depth. Several nonlinear equations relating the unsaturated soil shear strength to the matric suction and different backfill type of soils are considered.

2.2 Discretization-based kinematic analysis under seismic loading

The plastic limit theorems of Drucker and Prager (1952) may conveniently be employed to obtain lower and upper bounds of the collapse load for a wide variety of stability problems in geotechnical engineering, such as the critical heights of unsupported vertical cuts, the earth pressure of a retaining wall, the foundation capacity or the face pressure of a tunnel. The limit analysis method consists of two approaches, the kinematic and the static approaches also referred as upper bound and lower bound theorems respectively. These two theorems give upper and lower bounds on the collapse load enabling therefore, the required collapse load to be bracketed as closely as seems necessary for the problem under consideration.

The static theorem of limit analysis is based on the static equilibrium of an observed system. The application of this approach requires the construction of statically admissible stress field for the problem

under consideration, in which the equilibrium equations, the stress boundary conditions are satisfied and nowhere violates the yield criterion. The lower-bound can be stated as follows:

If a statically admissible stress distribution can be found, uncontained plastic flow will not occur at a lower load. From these rules, the lower-bound technique considers only equilibrium and yield. It does not consider to soil kinematics.

On the other hand, the kinematic theorem of limit analysis requires the construction of a kinematically admissible velocity field in which, the velocity boundary conditions, and the strain and velocity compatibility conditions are satisfied. The kinematic theorem of limit analysis is based on the work rate balance between the external forces and the internal energy dissipation for any kinematically admissible velocity field. The upper-bound theorem can be stated as follows:

If a kinematically admissible velocity field can be found, uncontained plastic flow must impend or have occur previously. The upper-bound technique considers only velocity or failure modes and energy dissipations. The stress distribution doesn't need to be in equilibrium and is only defined in the deforming regions of the mode.

The kinematical approach is the commonly used limit analysis approach in most previous stability analysis since it is difficult to construct a statically admissible stress field in the framework of the limit analysis static approach. In this thesis, the kinematical approach of limit analysis is applied to assess the seismic internal stability of geosynthetic reinforced soil retaining walls. This approach provides upper bound estimate to an active limit load that causes structure failure or a lower bound estimate to a reaction that offers resistance against structure failure. In our case, this theorem gives a rigorous lower bound to the reinforcement strength required to ensure the internal stability of reinforced soil retaining walls. For any assumed kinematically admissible failure mechanism, the reinforced wall fails if the external work rate exceeds the internal energy dissipation rate.
The upper-bound theorem states that the rate of work by external forces is less than or equal the energy dissipation rate for any kinematic admissible failure mechanism. This can be expressed by the equation of virtual work (Chen, 1975):

$$\int_S T_i \dot{u}_i^* dS + \int_V F_i \dot{u}_i^* dV \leq \int_V \sigma_{ij} \dot{\varepsilon}_{ij}^* dV \qquad (2\text{-}1)$$

Where $\dot{\varepsilon}_{ij}^*$ and $\dot{u}_i^*$ are, respectively, the strain rate and the velocity vector in the kinematically admissible velocity field; σ_{ij} is the stress tensor associated with $\dot{\varepsilon}_{ij}^*$; F_i and T_i refer respectively, to the external body forces distributed over the volume V and the external surface forces on the boundary S.

2.2.1 Basic assumptions

The stress-strain behavior of most real soils is characterized by an initial linear portion and a peak or failure stress followed by softening to a residual stress. In limit analysis, it is necessary to ignore the strain softening feature of the stress-strain diagram and to consider the stress-strain relationship of a soil in an idealized manner. This idealization, termed normality (or the flow rule), establishes the limit theorems on which limit analysis is based. Therefore, the application of the upper bound theorem of limit analysis requires an ideally rigid, perfectly plastic behavior of the soil mass according to an associated normality rule based on the Coulomb yield criterion.

In this chapter, the upper bound theorem is adopted to find a lower bound to the reinforcement forces required to prevent failure of the reinforced soil structures. A rigid block assumption is considered. The analysis concerns structure where the geosynthetic reinforcement layers are horizontal, finite in number uniformly distributed, and having a uniform length. The reinforcement provides forces acting in the horizontal direction that are given by the tensile strength or pull-out resistance. Resistance to shear, bending and compression of the geosynthetic reinforcement are negligible. Liquefaction potential are not considered. Examples of the application of limit analysis in reinforced soil can be found in many published papers (Michalowski, 1997-1998a-1998b; Ausilio et al., 2000; He et al., 2012, …).

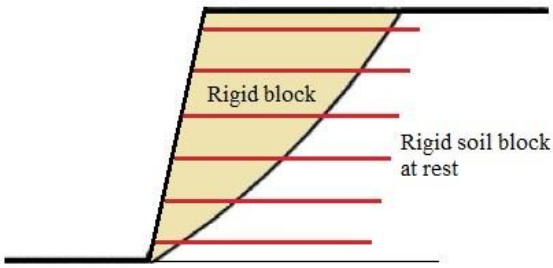

Figure 2-1 Schematic of the uniform spacing of the wall reinforcement

The failure of reinforced soil structures involves a three-dimensional phenomenon of sliding material (Figure 2-2). Gao et al. (2016) performed a three-dimensional stability analysis of reinforced slopes using the kinematic approach of limit analysis. They found that the conventional 2D plane-strain solutions will underestimate the stability of 3D reinforced slopes and that the differences between two-dimensional and three-dimensional solutions increase when the reinforced soil structure becomes narrower. These results are compatible with those obtained by Zhang et al. (2014) using the limit equilibrium, who proved that the most critical mechanisms are always achieved by two-dimensional analysis. In this work, the reinforced soil retaining wall is considered wide enough so that the differences between the two-dimensional solutions and the three dimensional ones are negligible and therefore, the three-dimensional phenomenon of sliding material is simplified to a prismatic volume obtained by extruding the two-dimensional area of the sliding mass along the out-of-plane direction (Utili, 2013). All the calculations and the reinforcement strength are expressed per unit width. However, performing

a two-dimensional analysis should not affect the fact that all the mechanisms considered are three-dimensional.

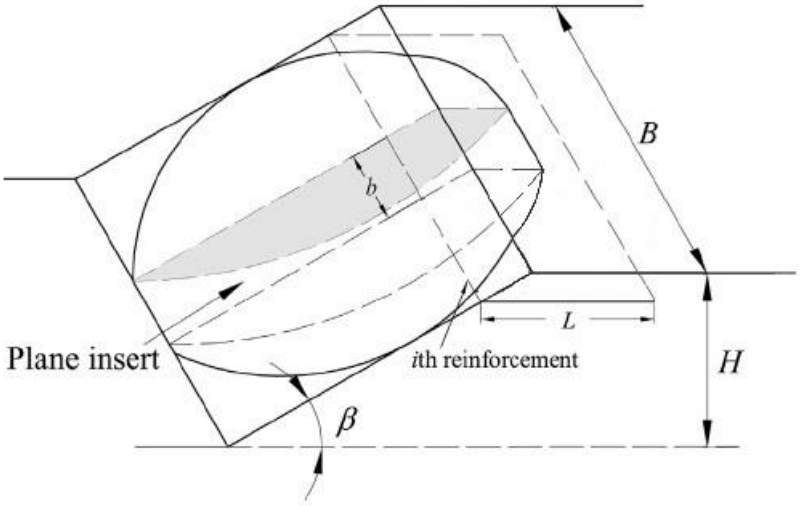

Figure 2-2 Three-dimensional rotational failure surface of reinforced slope (Gao et al., 2016)

A rotational log-spiral failure surface is assumed (Figure 1-16), since it was found that it is the most critical failure mechanism for reinforced soil retaining walls and coincident with the physical failure on-site (Michalowski, 1997; Sabermahani et al., 2009; Abd and Utili, 2017a; Alhajj Chehade et al., 2019a-2020). This type of failure mechanism can be divided into two types: toe log-spiral mechanism and below toe log-spiral mechanism. According to Chen et al. (1969), failures below the toe can occur only when the internal friction angle φ is less than 5^o for intact slopes. Therefore, it can be concluded that for reinforced soil structures with soil properties of engineering interest, the failures never occur below the toe.

2.2.2 Discretization technique

The traditional kinematic approach can be applied to the stability analysis of reinforced homogeneous soil retaining wall (Michalowski, 1997-1998a; Ausilio et al., 2000). However, the spatial discretization technique coupled with limit analysis was proposed by Mollon et al. (2011) to analyze the face stability of a pressurized tunnel under active and passive cases. It permits to overcome the main limitation of the traditional kinematic approach that can be only applied to the stability analysis of a homogeneous soil. This technique has further inspired many investigations on the topic of non-homogeneous or layered soil since slopes exhibit spatial variability in their soil properties (Ibrahim et al., 2015; Pan and Dias, 2017d; Qin and Chian, 2017-2018; Sun et al., 2018). Using this technique, the upper bound theorem of limit analysis can be applied to analyze the seismic stability of reinforced soil retaining walls considering the spatial variation of the soil friction angle and cohesion. In addition, the discretization method gives

the possibility to represent the earthquake loading with the pseudo-dynamic loading instead of the pseudo-static approach, since the former is more realistic.

2.2.2.1 Mechanical principles

The discretization technique is used to generate a rotational failure surface. The proposed discretization mechanism of the reinforced soil retaining wall is illustrated in Figure 2-3. The region of soil ABC, separated from the soil at rest by the sliding surface BC, is assumed to rotate rigidly around the center O with an angular velocity Ω. The process of discretization aims at defining a set of points located on the discontinuity surface using the previous known point on the contour of the surface. As mentioned before, toe log-spiral failure is considered and therefore, the slip surface is assumed to start at the wall toe (point B), as shown in Figure 2-3. In order to determine the next point in the velocity discontinuous lines, the kinematical admissibility condition must be satisfied. It requires that the failure surface meet the velocity vector with an angle equal to the soil internal friction one (Figures 1-16, 2-3).

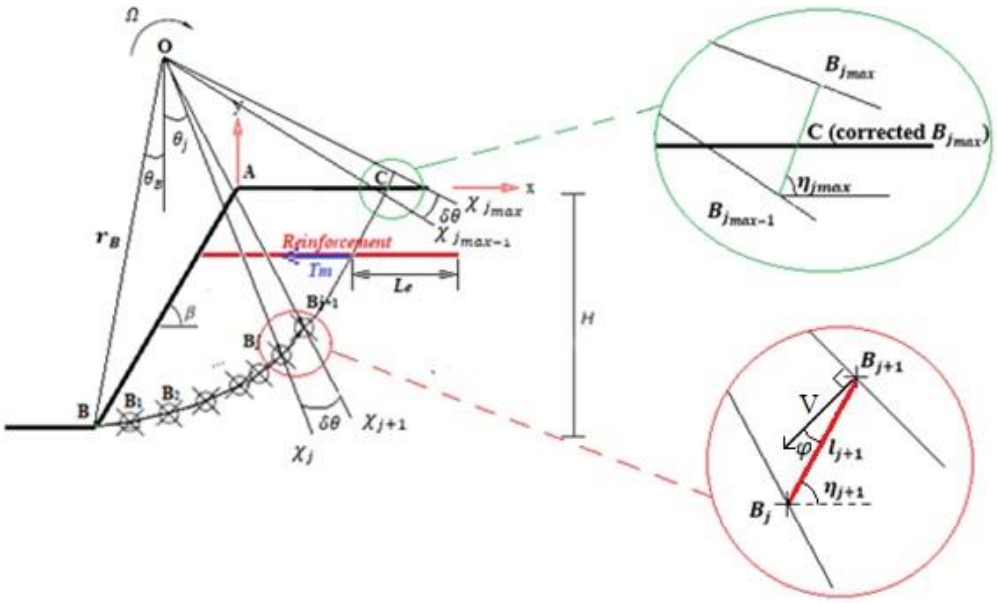

Figure 2-3 Discretization technique for the rotational failure surface of a reinforced soil retaining wall

2.2.2.2 Principle of generation of a new point.

A coordinate system is established with the point A at the top of the wall being the origin. The point O is defined by the two surface parameters r_B and θ_B, where r_B is the length of OB and θ_B is the angle between the y axis direction and the line OB. The moving block is discretized by several radial lines that all intersect at point O. In other words, all these lines are normal to the velocity field and the main idea is to generate the points of the failure surface in each of these radial lines.

A radial line is denoted χ_j with j varying from 0 to j_{max}, and therefore the number of radial lines is $j_{max}+1$. The first line denoted χ_0 correspond to (OB) and the last radial line denoted $\chi_{j_{max}}$ corresponds to (OC) where C is the intersection between the failure surface and the ground surface. Each line χ_j is defined by rotation of the former line χ_{j-1} by a constant angle $\delta\theta$: the discretization angle. The density of the points along the potential slip surface is defined by this angle. The smaller this angle, the larger the number of points generated, and the failure surface thus represents a closer match to the classical log-spiral failure mechanism. The point B_j corresponds to the point of the radial line χ_j at the failure surface. A radial line χ_j makes an angle θ_j with the vertical direction which is one of the polar coordinates of the point B_j with respect to O, and is given by:

$$\theta_j = \theta_B + j * \delta\theta \tag{2-2}$$

The basic idea for the generation procedure consists in computing the coordinates of each point B_{j+1} of line χ_{j+1}, using the coordinates of the point B_j in the previous line χ_j .

The generation of new points begins with the use of the point B. This point belongs to the line χ_0 and is defined by the parameters of the mechanism r_B and θ_B. From this point, a new point B_1 can be generated in the plane χ_1. More generally, it is possible to generate point B_{j+1} in any line χ_{j+1}, knowing the point B_j of the line χ_j using these two conditions:

1. The segment $[B_jB_{j+1}]$ should respect the normality condition, which requires that the normal vector to this segment pointing outside the mechanism should make an angle $\frac{\pi}{2}+\varphi$ with the velocity vector. This normality condition is necessary for the mechanism to be kinematically admissible and therefore, the kinematic theorem of the limit analysis could be applied.
2. The new point B_{j+1} belongs to the line χ_{j+1}.

Once the point B_j has been generated in χ_j, a new point B_{j+1} could be created in χ_{j+1}. The points are successively generated, until reaching the ground surface by the failure surface.

2.2.2.3 Mathematical formulation for the generation of a new point from the previous one.

Based on the established coordinate system, the coordinates of rotation center O (x_o, y_o) and wall toe B (x_B, y_B) are easily identified as follows:

$$\begin{cases} x_O = \frac{-H}{\tan\beta} - r_B \sin\ \theta_B \\ y_O = r_B \cos\theta_B - H \end{cases} \tag{2-3}$$

$$\begin{cases} x_B = \frac{-H}{\tan\beta} \\ y_B = -H \end{cases} \tag{2-4}$$

As mentioned before, the normality condition states that the line of each segment containing two consecutive points B_j and B_{j+1} should respect the normality condition. This mean that every line (OB_{j+1}) should make an angle $\frac{\pi}{2}+\varphi$ with (B_jB_{j+1}). From this condition and the geometrical and trigonometric relations, it is possible to calculate the length L_{j+1} of the segment $[OB_{j+1}]$, the length l_{j+1} of the segment $[B_jB_{j+1}]$ and the angle η_{j+1} that forms $[B_jB_{j+1}]$ with the horizontal line as follows:

$$L_{j+1} = \frac{L_j.cos(\varphi+\delta\theta)}{cos\,\varphi} \tag{2-5}$$

$$l_{j+1} = \frac{L_j.\sin(\delta\theta)}{\cos\varphi} \tag{2-6}$$

$$\eta_{j+1} = \theta_B + \varphi + (j+1).\delta\theta \tag{2-7}$$

Noting that for the line χ_0, L_0 is equal to r_B.

And then, the coordinates of the new point B_{j+1} will be easily computed as follows:

$$\begin{cases} x_{j+1} = x_j + l_{j+1}.\cos\eta_{j+1} \\ y_{j+1} = y_j + l_{j+1}.\sin\eta_{j+1} \end{cases} \tag{2-8}$$

2.2.2.4 Closure of the surface

The generation of the mechanism is stopped when the generated point B_{j+1} is located above the ground surface. Thus, if the ground surface is horizontal, the generation is stopped when the y-coordinate of the new point of the mechanism is positive. When the ground surface is inclined by an angle α from the horizontal axis, the mechanism is stopped when the angle ζ_{j+1} between the horizontal axis and the line (AB_{j+1}) is greater than α. The angle ζ_{j+1} is easily calculated as follows:

$$\zeta_{j+1} = \tan^{-1}\left(\frac{y_{j+1}}{x_{j+1}}\right) \tag{2-9}$$

After the detection of the first generated point above the ground surface B_{j+1}, this point is replaced by the intersection between segment B_jB_{j+1} and the ground surface using a linear interpolation. Knowing the equation of the ground surface, the coordinates of the point B_j and the angle η_{j+1}, the new coordinates of the point B_{j+1} are calculated as follows:

$$\begin{cases} x_{j+1} = \frac{(y_j - x_j.\tan\eta_{j+1})}{\tan\beta - \tan\eta_{j+1}} \\ y_{j+1} = x_{j+1}.\tan\alpha \end{cases} \tag{2-10}$$

2.2.3 Seismic loading

The most common approach used to represent the ground shaking in previous works (Michalowski, 1998a; He et al., 2012; Alhajj Chehade et al., 2019c) and design codes (Eurocode 8, 2004; FHWA, 2011) is the pseudo-static method. The effect of earthquake is represented by horizontal and vertical pseudo-static forces ($k_h g$ and $k_v g$ respectively). Despite the simplicity of the pseudo-static approach to consider the seismic action, this approach considers the dynamic behavior of seismic loading in an approximate manner without considering the acceleration amplification nor the time and spatial variation of the ground shaking. The pseudo-dynamic method, originally proposed by Steedman and Zeng (1990), considers these effects (Nimbalkar et al., 2006; Choudhury and Nimbalkar, 2006-2007; Basha and Sivakumar Babu, 2010; Qin and Chian, 2017), which is more realistic. The pseudo-dynamic approach has been applied to determine the seismic stability of geosynthetic reinforced homogeneous soil retaining walls with considering the time effects and phase change effects due to body waves propagating trough the reinforced backfill (Nimbalkar et al., 2006; Basha and Sivakumar Babu, 2011). The pseudo-dynamic approach is a more realistic method to represent the seismic action, compared to the pseudo-static one. The latter does not account for the space and time variation of the seismic effect, while the former considers these effects such as the motion amplification, earthquake duration and frequency. The pseudo dynamic method was used for various studies in geotechnical fields using the limit equilibrium method (Choudhury and Nimbalkar, 2007; Basha and Sivakumar Babu, 2009-2011; Choudhury et al., 2014; Zhou et al., 2018). Recently, Qin and Chian (2017), using the limit analysis method combined with the discretization method, conducted a seismic stability analysis of unreinforced slopes using the pseudo-dynamic method. Like all previous cited studies, a sinusoidal acceleration is adopted in this dissertation for simplicity, to consider the seismic loading (Figure 2-4).

The pseudo dynamic analysis considers a finite shear and primary wave velocities within the reinforced backfill. Under earthquake condition, the shear wave velocity $V_s = (G/\rho)^{0.5}$ and the primary wave velocity $V_p = [G.(2-2\upsilon)/\rho.(1-2\upsilon)]^{0.5}$ are assumed to be constant within the reinforced backfill, where G, ρ and υ are respectively the shear modulus, the density and the Poisson's ratio of the backfill material. Using these formulas, the following ratio can be expressed as $V_p/V_s = ((2-2\upsilon)/(1-2\upsilon))^{0.5}$. Knowing that $\upsilon = 0.3$ is commonly used for soils, $V_p/V_s = 1.87$ is considered in this work.

Along the depth of the reinforced backfill, it is assumed that the shear modulus is constant while the magnitude and phase of accelerations in both directions are varying. The acceleration is assumed to vary linearly from the input acceleration at the base to the amplified acceleration at the ground surface by an amplification factor f. This factor depends from many parameters related to the soil and the seismic input motion. However, the calculation of its value is not in the scope of this work. The linear variation of the magnitude of the seismic acceleration with the depth does not mean that the seismic acceleration

at any time t varies linearly with depth due to the phase difference of the waves' propagation. The waves periods in both directions are assumed to be equal to T. A phase difference t_0 is considered between the two input shakings to encompass the wider possible scenario. A value of t_0 equal to 0 gives the critical design criteria.

Assuming that the amplitudes of the horizontal and vertical harmonic vibrations are $k_h g$ and $k_v g$ respectively, where g is the acceleration due to gravity, and k_h and k_v are the horizontal and vertical seismic coefficients respectively, the horizontal and vertical accelerations at any depth y, and time, t, below the ground surface with an amplification factor f, can be expressed as:

$$\begin{cases} a_h = \left[f + \frac{y}{H}(f-1)\right].k_h g \sin\frac{2\pi}{T}\left(t - \frac{H+y}{V_s}\right) \\ a_v = \left[f + \frac{y}{H}(f-1)\right].k_v g \sin\frac{2\pi}{T}\left(t + t_0 - \frac{H+y}{V_p}\right) \end{cases} \quad (2\text{-}11)$$

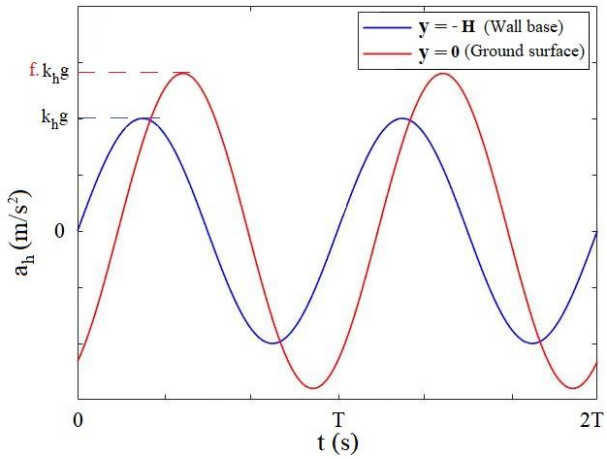

Figure 2-4 Horizontal accelerations at the wall base and ground surface

2.2.4 Work rate calculations

The kinematic approach of limit analysis is applied to determine the reinforcement strength required for the stability of reinforced earth retaining wall. Application of this theorem requires to equate the external work rate $\dot{W}$ to the internal energy dissipation $\dot{D}$ for any assumed kinematically admissible failure surface.

At failure, the applied external forces to the rotational rigid block are:

i. The weight of the soil composing the block.
ii. The inertia forces in the horizontal and vertical directions induced by the earthquake forces.
iii. The possible surcharge loading σ_s acting on the ground surface.
iv. The seepage force under the water table level (not considered in this section).

For each of the external force, the computation of the work of the force is achieved by the summation of the elementary rates of work. To achieve such goal, the computations of elementary surfaces are necessary. The trapezoidal element $B_j'B_{j+1}'\,B_{j+1}B_j$ as shown in Figure 2-5 is selected, where B_j and B_{j+1} belong to the potential failure surface and are two successive points obtained from the discretization technique.

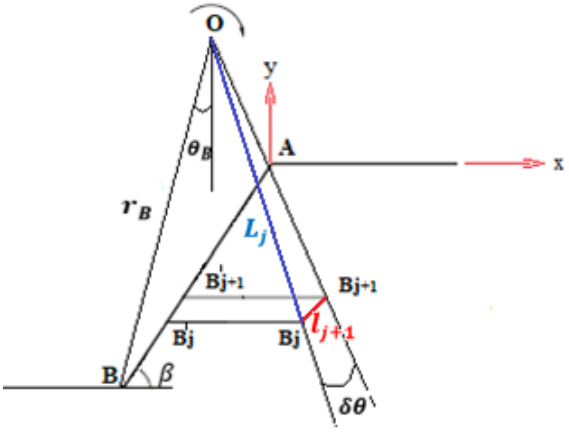

Figure 2-5 Elementary trapezoidal surface $B_j'B_{j+1}'\,B_{j+1}B_j$ for calculation of work rate

The x-coordinate of the point B_j' of the facing located at the same horizontal level of the point B_j is:

$$x_j' = \frac{y_j}{\tan\beta} \tag{2-12}$$

Then, the area of the elementary trapezoidal element $B_j'B_{j+1}'\,B_{j+1}B_j$:

$$A_{j+1} = \frac{1}{2} l_{j+1} \sin\eta_{j+1} \cdot \left[\left(x_{j+1} - x_{j+1}'\right) + \left(x_j - x_j'\right)\right] \tag{2-13}$$

Knowing the coordinates of B_j', B_j, B_{j+1}' and B_{j+1}, the coordinates of the center of gravity G_j for each elementary surface are computed.

In the case of inclined ground surface (Figure 2-6), the procedure is quite similar. For the points B_j generated above the horizontal axis (Ax), the corresponding point B_j' will be at the same horizontal level but belongs to the inclined ground surface, and then the x-coordinate of the point B_j' will be:

$$x_j' = \frac{y_j}{\tan\alpha} \tag{2-14}$$

In addition, when the first point B_{j+1} above the horizontal axis (Ax) is generated, the area of the elementary pentagon $B_j'A\,B_{j+1}'\,B_{j+1}B_j$ needs a special attention. This area will be the sum of the areas of the two elementary trapezoidal surfaces $AB_{j+1}'\,B_{j+1}C'$ and $B_j'AC'B_j$ with C' being the intersection between the horizontal axis and (B_jB_{j+1}).

Noting that in the case of horizontal ground surface, $C' \equiv C$ (see Figure 2-7).

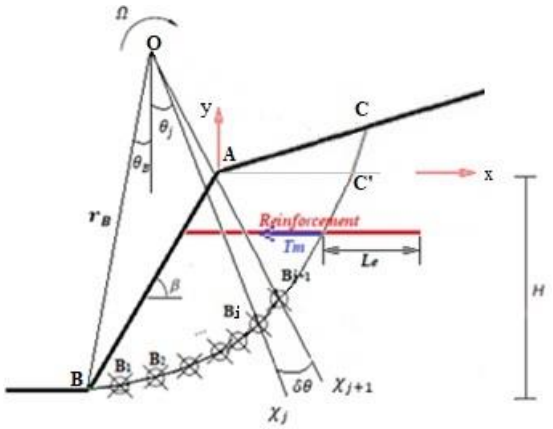

Figure 2-6 Reinforced soil wall with inclined ground surface

On the other hand, since a rigid block is considered, the rate of internal energy dissipation results from the part dissipated along the reinforcements and from the plastic soil deformation that occurs along the discontinuity surface that separates the movable block and the soil at rest.

The rate of external and internal forces can be computed as follows:

2.2.4.1 Rate of work of the soil weight:

The elementary rate of work done by the weight of an elementary trapezoidal surface A_j is equal to the vertical component of the velocity multiplied by the weight of the elementary surface:

$$d\dot{W}_\gamma = (\gamma . A_j).\left(\Omega.\left(x_{Gj} - x_O\right)\right) \tag{2-15}$$

where γ is the soil unit weight, $A_j$is the area of the trapezoidal element given by Eq. 2-13 and Ω is the rotation angular velocity of the block ABC. Then:

$$\dot{W}_\gamma = \sum_j(\gamma . A_j).\left(\Omega.\left(x_{Gj} - x_O\right)\right) \tag{2-16}$$

2.2.4.2 Rate of work of the horizontal and vertical inertia forces respectively:

The work rates of the horizontal and vertical seismic forces are calculated in a similar manner as a summation of the elementary rates of work of the trapezoidal elements. In case of pseudo-static approach, they are expressed as:

$$\dot{W}_{kh} = \sum_j(\gamma . A_j . k_h).\left(\Omega.\left(y_O - y_{Gj}\right)\right) \tag{2-17}$$

$$\dot{W}_{kv} = \sum_j (\gamma . A_j . k_v) . \left(\Omega . \left(x_{Gj} - x_O\right)\right) \quad (2\text{-}18)$$

On the other hand, in case of the pseudo-dynamic approach, they are expressed as:

$$\dot{W_{kh}} = \sum_j \left(\gamma . A_j . \left[f + \frac{y}{H}(f-1)\right] . k_h \sin\frac{2\pi}{T}\left(t - \frac{H+y}{V_s}\right)\right) . \left(\Omega . \left(y_O - y_{Gj}\right)\right) \quad (2\text{-}19)$$

$$\dot{W_{kv}} = \sum_j \left(\gamma . A_j . \left[f + \frac{y}{H}(f-1)\right] . k_v \sin\frac{2\pi}{T}\left(t + t_0 - \frac{H+y}{V_p}\right)\right) . \left(\Omega . \left(x_{Gj} - x_O\right)\right) \quad (2\text{-}20)$$

2.2.4.3 Rate of work of surcharge loading σ_s acting on the ground surface

Provided that a surcharge loading σ_s is positioned at a distance L_0 near the wall top as illustrated in Figure 2-7, only the 'effective' surcharge i.e. the surcharge loading within the region of failure block, between points A and C, has an unfavorable effect on the reinforced soil wall stability. The work rate of this surcharge can be defined as the dot product of uniformly distributed vertical surcharge and the velocity vector and therefore, it yields:

$$\dot{W}_{\sigma_s} = \sigma_s (x_c - L_0) . \Omega . \left(x_c - x_O - \frac{x_c - L_0}{2}\right) \quad (2\text{-}21)$$

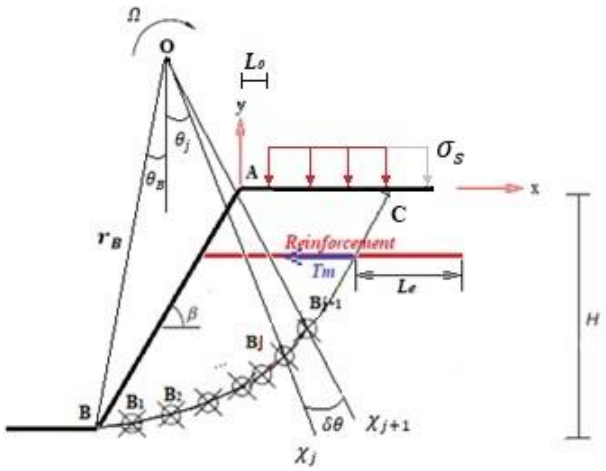

Figure 2-7 A surcharge loading near the wall top

2.2.4.4 Energy dissipation rate during rotational failure along the sliding surface BC:

At rotational failure surface, the rate of internal energy dissipation along an elementary velocity discontinuity surface l_j is $c.\delta v_t$, where δv_t is the tangential component of the deformation velocity with respect to the failure surface and c the soil cohesion.

$$d\dot{D}_c = c.\left(L_j.\Omega.\cos\varphi\right).l_j \quad (2\text{-}22)$$

Calculations of the internal energy dissipation along the sliding surface are made by the summation of the elementary energy dissipations along the different elementary surfaces:

$$\dot{D}_c = \sum_j \left(c. \left(L_j . \Omega . \cos \varphi \right) . l_j \right) \tag{2-23}$$

Therefore, $\dot{D}_c$ is equal to zero when a cohesionless soil is considered. Notice that the soil cohesion is not necessary a constant value. A heterogeneous soil could be considered, and the soil cohesion could be varied along the depth of the soil.

2.2.4.5 Energy dissipation rate in and/or along the reinforcements during rotational failure:

The resisting work rate of the reinforcements should be calculated in order to perform the stability analysis of the reinforced soil wall. As mentioned previously, resistance to shear, bending and compression of the geosynthetic reinforcements are negligible. They provide forces acting in the horizontal direction that are given by the tensile strength or pull-out resistance.

2.2.4.5.1 Rupture failure:

The computation of energy dissipation is presented here by the approach adopted by (Michalowski, 1998a, 1998b, 1997). The energy dissipation rate in a single reinforcement layer passing through a potential failure surface can be derived assuming that the "surface" (zone of velocity discontinuity) is a finite-thickness layer with a high velocity gradient, called the deformation zone (Figure 2-8), the synthetic reinforcement contributes to the stability of the structure only through its tensile strength, and assuming that the velocity of the reinforcement is the same as the one of the soil in the deformation zone.

The resisting work rate for the tensile rupture of a single reinforcing element is equal to the dot product of the force in the reinforcement and the velocity jump vector $\vec{v}$ (Figure 2-8), where $\vec{v}$ is the velocity discontinuity vector along the failure surface.

$$d\dot{D}_T = T_m \vec{n} . \vec{v} \tag{2-24}$$

where T_m is the tensile strength of a single reinforcement layer (per unit width) and $\vec{n}$ is a unit vector in the direction of the reinforcement.

Michalowski (1998a) represents the reinforcement in terms of average strength k_t expressed as:

$$k_t = \frac{n_r T_m}{H} \tag{2-25}$$

where n_r is the number of reinforcement layers and H the reinforced wall height.

For a log-spiral failure surface, the energy dissipation rate per infinitesimal length increment can be expressed as (see Figure 2-9):

$$d\dot{D}_T = k_t.r.\delta\theta.\frac{\cos(\theta-\varphi)}{\cos\varphi}\vec{n}.\vec{v} \tag{2-26}$$

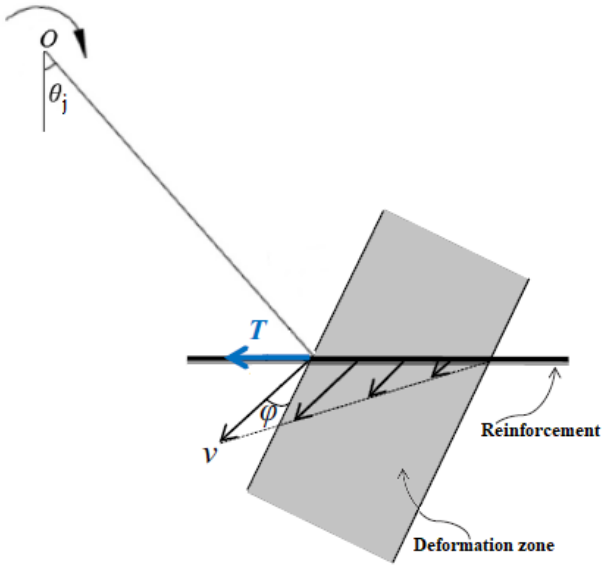

Figure 2-8 The tensile failure modes for geosynthetic

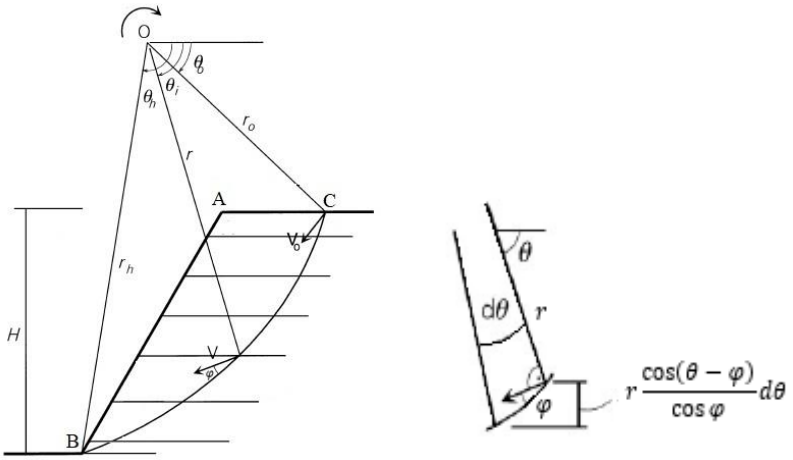

Figure 2-9 Schematic for calculation of the energy dissipation along a log-spiral failure surface (Michalowski, 1998a)

In the discretization technique and for an elementary length, the expression $r.\delta\theta.\frac{\cos(\theta-\varphi)}{\cos\varphi}$ is equivalent to $l_j.\sin\eta_j$, the velocity jump vector $\vec{v}$ is equivalent to $\Omega.L_j$ and the angle between the velocity discontinuity vector $\vec{v}$ and the unit vector in the direction of the reinforcement $\vec{n}$ is equal to $(\theta_B + j.\delta\theta)$.

Then, the energy dissipation rate per elementary length is:

$$d\dot{D}_T = k_t.l_j.\sin\eta_j.\Omega.L_j.\cos(\theta_B + j.\delta\theta) \tag{2-27}$$

Therefore, the energy dissipation rate during rotational failure along the reinforcements according to this approach is:

$$\dot{D_T} = \sum_j \left(k_t . l_j . \sin \eta_j \, . \Omega . L_j . \cos(\theta_B + j . \delta\theta)\right) \quad (2\text{-}28)$$

An identical energy dissipation rate results from an analysis with a discrete distribution (with uniform spacing) of reinforcement.

2.2.4.5.2 Pullout failure

So far, the expression of energy dissipation considers that the failure of reinforcement is a tensile failure. However, some reinforcements may be pulled out from the soil. The pullout force for a single layer of reinforcement is:

$$T_p = 2\gamma z^* L_e f^* \quad (2\text{-}29)$$

where z^* is the overburden depth; L_e is the effective length; f^* corresponds to the apparent friction coefficient at the soil/reinforcement interface. $f^* = F^* . \alpha$ where F^* is the pullout resistance factor and α is the correction factor to account for a nonlinear stress reduction over the embedded length of highly extensible reinforcement.

The energy dissipation along the reinforcements is therefore calculated considering both possibilities of reinforcement failures, rupture failure and pullout failure.

The energy dissipation rate during rotational failure along a single reinforcement being pulled out is:

$$d\dot{D}_p = T_p \Omega Y_i \quad (2\text{-}30)$$

where Y_i is the vertical distance between the reinforcement and the center of rotation O, calculated as:

$$Y_i = Y_O + (i - 0.5) * \frac{H}{n_r} \quad (2\text{-}31)$$

where i denotes the layer number from the top of the backfill.

2.2.5 Optimization process

A program is coded in Matlab for the generation of the rotational failure surface through the discretization technique and the work rates calculations. The inputs are the geometrical parameters (wall inclination and height), the soil properties, the seismic loading parameters, the reinforcement length, the reinforcement spacing and the discretization angle. The reinforcement average strength (defined on Eq. 2-25) and consequently, the reinforcement strength required to stabilize the reinforced soil wall and the corresponding critical failure surface (characterized by the parameters r_B, θ_B) are determined through

an optimization process. The objective function to be optimized is provided by equating the rates of external work and internal energy dissipation $\dot{W} = \dot{D}$. A two-step genetic algorithm, proposed by Guo et al. (2018), is used for the optimization process with regard to the geometrical parameters r_B, θ_B and the parameter t that represents the time involved in the pseudo-dynamic approach if this latter is considered to represent the seismic loading. The details of the proposed two-step are given in Guo et al. (2018).

2.2.6 Validation of the discretization method

To validate the robustness of the discretization technique to generate potential failure surface, combined with the kinematic analysis method applied to the reinforced soil structures, a comparison between the existing results of the conventional limit analysis method obtained by Michalowski (1998a) and the results obtained by the proposed method are presented.

Michalowski (1998a) used the conventional kinematic theorem of limit analysis to determine the strength of reinforcement necessary to maintain the slope stability using the pseudo-static approach. A cohesionless soil was considered and the vertical component of the seismic force was neglected. In addition, he assumes both linear (uniform) and triangular distribution of the reinforcement. The amount of reinforcements is presented in dimensionless form:

$$\frac{k_t}{\gamma H} = \frac{n_r T_m}{\gamma H^2} \tag{2-32}$$

To assess the internal stability of reinforced soil retaining walls using the limit analysis method, Michalowski (1997-1998a) considers only the failure of reinforcement by tension to calculate the reinforcement strength. The length of reinforcement is then determined in such manner that the required strength calculated does not need to be increased because of the possibility of pullout failure in some layers. In other words, the most critical failure mechanism involving the combination of the tensile failure in some layers and pullout in others needs to provide a required reinforcement strength, which is no larger than the value calculated considering only the tension failure of reinforcement. The required length obtained by this approach is unpractical in several cases, i.e. exceeds a reasonable length ($1.5H$, where H is the reinforced structure height). For instance, when the horizontal seismic coefficient k_h is equal to 0.3, the required length of reinforcement L_{req} for a reinforced structure where the backfill is a cohesionless soil φ=30^0, is equal to $1.75H$. The developed method, by fixing the reinforcement length and considering the two failures modes simultaneously, avoids this problem.

In order to validate the application of the discretization combined with the kinematic analysis method for the seismic analysis of reinforced soil structures, the results are obtained for a uniform distribution of the reinforcement force along wall height, since this distribution is used in practice, and under the same conditions used in the work of Michalowski (1998a), i.e. cohesionless soil, pseudo-static approach

without consideration of the vertical seismic force and considering only the tensile-failure of the reinforcement.

The comparisons of results are depicted in charts of Figure 2-10, for different horizontal seismic coefficient k_h, internal friction angle φ and facing inclination β. A total agreement can be observed between the results of Michalowski (1998a) and the present approach regarding the normalized required reinforcement $k_t/\gamma H$.

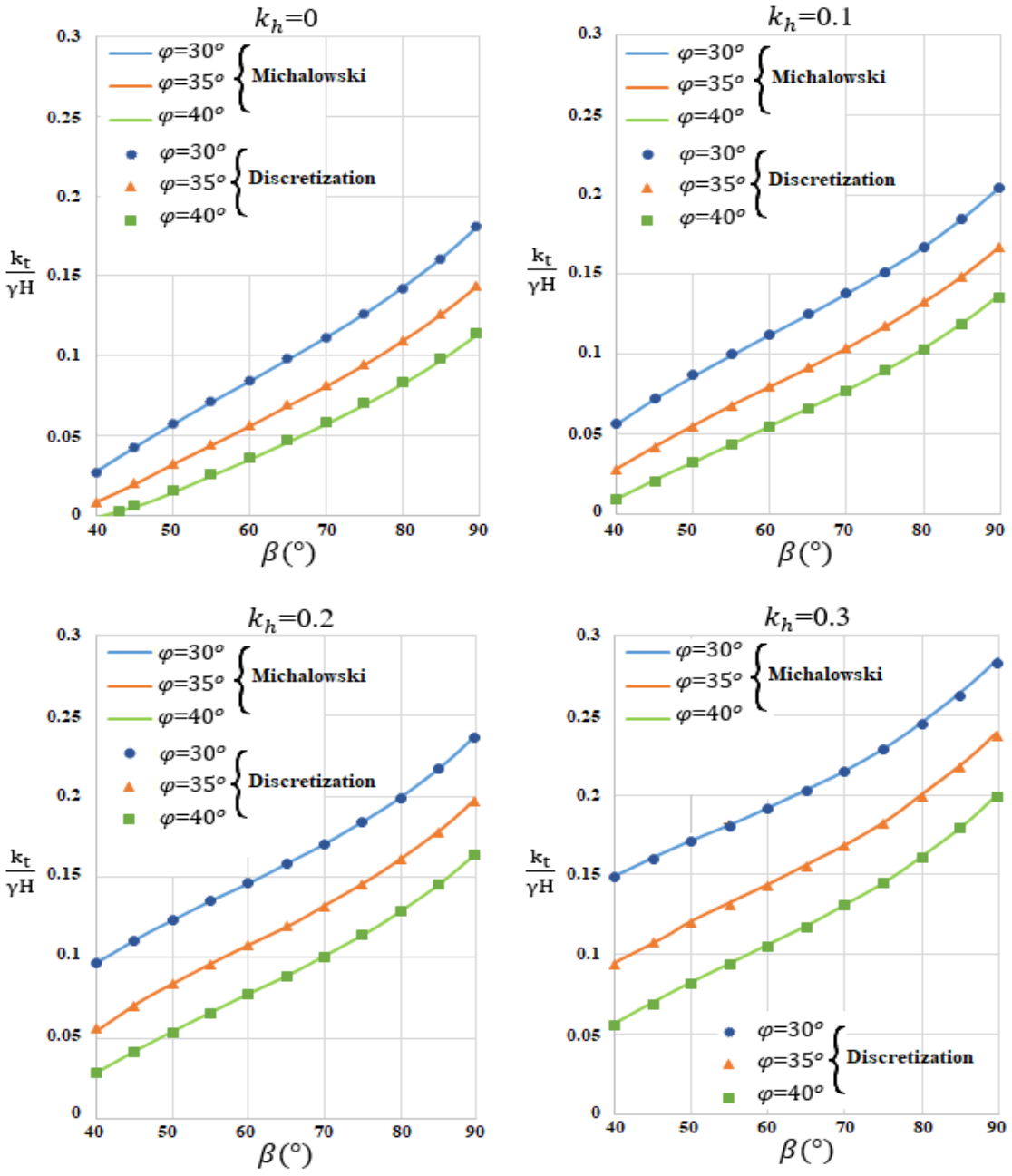

Figure 2-10 Comparison of results of the discretization method and the conventional limit analysis

As mentioned before, the discretization angle, $\delta\theta$, might have an impact on the accuracy of the failure mechanism generated. A decrease in the angle of discretization leads to an increase of the method accuracy. Considering a given slope with given geometry and soil properties: H = 7m, β = 75°, c = 0 kPa, $\varphi = 36^{o}$, $\gamma = 20\text{kN/m}^3$ and a given seismic coefficient $k_h = 0.2$. Four values of the discretization angle $\delta\theta$ are considered: $\delta\theta = 0.01^{o}$, $\delta\theta = 0.1^{o}$, $\delta\theta = 1^{o}$ and $\delta\theta = 5^{o}$. The required reinforcement strength is almost the same in all cases. The corresponding critical slip surface are plotted with different values of the discretization angle $\delta\theta$ as illustrated in Figure 2-11. The results indicate that taking $\delta\theta = 0.1^{o}$ is sufficient to satisfy the accuracy of the problem and therefore, this value is considered in this work.

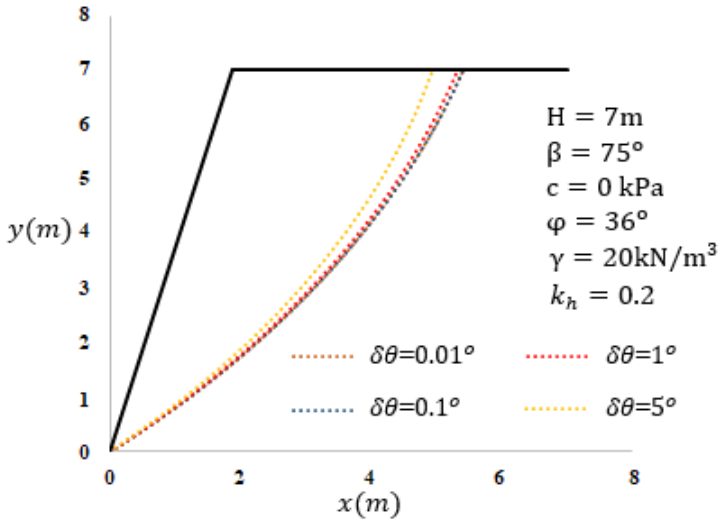

Figure 2-11 Generation of the rotational failure surface for different discretization angles

2.2.7 Crack presence

For conventional design codes (Eurocode 8, FHWA…), the backfill material is recommended to be cohesionless. Nevertheless, in regions where granular material is not locally available or expensive, the use of poorly draining backfill (cohesive soil) can be an attractive solution when geosynthetic reinforcements are used. The advantage of geosynthetic reinforcement is the absence of the corrosion risk, affecting the metallic reinforcement, requiring therefore the use of clean granular material with an appropriate drain system to ensure the durability of the retaining structure (Guler et al., 2007). On the other hand, the use of a poorly draining backfill leads to the loss of shear strength. However, this kind of soil have been successfully used as backfill for reinforced earth retaining wall (Benjamim et al., 2007). Fine grained soils from tropical areas, widely used in Brazil, showed good performances when used as backfill for reinforced soil-wall construction (Riccio et al., 2014). They show high percentage of fines, but high strength, low plasticity and good workability characteristics. In addition, experimental studies have been performed to investigate the behavior of geotextile reinforced cohesive slopes (Noorzad and Mirmoradi, 2010; Wang et al., 2011). As the poorly draining backfill are capable of

developing pore-water pressures, the hydraulic properties of permeable geosynthetics such as non-woven geotextiles and geogrids which are able to provide internal drainage, can help to dissipate these pressures, enhancing therefore, the internal stability of the structure (Portelinha et al., 2013-2014).

In general, cracks are found in cohesive soils, since their tensile strength is very limited (Abd and Utili, 2017a). The development of cracks presents an important factor affecting the stability of reinforced cohesive backfill retaining walls. This phenomenon of cracks development was observed in post-earthquake survey for reinforced cohesive slopes (Ling et al., 2001), as well as in experimental studies (Porbaha and Goodings, 1996).

Even though the issue of cracks in cohesive soils was first addressed by Terzaghi (1943), the analyses of unreinforced and reinforced slopes or walls with cracks are rare. The cracks introduce a discontinuity in both the static and kinematic fields, which means an extensive computational effort for numerical methods (e.g. finite element or finite difference method) to consider discrete discontinuities (Utili and Abd, 2016). Hence, to assess the stability of reinforced cohesive backfill retaining wall considering cracks through a parametric analysis, numerical methods are not suitable. Most of the studies conducted in the literature considering the presence of cracks have been carried out using the limit equilibrium method to assess their influence on the unreinforced slope stability (Baker, 1981; Chowdhury and Zhang, 1991; Kaniraj and Abdullah, 1993; Baker and Leshchinsky, 2001-2003). Most of them considered pre-existing cracks, considering that the crack depth or the crack position is known. However, it is not guaranteed that the analyzed crack is the most critical one (Zhao et al., 2016). More recently, based on the upper bound theorem of limit analysis suggested by Chen et al. (1969), several studies (Michalowski, 2012-2013; Utili, 2013; Utili and Abd, 2016; Zhao et al., 2016) investigated the stability of unreinforced slope taking into account both the effect of depth and location of cracks. While most of these analyses do not include the crack formation as a part of the failure mechanism, Michalowski (2012-2013) implemented the crack opening mechanism, requiring therefore energy during the crack formation process. Recently, Abd and Utili (2017a) first considered existing cracks referred as climate cracks, as well as tension crack formation as a part of the failure mechanism for geosynthetic reinforced slopes. However, a homogeneous reinforced slope is considered under static condition.

As mentioned above, Abd and Utili (2017a) considers, for the first time, the cracks on the design of reinforced slopes under static loading. However, earthquakes are significant for the cracks' formation. The kinematic theorem of limit analysis coupled with the discretization technique is used to generate a rotational failure mechanism for a geosynthetic reinforced heterogeneous backfill retaining wall accounting for the presence of cracks. Similar to Abd and Utili (2017a), this work accounts for the possibility of a single tension crack as a part of the failure mechanism, as well as the possibility of the pre-existing cracks presence generated by climate phenomenon's.

2.2.7.1 *Generation of discretized failure mechanism*

The proposed discretization mechanism of the reinforced earth retaining wall with cracks is presented in Figure 2-12, where block ABCD, composed of two sections, rotates around the center of rotation to be determined O, with an angular velocity Ω. Section 1 of the failure mechanism is delimited by a log-spiral surface BC where the soil fails purely in shear while section 2 is delimited by a vertical crack CD where the soil fails in tension/shear. For simplicity, like in the previous studies about the crack formation in cohesive soil (Michalowski, 2012-2013; Utili, 2013; Utili and Abd, 2016), the cracks are assumed to be vertical, despite that they may exhibit curved shapes (Hu et al., 2010).

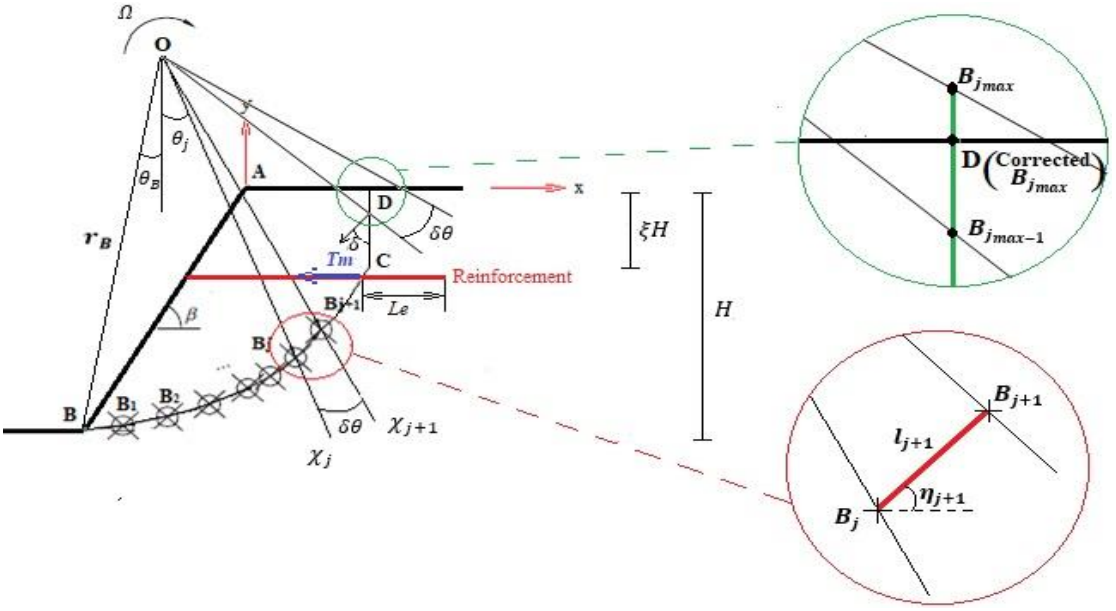

Figure 2-12 Discretization technique for the failure mechanism of a reinforced soil retaining wall with cracks

The failure mechanism is determined by the mechanism parameters r_B, θ_B and ξ, where r_B is the length of OB, θ_B is the angle between the y axis direction and the line OB and ξ is a parameter to define the crack depth (Figure 2-12). The discretized failure mechanism is generated by a series of points B_j as showed in Figure 2-12. Starting at the wall toe B, a new point B_1 on the failure mechanism is generated. The points are successively generated, until reaching the ground surface by the failure mechanism.

The mathematical formulation for the generation of a new point along the log-spiral part BC of the failure mechanism is well described in the section 2.2.2.3 with the difference that the generation process of the log-spiral part of the failure surface terminates when the ordinate, y_{j+1}, of the generated point B_{j+1} is greater than $-\xi H$, noting that the point A is the origin of the coordinate system used (Figure 2-12). The last point of the section 1 of the failure surface, C, is then adopted to ensure that their ordinate is equal to $-\xi H$.

For the crack CD as depicted in Figure 2-13, the abscissa of all the points in section 2 is constant and equal to x_C since a vertical crack is assumed. Knowing that the angle between two consecutives radial lines is $\delta\theta$, the vertical distance l_{j+1} of the segment $[B_jB_{j+1}]$ is obtained by:

$$l_{j+1} = (x_C - x_O).\left[\tan\left(\pi/2 - \theta_j^*\right) - \tan\left(\pi/2 - \theta_{j+1}^*\right)\right] \quad (2\text{-}33)$$

where θ_j^* is the corrected angle θ_j, after subtraction of the angle $\delta\theta_r$ due to replacement of the last point of the section 1 by the point C.

Therefore, the ordinate of any point B_{j+1} is defined by the ordinate of B_j as follows:

$$y_{j+1} = y_j + l_{j+1} \quad (2\text{-}34)$$

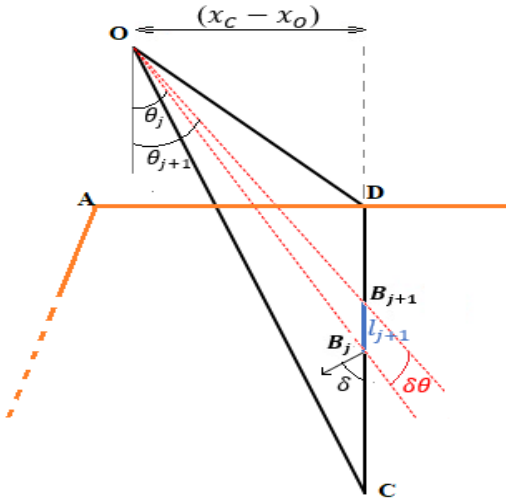

Figure 2-13 Generation of the crack

The generation of the mechanism is stopped when the generated point B_{j+1} is located above the ground surface, in other terms, when the ordinate of the new mechanism point is positive. In this case, the point B_{j+1}, is replaced by the intersection between the segment $[B_jB_{j+1}]$ and the ground surface: the point D $(x_C, 0)$.

2.2.7.2 Maximum depth of a vertical crack in soil

The depth of a vertical crack in the soil which is a part of the failure mechanism, is limited by the stability requirement of the crack boundaries since the new vertical reinforced slope formed at the right crack side after the failure should be stable (Abd and Utili, 2017a). A rigorous lower bound on the maximum critical depth can be found from the lower bound theorem of the limit analysis applied to the crack boundary. Many researchers (e.g. Terzaghi (1950) and Spencer (1967)) proposed the following equation for the lower bound of the maximum crack depth:

$$h_{max} = \frac{2c}{\gamma}\tan(\frac{\pi}{4} + \frac{\varphi}{2}) \quad (2\text{-}35)$$

A rigorous upper bound on the maximum critical depth can be obtained from the upper bound theorem of the limit analysis. The expression of the upper bound of the maximum crack depth (Spencer, 1968; Michalowski, 2013) is:

$$h_{max} = \frac{3.83c}{\gamma}\tan\left(\frac{\pi}{4} + \frac{\varphi}{2}\right) \quad (2\text{-}36)$$

The maximum stable vertical crack is located between these two values. To stay in the safe side, the upper bound value is used to limit the vertical crack depth.

2.2.7.3 Work rate calculations

The computation of the external work rate $\dot{W}$, done by the soil weight of the block $\dot{W}_\gamma$ and the inertia forces in the horizontal and vertical directions induced by the earthquake forces, $\dot{W_{kh}}$ and $\dot{W_{kv}}$ respectively, remains the same as the case without crack consideration (section 2.2.4). Whereas, the computation of the energy dissipation which takes place along the reinforcement $\dot{D}_T$, and along discontinuity surface (rigid block assumption) presents some differences.

The internal energy dissipated by soil, are divided into two parts. The first part is the dissipated energy along the log-spiral part of the failure surface $\dot{D}_c(BC)$, while the second part is the one dissipated along the vertical crack $\dot{D}_c(CD)$. If the crack is a pre-existing crack, $\dot{D}_c(CD)$=0 since the crack is already formed, contrary to the case of a crack formation as a part of the failure mechanism that require an amount of energy to be formed (Michalowski, 2012).

The expression of $\dot{D}_c(BC)$, obtained by the summation of the internal work rate per infinitesimal length l_j of the failure surface, is provided previously in the section (2.2.4):

$$\dot{D}_c(BC) = \sum\left(c_j.\left(L_j.\Omega.\cos\varphi_j\right).l_j\right) \quad (2\text{-}37)$$

where c_j and φ_j are the soil strength parameters at the point B_j, L_j is the length of $[OB_{j+1}]$ and l_j the length of $[B_jB_{j+1}]$.

As mentioned before, when the crack CD forms as part of the failure mechanism surface, the closed-form solution for the dissipation work rate per unit area is expressed as (Michalowski, 2012-2013):

$$\dot{D} = [v]\left(f_c\frac{1-\sin\delta}{2} + f_t\frac{\sin\delta-\sin\varphi}{1-\sin\varphi}\right) \quad (2\text{-}38)$$

Where f_c and f_t are the one-dimensional compressive and tensile strength, respectively, $[v]$ is the magnitude of the velocity discontinuity vector and δ the angle between the velocity vector with the vertical direction of an opening crack (Figure 2-13).

Considering a soil with no tensile strength ($f_t = 0$), which is generally assumed for safety reasons, and knowing that $f_c = 2c\cos\varphi/(1-\sin\varphi)$, Eq. 2-38 reduces to:

$$\dot{D} = c[v]\cos\varphi\,\frac{1-\sin\delta}{1-\sin\varphi} \tag{2-39}$$

This formula projected in our discretized analysis method gives the dissipation per elementary length l_j of $[B_jB_{j+1}]$ along the crack as:

$$\dot{d}_j = c_j\Omega L_j\cos\varphi_j\,\frac{1-\sin\delta_j}{1-\sin\varphi_j}\,l_j \tag{2-40}$$

And therefore

$$\dot{D}_c(CD) = \sum c_j\Omega L_j\cos\varphi_j\,\frac{1-\sin\delta_j}{1-\sin\varphi_j}\,l_j \tag{2-41}$$

On the other hand, the internal energy is dissipated by the reinforcement along the failure mechanism. Figure 2-14a and 2-14b illustrate the tensile failure modes for geosynthetics along the log-spiral and vertical crack parts of the failure mechanism, respectively.

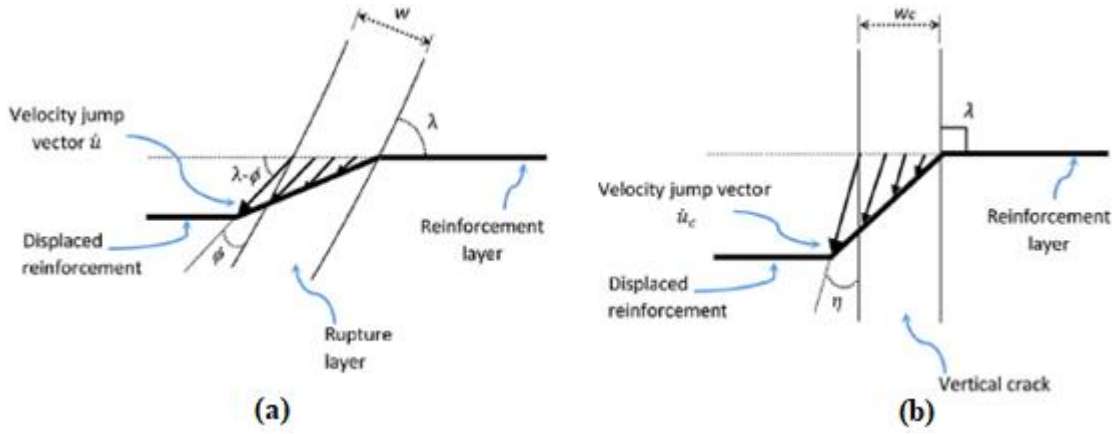

Figure 2-14 (a) Rupture of the geosynthetic element across the log-spiral part of the slip surface (b) Rupture of the geosynthetic element across the vertical crack based on (Abd and Utili, 2017a)

The energy dissipated by the reinforcement per infinitesimal length along the log-spiral part of the failure mechanism is provided previously in the section (2.2.4):

$$\dot{D}_t(BC) = \sum\left(k_t.\,l_j.\sin\eta_j\,.\,\Omega.\,L_j.\cos(\theta_B + j.\,\delta\theta)\right) \tag{2-42}$$

Along the crack CD, the energy dissipated by the reinforcement is similar for both types of cracks, pre-existing crack or crack formation as a part of the failure mechanism.

For a vertical velocity discontinuity, the equation giving the dissipated energy provided by Michalowski (1998a) is:

$$\dot{D}_t(CD) = \sum\left(k_t . l_j . \Omega . L_j . \cos(\theta_B + j . \delta\theta)\right) \tag{2-43}$$

According to the upper bound theorem, the energy balance equation, i.e. $\dot{W} = \dot{D}$, provides the objective function to be optimized in order to determine the required reinforcement strength. Four variables are considered in the optimization process using the two-step genetic algorithm, proposed by Guo et al. (2018), namely $[r_B, \theta_B, \xi, t]$ where r_B is the length of the segment $[OB]$, θ_B is the angle between the y axis direction and the line OB, ξ is the normalized crack depth and t the time involved in the pseudo-dynamic approach when this latter is used to represent the seismic loading.

2.2.7.4 Validation of the discretization technique involving crack presence

To validate the accuracy of the proposed method, a comparison with the results of Abd and Utili (2017a), who investigated the internal stability of geosynthetic reinforced slopes with cracks using the conventional method of limit analysis, is presented. These authors used the limit analysis to provide the amount of required reinforcement strength for a uniform $c - \varphi$ slopes under static condition, considering the pre-existing cracks and the crack formation as a part of the failure mechanism. They consider different slope inclination and soil tensile strength.

In order to assess the internal stability of reinforced soil retaining walls, Abd and Utili (2017a) among others (Michalowski, 1997-1998a; Ausilio et al., 2000), consider only the tension failure of reinforcement to calculate the reinforcement strength. The pullout failure is then investigated in the phase of determination of the required reinforcement length. Therefore, in this section, to validate the accuracy of the proposed method when dealing with cracks in terms of reinforcement strength, the reinforcement length is considered large enough so that only the tension failure of reinforcement is taken in consideration. A uniform distribution of the reinforcement, which is used generally in practice, is assumed.

The comparison results are shown in Figure 2-15 where the normalized required reinforcement strength $k_t/\gamma H$ is plotted against slope inclinations for different internal friction angles and for two different normalized cohesions of the backfill. Two distinct crack types are distinguished: pre-existing crack and crack formation as a part of the failure mechanism. Only tension cut-off cracks are considered.

A very satisfactory agreement is observed between the results of Abd and Utili (2017a) and the discretization method for both cases of normalized cohesion.

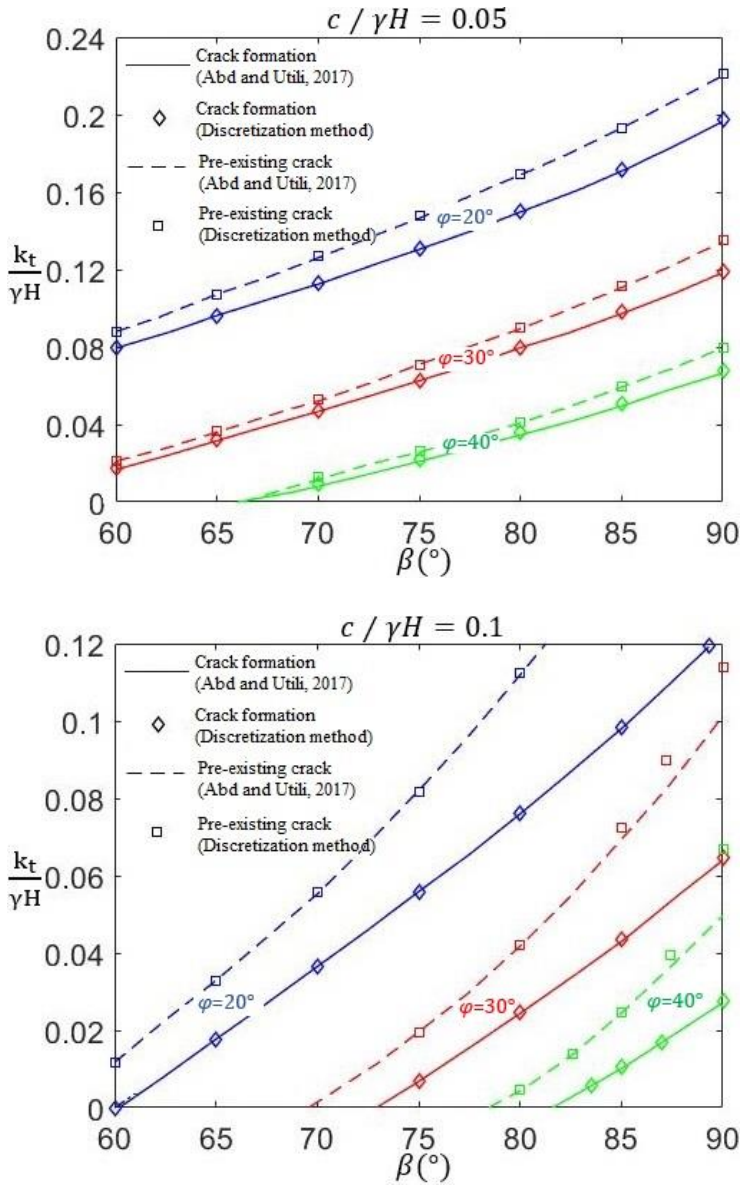

Figure 2-15 Comparison of results between the discretization method and the conventional limit analysis

2.3 Reinforced soil retaining walls: Dry soils

This section aims to illustrate the influence of key parameters on the stability of reinforced soil retaining walls for dry soils. Knowing that inclination of a reinforced soil retaining wall should not exceed 15^0, all simulations are conducted for two wall inclinations: 0^0 (vertical retaining wall) and 15^0, corresponding respectively to β=90^0 and β=75^0.

2.3.1 Kinematic stability analysis using pseudo-static approach

A 7 m reinforced soil wall (H=7 m), with a horizontal backfill ($\alpha = 0^0$) and a unit weight of the soil $\gamma = 20\ kN/m^3$, was used and a vertical reinforcement spacing equal to 70 cm was considered as in engineering practice. The initial and the minimum apparent friction coefficients at the soil/strip interface

are selected as f_0^*=1.2 and $f_1^* = 0.6$ respectively and $\delta\theta = 0.01^o$. The results are expressed in terms of the dimensionless factor of reinforcement strength $k_t/\gamma H$. The pseudo-static approach is adopted to model the seismic effect in this section.

2.3.1.1 *Influence of reinforcement length*

Figure 2-16 shows the effect of the reinforcement length L on the required reinforcement strength for β=75^0 and β=90^0. The soil cohesion c is taken equal to $c = 10\ kPa$, $k_h = 0.1$, $k_v = 0$. Four different internal friction angles φ are considered.

As can be seen in Figure 2-16, the required amount of reinforcement decreases with the increase of L until a specified value, beyond which the amount of reinforcement strength remains constant. The rate of decrease is greater for smaller values of φ. This optimal value of reinforcement length, specific for each internal friction angle in Figure 2-16, corresponds to the reinforcement length necessary to prevent the pullout failure of all reinforcement layers. It decreases with the increase of φ. For β=90^0 (respectively 75^0), when φ increases from 25^0 to 40^0, the optimal length decreases from $0.9H$ to $0.65H$ (respectively from $0.8H$ to $0.4H$).

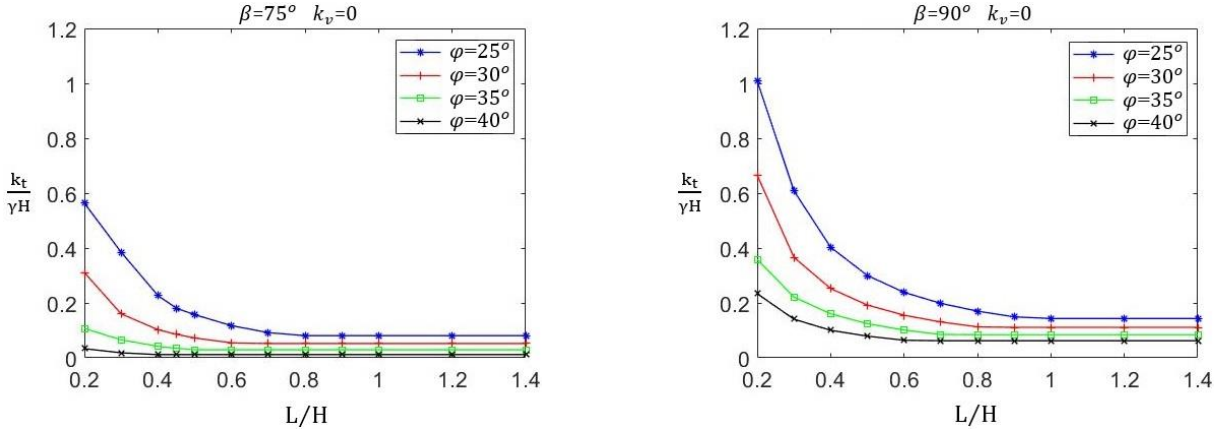

Figure 2-16 Influence of the reinforcement length

2.3.1.2 *Influence of seismic acceleration coefficients k_h and k_v*

Figure 2-17 shows the influence of the horizontal seismic acceleration coefficient k_h on the required normalized reinforcement strength for a cohesionless soil reinforced by reinforcement elements of length equal to the wall height i.e. $L = H$, for different values of φ, and for $k_v = 0$.

It is evident that the required value of reinforcement strength increases with the increase of k_h for different values of φ for the two wall inclinations. The rate of increase is lower for higher friction angles. For example, for β=90^0, the normalized reinforcement strength increases by 153% and 101% for $\varphi =$

30^0 and 40^0 respectively when k_h increases from 0 to 0.3. But the total reinforcement force for $\varphi = 30^0$ is approximately the double of the required reinforcement force for $\varphi = 40^0$. Same trends are obtained for β=75^0.

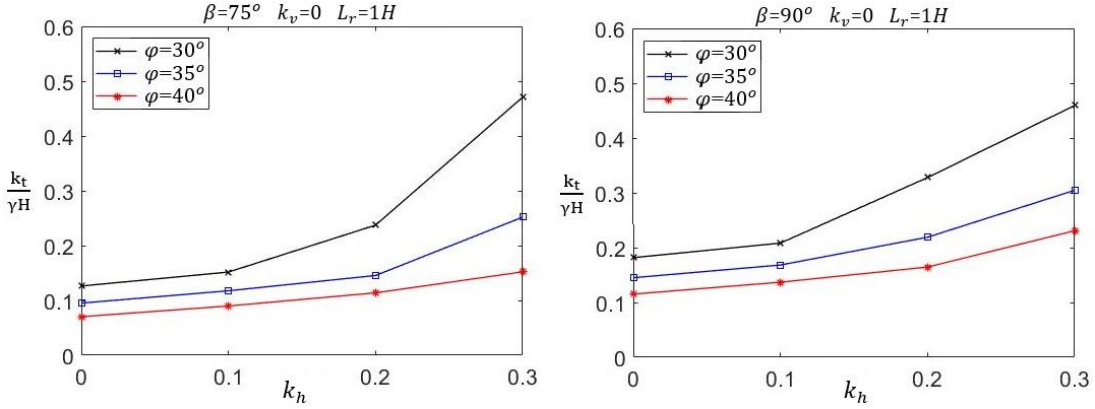

Figure 2-17 Influence of the horizontal seismic coefficient

In order to study the effect of the vertical acceleration on the required normalized reinforcement strength, Figure 2-18 shows the normalized strength of reinforcement for different values of φ, k_h and λ and for β=$75^0$and 90^0 respectively, where $\lambda = k_v/k_h$. A positive value of λ corresponds to a downward vertical seismic force, whereas a negative value corresponds to an upward vertical seismic force. A cohesionless soil reinforced by reinforcement elements of $L = H$ is considered.

Figure 2-18 illustrates the marginal influence of k_v on the results for all cases, showing the reliability of the assumption of neglecting the vertical acceleration in Eurocode 8. The results show that the downward vertical seismic force is unfavorable for the reinforced earth retaining wall, whereas, the upward vertical seismic force leads to a decrease in the required normalized reinforcement strength. That is why, despite its low impact, if the designer wants to take the vertical seismic acceleration into consideration in the seismic analysis of these structures, a downward force could be used. For example, for a vertical retaining structure of $\varphi = 35^0$, the required reinforcement strength increases only 8% when λ increases from 0 to 1 for $k_h = 0.1$, and 4.5% for $k_h = 0.2$.

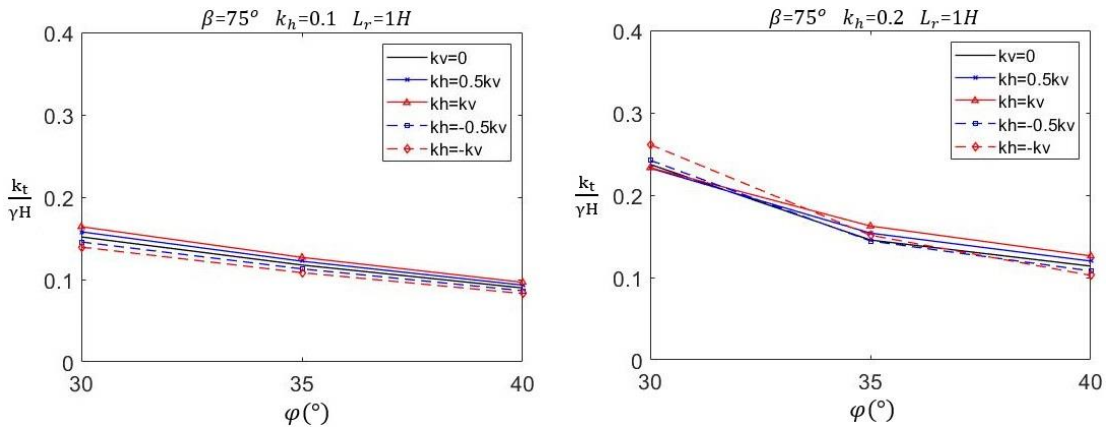

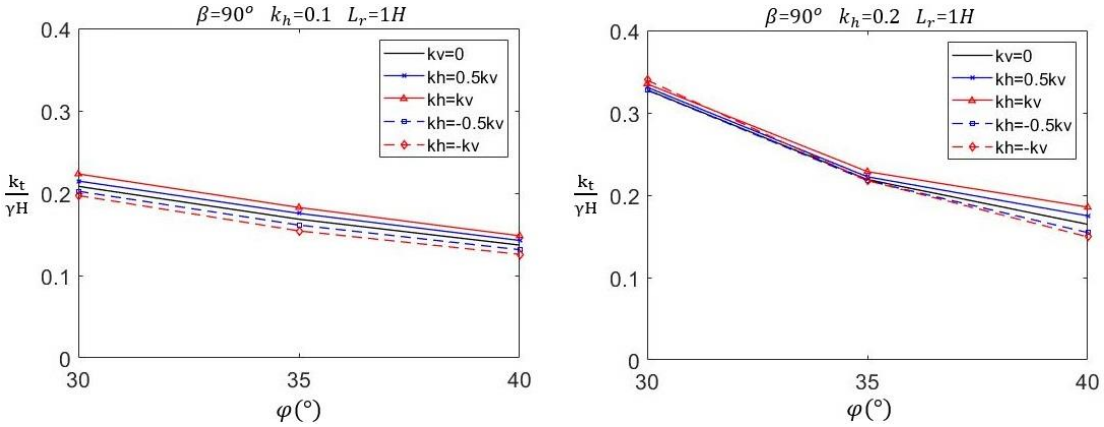

Figure 2-18 Influence of the vertical seismic coefficient

2.3.1.3 Influence of the soil strength parameters: Homogeneous and heterogeneous soil cases

Cohesionless soils are recommended for reinforced soil retaining walls. The design of these structures is performed by assuming a homogeneous backfill soil. However, the use of fine-grained soils as backfills can be done in regions where the granular soils are not available or expensive. These soils are nonhomogeneous in nature, which means that the soil strength parameters will exhibit a spatial variability. For the sake of simplicity, the soil strength parameters (internal friction angle and cohesion) are assumed to vary linearly only in the vertical direction, as shown in Figure 2-19. The soil unit weight variation is neglected in the whole domain. φ_1 and c_1 are respectively the soil friction angle and cohesion at the ground surface. φ_2 and c_2 are those at the wall toe level.

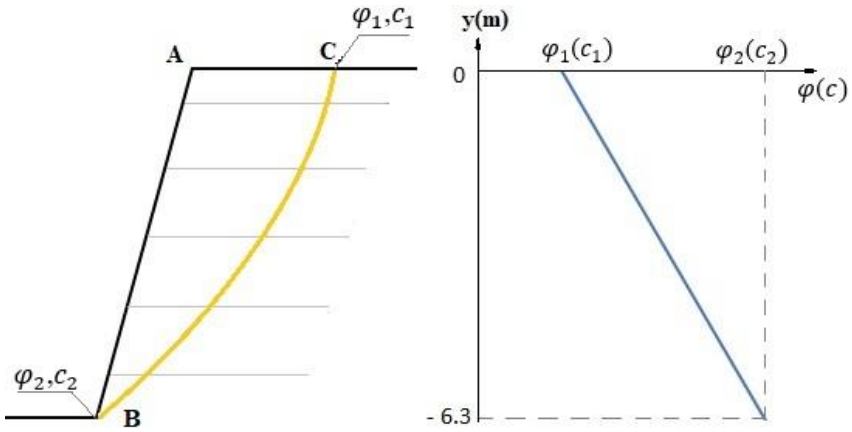

Figure 2-19 Variation of the friction angle with depth in the backfill

The effect of each soil strength parameter and its spatial variation is investigated apart. It means that when analyzing the influence of a parameter, the second is taken as constant. First, the impact of the soil friction angle variability is considered. A cohesionless soil is assumed, L is taken equal to the wall height H and no vertical component for the seismic acceleration is considered.

Figure 2-20 presents the required normalized reinforcement forces as a function of the soil friction angle at the wall toe level φ_2. The results are presented for two inclinations of the reinforced soil wall and three different values of the horizontal seismic coefficient: k_h= 0 (static case), 0.1 and 0.2. To better understand the impact of the soil friction angle variability, the results considering three cases are presented:

- Constant soil friction angle in the range from 30 to 45°,
- The soil friction angle at the ground surface is set equal to 75% and then 50% of its value at the wall toe level.

The results (Figure 2-20) show that for different values of the horizontal seismic coefficient and wall inclinations, the required reinforcement strength decreases with the increase of φ_2. The structure needs less reinforcement strength for higher friction angle values and inclined reinforced earth wall (β=75°). The linearity of the curves changes according to the value of the horizontal seismic coefficient k_h. When k_h is equal to zero (static case), a linear relationship exists between the required normalized reinforcement strength and the soil friction angle φ_2. With an increase of k_h, this relationship tends to be nonlinear. The nonlinearity exists in some curves (like for k_h=0.1) and all the curves becomes nonlinear for k_h=0.2.

The rate of decrease of the required reinforcement strength with the increase of φ_2 is greater for inclined reinforced soil walls. For example, for k_h=0 and β=75^0, the normalized reinforcement strength decreases respectively of about 60%, 55% and 49% for the three cases of soil friction angle variation (φ_1=φ_2, φ_1=0.75 φ_2 and φ_1=0.5 φ_2) when φ_2 increases from 30^0 to 45^0. These percentages decrease respectively to 50%, 46% and 43% for β=90^0. Similar trends are observed for k_h=0.1 and k_h=0.2. For k_h=0.1, the percentages are respectively 56%, 52% and 53% for β=75^0 and 47%, 49% and 50% for β=90^0. For k_h=0.2, the percentages are respectively 63%, 65% and 68% for β=75^0 and 58%, 61% and 63% for β=90^0.

In addition, Figure 2-20 shows that the rate of the soil friction variation plays an important role in the determination of the required reinforcement strength. More the soil friction angle exhibits variations, greater are the reinforcement forces required to maintain the structure stability. This is more pronounced for the lower friction angle values and important values of the horizontal seismic coefficients as presented in Figure 2-20. For example, for φ_2=30° and k_h=0.2, the rates of increase of the required reinforcement strength when passing from the case of a constant soil friction angle (φ_1=φ_2) to the third case (φ_1=0.5 φ_2) are respectively equal to 70% and 50% for β=75^0 and β=90^0. In addition, the variation rate of the soil friction angle can change the shape of the curves as shown in Figure 2-20 for the case of k_h=0.1. It means a change from a linear curve to a nonlinear one when the variation of the soil friction angle with the depth is important.

The impact of the soil cohesion variability is also considered (assuming a backfill soil friction angle constant and equal to 30°). *L* is taken equal to the wall height *H* and no vertical component of the seismic acceleration is assumed.

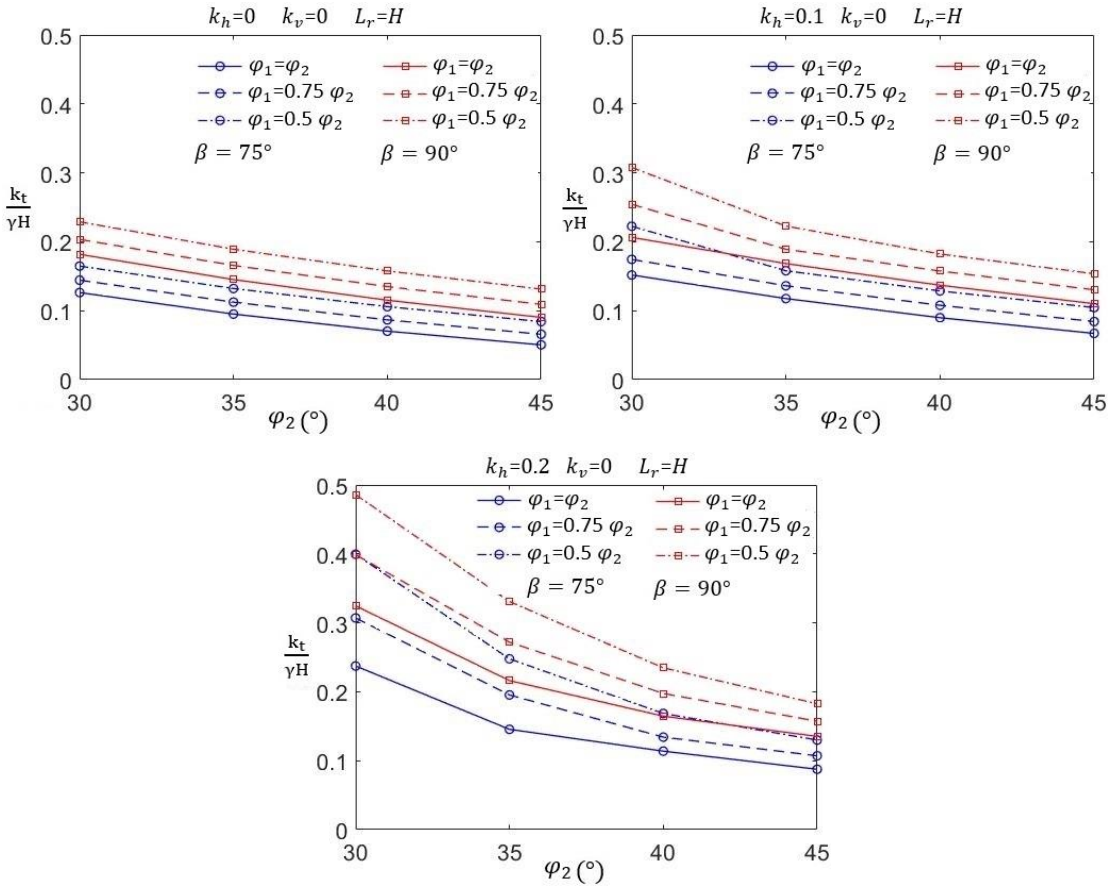

Figure 2-20 Influence of the friction angle

Figure 2-21 presents the required normalized reinforcement force as a function of the soil cohesion at the wall toe level c_2 for the two inclinations of the reinforced soil wall and the same three values of the horizontal seismic coefficient. The results are presented for three cases:

- Constant soil cohesion in the range from 0 to 15 kPa,
- The soil cohesion at the ground surface is set equal to 75% and then 50% of its value at the wall toe level.

As for the friction angle, the soil cohesion has a similar effect on the required normalized reinforcement strength. The latter decreases with the increase of the soil cohesion for all combinations of k_h and β. It is important to note that in the case of inclined reinforced soil retaining walls and $k_h = 0$, and for c_2 greater than respectively 12 kPa and 14.35 kPa, there is no need of reinforcement to maintain the system stability (cases of constant soil cohesion and c_1=0.75 c_2). In other terms, the energy dissipated along the sliding surface is greater than the work of the external forces in these cases.

The curves start from the same point since it corresponds to the case of a cohesionless soil. The effect of a linear variation of the soil cohesion has a lower effect on the required reinforcement force than the case of the soil friction angle variability. The influence of the soil cohesion variability increases with the increase of c_2.

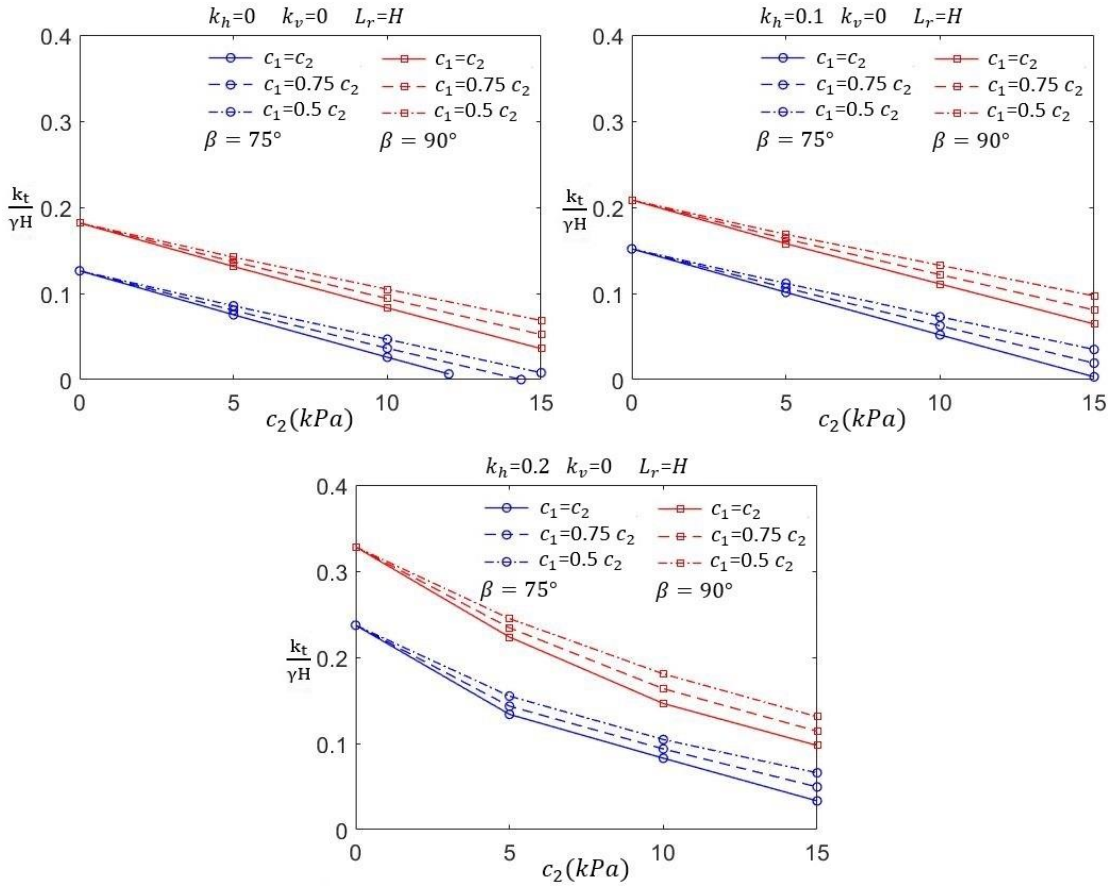

Figure 2-21 Influence of the cohesion

2.3.2 Kinematic stability analysis with crack consideration using pseudo-dynamic approach

2.3.2.1 Effect of considering pseudo-dynamic approach instead of pseudo-static

The pseudo-dynamic approach is more realistic to represent the seismic force than the pseudo-static one, since it considers the time and depth effects. In this section, the difference between the two approaches is investigated. A homogeneous backfill is considered with the basic input parameters: c=10 kPa, φ=25^0. The other parameters are taken as follows: λ=0.5 where λ=k_v/k_h with two wall inclinations 0^0 (vertical retaining wall) and 15^0, corresponding respectively to β=90^0 and β=75^0. The discretization angle is taken as $\delta\theta = 0.01^o$ which is sufficient to obtain a good accuracy with a reasonable time calculation for the optimization. The reinforcement length L is considered large enough to ensure that

only a tensile failure occurs. For dynamic analyses, the following parameters are considered: V_s=150 m/s, V_p=280.5 m/s, f=1.4, T=0.3 s, t_0=0 s.

Figure 2-22 shows the required reinforcement strength for the two reinforced soil retaining wall inclinations involving crack formation as a part of the failure mechanism, for different values of the horizontal seismic coefficient k_h. Only tension failure is assumed in the calculation of the required reinforcement strength.

It is clear from the curves that the difference between the two approaches increases with the increase of the seismic acceleration for the two wall inclinations. The normalized reinforcement strengths are equal for the static case, increase about 9.06% and 6.14% when considering a pseudo dynamic approach instead of pseudo-static one when k_h=0.1, for β=75° and β=90° respectively. The maximum percentages increases are 34.47% and 26.32% when k_h=0.5, for β=75° and β=90°. Figure 22 shows the difference between the two approaches for a single value of amplification factor f.

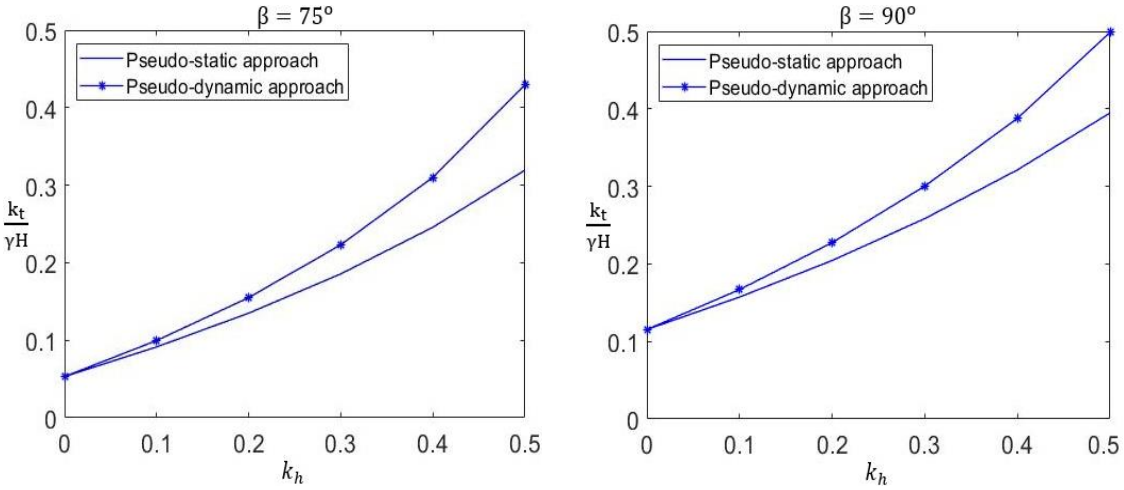

Figure 2-22 Comparison in terms of required reinforcement between the two approaches for different k_h

The required normalized reinforcement strength by the two approaches with different values of amplification factor f is also investigated. Figure 2-23 presents the cases of seismic coefficients equals to 0.1 and 0.2 for the two wall inclinations.

The required normalized reinforcement strength is constant in the case of a pseudo-static approach, since in such approach the amplification of the acceleration is not considered. However, in the case of the pseudo-dynamic approach, the required normalized reinforcement strength increases with the increase of the amplification factor. This increase is more pronounced for k_h=0.2 than for k_h=0.1, *i.e.* it is more pronounced when increasing the seismic acceleration. It is important to note that there is a small range of values of f where the required normalized reinforcement strength by the pseudo-dynamic approach is smaller than the one required by the pseudo-static approach. Therefore, the last approach in this case is more critical. This range depends generally of many factors like the pseudo-dynamic parameters (V_s, V_p, T, t_0) and the depth of the reinforced backfill.

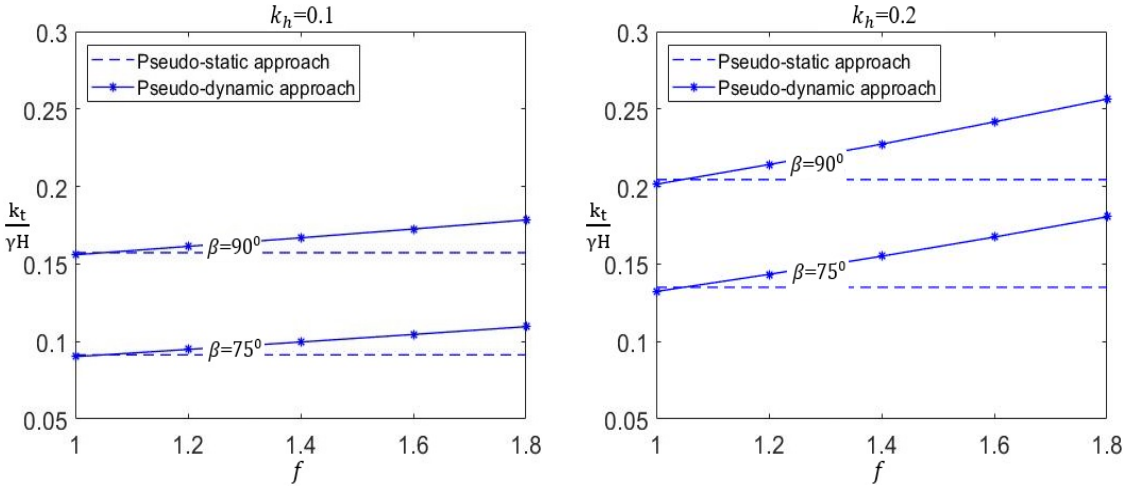

Figure 2-23 Comparison in terms of required reinforcement between the two approaches for different f

To justify these results, Figure 2-24 presents the horizontal seismic acceleration at the wall toe and at the ground surface for two different cases of amplification factor f (f=1 and f=1.4). In the case of f=1, the normalized reinforcement strength is lower for the pseudo-dynamic approach due to the phase between the signals at the wall toe and the ground surface. The maximum required reinforcement strength is obtained at t=0.103 $\mp$ T (s) when the values of horizontal accelerations, lower than the values of a pseudo-static approaches, are marked by a mark "+". In the case of f=1.4, the normalized reinforcement strength is greater for the pseudo-dynamic approach due to the amplification of the signal at the ground surface, despite the phase between the signals. The maximum required reinforcement strength is obtained at t=0.41 $\mp$ T (s) where the values of horizontal accelerations are marked by a circle mark "o". The peak of the accelerations varies linearly between the wall toe and the ground surface. Same variations are observed for the vertical accelerations.

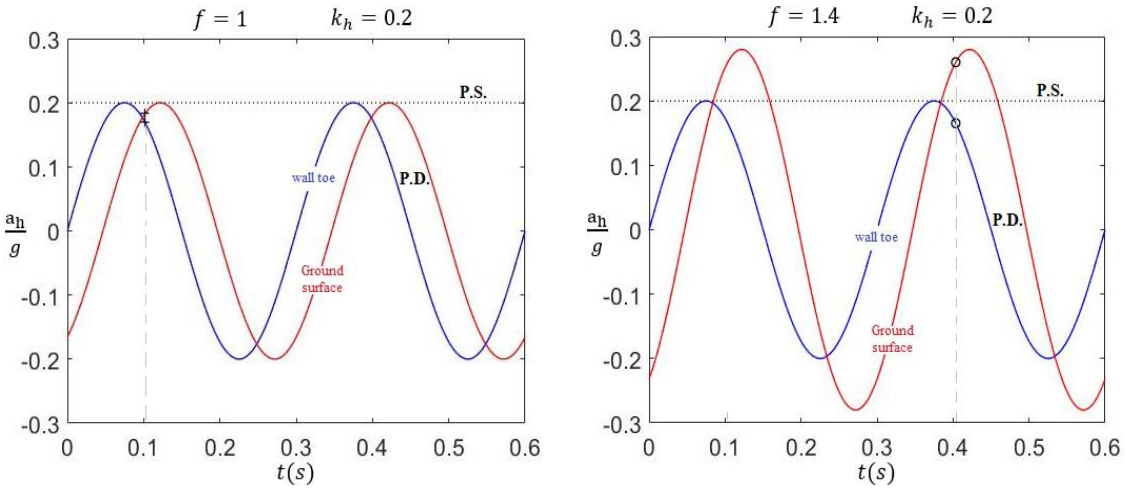

Figure 2-24 Horizontal seismic acceleration at the wall toe and the ground surface for different approaches

2.3.2.2 Effect of considering cracks in the analysis

To show the importance of considering the cracks in the analysis, Table 2-1 reports the required reinforcement strength of reinforced earth retaining walls for different values of k_h, for β=75° and β=90°. All the parameters used in the previous section are kept similar except the amplification factor which is set as constant equal to 1.2. Three cases of cracks are considered: No crack, crack formation as a part of the failure mechanism and pre-existing crack. In addition, the normalized depth of the crack ξ, is presented. The results indicate that the normalized reinforcement strengths for reinforced backfill with cracks (crack formation or pre-existing crack) are greater than those obtained for an analysis without consideration of cracks. Pre-existing cracks present the most critical case, requiring the greater reinforcement strength. These differences are more significant for a vertical retaining wall (β=90°) and lower values of k_h. One can observe that the crack depth decreases with the increase of k_h and β which justifies the rate of discrepancies observed. The lower the crack depth, the lower the differences. In addition, the crack depth in the case of a pre-existing crack is significantly greater than in the case of a crack formation.

Table 2-1 Required reinforcement strength and crack depth for different types of cracks

$\boldsymbol{\beta}$(°)		$\boldsymbol{k_h = 0}$		$\boldsymbol{k_h = 0.1}$	
		$\frac{k_t}{\gamma H}$	crack depth ξ	$\frac{k_t}{\gamma H}$	crack depth ξ
75°	No crack	0.051	-	0.092	-
	Crack formation	0.053	0.173	0.095	0.152
	Pre-existing crack	0.070	0.477	0.103	0.292
90°	No crack	0.113	-	0.158	-
	Crack formation	0.115	0.162	0.162	0.150
	Pre-existing crack	0.157	0.477	0.187	0.477

$\boldsymbol{\beta}$(°)		$\boldsymbol{k_h = 0.2}$		$\boldsymbol{k_h = 0.3}$	
		$\frac{k_t}{\gamma H}$	crack depth ξ	$\frac{k_t}{\gamma H}$	crack depth ξ
	No crack	0.140		0.197	

75°	Crack formation	0.143	0.136	0.201	0.126
	Pre-existing crack	0.147	0.183	0.203	0.142
90°	No crack	0.210	-	0.270	-
	Crack formation	0.214	0.138	0.276	0.132
	Pre-existing crack	0.217	0.173	0.277	0.141

2.3.2.3 Parametric analysis

In this section, to highlight the key parameters influence on the required normalized geosynthetic reinforcement strength, a parametric study was conducted for two reinforced soil wall inclinations: 0^o and 15^o. A combined failure (rupture and pullout) is assumed simultaneously in the calculation of the required reinforcement strength. Two cases are considered: a reinforced soil without presence of cracks and a reinforced soil which considers the crack as a part of the failure mechanism. The results are presented using graphs or tables. The effects of pseudo-dynamic seismic forces, soil and reinforcement properties are investigated using the following basic input parameters:

H=7 m, γ=18 kN/m^3, c=10 kPa, φ=25^o, $\delta\theta$=0.01^o, f=1.2, V_S=150 m/s, V_P=280.5 m/s, T=0.3 s, λ=0.5 and t_0=0 s, L_r=H, S_V=0.7 m, f_0^*=1.2, f_1^*=0.6.

where L_r is the reinforcement length, S_V is the vertical reinforcement spacing, f_0^* and f_1^* are the initial and the minimum apparent friction coefficients at the soil/strip interface.

When studying the influence of a parameter, the other parameters are maintained at their reference values.

2.3.2.3.1 Influence of reinforcement length

Figure 2-25 shows the effect of the reinforcement length L_r on the required normalized reinforcement strength $k_t/\gamma H$ with k_h=0.1 and for three different friction angles φ=20^o, 25^o, 30^o.

It can be seen that for both cases of crack presence or not, the normalized reinforcement strength decreases with the increase of the reinforcement length L_r until a specified value $L_{r\_optimum}$, beyond which there is no benefit of increasing L_r. This specified value corresponds to the reinforcement length with which the analysis considering only the tensile failure mode gives the same amount of reinforcement strength as the analysis considering the combined failure mode. This value increases for a larger inclination of the reinforced backfill (β=90°) and increases with the decrease of the soil friction

angle. In addition, for the same inclination and friction angle, the specified value of reinforcement length is slightly larger in case of a crack presence. In the range of reinforcement length smaller than $L_{r\_optimum}$, the rate of decrease of the required reinforcement strength with the increase of L_r is greater for smaller values of φ.

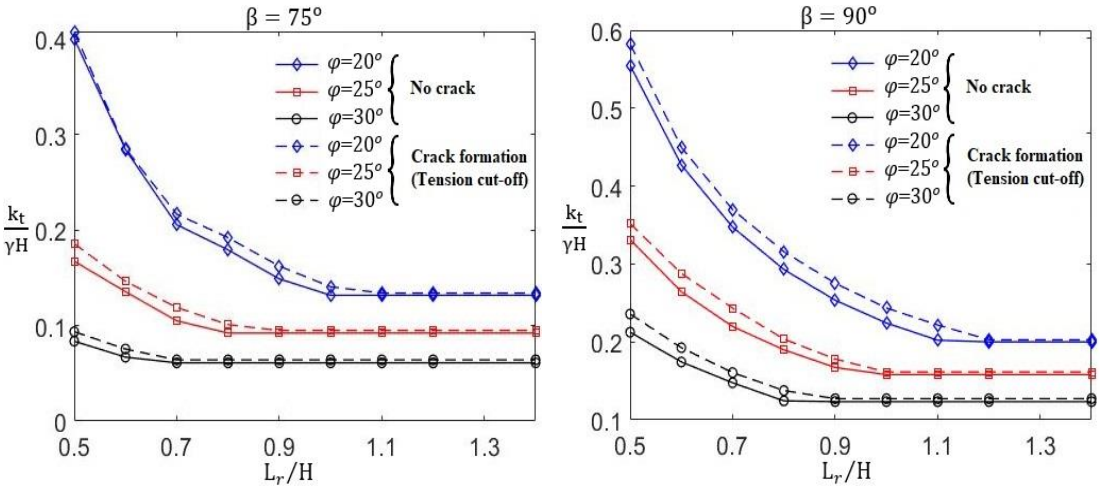

Figure 2-25 Influence of the reinforcement length

2.3.2.3.2 Effect of the amplification factor f

Figure 2-26 shows the effect of the amplification factor f on the required normalized reinforcement strength for different values of k_h for both vertical and inclined walls. As expected, the stability of the reinforced earth retaining wall decreases, requiring therefore greater reinforcement strength, when the amplification factor f increases. The influence of f is more significant for higher value of k_h.

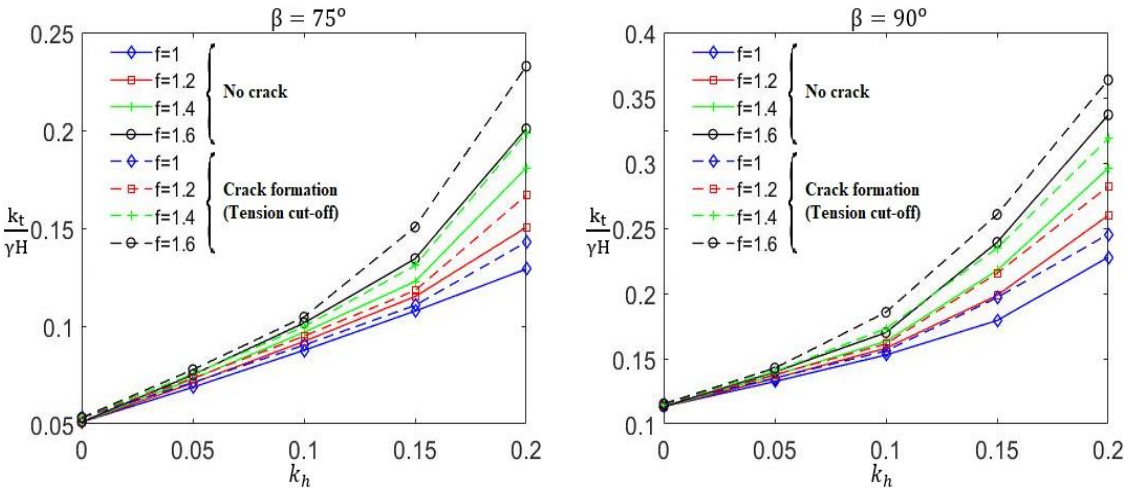

Figure 2-26 Influence of the amplification factor f

2.3.2.3.3 Influence of soil strength properties

Figure 2-27 shows the effect of the soil friction angle φ on the required normalized reinforcement strength for different values of k_h. The cohesion c, like the other parameters, is taken equal to its reference value ($10\ KPa$).

It is clear that with the presence of cracks or not, the normalized reinforcement strength decreases with the increase of the soil friction angle for different values of k_h, for both inclined and vertical reinforced soil structures. The influence of φ is greater for larger values of k_h. In addition, for the same k_h, the difference between the curves corresponding to the cases of crack presence and no crack decreases when increasing φ.

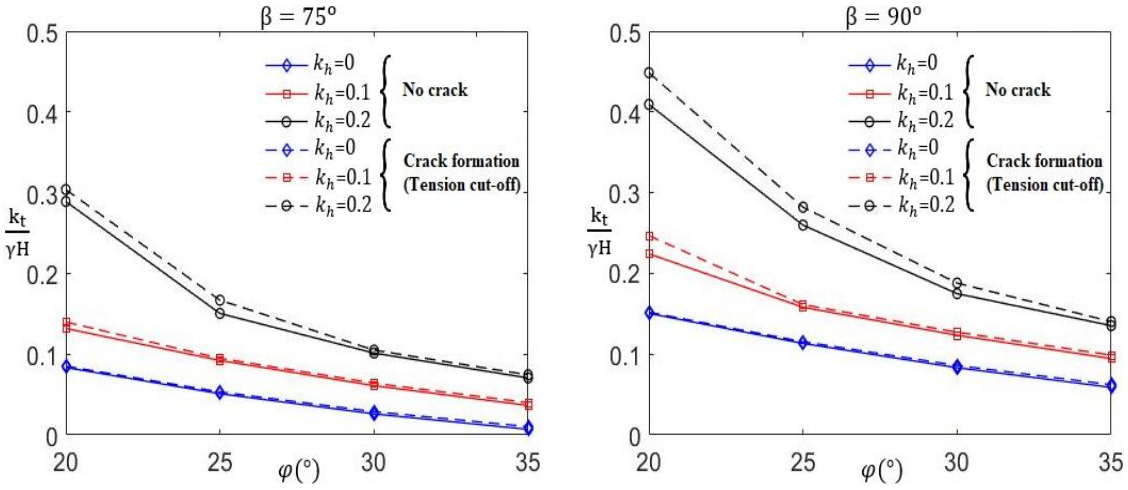

Figure 2-27 Influence of the soil friction angle

The influence of the cohesion c on the required normalized reinforcement strength is illustrated in Figure 2-28 for different values of k_h. The soil friction angle is also taken here, like the other parameters, equal to its reference value (25^o).

It can be seen that with the presence or not of cracks, the normalized reinforcement strength decreases with the soil cohesion increase for different values of k_h, for both inclined and vertical reinforced earth structures. The influence of c is greater for larger values of k_h. In the contrary of the case of friction angle, for the same k_h, the difference between the curves corresponding to the cases of crack presence and no crack decreases when decreasing c.

For the case of an inclined retaining wall under static loading, the normalized reinforcement strength required to ensure the stability of the system is zero for a cohesion c higher than $15\ kPa$. The system is stable without reinforcing the backfill with geosynthetics.

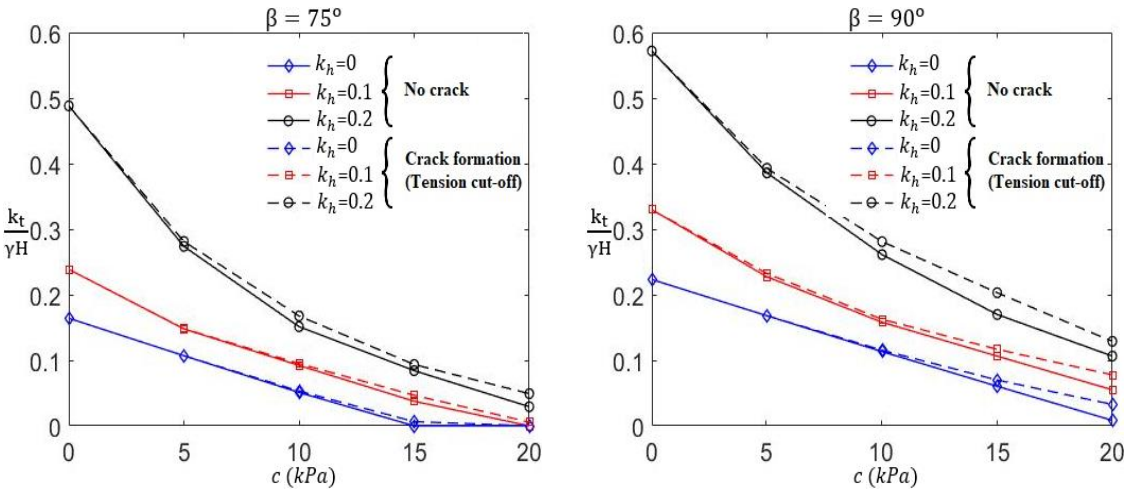

Figure 2-28 Influence of the soil cohesion

The influence of soil properties is investigated until now considering the backfill as a homogeneous medium. However, as mentioned before, both laboratory investigations and field observations show that the soil exhibit spatial variability in its properties, which can lead to an inappropriate design of the reinforced earth retaining wall when ignoring it. In the following section, the effect of the soil heterogeneity on the required normalized reinforcement strength is investigated considering the variation of the cohesion and friction angle, whereas the variation of the soil weight γ is neglected in the whole domain. For simplicity, it is assumed that the cohesion and the friction angle vary linearly in the vertical direction but are constant on the horizontal plane. The variation of the soil properties with the depth are shown in Figure 2-29, c_1 and φ_1 are the soil cohesion and friction angle at the ground surface, c_2 and φ_2 are the ones at wall toe.

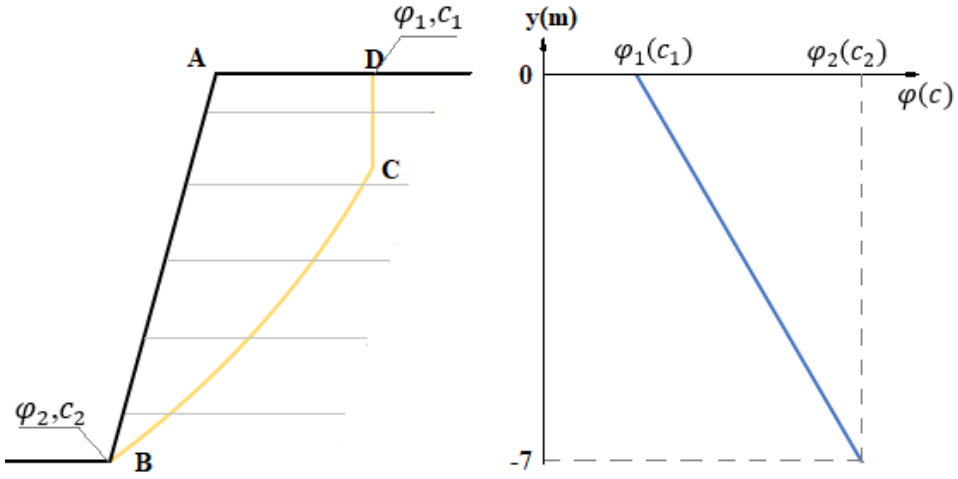

Figure 2-29 Variation of the soil properties in the backfill

Tables 2-2 and 2-3 present the required normalized reinforcement strength for four different cases of soil resistance properties and for different values of k_h. The first case considers constants values of soil properties, the second and third case take in consideration the variation of a soil parameter while

considering the value of the second one as constant, and finally, the last case considers the variation of the cohesion and friction angle simultaneously.

The results in the two tables are presented with three decimal digit numbers. Therefore, for two equal values in the table, a small difference exists in the exact values.

Table 2-2 Required reinforcement strength $k_t/\gamma H$: $\beta = 75°$

		c_1=10 kPa c_2=10 kPa $\varphi_1 = 25°$ $\varphi_2 = 25°$	c_1=10 kPa c_2=10 kPa $\varphi_1 = 20°$ $\varphi_2 = 30°$	c_1=5 kPa c_2=15 kPa $\varphi_1 = 25°$ $\varphi_2 = 25°$	c_1=5 kPa c_2=15 kPa $\varphi_1 = 20°$ $\varphi_2 = 30°$
k_h= 0	No crack	0.051	0.041	0.043	0.035
	Crack formation	0.053	0.043	0.044	0.036
k_h= 0.05	No crack	0.071	0.059	0.063	0.053
	Crack formation	0.073	0.062	0.064	0.054
k_h= 0.1	No crack	0.092	0.079	0.084	0.073
	Crack formation	0.095	0.082	0.085	0.074
k_h= 0.15	No crack	0.115	0.100	0.107	0.095
	Crack formation	0.118	0.104	0.108	0.096
k_h= 0.2	No crack	0.152	0.123	0.146	0.123
	Crack formation	0.168	0.138	0.151	0.128

It can be seen from the tables that the normalized reinforcement strength decreases with the increase of k_h in all cases. In addition, the normalized reinforcement strength is the highest in the first case when the soil parameters are considered constants and it is the smallest in the fourth case when both the soil friction angle and cohesion vary linearly in the backfill. More studies taking into account various coefficients of variations and different mean values of the soil properties, are needed to know if the results with the means values are the most critical. It is also noted that the difference in terms of normalized reinforcement strength between the cases of crack presence and no crack is the smallest when the soil is considered heterogeneous with linear variation of its properties, for the two inclinations of the reinforced soil wall considered in the study.

Table 2-3 Required reinforcement strength $k_t/\gamma H$: $\beta = 90°$

		c_1=10 kPa c_2=10 kPa $\varphi_1 = 25°$ $\varphi_2 = 25°$	c_1=10 kPa c_2=10 kPa $\varphi_1 = 20°$ $\varphi_2 = 30°$	c_1=5 kPa c_2=15 kPa $\varphi_1 = 25°$ $\varphi_2 = 25°$	c_1=5 kPa c_2=15 kPa $\varphi_1 = 20°$ $\varphi_2 = 30°$
k_h= 0	No crack	0.113	0.101	0.109	0.098
	Crack formation	0.115	0.104	0.109	0.099
k_h= 0.05	No crack	0.135	0.122	0.131	0.120
	Crack formation	0.138	0.126	0.132	0.120
k_h= 0.1	No crack	0.158	0.144	0.154	0.142
	Crack formation	0.161	0.148	0.155	0.144
k_h= 0.15	No crack	0.198	0.173	0.197	0.173
	Crack formation	0.216	0.188	0.202	0.186
k_h= 0.2	No crack	0.261	0.224	0.259	0.227
	Crack formation	0.282	0.242	0.265	0.232

2.4 Reinforced soil retaining walls: Saturated soils

2.4.1 Problem statement

The pore water effect within the backfill soil was not considered in the previous section since a dry backfill was considered. Knowing that the majority of the failure cases encountered in the literature were caused by the water presence, the pore water effect within the backfill soil is considered in this section, together with a possible crack opening in cohesive soils. This section concerns the seismic internal stability analysis of geosynthetic reinforced saturated soil retaining walls using the discretization technique with the upper bound theorem of limit analysis. The case of non-homogeneous and layered soils is investigated.

As mentioned previously, some of the most important design codes (e.g. FHWA-NHI-11-024, NF P 94-270) suggest a compacted cohesionless granular soil as a backfill in the reinforced zone with an appropriate drainage system. These requirements avoid the development of interstitial pore pressures behind the wall. However, the use of geosynthetic reinforcements, which do not have corrosion risk that can affect the metallic reinforcements, gives the opportunity to use poorly draining cohesive soils when

granular soils are not available or are expensive (Guler et al., 2007). This soil type was successfully used in the reinforced soil wall construction (Riccio et al., 2014). Nevertheless, the use of these soils can lead to several problematical issues and therefore, reduce the system stability (Abd and Utili, 2017a). Among these problems, the pore-water pressures development and the crack formation in the backfill zone are the most dangerous ones. Koerner and Koerner (2018) investigated 320 geosynthetic reinforced soil retaining walls failure cases. They reported that 73% of these failures occurred when the backfill in the reinforced zone was composed of cohesive soil and 63% were caused by the water presence. The water presence in the cohesive backfill must be addressed due to the low soil permeability and drainage system malfunction that can be caused by its clogging by fines. The system shear strength can then be significantly reduced.

2.4.2 Calculation of work rate of pore-water pressure in limit analysis

The whole failure mechanism $ABCD$ is limited by the log-spiral part BC where the soil fails purely in shear and the potential crack CD where the soil fails in tension/shear as shown in Figure 2-30.

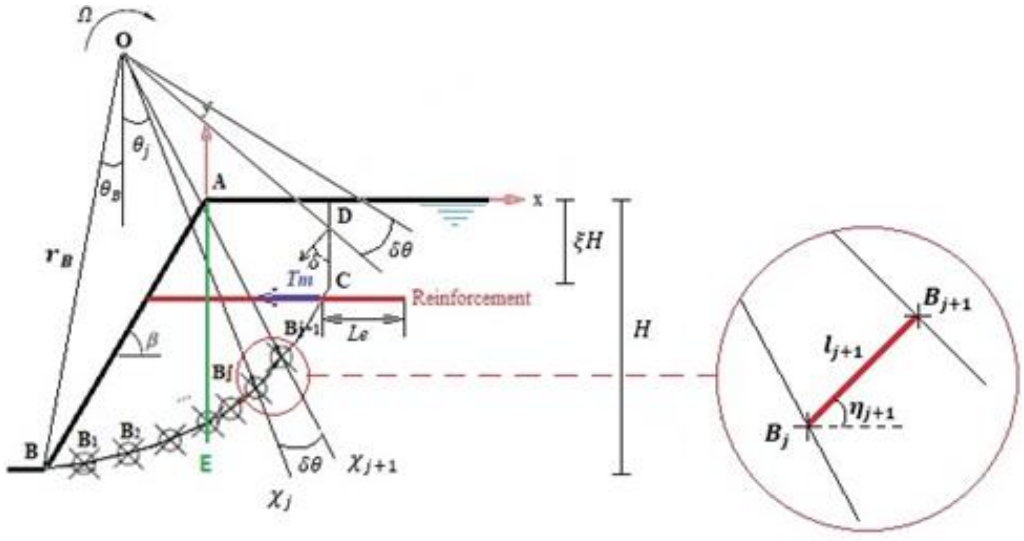

Figure 2-30 Discretization technique for the failure mechanism

The internal energy dissipation during the failure process takes place along the geosynthetic reinforcement elements by tensile or pullout failure and comes from the soil plastic deformation along the failure surface based on the rigid block assumptions. On the other hand, the external work rate comes from the work rate of the soil block weight $ABCD$, the inertia forces representing the seismic loading in both directions and the work rate produced by the pore pressure.

According to the upper bound theorem, the energy balance equation provides the objective function to be optimized in order to determine the required tensile reinforcement strength to ensure the reinforced soil retaining wall stability.

$$\dot{W_\gamma} + \dot{W_{kh}} + \dot{W_{kv}} + \dot{W_u} = \dot{D_c} + \dot{D_T} \quad (2\text{-}44)$$

Where $\dot{W_u}$ is the pore-water pressure work rate; $\dot{D_c}$ is the internal energy dissipation along the sliding surface composed of the energy dissipated along the log-spiral part BC and the energy dissipated along the vertical crack CD; and $\dot{D_T}$ the internal energy dissipation rate along the reinforcement. The computation of the pore-water pressure work rate is performed by summation of the elementary work rates by considering the same elementary trapezoidal surface $B_j' B_j B_{j+1}' B_{j+1}$ shown in Figure 2-5 and presented in the next paragraph.

For saturated soils, the effect of water must be included as an external loading applied to the soil skeleton and the boundary. As presented in Viratjandr and Michalowski (2006), the work of both seepage and buoyancy forces must be included in the analysis. In order to include both forces works in the kinematic approach of limit analysis, the pore water pressure is employed by using the so-called pore-water pressure coefficient r_u introduced by Bishop and Morgenstern (1960). The pore-water pressure u at a depth h below the surface, is then assumed to be equal to $r_u \gamma h$ where γ is the soil unit weight. The work rate of the pore-water pressure $\dot{W_u}$ can be expressed as a summation of both forces works as follows:

$$\dot{W_u} = -\gamma_w \int_V \frac{\partial h}{\partial x_i} . v_i dV + \gamma_w \int_V \frac{\partial Z}{\partial x_i} . v_i dV \quad (2\text{-}45)$$

where the first term represents the seepage force work rate over the entire collapse volume and the second one is the buoyancy force work rate, γ_w is the water unit weight, h is the hydraulic head, Z is the elevation head, v_i the velocity vector in the collapse block and V is the volume of the failure block. Alternatively, Viratjandr and Michalowski (2006) by developing the derivative $\frac{\partial}{\partial x_i}$ of the product uv_i, showed that the expression of the water pressure work rate can be written as a sum of the pore pressure work rate on skeleton expansion and on the boundary as follows:

$$\dot{W_u} = -\int_V u . \dot{\varepsilon_{ii}} dV - \int_S u . n_i . v_i dS \quad (2\text{-}46)$$

where $\dot{\varepsilon_{ii}}$ is the volumetric strain rate, S the boundary surface of the failure block, n_i the outward unit vector normal to the surface S.

The first term in Eq. 2-46 is assumed to be zero since a rigid block is considered. In the framework of the discretization technique to generate the failure surface, the kinematical admissibility condition must be satisfied and therefore, the angle between the velocity vector and the failure surface must be equal to the friction angle φ. Hence the angle between the vector n_i and the velocity vector is equal to $\frac{\pi}{2} + \varphi$. Knowing that the velocity at a point B_j on the failure surface is equal to $\Omega . L_j$ where L_j is the length of $[OB_j]$, the work rate of the pore pressure effect along the discontinuity surface is then given by the summation of the elementary work rates as follows:

$$\begin{cases} \dot{W}_u = \sum_j r_u.\gamma.\left(x_j.\tan\beta - y_j\right).l_j.\Omega.L_j.\sin\varphi & \text{along the boundary } BE \\ \dot{W}_u = \sum_j r_u.\gamma.\left(-y_j\right).l_j.\Omega.L_j.\sin\varphi & \text{along the boundary } ED \end{cases} \quad (2\text{-}47)$$

where x_j and y_j are the coordinates of point B_j and l_j is the length of $[B_{j-1}B_j]$.

It is worth noting that when calculating the internal energy dissipation rate along the reinforcement, the pullout force should account for the water presence. It can then be written as:

$$T_p = 2\gamma z^*(1 - r_u)L_e f^* \quad (2\text{-}48)$$

where z^* is the overburden depth; L_e is the effective length; f^* corresponds to the apparent friction coefficient at the soil/reinforcement interface.

Four variables are considered in the optimization process, namely $[r_B, \theta_B, \xi, t]$ where r_B is the length of OB, θ_B is the angle between the y axis direction and the line OB, ξ is a parameter to define the crack depth and t the time involved in the pseudo-dynamic approach.

2.4.3 Comparison

To validate the robustness of the proposed discretization method in the case of saturated soil, a comparison between the existing results of the conventional limit analysis method obtained by Abd and Utili (2017a) and the results obtained by the discretization-based kinematic analysis is presented. Abd and Utili (2017a) used the conventional kinematic theorem of limit analysis to investigate the internal stability of geosynthetic reinforced slopes with cracks under static loading and considering only the reinforcement tensile failure to calculate the required reinforcement strength. The pore water pressure effect on the required level of reinforcement was analyzed by employing the same approach used here through the so-called pore-water pressure coefficient r_u.

In order to validate the application of the discretization method in this study, the results of the discrete method are obtained under the same conditions used in the work of Abd and Utili (2017a). The case of crack formation as a part of the failure mechanism with tension cut-off is considered. The comparisons of results are depicted in Figure 2-31. for different slopes inclinations β and coefficients r_u. A total agreement can be observed between the two methods.

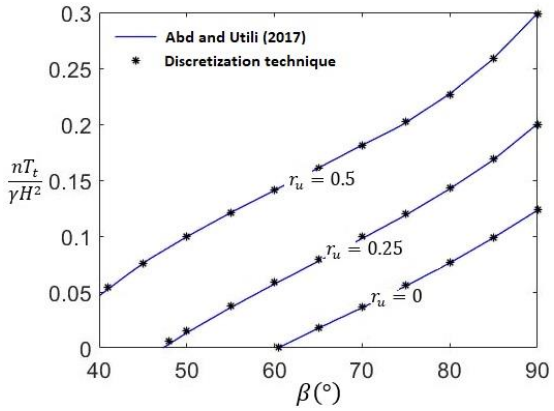

Figure 2-31 Comparison of the conventional limit analysis and the discretization technique ($\varphi = 20°$ and $c/\gamma H = 0.1$)

2.4.4 Results and discussions

2.4.4.1 Homogeneous soil

To investigate the pore-water pressure effect, tension crack and seismic loading, the results in terms of required reinforcement strength in a normalized form are presented for two wall inclinations $\beta = 75°$ and $\beta = 90°$. The two reinforcement failures modes are considered simultaneously. The following parameters are considered: H=7 m, γ=18 kN/m^3, φ=25°, c=12.6 kPa, $\delta\theta$=0.01^o, λ=0.5, L_r=1.2 H, n=10, f_0^*=1.2, f_1^*=0.6, f=1.2, V_S=150 m/s, V_P=280.5 m/s, and T=0.3 s, where λ=k_v/k_h, n the reinforcement number, L_r the reinforcement length and c the soil cohesion.

According to Figure 2-32, it is observed that the required reinforcement strength increases with the horizontal seismic coefficient, the pore-water ratio and the wall inclination (β). In addition, the normalized reinforcement strength values for the reinforced backfill with cracks are greater than the values obtained when considering an intact soil.

It is evident that the required reinforcement strength increases with the increase of k_h. Moreover, as expected, the pore-water pressure is unfavorable to the reinforced soil wall stability. The presence of cracks leads to an increase of the required normalized reinforcement strength. In particular, when the value of the pore-water pressure or of the seismic loading is important, the increase of the required reinforcement strength is more obvious. Hence, it is critical to consider these effects when poorly draining cohesive soils are used in seismic zones as backfill materials for economic reasons.

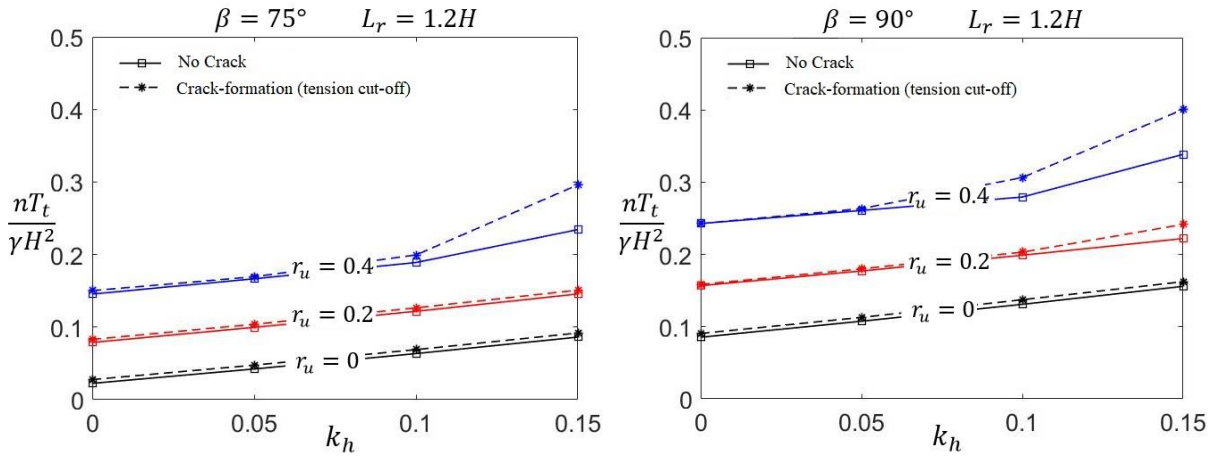

Figure 2-32 Required reinforcement strength against seismic coefficient for intact and cracked backfills

Figure 2-33 shows the soil cohesion effect on the required reinforcement strength to ensure the reinforced earth wall stability under different values of pore-water coefficients for a uniform backfill soil. The horizontal seismic coefficient is equal to 0.1. The normalized reinforcement strength is significantly increased with the pore pressure coefficient increase. It is clear that the wall performance is improved by increasing the soil cohesion. When the soil cohesion increases, the normalized required reinforcement strength decreases for different values of r_u, for both reinforced earth walls inclinations. The influence of c is greater for the case of a pore-water coefficient r_u equal to 0.4. The required reinforcement strength is slightly greater for the crack presence case. The discrepancy between the curves corresponding to the cases of crack formation as a part of the failure mechanism and no crack is more noticeable when the soil cohesion increases.

For the inclined retaining wall with $\beta = 75°$, the normalized reinforcement strength required to ensure the reinforced earth wall stability is equal to zero for a soil cohesion c higher than 19 kPa and a pore-water coefficient r_u equal to zero. The structure is stable without reinforcing the backfill with geosynthetics elements.

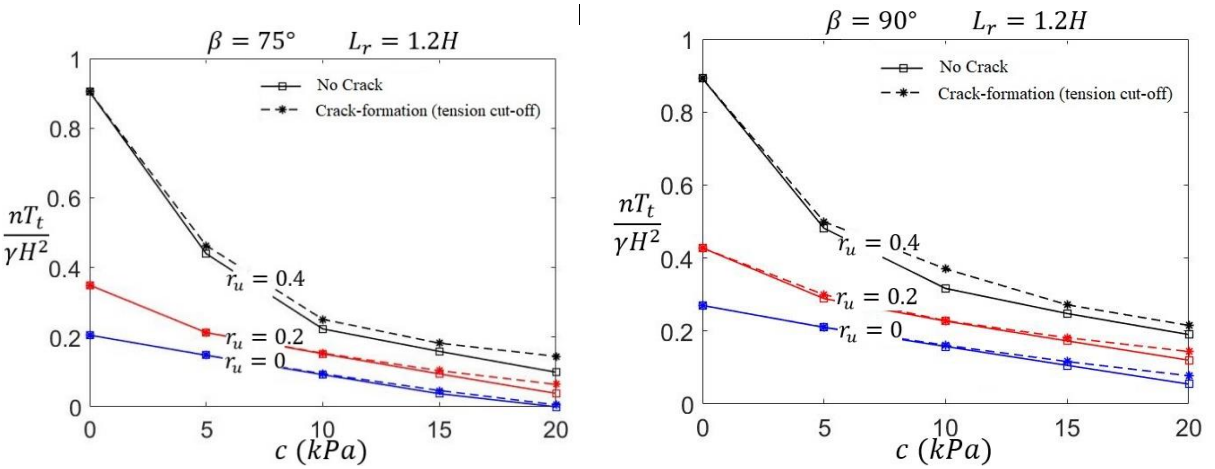

Figure 2-33 Required reinforcement strength against soil cohesion for intact and cracked backfill

The influence of the soil friction angle on the required reinforcement strength for the reinforced soil wall is presented in Figure 2-34 for different pore pressure coefficients. A uniform backfill soil and a horizontal seismic coefficient equal to 0.1 are considered. It is clear that higher friction angle implies better quality backfills and therefore, that the normalized required reinforcement strength decreases with the increase of the soil friction angle considering the presence of cracks or not, for different values of r_u and for both reinforced earth structures inclinations. The influence of φ is greater for larger values of r_u. The required reinforcement strength is slightly greater for the crack presence case. In addition, the difference between the curves corresponding to the cases of crack presence and no crack decreases when increasing φ as well as when decreasing r_u and the wall inclination.

For the inclined retaining wall with $\beta = 75°$, the normalized reinforcement strength required to ensure the reinforced soil wall stability is equal to zero for a soil friction angle higher than 37° and a pore-water coefficient r_u equal to zero.

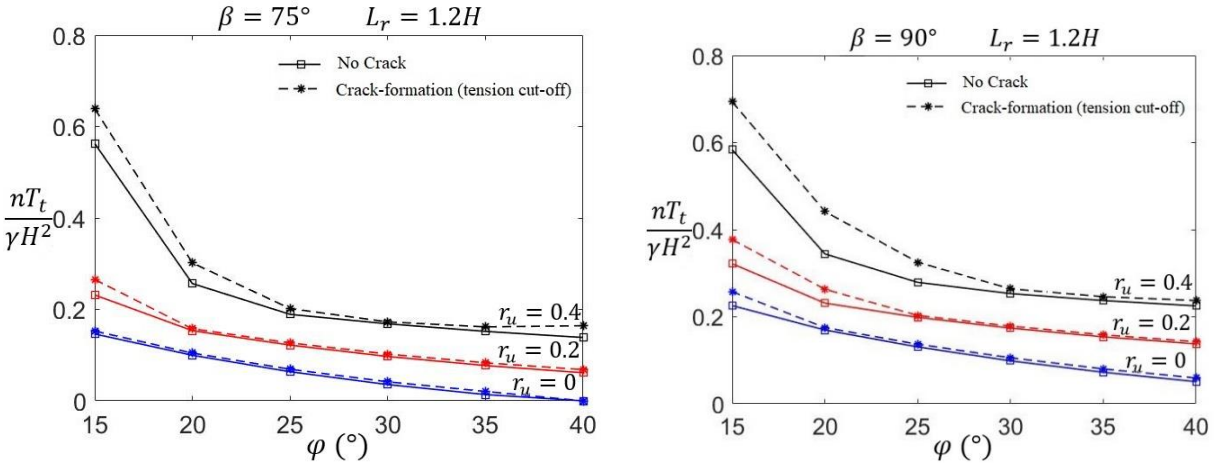

Figure 2-34 Required reinforcement strength against soil friction angle for intact and cracked backfill

2.4.4.2 Heterogeneous soil

Most analysis of reinforced soil retaining walls assume a homogeneous soil. However, soils are nonhomogeneous in nature and exhibit spatial variability in their properties (Pan and Dias, 2015). This heterogeneity affects the reinforced soil retaining walls stability. Hence, it is important to consider it in the reinforced wall design. The traditional kinematic approach can only be applied to homogeneous soils. The discretization-based kinematic analysis method gives the ability to overcome this limitation, and to consider the soil heterogeneity. The variation of the soil strength parameters, the soil cohesion and friction angle, are considered, whereas the soil unit weight γ is considered constant in the whole domain. For convenience and simplicity, two cases are considered in this study. In the first case, the soil

properties are assumed to increase linearly with depth. In the second one, a layered backfill soil profile is analyzed.

2.4.4.2.1 Linearly increased soil strength profile

The soil strength parameters are assumed to vary linearly only in the vertical direction, as shown in Figure 2-35 but are constant on the horizontal plane. The soil unit weight variation is neglected in the whole domain. φ_1 and c_1 are respectively the soil friction angle and cohesion at the ground surface. φ_2 and c_2 are those at the wall toe level.

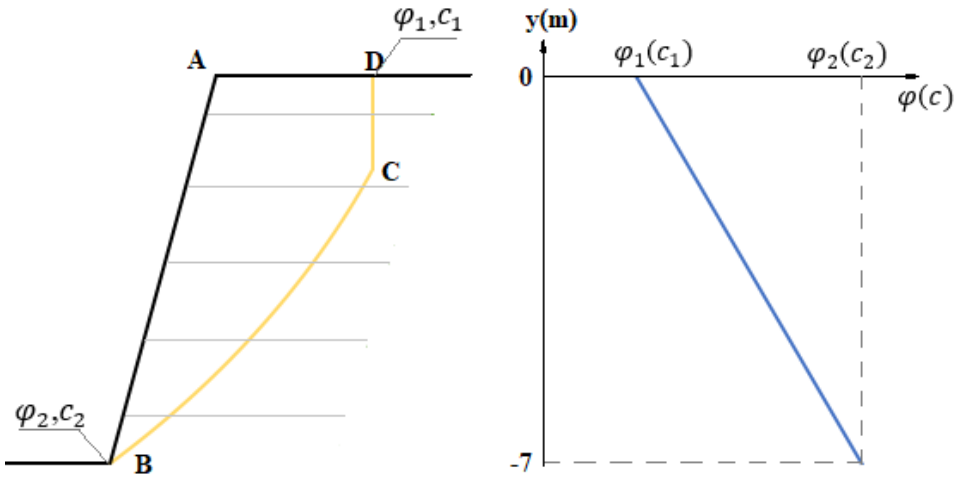

Figure 2-35 Variation of the soil properties in the backfill

The effect of each soil strength parameters variability is investigated separately. When analyzing the influence of a parameter, the second one is taken as constant. An inclined reinforced soil wall with β=75° is considered. The other parameters are kept the same as the previous section: H=7 m, γ=18 kN/m^3, $\delta\theta$=0.01^o, λ=0.5, L_r=1.2 H, n=10, f_0^*=1.2, f_1^*=0.6, f=1.2, V_S=150 m/s, V_P=280.5 m/s, and T=0.3 s

First, the effect of the soil cohesion variability is considered. The required normalized reinforcement strength is plotted against different soil cohesions c_1 at the ground surface as shown in Figure 2-36. The soil cohesion at the wall toe level is kept equal to c_2=12.6 kPa. The soil friction angle is considered constant across the whole field φ_1=φ_2=25°.

A decrease of the required reinforcement strength is observed when c_1 increases from 2.5 to 22.5 kPa for both cases of intact or cracked soil. The required reinforcement strength in the crack presence is greater than for an intact soil. The difference between the two cases is more pronounced for greater values of c_1. The required reinforcement strength decreases linearly with c_1 for the case of water-pressure coefficients r_u equals to 0 and 0.2. However, for $r_u = 0.4$, the rate of decrease is greater for c_1 smaller than 7.5 kPa. This is due to the pullout failure in some reinforcement layers in this case.

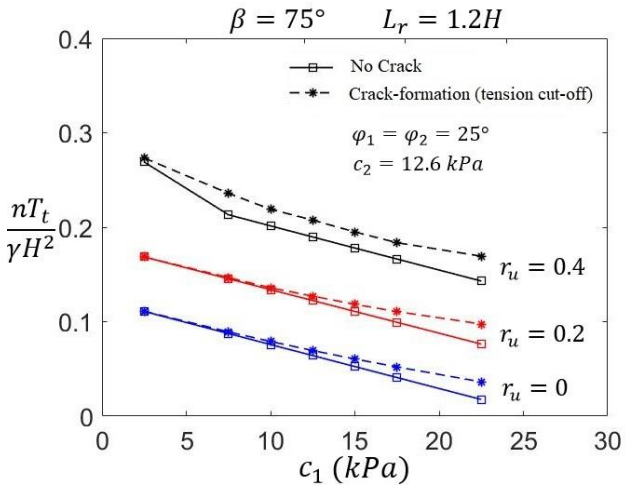

Figure 2-36 Required reinforcement strength against non-uniform soil cohesion for intact and cracked backfill

The effect of the soil friction angle variability is also considered. Figure 2-37 shows the required normalized reinforcement strength against different soil friction angles φ_1 at the ground surface. The soil friction angle at the wall toe level is kept equal to φ_2=25°. The soil cohesion is considered constant across the whole field c_1=c_2=12.6 kPa.

The increase of φ_1 from 15° to 35° decreases slightly the required normalized reinforcement strength and therefore, this increase slightly enhances the reinforced soil wall stability for both intact and cracked soils and different values of r_u. The required reinforcement strength is slightly greater for the crack presence case except when the soil friction angle φ_1 at the wall toe is smaller than 25° and the pore-water pressure $r_u$is equal to 0.4. Wherein that case, the difference between the intact soil case and the cracked soil one becomes significant, and increases with the soil friction angle φ_1 decrease. This is due to the pullout failure in some reinforcement layers in the case of cracked soils.

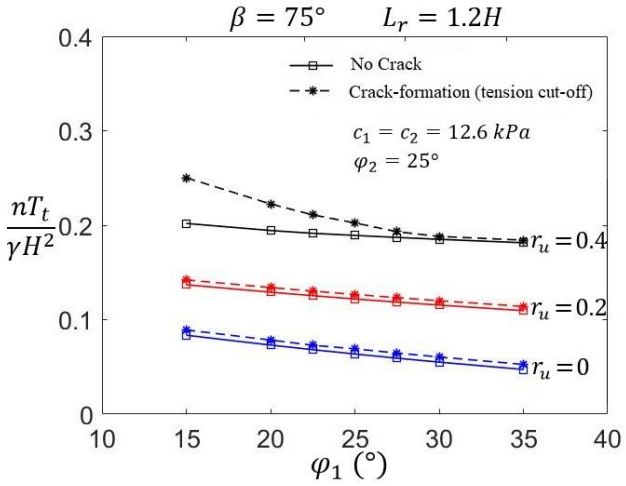

Figure 2-37 Required reinforcement strength against non-uniform soil friction angle for intact and cracked backfill

2.4.4.2.2 Layered soil profile

In most of the real cases, the soil profile is a layered one. In this section, a reinforced soil retaining wall with a backfill composed of two soil layers with different soil strength parameters, as shown in Figure 2-38, is analyzed using the proposed mechanism. A coefficient m is defined to distinguish the stratified condition as the ratio of the upper layer height to the wall height. The soil strength parameters are φ_1 and c_1 in the upper layer and φ_2 and c_2 in the lower layer.

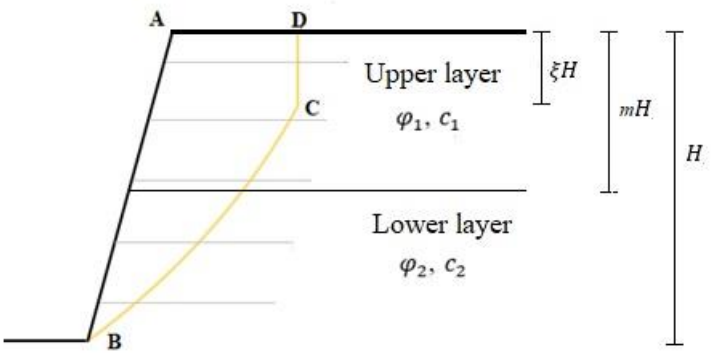

Figure 2-38 Heterogeneous backfill with two soil layers

The reinforced soil wall considered is inclined with β=75° and all the parameters are kept the same as the previous sections except the soil strength parameters. Figure 2-39 shows the pore-water pressure coefficient r_u and soil cohesion c_2 of the lower layer influences on the normalized required reinforcement strength. Two crack cases are considered: No-crack and crack-formation as a part of the failure mechanism. A two-layered backfill required a greater reinforcement strength to ensure the structure stability when the coefficient r_u increased and when the soil cohesion c_2 in the lower layer decreased.

The required reinforcement strength is slightly greater when considering the crack in the failure mechanism. An increase in the lower layer soil cohesion c_2 from 10 to 20 kPa leads to 35.37% and 36.73% reduction of the normalized required reinforcement strength for intact and cracked soil respectively, for a pore-water pressure coefficient equal to 0.4. These reductions become respectively equal to 57.21% and 56.35% for intact and cracked soils when the pore-water pressure coefficient is equal to zero.

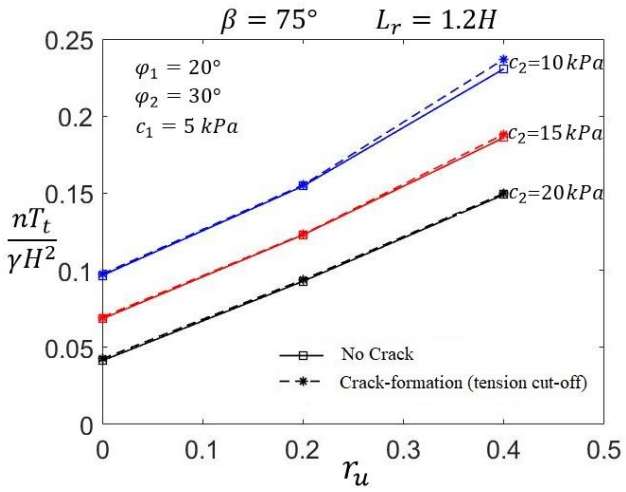

Figure 2-39 Required reinforcement strength against r_u and soil cohesion c_2 for a two-layered backfill

Figure 2-40 illustrates the influence of the pore-water pressure coefficient r_u and lower layer soil friction angle φ_2 on the normalized required reinforcement strength. The same two crack cases are considered. A reinforced soil wall is more stable when the coefficient r_u decreased and when the soil friction angle φ_2 in the lower layer increased. This is logical since the water has a destabilizing effect and the soil friction angle increase enhances the wall stability by providing an additional resistance.

The required reinforcement strength is also slightly greater for the crack-formation case as a part of the failure mechanism. A decrease in the lower layer soil friction angle φ_2 from 35 to 25° leads to respectively 75.8% and 77.12% of normalized required reinforcement strength increase for intact and cracked soil, for a pore-water pressure coefficient equal to zero. These increases become respectively equal to 25.73% and 29.84% for intact and cracked soil when the pore-water pressure coefficient is equal to 0.4.

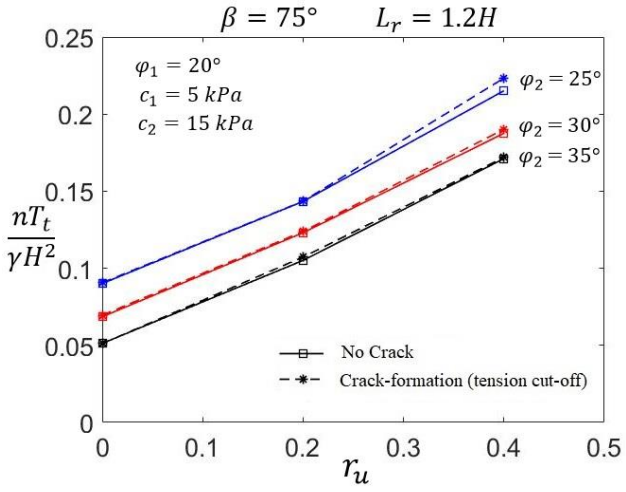

Figure 2-40 Required reinforcement strength against r_u and soil friction angle φ_2 for a two-layered backfill

2.5 Reinforced soil retaining walls: Unsaturated soils

2.5.1 Problem statement

Most previous studies of the internal stability of reinforced soil walls analysis are conducted assuming dry soils. On the other hand, when the water is considered, a saturated soil is generally assumed like in the previous section. However, natural soils are unsaturated in nature and the unsaturated soil properties are greatly different from dry or saturated ones. The soil matric suction increases the soil shear strength (Li and Yang, 2019). Therefore, it should be taken into consideration when performing a stability analysis to avoid an underestimation of the reinforced soil structures safety factor and for the sake of realistic designs (Vahedifard et al., 2016; Li and Yang, 2019). Recently, several works have been conducted to analyze geotechnical structures with partially saturated soils (Vahedifard et al., 2016; Yao and Yang, 2017; Huang et al., 2018; Xu and Yang, 2018; Li and Yang, 2019; Yang and Chen, 2019; Yang et al., 2019). Portelinha and Bueno (2012), Vahedifard et al. (2016) and Yang and Chen (2019) among others, investigated the stability of reinforced soil structures with unsaturated soils, numerically, analytically and experimentally. However, their studies are limited to static cases. Several formulas are proposed to describe the shear strength of unsaturated soils in the literature starting since Fredlund et al. (1978).

This section investigates the internal seismic stability of geosynthetic-reinforced unsaturated soil retaining walls. The groundwater level can be located at any reinforced backfill depth. Several nonlinear equations relating the unsaturated soil shear strength to the matric suction and different backfill type of soils are considered in this study.

The pseudo-dynamic approach is used to represent the seismic loading.

The reinforced soil structure of height H, reinforcement length L, reinforcement tensile strength T_m and wall inclination from the horizontal surface β is sketched in Figure 2-41. The water level depth is defined by the parameter ξ_w. The whole rigid block ABDC rotates around the point O with an angular velocity Ω. The geometry of the failure mechanism is determined by two parameters r_B and θ_B.

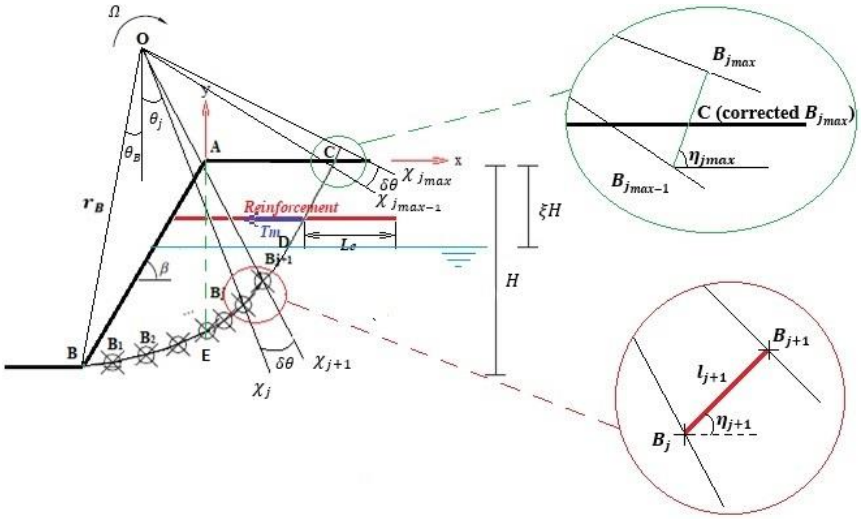

Figure 2-41 Discretization technique for the generation of the log-spiral failure mechanism

2.5.2 Nonlinear shear strength of unsaturated soils

For unsaturated soils, the existence of the soil suction tends to increase the soil cohesion and consequently the shear strength. Initially, the unsaturated shear strength was considered to be a linear function with the matric suction. Fredlund et al. (1978) extends the classical Mohr-Coulomb shear strength equation to include the linear increase of the shear strength due to soil suction. It is given as:

$$\tau_f = c' + (\sigma_n - u_a)\tan\varphi' + (u_a - u_w)\tan\varphi^b \tag{2-49}$$

where τ_f is the unsaturated soil shear strength, c' the effective cohesion, $(\sigma_n - u_a)$ is the net normal stress on the failure plane, φ' the effective friction angle, $(u_a - u_w)$ the matric suction with u_a and u_w being respectively, the pore air pressure and the pore water pressure. φ^b represents the rate of the shear strength increase relative to the matric suction and it is commonly taken in the order of 15° based on a limited number of datasets (Zhang et al., 2014; Xu and Yang, 2018).

The assumption of linearity of the unsaturated soil shear strength was revoked after experimental results conducted later that cover a wide range of matric suctions (Escario and Sáez, 1986; Fredlund et al., 1987; Yang and Chen, 2019; Li and Yang, 2019). It was clearly found that the relation between the shear strength envelope and the matric suction is not linear. These experimental results in addition, have showed that there is a relation between the unsaturated shear strength and the soil-water characteristic curve (SWCC) (Zhang et al., 2014). Figure 2-42 shows the entire shear strength envelope of a typical unsaturated soil. It can be divided into three sections. The unsaturated soil behaves as a saturated soil when the matric suction is lower than the air-entry value (AEV). The non-linearity begins once the matric suction exceeds the AEV. When the matric suction is greater than the residual suction, the behavior is highly dependent on the soil type. The shear strength becomes generally horizontal in the residual zone for plastic clays and silts. On the other hand, cohesionless soils show a reduction in their

shear strength in this zone. To highlight the behavior divergence of different types of unsaturated soils, four different soils are used in this study (Fredlund and Xing, 1994). The main parameters of the four SWCCs are given in Table 2-4, where SWCCs 1-4 represent respectively, a sandy soil, fine-grained soil (silt), clay and extremely fine-grained soil.

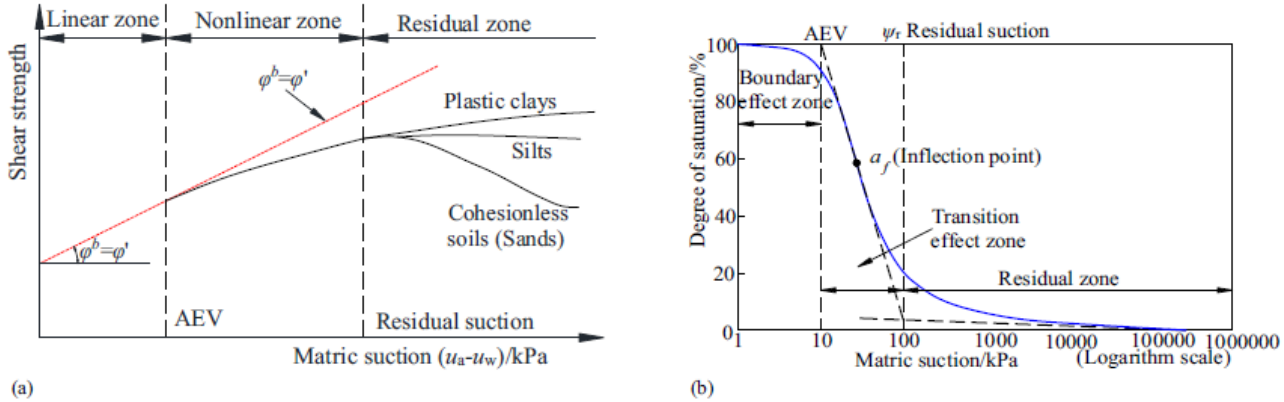

Figure 2-42 Relationship between unsaturated soils and SWCC from Zhang et al. (2014): (a) typical unsaturated shear strength envelopes; (b) SWCC for typical soil

Table 2-4 SWCC parameters by Fredlund and Xing (1994)

SWCC	$\boldsymbol{\theta_s}$	$\boldsymbol{a_f(kPa)}$	$\boldsymbol{n_f}$	$\boldsymbol{m_f}$	$\boldsymbol{\psi_r(kPa)}$	AEV($\boldsymbol{kPa}$)	$\boldsymbol{\theta_r}$	$\boldsymbol{k}$	$\boldsymbol{c_{ult}(kPa)}$
1	0.4	1	2	1	10	0.5	0.081	1.0	11.4
2	0.4	10	2	1	100	5	0.080	1.8	13.7
3	0.4	100	2	1	1000	50	0.078	2.2	28.4
4	0.4	1000	2	1	10000	500	0.073	2.5	107.3

Several equations have been proposed to define the nonlinear relationship between the unsaturated soil shear strength and the matric suction (Fredlund et al., 1996; Vanapalli et al., 1996; Bao et al., 1998; Khalili and Khabbaz, 1998; Vilar, 2006). These equations are grouped and presented in Table 2-5, Where θ_w, θ_s and θ_r are the volumetric water content, saturated volumetric water content and residual volumetric water content, respectively; S is the degree of saturation; S_r is the residual degree of saturation; c_{ult} is the ultimate undrained shear strength of an air-dried soil sample and ψ_r is the residual suction. According to Fredlund and Xing (1994), θ_w can be calculated using the SWCCs parameters as follow:

$$\theta_w = \left[1 - \frac{ln\left(1+{}^{\psi}/_{\psi_r}\right)}{ln\left(1+{}^{10^6}/_{\psi_r}\right)}\right] \frac{\theta_s}{\left\{ln\left[\exp(1)+\left({}^{\psi}/_{a_f}\right)^{n_f}\right]\right\}^{m_f}} \tag{2-50}$$

Where ψ is the matric suction.

Table 2-5 Apparent cohesion due to matric suction

Unsaturated shear strength equation	Cohesion due to the matric suction
Fredlund et al. (1978)	$c_{(u_a-u_w)} = (u_a - u_w)\tan\varphi^b$
Fredlund et al. (1996)	$c_{(u_a-u_w)} = (u_a - u_w)\Theta_d^k \tan\varphi'$ where $\Theta_d = \theta_w/\theta_s$, k is a fitting parameter.
Vanapalli et al. (1996)	$c_{(u_a-u_w)} = (u_a - u_w)\left[\tan\varphi' . \left(\frac{\theta_w - \theta_r}{\theta_s - \theta_r}\right)\right]$ or $c_{(u_a-u_w)} = (u_a - u_w)\left[\tan\varphi' . \left(\frac{S - S_r}{100 - S_r}\right)\right]$
Vilar (2006)	$c_{(u_a-u_w)} = \frac{(u_a - u_w)}{a + b(u_a - u_w)}$ Where $a = \frac{1}{\tan\varphi'}$, $b = \frac{1}{(c_{ult}-c')}$ Or $b = \frac{1}{(c_{measured}-c')} - \frac{a}{\psi_{measured}}$
Khalili and Khabbaz (1998)	$c_{(u_a-u_w)} = (u_a - u_w)[\lambda']\tan\varphi'$ Where $[\lambda'] = 1.0$ if $(u_a - u_w) \le AEV$ $[\lambda'] = \left(\frac{u_a-u_w}{AEV}\right)^{-0.55}$ if $(u_a - u_w) > AEV$
Bao et al. (1998)	$c_{(u_a-u_w)} = (u_a - u_w)[\zeta]\tan\varphi'$ Where $[\zeta] = 1.0$ if $(u_a - u_w) \le AEV$ $[\zeta] = \frac{\log(u_a-u_w)_r - \log(u_a-u_w)}{\log(u_a-u_w)_r - \log(AEV)}$ if $AEV < (u_a - u_w) < \psi_r$ $[\zeta] = 1.0$ if $(u_a - u_w) \ge \psi_r$

With regard to the matric suction distribution in unsaturated soils, it is affected by the hydrologic properties and the environmental factors among other factors (Yao and Yang, 2017). The widely used distribution in the literature is the uniform one (Figure 2-39a). However, another estimation of the matric suction distribution is the linear variation of matric suction with depth (Yao and Yang, 2017; Xu and Yang, 2018). The matric suction of the unsaturated part in this case is taken equal to zero at the water table level and increases proportionally with the distance between the water table level and the calculation point as illustrated in Figure 2-43b (ρ is the magnitude of linearly distributed matric suction).

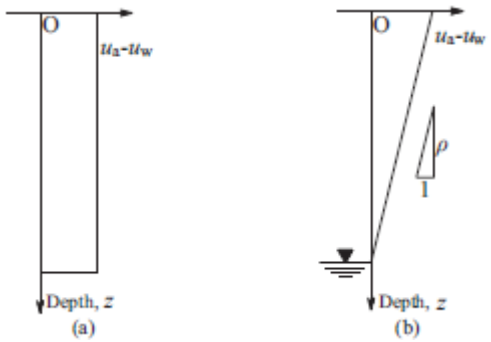

Figure 2-43 Distributions of matric suction: (a) Uniform distribution with depth; (b) Linear distribution of the matric suction

The required reinforcement strength to stabilize the reinforced soil walls is determined by equating the external work rates and the internal energy dissipation rates as follows:

$$\dot{W}_\gamma + \dot{W}_{kh} + \dot{W}_{kv} + \dot{W}_u = \dot{D}_c + \dot{D}_T \tag{2-51}$$

The internal energy dissipation expression along the sliding surface $\dot{D}_c$ is expressed as:

$$\dot{D}_c = \sum\left(c_{tot}.\left(L_j.\Omega.\cos\varphi\right).l_j\right) \tag{2-52}$$

c_{tot} used in the internal energy dissipation expression along the sliding surface $\dot{D}_c$, is the total cohesion; it is equal to the effective cohesion c' in the saturated zone and to the sum of c' and the apparent cohesion c_u due to the matric suction in the unsaturated zone which is given in Table 2-5.

The pullout force for a single layer of reinforcement is divided into two cases:

$$T_p = 2\gamma z^*(1 - r_u)L_e f^* \qquad in\ the\ saturated\ zone \tag{2-53}$$

$$T_p = 2\gamma z^* L_e f^* \mu_{(u_a - u_w)} \qquad in\ the\ unsaturated\ zone \tag{2-54}$$

where z^* is the overburden depth; L_e is the effective length; f^* corresponds to the apparent friction coefficient at the soil/reinforcement interface. $f^* = F^*.\alpha$ where F^* is the pullout resistance factor and α is the correction factor to account for a nonlinear stress reduction over the embedded length of highly extensible reinforcement, $\mu_{(u_a - u_w)}$ is a coefficient to explicitly account for the influence of the soil suction on the soil reinforcement pullout capacity. There is no presence of an expression in the literature for the parameter $\mu_{(u_a - u_w)}$. However, some researchers such as Esmaili et al. (2014), investigated the influence of matric suction on the pullout capacity of geotextile reinforcement. This study provides some graphs for this additional parameter that must be included in the equation of the pullout force at the interface reinforcement/soil in function of the water content w and the parameter value are always within the range of 0.6 - 1.15 depending on the test and the water content. In this thesis, a value of 0.85 is used for $\mu_{(u_a - u_w)}$.

The pore-water pressure work rate in the saturated zone is included as an external loading. Since a rigid block is assumed in this study, the work rate of the pore pressure effect along the discontinuity surface is then given as follows:

$$\dot{W}_u = -\int_S u.n_i.v_i dS \tag{2-55}$$

Where u is the pore-water pressure; S the boundary surface of the failure mechanism; n_i the outward unit vector normal to the surface S; v_i the velocity vector in the collapse block, respectively.

The so-called pore-water pressure coefficient r_u is used to represent the pore water pressure u as in the previous section. At a depth h below the water table level, u is assumed to be equal to $r_u \gamma h$.

The calculations of the pore water pressure work rate should be divided into two different cases, which are as follows:

In Figure 2-40, if the point D, that locates the water-table level, is above the point E:

$$\begin{cases} \dot{W}_u = \sum_j r_u.\gamma.\left(x_j.\tan\beta - y_j\right).l_j.\Omega.L_j.\sin\varphi & \text{along the boundary } BE \\ \dot{W}_u = \sum_j r_u.\gamma.\left(-y_j - \xi H\right).l_j.\Omega.L_j.\sin\varphi & \text{along the boundary } ED \end{cases} \tag{2-56}$$

Where x_j and y_j are the coordinates of point B_j.

Otherwise, if the point D is located below the point E, then:

$$\dot{W}_u = \sum_j r_u.\gamma.\left(x_j.\tan\beta - y_j\right).l_j.\Omega.L_j.\sin\varphi \quad \text{along the boundary } BD \tag{2-57}$$

According to the upper bound theorem, equating the internal energy dissipation with the external work rates, a lower bound to the required reinforcement strength is obtained through an optimization process, using three parameters as variables, namely the mechanism parameters r_B and θ_B and t the time involved in the pseudo-dynamic.

2.5.3 Results and discussions

In this section, the influence of key parameters on the reinforcement strength required to maintain the reinforced soil wall stability are investigated. These parameters include the soil friction angle, the horizontal seismic coefficient, the SWCC models corresponding to different soil types, the water table level, the soil suction distribution and different equations suggested for the apparent cohesion contributed by soil suction. The numerical results are obtained using the following input parameters:

H=7m, β=80°, γ=18 kN/m^3, c=6 kPa, $\delta\theta$=0.01^o, L_r=H, S_v=70 cm, F^*=$\frac{2}{3}\tan\varphi$, α=0.8, $\mu_{(u_a-u_w)}$ =0.85, f=1.2, V_S=150 m/s, V_P=280.5 m/s, T=0.3 s, λ=0.5 and t_0=0 s, where H is the wall height, β the wall inclination to the horizontal, γ the soil unit weight, c the soil cohesion, $\delta\theta$ the discretization angle, L_r the reinforcement length, S_v the reinforcement vertical spacing, F^* the pullout resistance factor, α is the correction factor, λ=k_v/k_h.

The results are provided in the form of graphs and tables and the required reinforcement strength is presented in a normalized form ($k_t/\gamma H$ where k_t is the average reinforcement strength).

2.5.3.1 Effect of the soil friction angle

To investigate the effect of the soil internal friction angle, the model of Fredlund et al. (1996) is used for the four different SWCC models as illustrated in Figure 2-44. A fully unsaturated soil and a uniform soil suction distribution are considered. The results are obtained for a seismic horizontal coefficient k_h equal to 0.15.

It can be seen from Figure 2-44 that the normalized required reinforcement strength decreases with the increase of the soil friction angle for different SWCC models and soil suction values. The decrease rate is important for $\varphi \leq 20°$ and this rate decreases for larger friction angle values. In addition, it can be seen that the soil matric suction enhanced the reinforced earth wall stability, especially for the soil models SWCC3 and SWCC4 where the normalized required reinforcement strength decreases significantly with the soil suction. However, for the SWCC1 and SWCC2 cases, the enhancement due to the soil suction is clearly reduced for important soil friction angles.

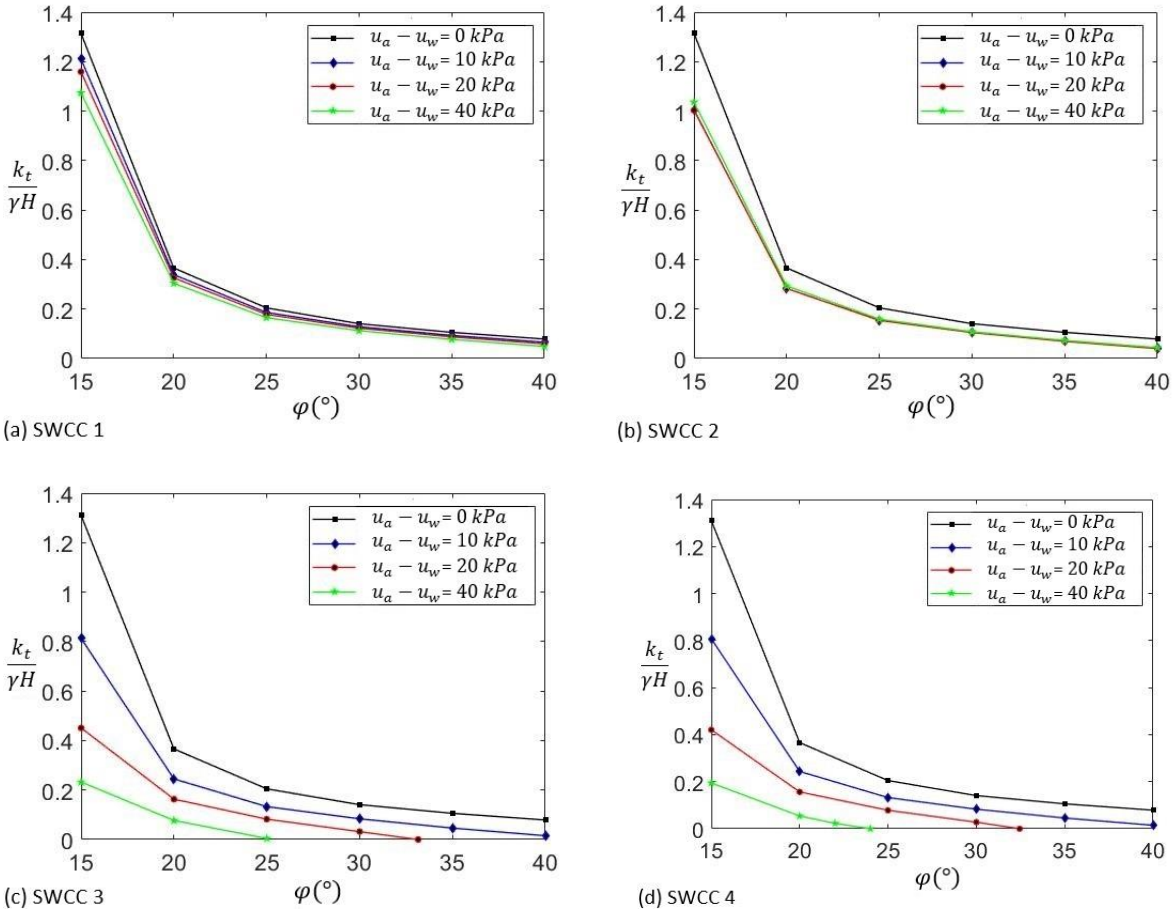

Figure 2-44 Influence of the soil internal friction angle: (a) SWCC 1; (b) SWCC 2; (c) SWCC 3; (d) SWCC 4

2.5.3.2 *Effect of the horizontal seismic coefficient*

Using the Fredlund et al. (1996) model for the four types of soil, the effect of the horizontal seismic coefficient for different soil matric suction values are presented in Figure 2-45. Fully unsaturated soils with a uniform soil distribution are considered. The soil friction angle is fixed here equal to 20°. Contrary to the friction angle influence part, the normalized required reinforcement strength increases with the increase of the horizontal seismic coefficient for different SWCC models. This is intuitive. For a soil matric suction equal to zero, the results are the same for different SWCC models since there is no apparent cohesion in all the models. However, for any soil matric suction value, the normalized required reinforcement strength is greater for the SWCC1 model and lower for the SWCC3 and SWCC4 ones which almost present the same value. It is also important to note that the required reinforcement strength decreases with the soil suction increase for all soil models except for the SWCC2 model which breaks this rule for the range of suctions considered.

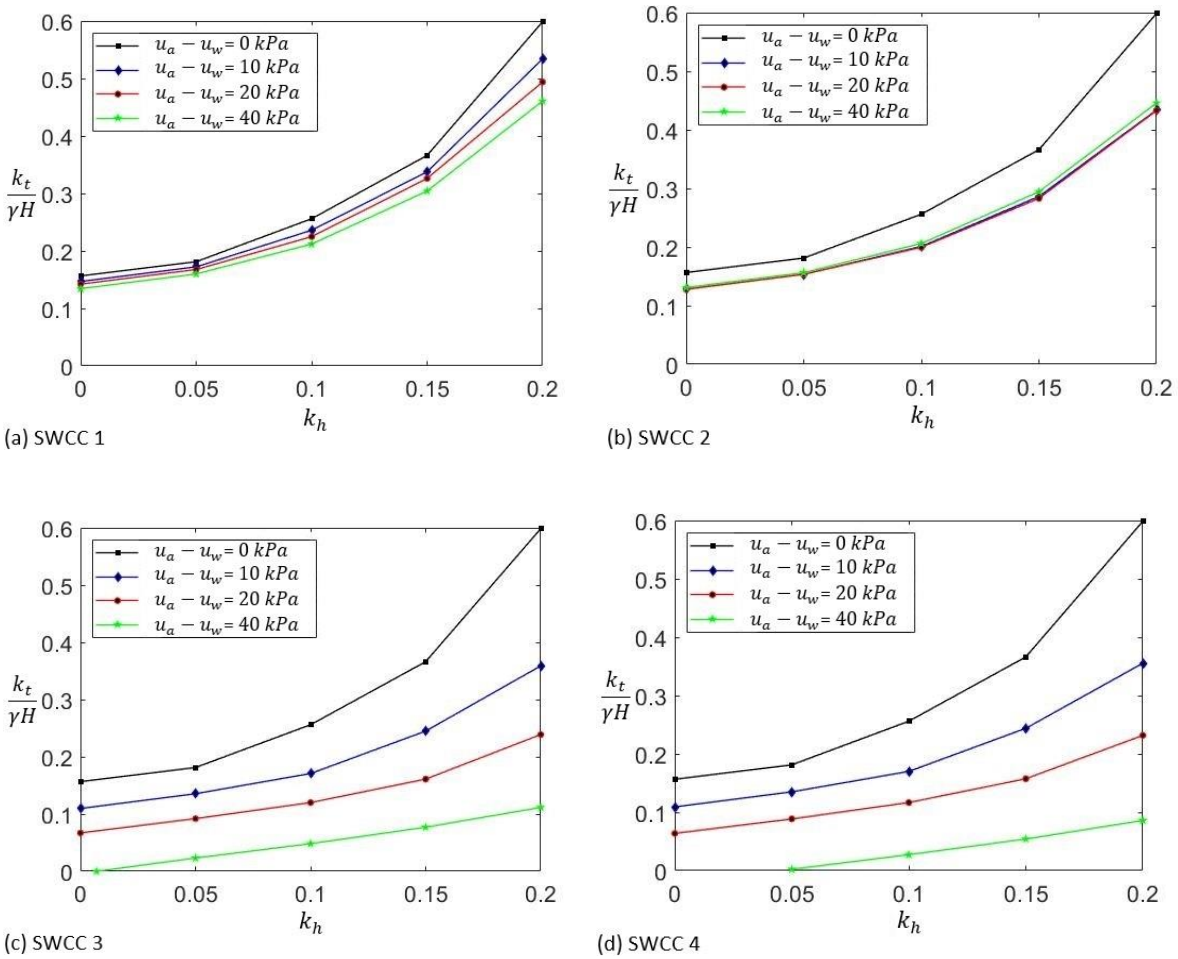

Figure 2-45 Influence of the horizontal seismic coefficient: (a) SWCC 1; (b) SWCC 2; (c) SWCC 3; (d) SWCC 4

2.5.3.3 Influence of the water table level

To investigate the effect of the water table level, the parameter ξ_w is considered. Numerical results are shown in Figure 2-46, considering a soil friction angle φ=25°, k_h=0.15. The equation proposed by Fredlund et al. (1996) is also used here to estimate the cohesion increment due to the matric suction in the unsaturated backfill zone. In the saturated zone, the pore-water pressure, as explained before, is considered as an external work and the pore-water pressure coefficient r_u is used to represent it (taken equal to 0.4). Figure 2-46 presents the normalized required reinforcement strength for different matric suctions in the unsaturated backfill zone, for different soil SWCC models, versus ξ_w. The matric suction in the unsaturated zone is uniformly distributed with depth until reaching the water table level above which the soil is saturated. When ξ_w is equal to zero, a saturated soil is considered. When it is equal to one, a fully unsaturated zone is considered. It can be seen that the starting point of all graphs is the same for all soil models. This is logic since the starting point corresponds to the fully saturated backfill case. The normalized required reinforcement strength decreases with the water table level depth increase for different soil models and matric suctions in the unsaturated zone. For the case of a matric suction equal to zero, the required reinforcement strength is the same for different soil models and water table levels. This is because there is no consideration for the apparent cohesion in the unsaturated zone. The effect of soil suction is more pronounced for deep water table levels and especially for soil models SWCC 3 and SWCC 4.

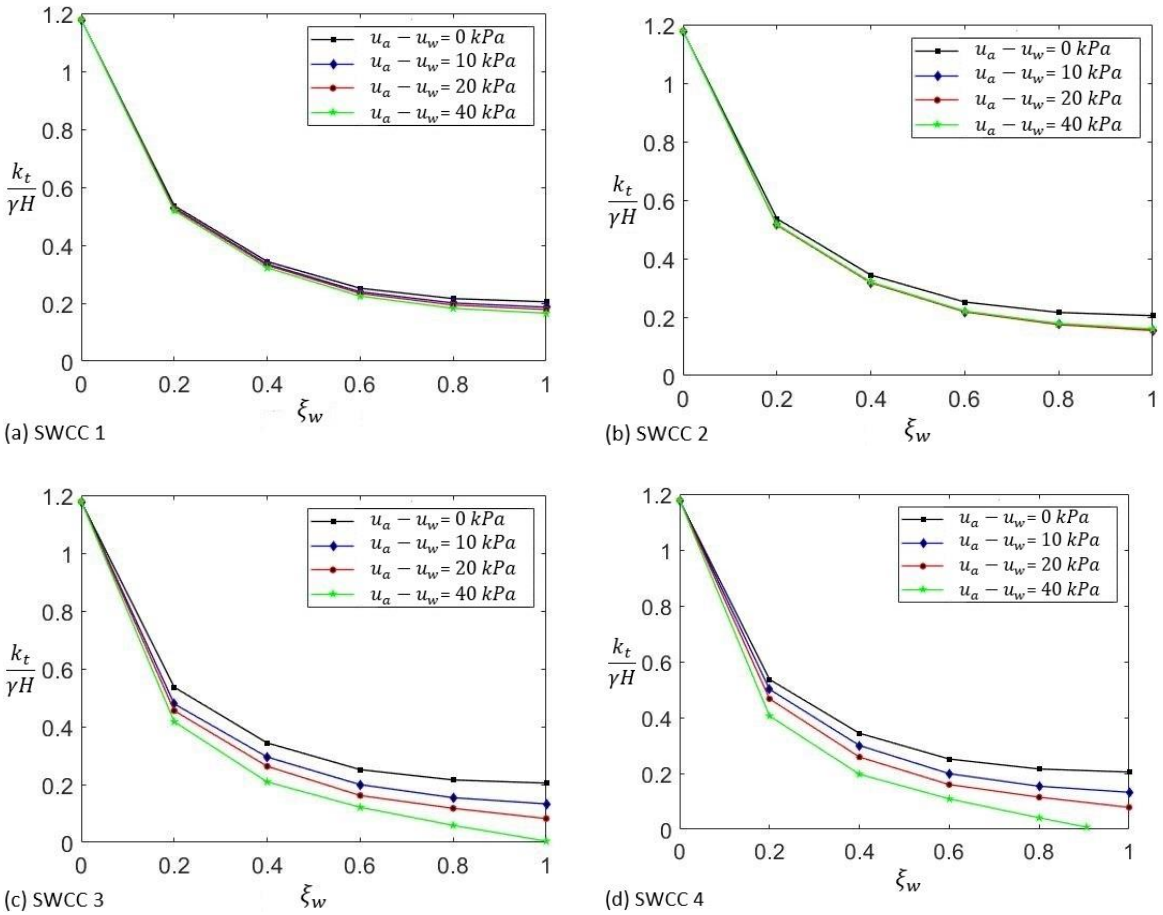

Figure 2-46 Effect of water table level under different matric suction: (a) SWCC 1; (b) SWCC 2; (c) SWCC 3; (d) SWCC 4

2.5.3.4 Influence of the saturation condition

In order to investigate the differences between the fully saturated and fully unsaturated cases, the normalized reinforcement strength required to maintain the structure stability are presented in Table 2-6 for different values of soil friction angle φ and horizontal seismic coefficient k_h. In the case of a fully unsaturated backfill soil, the soil matric suction is taken equal to $20\ kPa$, it is uniformly distributed with depth and the results are obtained for the four different types of soil. In the case of a saturated soil, the results are obtained considering two values of the pore-water pressure coefficient r_u: 0.3 and 0.4 (Table 2-6).

As concluded early, it can be seen from this table that the required reinforcement strength increases with the increase of the horizontal seismic coefficient k_h and the decrease of the soil friction angle φ for all the soil types and for both cases of fully saturated and unsaturated backfill. Concerning the fully unsaturated soil, it is obvious from the results that for the matric suction value $(u_a - u_w)$ equal to $20\ kPa$, the normalized reinforcement strength required for the wall stability is the largest in the case

of soil type SWCC1 that corresponds to sandy soils. It decreases for the case of SWCC2 corresponding to fine-grained soils. The lowest reinforcement strength required is for the case of soil type SWCC4 that corresponds to extremely fine-grained soils. This case is slightly greater than the case of SWCC3 corresponding to clays. On the other hand, for the fully saturated case, it is clear that the required reinforcement strength increases with the pore-water pressure coefficient r_u for all the values of φ and k_h. Comparing the saturated and unsaturated soil backfills, the required reinforcement strength in the case of saturated soil is higher than for the unsaturated cases. It can be ten times greater than the fully unsaturated soil depending on the soil types, the soil friction angle and the horizontal seismic coefficient. These results show the importance of considering the soil apparent cohesion in the stability analysis of these structure and the economic benefits that can results from this consideration.

Table 2-6 Required reinforcement strength $k_t/\gamma H$ with respect to the different saturation condition

$\boldsymbol{\varphi}(°)$	$\boldsymbol{k_h}$	Unsaturated				Saturated	
		SWCC1	SWCC2	SWCC3	SWCC4	$r_u = 0.3$	$r_u = 0.4$
15	0	0.208	0.188	0.135	0.132	0.55	0.958
	0.05	0.302	0.282	0.175	0.171	1.142	1.616
	0.1	0.522	0.453	0.261	0.256	1.86	2.286
	0.15	1.159	1.003	0.467	0.431	2.632	3.086
	0.2	1.914	1.734	1.039	1.004	3.522	4.054
20	0	0.142	0.128	0.067	0.064	0.291	0.414
	0.05	0.168	0.153	0.092	0.089	0.437	0.664
	0.1	0.225	0.20	0.12	0.117	0.877	1.425
	0.15	0.322	0.283	0.163	0.157	1.531	2.118
	0.2	0.494	0.411	0.239	0.232	2.277	2.898
25	0	0.098	0.083	0.016	0.013	0.221	0.269
	0.05	0.119	0.103	0.037	0.033	0.266	0.377
	0.1	0.143	0.127	0.059	0.055	0.366	0.587
	0.15	0.178	0.154	0.082	0.078	0.569	1.173
	0.2	0.241	0.211	0.111	0.107	1.106	1.84
30	0	0.065	0.048	0	0	0.194	0.238
	0.05	0.083	0.066	0	0	0.211	0.258
	0.1	0.102	0.085	0.012	0.008	0.247	0.35
	0.15	0.123	0.105	0.032	0.028	0.326	0.49
	0.2	0.148	0.13	0.053	0.049	0.453	0.75

2.5.3.5 Effect of the matric suction distribution

As discussed before, the matric suction distribution with depth is considered by the means of two estimations: a uniform distribution and a linear one. All the results presented before are based on a uniform distribution estimation. However, to investigate the effect of the matric suction distribution, Figures 2-47 and 2-48 show the required reinforcement strength for different soil types considering a uniform matric suction distribution and a linear increase with depth. The results are obtained for different water table levels and different matric suction values in the unsaturated zone. The pore-water pressure coefficient r_u is taken equal to 0.3 in the saturated zone. The soil friction angle and the horizontal seismic coefficient are respectively equal to 25° and 0.15. Five different water table levels are considered by taking five different values of the parameter ξ_w: 0.4, 0.7, 1, 1.3 and 1.6. In the case of the matric suction uniform distribution, the last three values correspond to the same case.

The results show that for both matric suction distribution cases, the required reinforcement strength decreases with the matric suction for any water table levels for the three soil types SWCC1, SWCC3 and SWCC4. The rate of increase is greater for the soil type models SWCC3 and SWCC4. However, for the soil type model SWCC2 corresponding to a fine-grained soil, the results show that the required reinforcement strength remains the same for a matric suction greater than $10\ kPa$. Comparing the different soil types, SWCC4 requires in both cases of matric suction distribution, the least amount of reinforcement. The required reinforcement strength in the case of SWCC3 is slightly greater than for the soil type model SWCC4. The first two soil type models SWCC1 and SWCC2 require a larger one than the SWCC3 and SWCC4 cases. The soil model SWCC1 requires a greater amount than the model SWCC2 for a matric suction lower than $80\ kPa$ in the case of matric suction uniformly distributed and lower than $40\ kPa$ in the case of a linear distribution.

Concerning the effect of the matric suction distribution, it is clear that the normalized reinforcement strength required for the wall stability is greater when considering a linear distribution for all the soil type models. This is because the matric suction linearly increases with depth results are lower than the matric suction uniformly distributed one. An exception exists at the ground surface where the values are equal. This results in a decrease of the apparent cohesion and therefore of the total soil cohesion. The differences in values between the two estimations increase with the increase of the parameter ξ_w i.e. when the water table is deeper in the soil mass. When the water table is below the wall toe (ξ_w greater than one), the required reinforcement strength remains the same in the case of a uniformly distributed matric suction and it continues to decrease in the other case. Therefore, for a fully unsaturated backfill, when the water table becomes deeper, the difference between the two distribution estimations becomes lower.

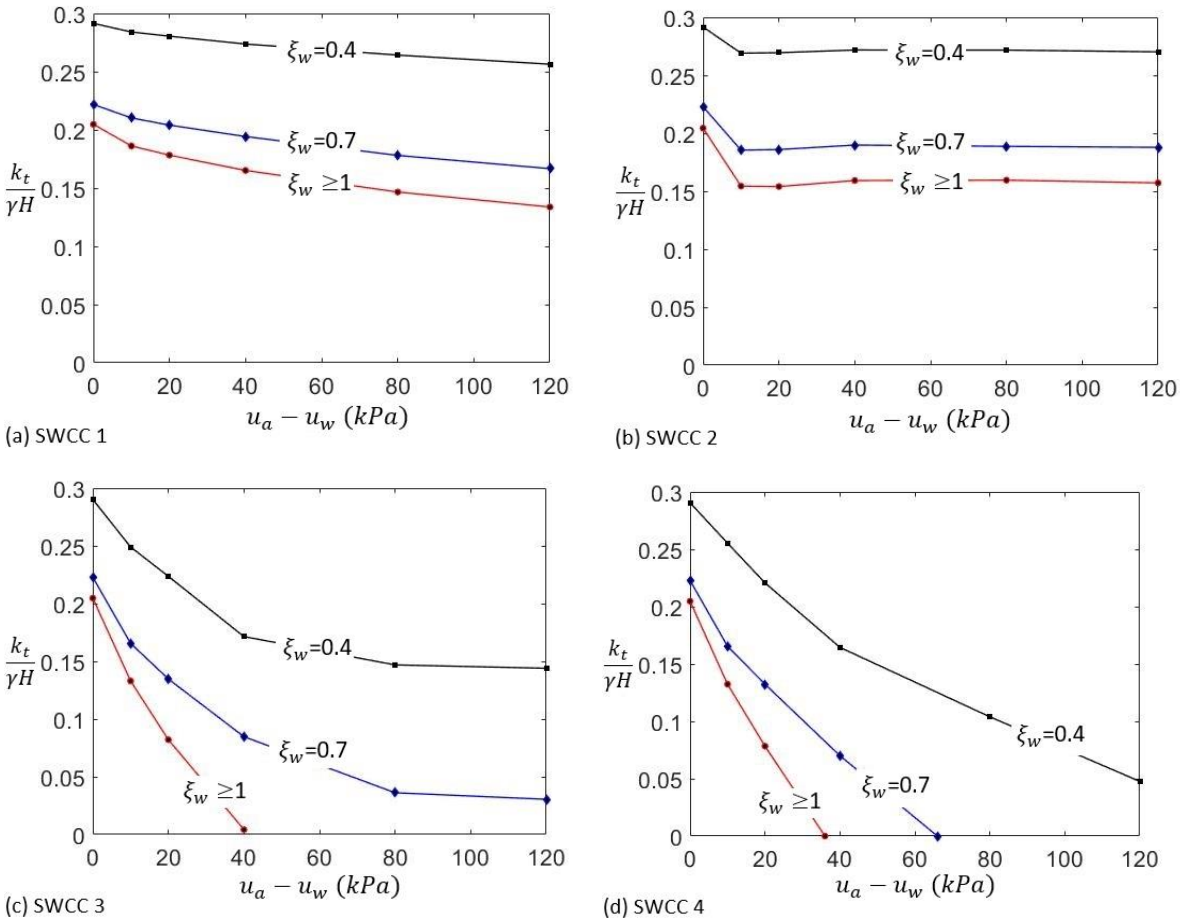

Figure 2-47 Required reinforcement strength for uniformly distributed soil matric suction (a) SWCC 1; (b) SWCC 2; (c) SWCC 3; (d) SWCC 4

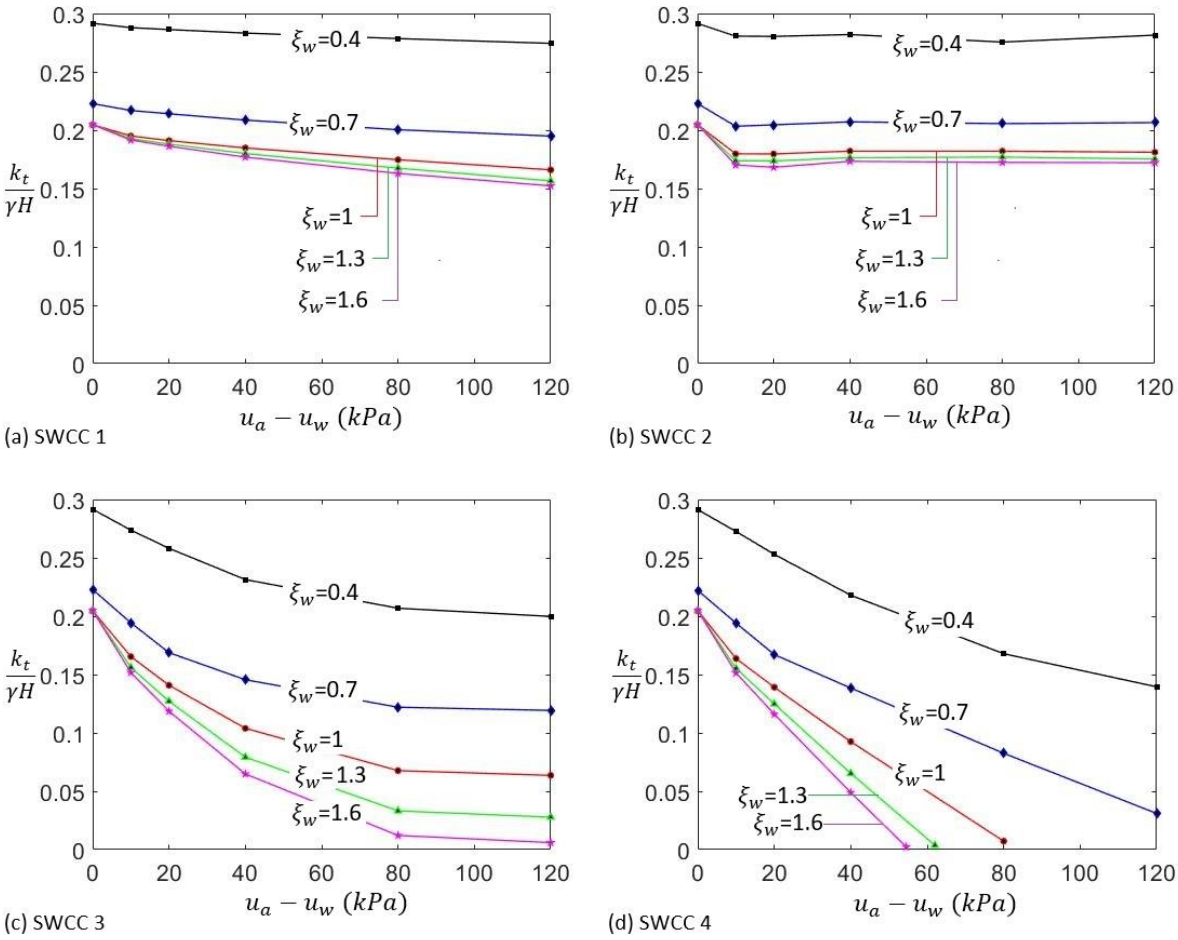

Figure 2-48 Required reinforcement strength for linearly distributed soil matric suction (a) SWCC 1; (b) SWCC 2; (c) SWCC 3; (d) SWCC 4

2.5.3.6 Effect of the shear strength model

All the results presented in the paper until now are based on the unsaturated soil shear strength proposed by Fredlund et al. (1996). However, Figure 2-49 presents the normalized required reinforcement strength versus the matric suction for various shear strength models of unsaturated soils and for four soils types. In addition to the basic input parameters presented in the introduction of the parametric study section, the backfill soil friction angle is considered equal to 20° and the horizontal seismic coefficient to 0.15. A fully unsaturated backfill soil and a uniform distribution for the matric suction are considered.

Regarding the soil type SWCC1 representing a sandy soil, as illustrated in Figure 2-49, the required reinforcement strength obtained using nonlinear models are greater than those obtained using the linear model proposed by Fredlund et al. (1978). The curve obtained under the model proposed by Vanapalli et al. (1996) presents the greater amount of required reinforcement strength that increases with the matric suction. The curves obtained under the model proposed by Bao et al. (1998) is horizontal. For the curve based on the model of Vilar (2006), the required reinforcement strength decreases nonlinearly for a

matric suction below $40\ kPa$, and then tends to decrease linearly. This decrease is not obvious and can be neglected. For the other two models proposed by Fredlund et al. (1996) and Khalili and Khabbaz (1998), the required reinforcement strength decreases linearly with the matric suction.

Regarding the soil type SWCC2 representing fine-grained soils, the required reinforcement strengths obtained using nonlinear models are also greater than those obtained using the linear model proposed by Fredlund et al. (1978). For the curves obtained by the model proposed by Fredlund et al. (1996), the required reinforcement strength decreases within a matric suction below $10\ kPa$ and then remains constant above this value. The curves of required reinforcement strength under the models proposed by Khalili and Khabbaz (1998) and Vilar (2006) present similar trends and the differences between the two curves are very small. For the models proposed by Vanapalli et al. (1996) and Bao et al. (1998), the curves show a similar trend but the required reinforcement strength obtained by the first model are greater than those obtained by the second.

For the soil type SWCC3 representing clays, the curves under all the nonlinear models except the model proposed by Vilar (2006), overlapped with a matric suction below $40\ kPa$. Above this value, the curves by the models of Bao et al. (1998) and Khalili and Khabbaz (1998) remain overlapped but the rate of nonlinearity for the two other models decreases and therefore, the required reinforcement strength are greater by the models proposed by Vanapalli et al. (1996) and Fredlund et al. (1996). The nonlinearity rate of the latter decreases more for the second. The required reinforcement strength obtained by the model proposed by Vilar (2006) are the larger among all the models, even for the linear one. This latter based on the linear model of Fredlund et al. (1978) falls between the curves of the model of Vilar (2006) and the other nonlinear models.

With regard to the extremely fine-grained soil presented by the soil model SWCC4, the curves of all nonlinear models, except the model of Vilar (2006), are overlapped. The required reinforcement strengths obtained by the linear model proposed by Fredlund et al. (1978) are the larger among all the models and the curves obtained by the model proposed by Vilar (2006) falls between the linear model curve and the overlapped nonlinear model curves.

From Figure 2-49, it can be concluded that the required reinforcement strength for the reinforced earth retaining walls is affected by the matric suction, soil types and the shear strength models used to calculate the apparent cohesion. It permits to highlight the importance of a careful choice of the shear strength models for unsaturated soils in order to obtain realistic solutions.

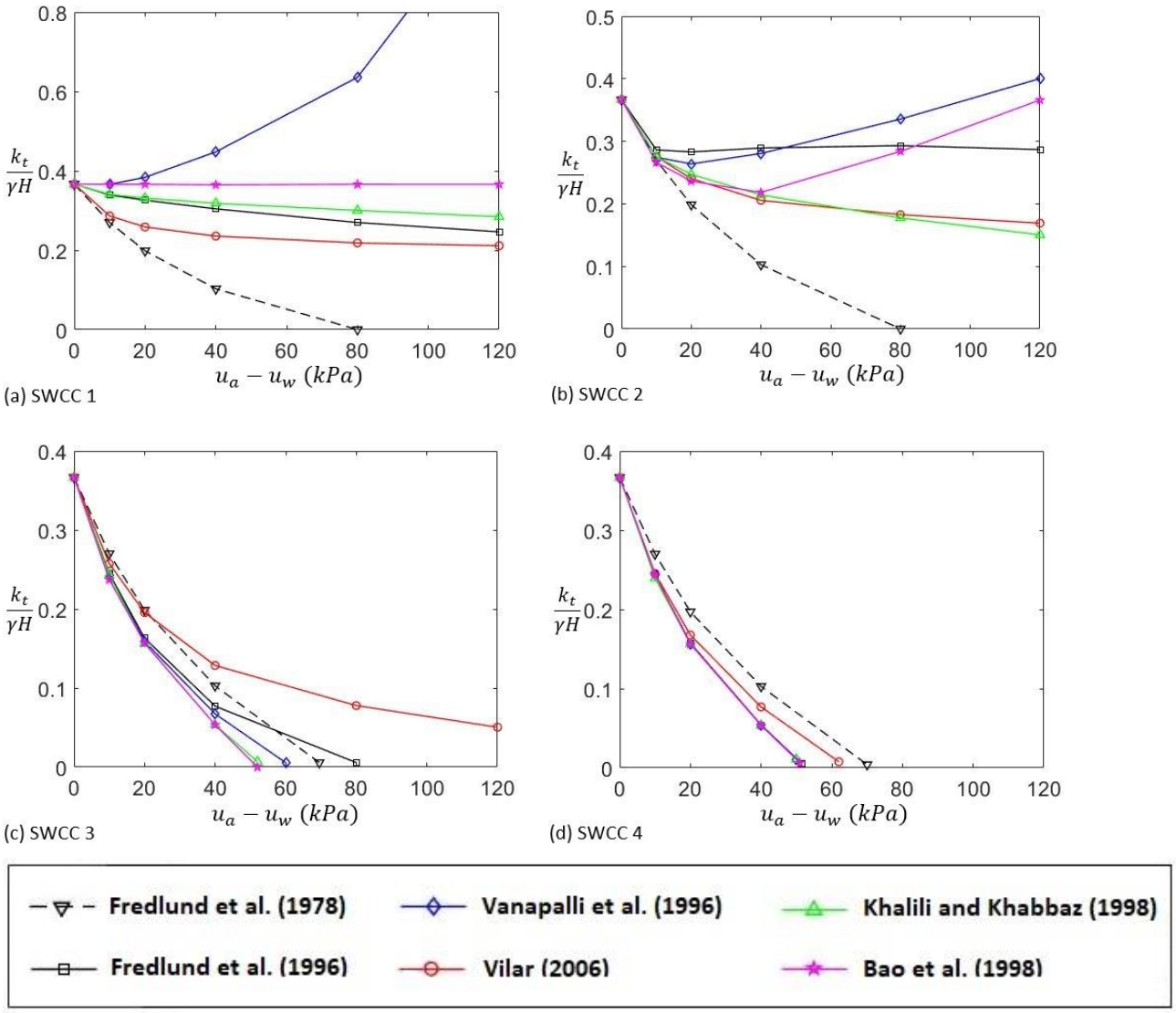

Figure 2-49 Effect of shear strength model on the required reinforcement strength with different soil types (a) SWCC 1; (b) SWCC 2; (c) SWCC 3; (d) SWCC 4

2.6 Conclusion

This chapter aims to investigate the seismic internal stability of reinforced soil retaining walls using the kinematic approach of limit analysis. The analysis is performed with an extension of the discretization technique proposed by Mollon et al. (2011). This technique is used to generate a rotational log-spiral mechanism point-by-point, which allows the possibility of presenting the seismic loading with a pseudo-dynamic approach and considers the soil heterogeneity. The crack-formation as a part of the failure mechanism as well as the pre-existing crack are considered. Three soil cases are considered, dry, saturated and unsaturated backfill soils. The proposed method is validated by comparison with results of existing studies based on the conventional kinematic approach.

The following conclusions are made:

The required normalized reinforcement strength decreases with the increase of the reinforcement length until a limit value above which, there is no benefit of the length increase.

The required normalized reinforcement strength is highly dependent on the soil properties. It decreases when increasing the soil friction angle and the cohesion, and their importance is more significant for higher values of horizontal seismic coefficient k_h.

From the analysis, the effects of the horizontal seismic coefficient k_h on the required reinforcement strength is also evident. Increasing k_h leads to an increase in the required reinforcement strength, and this is more pronounced for lower friction angles values.

For nonhomogeneous backfills, the soil friction angle distribution has an important effect on the required normalized reinforcements. More the soil friction angle exhibits variation, greater are the reinforcement forces required to maintain the structure stability. The effect of a variation of the soil cohesion has a lower effect on the required reinforcement force than the soil friction angle variation one.

The presence of the crack leads to an increase of the required reinforcement strength to ensure the stability of the reinforced soil wall, hence the importance of considering the cracks when using a cohesive soil.

The required normalized reinforcement strength obtained when using the pseudo-dynamic approach is generally larger than the one obtained using the pseudo-static approach. For a range of values of amplification factors f near to 1, the opposite occurs. Therefore, for a safety design, engineers must check the reinforcement using the two approaches for a soil class characterized by a low amplification factor. Otherwise, they should use the pseudo-dynamic approach to obtain a safe design.

More the water table is deep, less is the required reinforcement strength for the reinforced soil wall. This is generally more pronounced when the matric suction in the unsaturated zone is greater. Therefore, it is important to carefully estimate the water table level and to account for a possible variation of this level due to the weather or other possible reasons.

A comparison is presented for the two cases of fully unsaturated and fully saturated backfill soils. The results show a large reduction of the required reinforcement strength from saturated conditions to fully unsaturated conditions. Hence the importance of considering unsaturated soil properties instead of saturated ones can deal with economic benefits.

The required reinforcement strength is greater when considering a linear increased matric suction distribution than in the case of a uniform one.

The soil types represented by different SWCC models have a major influence on the required reinforcement strength for the wall stability. In addition, the increase of the soil matric suction decreases

the required reinforcement strength except for the case of fine-grained soils where the required reinforcement strength remains the same.

3 Chapter 3: Probabilistic stability analysis using random variables approach

3.1 Introduction

Despite being familiar to geotechnical engineers, the deterministic models based on the global factor of safety cannot reflect accurately all the uncertainties and can result in an overdesigns or instabilities when uncertainties are respectively smaller or greater than anticipated.

The objective of this chapter is to perform reliability-based analyses of the internal seismic stability of geosynthetic reinforced soil retaining walls. The uncertainty and variability of the soil shear strength parameters, reinforcement strength and characteristics of seismic loading are considered using random variables. When considering the reliability through random variables, in each simulation, the soil properties, the tensile reinforcement resistance and the soil-reinforcement interaction properties are considered to be the same in the entire physical domain but varied among different simulations following a given distribution. Therefore, the random variables approach cannot model the soil spatial variability since the soil properties changes in both the vertical and horizontal directions even in one soil stratum. However, this approach is adopted in this chapter due to its simplicity and the fast estimation of the reliability results comparing to the random fields approach. It is used to perform the reinforced soil wall reliability stability analysis. The response surface method based on the Sparse Polynomial Chaos Expansion (SPCE) combined with Monte Carlo Simulation is the reliability method considered to carry out the probabilistic analysis. The Sparse Polynomial Chaos Expansion could successfully deal with many random variables and provide an interesting alternative to the full Polynomial Chaos Expansion (PCE) approach.

The deterministic computation of the structure safety factor is based on the upper bound theorem of limit analysis, to ensure rigorous results. The discretization technique is used to generate the rotational failure mechanism so that the seismic loading could be implemented by the pseudo-dynamic approach (Alhajj Chehade et al., 2019a-2019b). The influence of the correlation between the soil parameters, the random variables distribution type and the uncertain parameters coefficients of variation on the probabilistic results are investigated and discussed. A global sensitivity analysis is performed in order to specify the contribution of each random variable on the reinforced soil retaining wall safety factor.

3.2 Reliability analysis for geosynthetic Reinforced Soil Retaining Walls

Reliability analyses through the random variables approach, were used by many researchers for the study of reinforced soil system problems (Chalermyanont and Benson, 2004-2005; Sayed et al., 2008; Basha and Sivakumar Babu, 2009-2010-2011-2012; Sivakumar Babu and Singh, 2011; Bathurst and Miyata,

2015; Luo et al., 2016; Ferreira et al., 2016; Zevgolis and Bourdeau, 2017; Javankhoshdel and Bathurst, 2017; Yu and Bathurst, 2017; Bathurst et al., 2019b). The majority of these works were conducted using deterministic limit equilibrium methods and deterministic finite or difference elements methods. The objective of this chapter is to perform a reliability analysis of geosynthetic reinforced soil retaining walls in which, the deterministic model is based on the kinematic approach of the limit analysis theory. This latter is combined with the discretization method (Alhajj Chehade et al., 2019a-2019b-2019d) to implement the pseudo-dynamic method of seismic loading that represents the earthquake acceleration better than the pseudo-static approach. Geosynthetic reinforcement resistance to shear, torsion and bending is negligible. In addition, the pore water pressure and the soil liquefaction phenomenon are not considered. The uncertainty and variability of the soil shear strength parameters, reinforcement strength and characteristics of seismic loading are considered using random variables.

3.2.1 Deterministic problem: Limit analysis model

The deterministic model is based on the kinematic approach of limit analysis combined with the discretization method. This combined analysis method was presented in Alhajj Chehade et al. (2019b-2021) and validated using the results of traditional limit analysis method available in literature (Michalowski, 1998a) as shown in chapter 2. The upper bound theorem of limit analysis is based on the work rate balance of the internal and external forces for any kinematically admissible velocity field. The use of this theorem in the internal stability assessment of geosynthetic reinforced soil retaining walls, gives a rigorous upper bound of the structure safety factor. A rotational toe two-dimensional mechanism is assumed since the previous results show that it represents the most frequently failure surface occurring for this type of retaining walls (Michalowski, 1997-1998a; Sabermahani et al., 2009). However, to implement the pseudo-dynamic approach in the seismic assessment, the discretization method is used for the generation of this log-spiral mechanism (Figure 3-1). In this figure, a backfill is considered (Horizontal surface), H denotes the wall height and β is the wall inclination. The region of soil ABC rotates around the point O with an angular velocity Ω. The idea of the discretization method is to define the failure surface by a set of points iteratively. The angle between two consecutives radial lines denoted χ_j which controls the discretization, is noted $\delta\theta$. It defines the accuracy of the failure mechanism. The finer is the value of the discretization angle, the more accurate is the log-spiral failure mechanism. An angle $\delta\theta = 0.1°$ is taken since it gives accurate results (Alhajj Chehade et al., 2021).

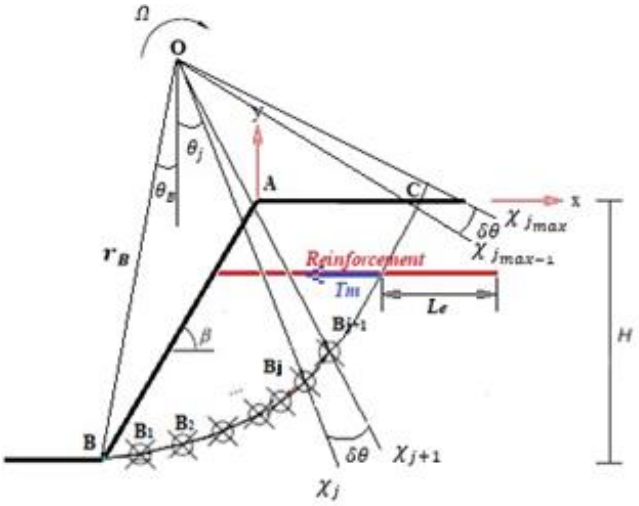

Figure 3-1 Discretization technique for the collapse mechanism of a reinforced earth retaining wall

Starting at the point B at the wall toe, each point B_j is defined using the previous known point, until reaching the surface by the point C. The point B is defined by the mechanism parameters r_B and θ_B where r_B is the length of $[OB]$ and θ_B is the angle between the y axis direction and the line (OB). Considering the point A as the origin of the coordinate system, the coordinates of the point B are calculated in terms of the mechanism parameters. The coordinates of the successively generated points are calculated using the trigonometrical and geometrical relations. Through the generation procedure, the mechanism must be kinematically admissible and therefore should respect the normality condition, requiring that the angle between the velocity vector and the discontinuity surface is equal to the internal friction angle φ. Chapter 2 provides more details about the discretization method and the generation process.

The pseudo-dynamic approach developed by Steedman and Zeng (1990) is used to represent the seismic loading instead of the commonly used pseudo-static approach. It considers the space and time variation of the dynamic loading. Many researchers used this approach in their studies (Choudhury and Nimbalkar, 2006-2007; Basha and Sivakumar Babu, 2009-2010-2011-2012; Choudhury et al., 2014; Qin and Chian, 2017; Zhou et al., 2018; Alhajj Chehade et al., 2019b-2020).

For a sinusoidal base shaking, the horizontal and vertical acceleration at any depth y and time t with a soil amplification f can be expressed as:

$$\begin{cases} a_h = \left[f + \frac{y}{H}(f-1)\right].k_h g \sin\frac{2\pi}{T}\left(t - \frac{H+y}{V_s}\right) \\ a_v = \left[f + \frac{y}{H}(f-1)\right].k_v g \sin\frac{2\pi}{T}\left(t + t_0 - \frac{H+y}{V_p}\right) \end{cases} \quad (3\text{-}1)$$

Where k_h and k_v are respectively, the horizontal and vertical seismic coefficients, g is the acceleration due to gravity and t_0 the phase difference between the two input shakings.

As mentioned above, the upper bound theorem of limit analysis is based on the work rate balance between the external forces, $\dot{W}$, and the internal energy dissipation, $\dot{D}$. Its application gives an upper bound to the reinforced soil wall safety factor FoS. The internal energy dissipation during the incipient plastic failure process took place in the soil along the discontinuity surface and along the geosynthetic reinforcement elements. In the other hand, the external work rate is due to the soil weight of the block ABC, the inertia forces induced by the seismic loading in both directions and the surcharge boundary loads when existing. This latter is not considered here. The external work rate and internal energy dissipation are obtained by summation of the elementary work rates. The details of the calculations of the elementary surfaces and theirs corresponding internal and external work rates are detailed in chapter 2 with the difference that in chapter 2, the application of the kinematic theorem gives a lower bound to the required reinforcement strength that ensure the reinforced soil wall stability. In this chapter, the reinforcement strength is defined and the upper bound approach gives the wall safety factor corresponding to the defined reinforcement strength. The energy dissipation rate during rotational failure due to reinforcements is given as:

$$\dot{D}_r = \sum_1^{n_r} T_i \Omega Y_i \tag{3-2}$$

Where n_r is the number of reinforcement layers, T_i is the reinforcement force in the layer i at failure, and Y_i is the vertical distance between the reinforcement and the center of rotation O. This latter can be expressed as:

$$Y_i = Y_0 + (i - 0.5) * \frac{H}{n_r} \tag{3-3}$$

The energy dissipation along the reinforcements is calculated considering both the reinforcement layers failing in tension and those being pulled out. Therefore, $T_i = min[T_u, T_p]$, where T_u is the reinforcement tensile strength and T_p is the reinforcement pullout force expressed as:

$$T_p = 2\gamma z^* L_e f^* \tag{3-4}$$

where z^* is the overburden depth; L_e is the effective length (Figure 3-1)

The safety factor FoS is calculated for each possible slip surface of the reinforced soil system. Then, the critical failure surface and its corresponding safety factor $FoS_{critical}$ are determined through an optimization process. The safety factor is traditionally defined as the coefficient by which the soil shear strength would have to be reduced to bring the system to the verge of failure. Hence, the method is known as the strength reduction method. In the framework of the kinematic theorem of limit analysis, the criterion of the critical state is the work rates balance. FoS is therefore, the ratio of the soil shear

strength and the minimum shear strength that provides a balance between the external work rate $\dot{W}$ and the internal energy dissipation $\dot{D}$.

A two-step genetic algorithm, proposed by Guo et al. (2018), is used for the optimization process with regard to the geometrical parameters r_B, θ_B and t the time involved in the pseudo-dynamic approach. The details of the proposed two-step are given in Guo et al. (2018).

3.2.2 Performance function

The assessment of the internal stability of geosynthetic reinforced soil walls requires the consideration of the tensile and pullout failure of reinforcements. The common procedure, used when the upper bound theorem of limit analysis is used for the internal stability analysis (Michalowski, 1997-1998a; He et al., 2012, among other), is composed of two steps: first, the reinforcement strength is determined considering only the reinforcement tensile failure. Then, the length of reinforcement is adjusted in such a way that the required reinforcement strength calculated does not need to be increased when considering the reinforcement pullout failure in addition to the reinforcement tensile failure. In such procedure where every type of reinforcement failure is considered apart, a performance function for each failure type is required (Basha and Sivakumar Babu, 2010). Most design codes (FHWA, 2009; NF P 94-270, 2009) recommend a reinforcement length between 0.7H and 1.2H depending on the loading level, where H is the wall height. However, this traditional analysis and design procedure gives impractical values of reinforcement length going to 2H, especially when the horizontal seismic coefficient is important ($k_h \geq 0.2$). Chapter 2 presented an improved method by fixing initially the reinforcement length, to calculate the reinforcement strength required for the system stability considering both the tensile and pullout failures of the reinforcements. The reinforcement force in the work calculation is taken the minimum between the reinforcement strength and the pullout force at each reinforcement layer. A unique performance function G is used consequently in the reliability analysis and is defined as follows:

$$G = FoS - 1 \tag{3-5}$$

where FoS is the safety factor determined using the strength reduction method.

3.2.3 Combination of the SPCE and MCS for the reliability analysis

This section presents the combination between the Sparse Polynomial Chaos Expansion metamodeling technique and the Monte Carlo Simulation technique (called SPCE-MCS procedure). SPCE-MCS consists of replacing the expensive deterministic model by a meta-model (also known as surrogate model) whose computation time is quasi-negligible. Then, the obtained surrogate model is used to perform a direct MCS. The probability distribution function PDF, statistical moments and failure

probability can be easily computed. The MCS and the SPCE are presented in details separately in Sections 1.5.2.2.1 and 1.5.2.3.4 of chapter 1.

The procedure of performing reliability analysis using the SPCE-MCS method:

- Identify the input parameters uncertainties (distribution type and relating statistical parameters). This is carried out through experimental tests. This step is not considered in this thesis although it is important. However, the input parameters uncertainties are taken from the literature.
- Construct a SPCE meta-model using the iterative algorithm described in chapter 1 (section 1.5.2.3.4).
- Perform a MCS using the created SPCE metamodel. For an MCS with N_{total} metamodel runs, the failure probability can be computed using Eq. 1-23 in Section 1.5.2.2.1 of chapter 1.
  A large number of N_{total} should be considered so that the method converges and consequently to obtain an accurate failure probability, e.g., the coefficient of variation of P_f given in Eq. 1-24 is smaller than ε_{tgt}.
- The outputs of the methods are the probability distribution function PDF, failure probability, statistical moments and the Kucherenko sensitivity indices of each random variable since correlated ones are considered.

In this chapter, similar to several works (Pan and Dias, 2017b; Guo et al., 2018-2019a), the target accuracy Q_{tgt}^2 of the SPCE is set equal to 0.999, the cutoff values ε_1 and ε_2 are equal to $5 \times 10^{-5}$and the maximum PCE order p_{max} is set equal to 15. On the other hand, the q-quasi-norm q is taken 0.75. N_{total} is set equal to 2×10^6 and $\varepsilon_{tgt} = 5\%$.

3.2.4 Parametric sensitivity study

In the reliability analysis, all the input parameters can be considered as random variables. However, such option will result in heavy computation efforts. Hence, the aim of this parametric study is to show how the variability of each input parameters could affect the model response. The dimension of the problem and therefore, the expensive computation efforts, is then reduced by specifying the group of input parameters which influence the model response and the other ones which have a minor effect. Only the parameters of the first group will be modeled by random variables.

The geosynthetic reinforced soil retaining wall reference model considered in this study is showed in Figure 3-2. It is composed of a vertical wall of height $H = 6m$. The reinforcement consists of 10 geogrids layers with constant length L_r=1.2H, vertical spacing S_v=60cm and a tensile resistance strength T_u=28.7 kN/m. The backfill material is composed of a soil with a cohesion c=5kPa, a friction angle φ=28° and unit weight γ=18 kN/m^3. Since the reinforcement used are geogrids layers, the pullout interaction factor designated by f^*, is equal to (FHWA, 2009):

$$f^* = F^*.\alpha \tag{3-6}$$

where $F^* = {}^{2}/_{3}.\tan(\varphi)$ is the pullout resistance factor and α is the correction factor equal to 0.8 in the absence of geogrids test data. The other parameters are as follows: k_h=0.15, λ=0.5, f=1.2, T=0.3 s, t_0=0 s, V_s=150 m/s, V_P=280.5 m/s, $\delta\theta$=0.1^o where λ=k_v/k_h.

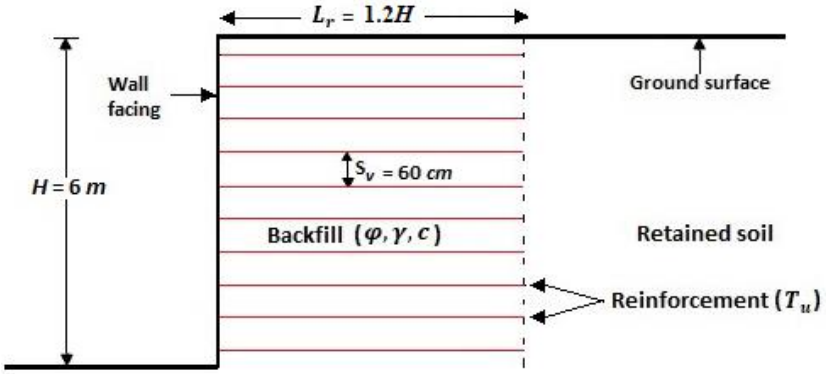

Figure 3-2 Schematic illustration of the geogrids-reinforced soil wall model

The deterministic limit analysis model gives a safety factor $FoS = 1.5$ for the reinforced soil wall reference model.

To study the effects of each input parameter, calculations were carried out by varying the evaluated parameter over a given range determined by a minimum and a maximum value, while maintaining the other parameters at their reference values. The minimum and maximum values are taken in such a way that the difference between most of them and the reference value is almost equal to 2σ, with σ being the standard deviation.

Table 3-1 shows the considered ranges for all the parameters and the results of the parametric study. The main parameters which influence the safety factor, are the soil friction angle φ, cohesion $\boldsymbol{c}$ and unit weight γ, the ultimate strength of geogrids T_u, the horizontal seismic coefficient k_h and the amplification f of the seismic loading. The other parameters have a lower impact (less than 5%).

Table 3-1. Influence of the input parameters

Parameters	**Reference value**	**Variation**		$\frac{\Delta FS}{FS(ref)}$ (%)
		Min	**Max**	
Soil properties				

$\boldsymbol{\varphi}$ (°)	28	17	39	-37.25	46.11
$\boldsymbol{c}$ $(\boldsymbol{kPa})$	5	1	9	-11.47	10.87
$\boldsymbol{\gamma}$ $(\boldsymbol{kN/m\text{^}3})$	18	15.5	20.5	9.31	-8.18
Reinforcement strength					
$\boldsymbol{T_u}$ $(\boldsymbol{kN/m})$	28.7	20	37.5	-14.91	10.01
Seismic loading					
$\boldsymbol{k_h}$ $(-)$	0.15	0.05	0.25	34.93	-21.79
$\boldsymbol{\lambda}$ $(-)$	0.5	0	1	1.42	-2.02
$\boldsymbol{f}$ $(-)$	1.2	0.8	1.6	10.01	-8.89
$\boldsymbol{V_s}$ $(\boldsymbol{m/s})$	150	100	250	1.42	-0.30
$\boldsymbol{T}$ $(\boldsymbol{s})$	0.3	0.15	0.45	0.56	-0.3

3.2.5 Parameter characterization

Six random input parameters are treated as random variables in this study to characterize the variability of soil properties, seismic loading and reinforcement strength parameters. In addition to the six variables determined in the previous paragraph, two other variables having an important effect on the safety factor, the vertical seismic coefficient k_v which is a dependent random variable that is directly linked to k_h ($k_v = 0.5\ k_h$) and, the pullout resistance factor F^* which is a function of the soil friction angle, are also considered. Concerning the soil properties, different values of the coefficient of variation (COV) of the friction angle φ, soil cohesion c and unit weight γ are proposed. The soil friction angle is generally comprised between 20° and 45° for most soils; within this range, the COV proposed in the literature is essentially between 2 and 20% (Phoon and Kulhawy, 1999; Chalermyanont and Benson, 2004; Luo et al., 2016; Javankhoshdel and Bathurst, 2017). For the soil cohesion, the value of the COV could reach 50% (Phoon and Kulhawy, 1999; Sivakumar Babu and Singh, 2011; Javankhoshdel and Bathurst, 2017; Javankhoshdel et al., 2019). The COV of the soil unit weight γ ranges from 3 to 10% (Phoon and Kulhawy, 1999; Ferreira et al., 2016; Luo et al., 2016). In addition, correlations exist between the soil shear strength parameters and soil unit weight random variables. Previous literature studies reported that a negative correlation exists between the soil cohesion and friction angle (Lumb, 1970; Yucemen et al., 1973; Hata et al., 2012). A value of $\rho_{c\varphi}$=−0.5 is assumed in this study. Positives correlations exist

between the soil unit weight γ and soil cohesion c and between c and the soil friction angle φ (Fenton and Griffiths, 2005; Sivakumar Babu and Srivastava, 2007; Parker et al., 2008; Stuedlein et al., 2012; Javankhoshdel and Bathurst, 2017). Values of $\rho_{\varphi\gamma} = \rho_{c\gamma}$=0.4 are considered in this study. Concerning the reinforcement strength, the COV according to Bathurst and Miyata (2015) who analyzed a large database of geogrids tensile strength after the installation damage and creep, could reach 20% in some extreme cases. For the seismic loading parameters modeled as random variables, the COV of the horizontal seismic coefficient k_h is assumed to be equal to COV_{k_h}=30%. For the amplification factor f, there is no previous information or data about its coefficient of variation (COV) or its probabilistic distribution function. However, COV_f=15% is assumed here.

Table 3-2 summarizes the mean, coefficient of variation and the considered probabilistic distributions of the random variables.

Table 3-2. Statistics of random input parameters.

Random variables	**Mean (μ)**	**COV**	**Distribution**
Soil properties			
$\boldsymbol{\varphi}$ (°)	28	20%	Log-normal
$\boldsymbol{c}$ ($\boldsymbol{kPa}$)	5	40%	Log-normal
$\boldsymbol{\gamma}$ ($\boldsymbol{kN/m\text{^}3}$)	18	7%	Log-normal
Reinforcement strength			
$\boldsymbol{T}$ ($\boldsymbol{kN/m}$)	28.7	15%	Log-normal
Seismic loading			
$\boldsymbol{k_h}$ (−)	0.15	30%	Log-normal
$\boldsymbol{f}$ (−)	1.2	15%	Log-normal

3.2.6 Probabilistic failure surface

When a deterministic limit analysis model is performed, an optimization process is conducted by varying the potential failures surfaces through the geometrical mechanism parameters r_B and $\theta_B$variation . This process aims to find the most critical failure surface that corresponds to the surface with the lowest safety factor or alternatively, the most required amount of reinforcement strength. This critical failure surface is referred as the critical deterministic failure surface. However, in the reliability analysis, there is two types of probabilistic stability analysis which can be carried out.

In the first approach, the reliability analysis is carried out on the defined deterministic failure surface (Youssef Abdel Massih et al., 2008). Nevertheless, even though the failure probability calculated is considered representative of the failure probability of the reinforced soil wall, it is in reality the failure probability of the deterministic failure surface.

Within the second approach, the reliability analysis results are more rigorous. The search of the critical failure surface is performed in each deterministic simulation. Since several critical failure surfaces are generally obtained with this approach, the failure probability calculated from the reliability analysis is not associated to a unique failure surface. Here the failure probability of the reinforced structure is not assumed to be equal to the failure probability of the critical deterministic failure surface. However, this approach requires greater computation time since the optimization process is repeated in each evaluation of the deterministic limit analysis model. Therefore, we introduced an efficient reliability method, so this problem can be addressed. In all subsequent results, the failure probability is calculated using the second approach.

3.2.7 Results and discussion

A set of simulations was conducted for the reference model of Geosynthetic reinforced soil retaining wall for the parametric sensitivity analysis. The vertical reinforced soil wall (β=90°) is 6 m high. The reinforcement layers with constant length L_r=1.2H, were placed horizontally and spaced 60 cm. The mean, the coefficient of variation and the probabilistic distributions of the random variables considered are presented in Table 3-2. The other parameters are treated as deterministic. The deterministic calculation with the mean values of the parameters modeled as random variables, gives a safety factor $FoS \cong 1.5$.

Knowing that inclination of a reinforced soil retaining wall should not exceed 15^0, the results of an inclined reinforced soil wall with β=75° are also presented. All the input deterministic and random variables are equal to those for the reference model except the reinforcement strength mean value.

It is worth noting that the consuming time for a deterministic calculation of the safety factor on an Intel Xeon CPU E5-2620 v4 2.10 GHz (2 processors) PC is around 1 min. Around 200 deterministic calculations are needed to construct the SPCE metamodel. This showed the efficiency of using the SPCE method to perform a reliability analysis of the reinforced soil retaining wall under dynamic loading since for example, an analysis with a $P_f = 0.02$ required around 20000 model evaluations to reach a converged result using the MCS reliability method according to Eq. 3. The reliability analysis results are presented in terms of failure probability, probability density functions of the safety factor FoS and Kucherenko sensitivity indices.

3.2.7.1 Influence of the correlation coefficients

In order to discuss the influence of the correlation coefficients between soil parameters, the cases of uncorrelated random variables and correlated ones are investigated and compared in this study. As mentioned before, a correlation coefficient of $\rho_{c\varphi}$=-0.5 is assumed in this study between the soil shear strength parameters and $\rho_{\varphi\gamma} = \rho_{c\gamma}$=0.4 are assumed between the soil unit weight γ and both shear strength parameters. Two calculations are conducted in the case of correlated variables. The first considers only the cross correlation between c and φ, while the second considers also the cross correlation between c and γ and φ and γ.

The probability density functions of the safety factor for the cases of correlated and independent variables are given in Figure 3-3. The correlation impacts the PDFs' shapes for the two walls inclinations. The PDF curves are shorter and wider in the case of independent variables. In the case of correlated variables, the PDF curves are higher and narrower when considering the cross correlation between γ and both shear strength parameters. In all cases, the curves are positively skewed, with the bigger tail at the right in the case of independent variables and the smaller one in the case of three correlated variables. This means that the consideration of the correlation between the three soil parameters gives results with a small uncertainty manifested by the higher peak curve. Ignoring the three correlation coefficients in the independent variables case, gives the results with the larger uncertainty in FoS.

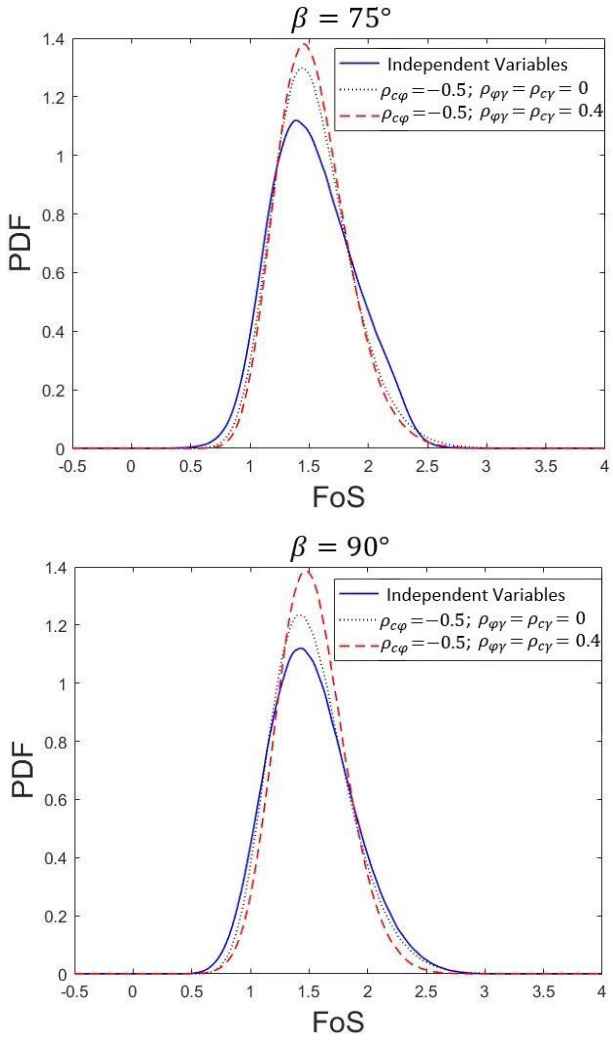

Figure 3-3 Influence of the correlation on the probability density functions of the safety factor FoS

According to Table 3-3, it is observed that the obtained failure probabilities in terms of independent variables are bigger than those of correlated variables for both wall inclinations. For correlated variables, considering only the cross correlation between c and φ gives greater failure probabilities than the three cross correlation coefficient case. For independent variables, the failure probabilities are equal to 0.048 and 0.061 for respectively $\beta = 75°$ and $\beta = 90°$ and decrease respectively to 0.03 and 0.041 in the case of a single correlation between c and φ and respectively to 0.022 and 0.029 in the case of three correlation coefficients. The PDF of the FoS obtained within small values is the highest in case of independent variables and the lowest in case of three correlated variables as shown in Figure 3-3 which, justify the highest failure probability obtained in the first case and the lowest one in the second case. It can be concluded that for this reinforced soil wall case study, neglecting the correlations between the soil parameters leads to conservative reinforced soil retaining wall design. This permits safer design but may not be economical.

Concerning the FoS first two statistical moments, for both wall inclinations, the independent variables cases give almost the same mean values and higher standard deviations compared to those for correlated variables. The insignificant differences in terms of mean values even if the probability density function modes are differents and smaller in independent variables cases can be explained by the bigger tails at the right side of the positively skewed curves for these variables. The increases of the standard deviation values in case of independent variables, for both inclinations, are results of the shorter and wider probability density function curves that reflect larger results uncertainties. For correlated variables, considering only the cross correlation between c and φ gives higher standard deviations compared to the three correlation coefficients case, for both wall inclinations. It is important to note that the two reinforced soil walls ($\beta = 75°$ and $\beta = 90°$) that had the same factor of safety based on the deterministic approach considering the means values ($FoS \cong 1.5$), have a different failure probability in the probabilistic approach although the same degree of uncertainty is involved in the calculation. The vertical reinforced soil retaining wall presents a higher failure probability than the inclined one. These results showed the advantage of the probabilistic approach over the deterministic one.

Table 3-3. Correlation influence on the reliability results.

Wall inclination	Case	P_f	μ_{FoS}	σ_{FoS}
$\boldsymbol{\beta = 75°}$	Independent variables	0.048	1.5325	0.352
	$\rho_{c\varphi} = -0.5$; $\rho_{\varphi\gamma} = \rho_{c\gamma} = 0$	0.030	1.5311	0.323
	$\rho_{c\varphi} = -0.5$; $\rho_{\varphi\gamma} = \rho_{c\gamma} = 0.4$	0.022	1.5282	0.298
$\boldsymbol{\beta = 90°}$	Independent variables	0.061	1.5164	0.359
	$\rho_{c\varphi} = -0.5$; $\rho_{\varphi\gamma} = \rho_{c\gamma} = 0$	0.041	1.5181	0.335
	$\rho_{c\varphi} = -0.5$; $\rho_{\varphi\gamma} = \rho_{c\gamma} = 0.4$	0.029	1.5185	0.293

Figure 3-4 presents the total Kucherenko indices of random variables for independent and correlated variables cases. The correlation effect can be considered using the total Kucherenko indices contrary to the case of the first order indices which represent the contribution of each variable separately. By observing Figure 3-4, one can have an insight into the contribution of each variable on the FoS variance

and the influence of the correlation between the soil parameters on these indices. One can see that the sensitivity results are almost the same for both wall inclinations. The correlation between the soil parameters significantly impacts the Kucherenko indices for most variables. The impact is more pronounced when considering the cross correlation between γ and both soil shear strength in addition to the cross correlation between c and φ.

For the inclined reinforced soil wall model ($\beta = 75°$), the total Kucherenko indices for φ, k_h, c, T_u, f and γ are respectively, 0.695, 0.184, 0.049, 0.031,0.015 and 0.009 for the case of independent variables. These indices become respectively 0.609, 0.27, 0.054, 0.020, 0.029 and 0.020 when considering only the cross correlation between c and φ. When considering the cross correlation between c and φ, γ and c and γ and φ, they become respectively, 0.338, 0.279, 0.034, 0.037, 0.027 and 0.015. It can be observed that in all cases, correlated and independent variables, the soil friction angle has the highest Kucherenko index and the horizontal seismic coefficient k_h has the second highest one. However, the difference between these two indices decreases when the correlation between the soil shear strength parameters is considered and the impacts of these two variables become almost the same when all the correlations between the soil parameters are considered. The soil cohesion c, the reinforcement strength T_u and the soil amplification f have almost the same influence on the FoS variance and the soil unit weight has the least one and therefore the least influence on the FoS variability.

For the vertical reinforced soil wall model, the total Kucherenko indices for φ, k_h, T_u, c, γ and f are respectively equal to, 0.648, 0.206, 0.054, 0.04, 0.028 and 0.026 when neglecting the three correlation coefficients between the soil parameters. These indices become respectively 0.585, 0.23, 0.095, 0.072, 0.023 and 0.046 for the single cross correlation coefficient case between c and φ. The total Kucherenko indices become respectively, 0.297, 0.334, 0.049, 0.027, 0.016 and 0.031 for the three correlation coefficients case. The same remarks as for inclined reinforced soil wall, are addressed on the influence of the correlation on the total Kucherenko indices of the most important variables φ and k_h with the difference that the impact of k_h becomes greater than φ in case of three correlated variables. The other remaining variables are ranked in the following order: T_u, c and f. For these three variables, the single cross correlation coefficient case between c and φ shows a higher total Kucherenko index compared to other cases. The least important variable is γ whose the total Kucherenko indices are the lowest.

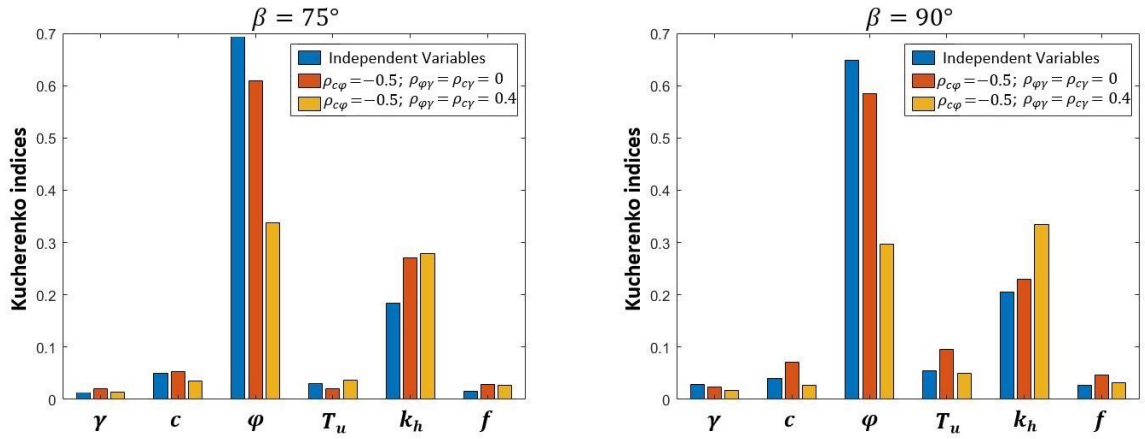

Figure 3-4 Kucherenko indices of each variable for correlated and independent variables cases

3.2.7.2 Influence of the distribution types

In the previous section, all the variables were assumed to be lognormally distributed. The effect of using different distribution types of input variables on the probabilistic results is investigated. The random input variables are assumed to follow truncated normal distributions instead of log-normal ones. The results are compared to those obtained in the case of lognormal distributions.

The probability density functions of the safety factor FoS for the cases of normal and lognormal distribution types of random variables are given in Figure 3-5. It is shown that for the inclined reinforced soil wall, the distribution type hardly impacts the PDFs' shapes. The PDF is slightly shorter and wider in case of normal distribution type for the random variables. The impact is more significant for the case of vertical reinforced soil retaining wall ($\beta = 90°$) where the PDF is clearly shorter and wider in case of normal distribution type for the random variables. And therefore, assuming normal distributions appears to lead to a shorter and a more spread out distribution at the tail region for both wall inclinations and this is more significant in the vertical wall case. In addition, the curves for both distribution types are slightly positively skewed.

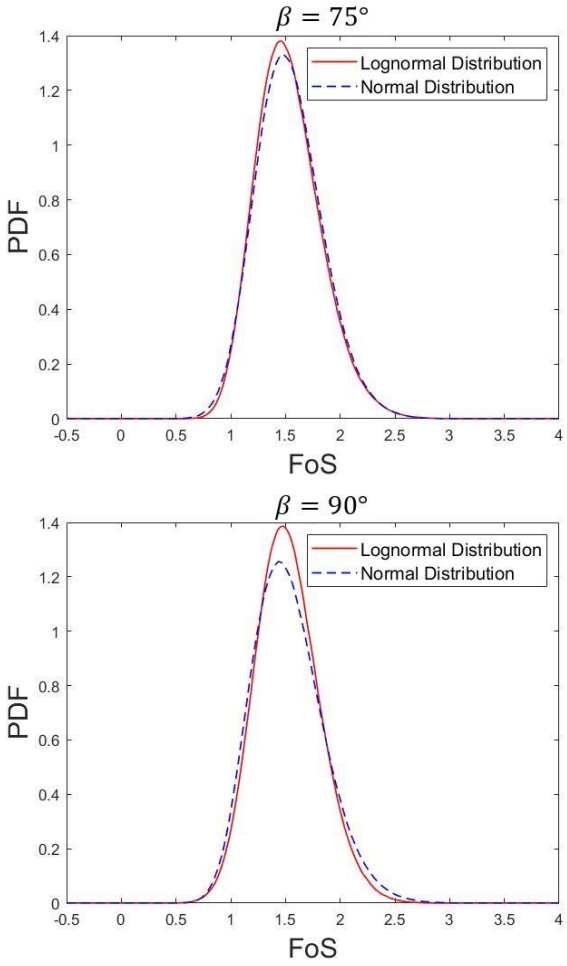

Figure 3-5 Influence of the distribution on the probability density functions of the safety factor FoS

Table 3-4 summarizes the obtained failure probabilities and the FoS first two statistical moments for both distribution types and both wall inclinations. The failure probabilities, for lognormally distributed variables, are equal to 2.15×10^{-2} and 2.86×10^{-2} for respectively $\beta = 75°$ and $\beta = 90°$ and increase to 2.86×10^{-2} and 3.60×10^{-2} respectively for truncated normally distributed variables. One can conclude that considering the truncated normal distribution for the input variables gives slightly higher failure probability than lognormal distributions, for both reinforced soil retaining wall inclinations. These results can be explained graphically by the slightly bigger tail at the left side of the PDF curves in case of normal distribution for the input variables.

Concerning the first two moments of FoS, the type of distribution of random variables hardly influences the mean values μ_{FoS} and the standard deviations σ_{FoS} of the reinforced soil wall safety factor FoS. This is in agreement with the observation of the PDF shapes in Figure 3-5. The mean values μ_{FoS} and the standard deviations σ_{FoS} are smaller in the case of lognormal distribution for the input variables for both wall inclinations. It is important to note that for the vertical reinforced soil wall, the mean value μ_{FoS} is lower for the lognormally distributed input variables case even though the mode of the PDF

curve is higher for this distribution type of input variables. This is explained by the bigger tail at the right side in the case of normally distributed input variables. For both wall inclinations, the higher values of standard deviations σ_{FoS} for the case of normally distributed input variables comparing to the case of lognormally distributed ones, show that the former case results in a higher uncertainty of the model response.

Table 3-4. Influence of the distribution types on the reliability results.

Wall inclination	Case	P_f	μ_{FoS}	σ_{FoS}
$\beta = 75°$	Lognormal Distribution	2.15×10^{-2}	1.528	0.2984
	Normal Distribution	2.82×10^{-2}	1.535	0.3064
$\beta = 90°$	Lognormal Distribution	2.86×10^{-2}	1.518	0.2929
	Normal Distribution	3.60×10^{-2}	1.524	0.3252

Figure 3-6 gives for both wall inclinations, a comparison between the Kucherenko indices for lognormal and normal distributions. For the vertical reinforced soil wall, similar results are obtained from the two distributions types. The distribution type slightly influences the Kucherenko indices and give quite similar indices for most input variable without changing their ranking order. The horizontal seismic coefficient k_h and the soil friction angle φ appear to have the biggest impact on the FoS. The horizontal seismic coefficient k_h have the higher Kucherenko index and therefore the higher impact on the FoS. The second most important variable is the soil friction angle φ. When the truncated normal distribution is used, the Kucherenko index of the horizontal seismic coefficient k_h increases comparing to the case of lognormal distribution type of input variables while the one of the soil friction angle decreases. Therefore, in case of lognormally distributed variables, the difference between the Kucherenko indices of these two variables is reduced. The third most important variable is the reinforcement strength T_u, followed by the soil amplification f, the soil cohesion c and finally the soil unit weight that has the lower Kucherenko index and therefore, the lower impact.

For the inclined reinforced soil wall ($\beta = 75°$), the distribution type greatly influences the Kucherenko indices for the two most important variables, k_h and φ. Similar to the case of vertical reinforced soil wall, the Kucherenko index of the horizontal seismic coefficient k_h increases when the truncated normal distribution is used instead of the lognormal distribution and it decreases for the case of the soil friction angle. However, the ranking order here changes in such a way that φ becomes the most important variable in case of lognormal distribution and k_h remains the most important one in case of normal distribution. The use of truncated normal distribution leads to an increase in the Kucherenko index for f and a decrease for T_u and c. However, it can be noted that the impact of T_u, f and c are almost the

same on the FoS, for both distribution types. The soil unit weight has the lowest impact as in the case of vertical reinforced soil wall. It can be concluded from the results of both wall inclinations, that k_h and φ have the highest impact regardless of the distribution type used.

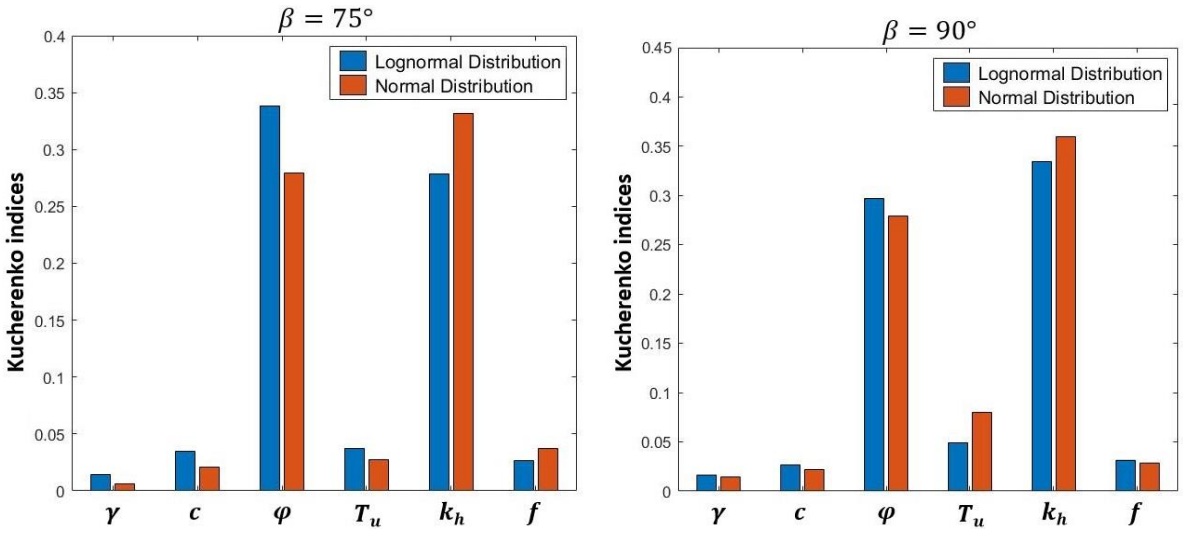

Figure 3-6 Kucherenko indices of each variable for Lognormal and Normal Distributions

3.2.7.3 Influence of the coefficient of variation (COV)

The previous results are based on the values of COV presented in Table 3-2. To assess the effect of the COV of different random variables on the probabilistic results, different values of COV that range between 0% and 40% were used to perform the probabilistic analysis. A coefficient of variation equal to 0% means that the parameter is considered as deterministic. When the COV of a given random variable is investigated, the rest of parameters were maintained at their reference values (Table 3-2). The results are presented for the two wall inclinations. For the sake of clarity, for each wall inclination, the results are presented in two separate figures. The first contains the influence of the variability of soil properties (Figure 3-7) while the second presents the influence of the rest of random variables, i.e. the reinforcement strength and the seismic random parameters (Figure 3-8).

Figure 3-7 presents the failure probability as a function of the soil unit weight coefficient of variation $COV_{\gamma,}$ the soil cohesion coefficient of variation COV_c and the soil friction angle coefficient of variation COV_φ. For the inclined retained wall ($\beta = 75°$), the wall failure probability is almost the same (4×10^{-3}) for a COV_φ between 0% and 10%. Then, the failure probability increases rapidly when COV_φ increases from 10% to 40%. The same trend is shown for the vertical wall where the failure probability remains almost constant for a COV_φ between 0% and 10% and then, increases rapidly with the increase of COV_φ. Concerning the soil cohesion, the failure probability decreases with the increase of COV_c for both wall inclinations. However, the variations in the failure probability with the variation of COV is

much more important in the case of soil friction angle compared to the soil cohesion case. For the soil unit weight, both wall inclinations presented the same trend. Firstly, the failure probability decreased with the increase of the coefficient of variation COV_γ until a specified value of COV_γ where the failure probability presented its lower value. Beyond this specified value, the failure probability increased with the increase of COV_γ. The specified value of COV_γ is almost equal to 25% for the inclined wall and about 20% for the vertical wall. Similar to the soil cohesion case, the variations in the failure probability with the variation of COV is much more important in the case of soil friction angle compared to the soil unit weight case. It is important to note that in practice, reducing the input uncertainty leads to a decrease in the probability failure. However, it can be shown here that reducing the coefficient of variation of the soil cohesion gives greater failures probabilities. In addition, the same trend is observed for a given range of coefficient of variations of the soil unit weight ($0 \leq COV_\gamma \leq 20 - 25\%$). Generally, one seeks to reduce the input uncertainty in order to obtain a smaller failure probability P_f hence the importance of the findings here. Concerning the coefficient of variation of the soil cohesion, these results are explained by the correlation that exists between the soil cohesion and the soil friction angle. Increasing the coefficient of variation of the soil cohesion gives more small samples values of the soil cohesion. These values are associated with high values of soil friction angle due to the negative correlation, and therefore low failure probability since this latter is more sensitive to the value of the soil friction angle. In fact, the probabilistic analysis conducted considering the same random variables as here, but without consideration of the correlation between the soil properties gave higher failure probability when increasing the coefficient of variation of the soil cohesion. On the other hand, concerning the coefficient of variation of the soil unit weight, similar trend was reported by Chalermyanont and Benson (2004) and Sayed et al. (2008). This can be justified by the combination of two factors: the correlation effect and the fact that the soil unit weight has an effect on both driving and resisting moments.

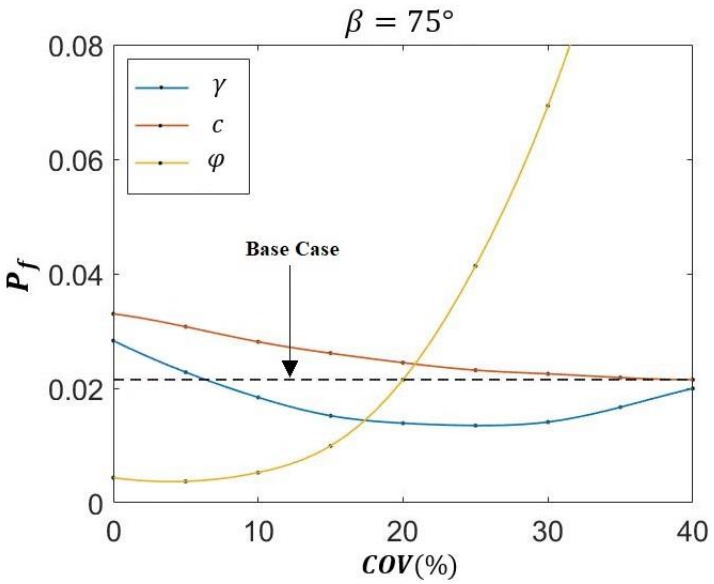

(a)

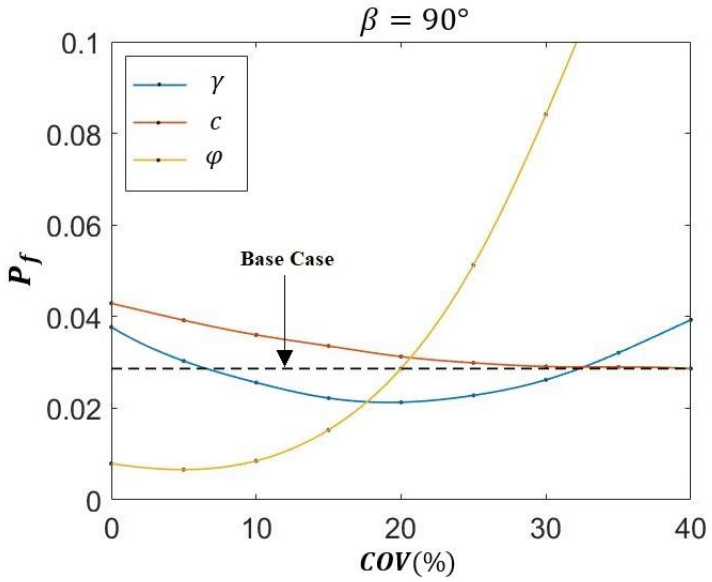

(b)

Figure 3-7 Effect of the variability of soil properties on the failure probability: (a) $\beta = 75°$, (b) $\beta = 90°$

Figure 3-8 presents the failure probability as a function of the reinforcement strength coefficient of variation $COV_{T_u,}$ the coefficient of variation COV_{k_h} of the horizontal seismic coefficient and the seismic loading amplification coefficient of variation COV_f. For the three different parameters and both wall inclinations, the increase of the coefficient of variation leads to an increase in the failure probability. However, the rate of increase is different. The effect of the variation of COV is more pronounced in cases of T_u and k_h, where the failure probability increases respectively from 1.78×10^{-2} and 3.81×10^{-3} to 5.09×10^{-2} and 3.68×10^{-2} when the COV increases from 0% to 40% for the inclined reinforced soil wall case. For $\beta = 90°$, these values become respectively 2.23×10^{-2} and 6.34×10^{-3} for $COV = 0\%$ and increase to 8.97×10^{-2} and 4.72×10^{-2} when the COV increase to 40%. For the amplification factor, the failure probability increases from 1.89×10^{-2} to 3.39×10^{-2} when the COV increases from 0% to 40% for the inclined reinforced soil wall and from 2.57×10^{-2} to 4.49×10^{-2} for the vertical reinforced soil wall case.

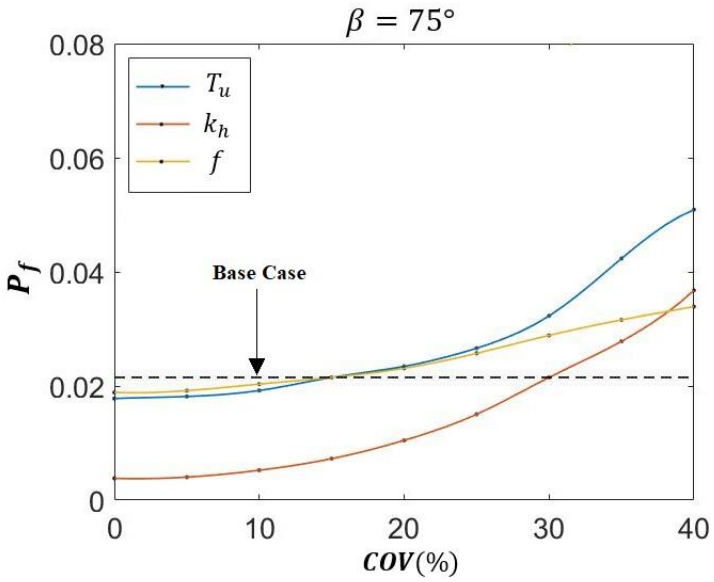

(a)

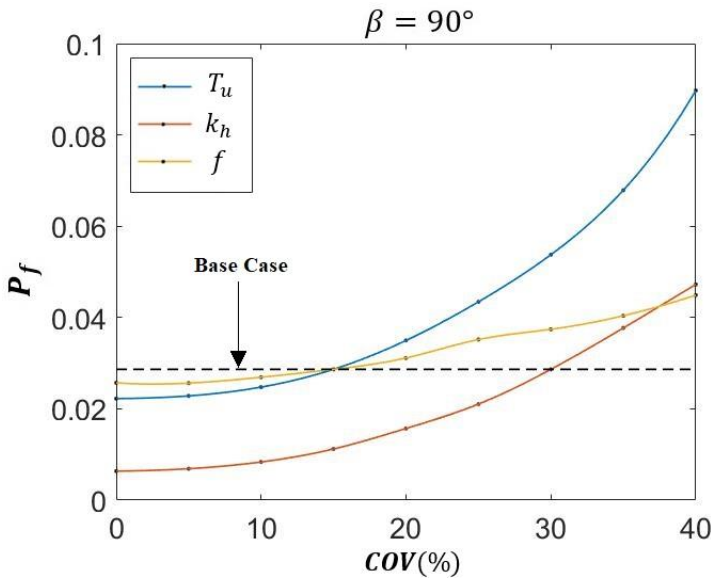

(b)

Figure 3-8 Effect of the variability of reinforcement and seismic random parameters on the failure probability: (a) $\beta = 75°$, (b) $\beta = 90°$

It may be noted that the wall reliability is reduced significantly with the increase in the friction angle coefficient of variation and that the variability of soil friction angle plays an important in the reinforced soil wall design and stability.

3.2.7.4 Comparison between deterministic and probabilistic approaches

Figure 3-9 presents the failure probability obtained by the probabilistic approach versus the deterministic safety factor for the reference model of Geosynthetic reinforced soil retaining wall (β=90°) and for the

inclined reinforced soil wall (β=75°). A deterministic safety factor refers to the safety factor obtained within a deterministic calculation using the mean values of the parameters modeled as random variables in the probabilistic approach. All the input parameters are maintained equal to those used previously except the reinforcement strength mean value which is changed in order to have a desired deterministic safety factor. In other words, mean value of the reinforcement strength modeled as a random variable in the probabilistic approach, is taken as the required reinforcement strength that gives the related safety factor in the deterministic approach.

It can be observed that the two reinforced soil walls ($\beta = 75°$ and $\beta = 90°$) that had the same factor of safety based on the deterministic approach considering the means values ($FoS \cong 1.5$), have different failure probability in the probabilistic approach although the same degree of uncertainty is involved in the calculations. For the same deterministic safety factor of the reinforced soil retaining wall, the failure probability increased progressively with the wall inclination β. These results are in agreement with the results reported by Javankhoshdel and Bathurst (2017). For the two wall inclinations, the failure probability decreased dramatically when the safety factor FoS increased from 1 to 1.4. Then, the rate of decrease became lower for higher safety factors. The results showed the main limitation of the deterministic approach. Two reinforced soil walls that have the same deterministic safety factors present two different reliability levels by obtaining different probability of failures. This means that when designing two reinforced earth walls for a target safety factor using the deterministic approach, the reliability levels of these two walls are different.

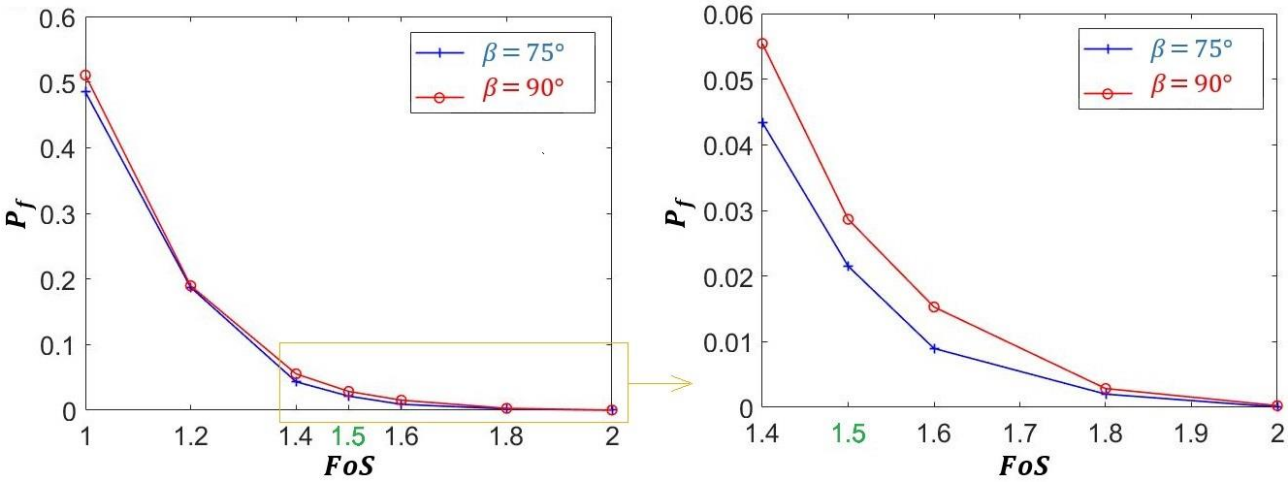

Figure 3-9 Failure probability versus deterministic factor of safety for reinforced earth retaining walls for the two wall inclinations

3.3 Conclusion

The seismic internal stability of geosynthetic reinforced soil retaining walls is presented in this chapter in a probabilistic framework using the random variables approach. The deterministic computation of the safety factor is based on the kinematic theorem of limit analysis. The point-to-point method is used to

generate the rotational failure mechanism so that the pseudo-dynamic approach is adopted in order to account for the dynamic effect of a ground shaking. The Sparse Polynomial Chaos Expansion (SPCE) in combination with the Monte Carlo Simulation MCS is used to perform the probabilistic analysis. Six input parameters were considered as random input variables including the soil (γ, c and φ), seismic loading (k_h and f) and reinforcement strength (T_u) parameters. In addition to these six variables, two dependent random variables are involved in the reliability analysis: the vertical seismic coefficient k_v which is a dependent random variable of k_h and the pullout resistance factor F^* which is a function of the soil friction angle φ. As a result, eight input parameters were considered as random input variables in this study. The influences of the correlation coefficients, distributions types and coefficient of variation of the input parameters on PDFs of the Geosynthetic reinforced soil wall safety factor FoS, mean and standard deviation of the FoS and system failure probability, were investigated. The contribution of each input variable to the FoS variance is also obtained by computing the Kucherenko sensitivity indices. The following conclusions can be drawn from this research:

The correlation between the soil parameters impacts the PDFs shape of the safety factor FoS. Considering the correlation between the soil parameters gives taller and narrower curves and smaller failure probabilities. The PDFs of the FoS are positively skewed in all cases of independent and correlated variables. The distribution is highly skewed in the case of independent variables and the skewness decreases with the increase of correlated variables. Neglecting some correlation structures between the soil parameters ensure a conservative design. With respect to the sensitivity analysis, the correlation between the soil parameters have a significant influence on the Kucherenko indices.

The normal distribution of random variables increases the failure probability, mean value and standard deviation of the reinforced soil wall safety factor FoS. A normal distribution induces a slightly shorter and wider PDF curve than the lognormal distribution one. With respect to the sensitivity analysis, the two distribution types of random variables give almost similar Kucherenko sensitivity indices for each variable.

For the two distribution types, the Kucherenko sensitivity analysis helps to identify significant input parameters and shows that the soil friction angle and the horizontal seismic coefficient are the most important parameters in the reinforced soil retaining wall analysis. On the other hand, the soil unit weight has the lowest impact on the FoS variability.

The failure probability decreased dramatically when the safety factor FoS increased from 1 to 1.4. For the same deterministic safety factor of the reinforced soil retaining wall and the same degree of uncertainty involved in the probabilistic calculations for the input random variables, the failure probability increased progressively with β, the angle forming the wall with the horizontal. This result reflects the advantage of a probabilistic approach over a deterministic one since two systems that have

the same deterministic safety factor present different failures probability in the framework of probabilistic analysis.

The variability associated with the backfill soil friction angle plays a vital role in the design of reinforced soil retaining wall and therefore, it is important to carefully specify the statistical parameters of this random variable through measurement data or laboratory test results.

In this chapter, the uncertainty of the soil shear strength parameters, reinforcement strength and characteristics of seismic loading are considered using random variables. This approach is selected in this study since it is simpler and faster than the random field approach. In addition, this approach provides conservative results for most cases and ensure thereafter, a safer design. However, this approach presents a limitation since it neglects the backfill soil spatial variability. When considering the variability through the random variables approach, the soil properties are assumed to be homogeneous across the whole backfill in each simulation. This assumption is not realistic since the soil properties changes in both the vertical and horizontal directions even in one soil stratum. To address this problem, random fields will be employed where each random field is represented using a series of indexed random variables. The next chapter carry out a probabilistic seismic internal stability analysis of reinforced soil retaining wall considering the soil spatial variability of the backfill soil.

4 Chapter 4: Probabilistic stability analysis using random fields approach

4.1 Introduction

In the previous chapter, the reliability analysis of geosynthetic reinforced soil retaining walls was performed using the random variables approach. This assumption cannot model realistically the variability of the soil properties. To address this problem, this chapter aims to investigate the effect of the soil spatial variability, ignored in the previous chapter, on the seismic internal stability analysis of geosynthetic reinforced soil retaining walls. It can thus predict more accurately the structure reliability level. The soil strength parameters are modeled by random fields (RFs) characterized by their autocorrelation functions in addition to their marginal probability density functions. Like in the previous chapter, the input parameters uncertainties (autocorrelation distance, distribution type and relating statistical parameters) used for the RFs are adopted based on hypothetical values taken from the literature. In the random fields approach which models the soil properties inherent variability, one needs to discretize the random field into a certain number of random variables and each random field is represented using a series of indexed random variables. In order to obtain accurate results, a larger number of these variables is required. Several methods were developed for the random field discretization. The series expansion methods (Karhunen-Loève expansion, Orthogonal Series Expansion, Expansion Optimal Linear Estimation) are the most efficient in terms of required random variables for an accurate random field presentation. Among these approaches, the Karhunen-Loève expansion method (K-L expansion) is the most efficient and hence is employed in this chapter to generate the random fields. To deal with the high dimensional stochastic problem considered, the SIR/A-bSPCE method is the reliability method considered to carry out the probabilistic analyses. The idea consists in reducing the original input space dimension. Then, an active learning sparse polynomial chaos expansion (A-bSPCE) is used to construct a metamodel in a lower-dimensional subspace and the total computational time of the probabilistic analysis is significantly reduced compared to directly running the classical probabilistic method. The results provided within the SIR/A-bSPCE approach combined with the MCS, include the probability distribution function PDF, statistical moments and failure probability. The same deterministic model with the same hypothesis used in the previous chapter are adopted here. It is based on the kinematic approach of limit analysis to compute the reinforced soil wall safety factor. The discretization technique is used to generate the rotational failure mechanism so that the pseudo-dynamic approach can be used to represent the seismic loading (Alhajj Chehade et al., 2019b-2020). The soil friction angle and cohesion are modelled as two anisotropic cross-correlated lognormal random fields. The effects of the spatial variability, cross-correlation between the soil

strength parameters and coefficient of variation of these two random fields on probability density functions (PDFs) of the structure safety factor and on failure probabilities are investigated and discussed.

4.2 Random field model

4.2.1 Discretization of random fields

A random field can be represented by a collection of indexed random variables. Several methods have been developed to discretize a continuous parameter random field into a certain number of random variables. These methods could be grouped into three categories: point discretization methods (Midpoint, Shape Function, Integration Point, Optimal Linear Estimation), average discretization methods (Spatial Average, Weighted Integral) and series expansion methods (Karhunen-Loève expansion, Orthogonal Series Expansion, Expansion Optimal Linear Estimation). The first and second approaches require a large number of random variables for a good approximation of the random field. On the other hand, the third approaches are the most efficient in terms of random variables number required for an accurate random field presentation. In fact, the random field is exactly represented using a series of random variables and deterministic spatial functions using these approaches. The approximate random field is defined by truncating the series expansion to a finite number of terms. Among these approaches, the Karhunen-Loève expansion method (K-L expansion) is the most efficient since the required size of the series expansions for a given accuracy is the smallest. The K-L expansion approach was adopted by many researchers to simulate the random fields in the framework of reliability analysis of geotechnical structures such as slopes, tunnels and foundations considering soil spatial variability.

The discretization of the random fields using K-L expansion is carried out in the Gaussian space. In the case of non-Gaussian random fields, the generated Gaussian random field must be transformed to the non-Gaussian space by applying specified corrections functions that will be presented later in the chapter. A Gaussian random field is completely described by constant mean μ, constant standard deviation σ and an autocorrelation function $\rho(x, x')$ which is an index of correlation used to describe the spatial extent within which there is a strong correlation between soil properties. A Non-Gaussian marginal cumulative density function is required in the case of non-Gaussian random field. The exponential form of the autocorrelation function is commonly used for spatially varying soils. Its square form is the one used in this study, and is expressed as:

$$\rho(x, y) = exp\left(-\left(\frac{|x-x'|}{l_x}\right)^2 - \left(\frac{|y-y'|}{l_y}\right)^2\right) \quad (4\text{-}1)$$

Where (x, y) and (x', y') are the coordinates of two arbitrary points, l_x and l_y are the autocorrelation distances along the horizontal and vertical directions respectively.

A small fluctuation of the soil property, which means that it is highly correlated over a large spatial extent, is reflected with a large autocorrelation distance. However, a small autocorrelation distance shows that the spatial extent where the soil property is highly correlated is small and a large soil property fluctuation exists within the field.

4.2.2 The K-L expansion

A random field $H(x,\theta)$ can be represented by a collection of random variables indexed by a continuous parameter $x \in \Omega$ where Ω is a bounded domain of R^2 in the case of two-dimensional fields and $\theta \in \boldsymbol{\Theta}$ where θ is a realization of the random field and $\boldsymbol{\Theta}$ is the outcome space (all the possible outcomes). The K-L expansion of a random field is based on the spectral decomposition of its autocovariance which is bounded, symmetric and positive definite. Any realization of $H(x.\theta)$ can be expanded over this basis as follows:

$$H(x,\theta) = \mu + \sum_{i=1}^{\infty} \sigma\sqrt{\lambda_i}\varphi_i(x)\xi_i(\theta) \tag{4-2}$$

where μ and σ are respectively the random field mean and standard deviation, λ_i and φ_i are the eigenvalues and eigenfunctions of the covariance function and $\xi_i(\theta)$ is a vector of standard uncorrelated random variables. For practical implementation, the approximate random process is defined by truncating the series expansion to a finite number of terms S, which depends on the desired accuracy, the autocorrelation function and the dimension of the random field. The approximated field is then given by:

$$H(x,\theta) \cong \mu + \sum_{i=1}^{S} \sigma\sqrt{\lambda_i}\varphi_i(x)\xi_i(\theta) \tag{4-3}$$

The accuracy of the treated problem is determined by the calculation of the error estimate, which is based on the variance of the truncated error for a K-L expansion with S terms as follows (Phoon and Ching, 2014):

$$\varepsilon = \frac{1}{\Omega}\int_{\Omega}\left[1 - \sum_{i=1}^{S}\lambda_i\varphi_i^2(x)\right]d\Omega \tag{4-4}$$

4.2.3 Cross-correlated Gaussian random fields

Typically, many random soil properties are involved in geotechnical problems, such as the friction angle, cohesion, unit weight, Young's modulus and Poisson's ratio. All these properties can be modeled by random fields.

In this chapter, only the soil cohesion and the soil friction angle are considered as random fields due to the relatively low effect of the elastic properties on the internal stability of geosynthetic reinforced soil

retaining wall ultimate limit state. Being always positive, a lognormal random field is considered for each of these random fields. The soil properties are assumed to share an identical autocorrelation function (identical autocorrelation distances l_x and l_y) in the soil region Ω. In addition, it is known that a negative correlation exist between the soil cohesion and friction angle (Lumb, 1970; Yucemen et al., 1973; Hata et al., 2012). This cross correlation structure is simply defined by a cross correlation coefficient.

If a random field $H(.)$ is assumed to follow a lognormal distribution, $\ln(H)$ will follow a normal distribution with mean value μ_{ln} and standard deviation σ_{ln}. Consequently, the K-L expansion given in Eq. (4-3) becomes:

$$H(x,\theta) \cong exp\left[\mu_{ln} + \sigma_{ln}\sum_{i=1}^{S}\sqrt{\lambda_i}\varphi_i(x)\xi_i(\theta)\right] = exp[\mu_{ln} + \sigma_{ln}G(x,\theta)] \qquad (4\text{-}5)$$

where $G(x,\theta)$ is the standard normal random field.

When the cross correlation $\rho_{c,\varphi}$ existed between the soil cohesion c and the soil friction angle φ, it must be considered also in the framework of the random field transformation. For the case of c,φ soil considered here, the two cross-correlated lognormal random fields with a cross-correlation $\rho_{c,\varphi}^{ln}$ can be expressed as:

$$H_c(x,\theta) = exp[\mu_{lnc} + \sigma_{lnc}G_c(x,\theta)] \qquad (4\text{-}6)$$

$$H_\varphi(x,\theta) = exp\left\{\mu_{ln\varphi} + \sigma_{ln\varphi}\left[G_c(x,\theta).\rho_{c,\varphi}^{ln} + G_\varphi(x,\theta).\sqrt{1-\left(\rho_{c,\varphi}^{ln}\right)^2}\right]\right\} \qquad (4\text{-}7)$$

where $\rho_{c,\varphi}^{ln}$ is the cross-correlation coefficient between $\ln(\varphi)$ and $\ln(c)$.

4.3 SIR/A-bSPCE method

This section presents the SIR/A-bSPCE method, used in this chapter in order to perform geosynthetic reinforced soil retaining wall probabilistic stability analysis. It is started by the presentation of the bootstrap-based resampling technique that provide local error estimate for SPCE predictions. This approach is referred as bootstrap-SPCE (bSPCE). Then, an active learning algorithm is presented that iteratively enriches an initial experimental design in order to improve the accuracy of the reliability analysis results. The method that combines the SPCE with the active learning algorithm is referred as A-bSPCE. After that, the principles of the Sliced Inverse Regression (SIR) are described. In the end, the A-bSPCE is combined with the SIR for the reliability analysis.

4.3.1 Bootstrap-based local error estimation for SPCE predictions

The metamodeling tool Polynomial Chaos Expansion (PCE) and its extension SPCE are well described in chapter 1. This latter was used in the previous chapter to perform reliability analysis of geosynthetic reinforced soil retaining wall using the random variables approach. It was mentioned that the metamodel accuracy and the computation time increase with the PCE order and consequently, one should increase the PCE order successively until obtaining the target accuracy with the minimum possible PCE order. Two estimate measures of the generalization error are presented, the empirical mean-square residual error and the leave-one-out error and their coefficients of determination R^2 and Q^2 (Blatman and Sudret, 2010a). However, these two errors are used to estimate the global accuracy of the PCE. Nevertheless, there is lack of local error estimates to the PCE or SPCE predictions such as variability or confidence bounds for each PCE or SPCE prediction.

To address this issue, Marelli and Sudret (2018) proposed to combine the bootstrap-based resampling strategy with the PCE metamodeling technique. This combination between PCE and bootstrap technique consists in getting, using a reference Experimental Design ($ED^{(ref)}$), multiple metamodeling models using different boosting training sets. This $ED^{(ref)}$ includes a set of N realizations $\mathcal{X} = \{x^{(1)}, \dots, x^{(N)}\}$, selected randomly by using a sampling scheme (e.g. MC simulations, Latin Hypercube sampling or Sobol set). For each sample $x^{(i)}$, the corresponding response $y^{(i)}$, is evaluated using the deterministic model to obtain $\hat{Y}$, the model response of the of the N realizations of the $ED^{(ref)}$. Then, a set of B bootstrap-resampled experimental designs EDs are generated based on the $ED^{(ref)}$ by randomly assembling B times N realizations of $x^{(i)}$ $(i = 1 \dots N)$ and the corresponding $y^{(i)}$ which are already calculated. In each of the B bootstrap-resampled experimental designs EDs, the input sample $x^{(i)}$ could be present for zero, one or more times. The B bootstrap-resampled experimental designs EDs result in B different PCEs where, for each of the generated EDs, the PCE unknown coefficients are computed based on the least-square minimization method as shown in Eq. (1-35) of chapter 1. As a result, B different predictions can be obtained for any points not included in the $ED^{(ref)}$. Consequently, empirical quantiles can be employed to provide local error bounds on the PCE prediction for any realization.

In the case of SPCE, Marelli and Sudret (2018) proposed a fast bSPCE approach in order to reduce the expensive time computation that may results from performing B times sparse least-square analysis. In this approach, the sparse polynomial basis identified by the $ED^{(ref)}$ is effective for the other B bootstrap-resampled experimental designs EDs and therefore, bootstrapping is applied only to the unknown coefficient estimation based on a classic ordinary least-square regression on the sparse basis (Blatman and Sudret, 2011).

4.3.2 Active learning Sparse Polynomial Chaos Expansions (A-bSPCE)

The metamodeling methods are found to be an efficient tool to perform reliability analysis of various geotechnical problems. They consist of replacing the expensive deterministic model by a meta-model whose computation time is quasi-negligible. Then, a direct MCS can be performed on the obtained metamodel. This procedure is used to perform the reliability analysis in chapter 3, where the SPCE is combined with the MCS. However, this procedure can be enhanced by an adaptive experimental design algorithm. The idea of building a metamodel starting with initial ED and gradually enriching it, was developed to enhance the accuracy of the surrogate-model since the reliance on a single set of ED could be insufficient to cover the limit state surface vicinity which is the region of interest in the reliability analysis. Recently, Marelli and Sudret (2018) presented an active learning method to construct the SPCE model and the approach is noted A-bSPCE in this chapter.

The approach starts with an initial ED which is updated iteratively by adding new samples located close to the limit state surface to improve the accuracy of the reliability analysis results. After each update of the ED, a new SPCE model is obtained. Consequently, two key elements should be defined for the adaptive experimental design algorithm: the learning function which identifies the best candidate sample to enrich the current ED in order to improve the metamodel accuracy in estimating the failure probability, and the stopping condition of the active learning SPCE that is used to stop the ED enrichment process when the preset target accuracy is satisfied.

Marelli and Sudret (2018) used the bootstrap-based local error estimate introduced in the previous section, to define a solution for the learning function and the stopping condition in an adaptive SPCE. They proved the method efficiency for reliability analysis by its application on a set of benchmark applications.

The former is based on the probability of misclassification of a candidate sample and it is expressed at each sample $x^{(i)}$ as follows:

$$LF_{bSPCE}\left(x^{(i)}\right) = \left|\frac{Num_S\left(x^{(i)}\right) - Num_F\left(x^{(i)}\right)}{B}\right| \tag{4-8}$$

where B is the number of the bootstrap SPCE models obtained after each enrichment, $Num_S\left(x^{(i)}\right)$ and $Num_F\left(x^{(i)}\right)$ are the number of safe (respectively failed) predictions obtained by the B different SPCE models at the sample $x^{(i)}$. The learning function is then evaluated on the MCS samples and the one which can minimize the value of LF_{bSPCE} is added to the current ED. The number of samples to be added in each iteration can be more than one.

The latter, which is necessary to define a stopping condition of the adaptive process, is based on the convergence of the P_f values estimated by the B SPCE models after each iteration and it is given as follows:

$$\frac{P_f^+ - P_f^-}{P_f} \leq \varepsilon_{P_f} \tag{4-9}$$

where ε_{P_f} is an the target accuracy in a range between 0.05 and 0.15 for typical usage scenarios (Marelli and Sudret, 2018), P_f is the failure probability obtained by the SPCE which is based on the full set of the $ED^{(ref)}$, and P_f^+ and P_f^- are respectively the maximum and minimum of the P_f values estimated by the B different SPCE models. The adaptive process is considered as convergence when this condition is satisfied for two consecutive iterations (Marelli and Sudret, 2018).

4.3.3 Sliced Inverse Regression (SIR)

The random field discretization could result in a large number of input random variables. Using the SPCE for high dimensional stochastic problems is found to be very time-consuming. Although the adaptive SPCE is more efficient than the SPCE and intuitively the PCE, when the dimension is high, it is still difficult to build the metamodel using adaptive SPCE with reasonable accuracy and computation time (Al-Bittar and Soubra, 2014a; Pan and Dias, 2017c). To overcome the problem of dimensionality, a dimension reduction technique should be incorporated in order to reduce the original high-dimensional input random variable vector. The output response in many problems handling a large number of input random variables depends only on a limited number of parameters varying within a low-dimensional subspace (Li et al., 2016). Therefore, these problems are in practice low-dimensional. Generally, the dimension reduction is achieved by using the global Sensitivity Analysis GSA (Sudret, 2008). The SPCE-based GSA has been widely used to perform reliability analysis (Al-Bittar and Soubra, 2014a; Pan and Dias, 2017b; Guo et al., 2019a-2019b) and it has shown a good performance. In the framework of this approach, a GSA based on a SPCE of 2nd order is performed to select the significant variables. A SPCE of second order requires a smaller ED and therefore a smaller number of calls to the deterministic model comparing to a high-order one. In addition, the change in Sobol indices with the SPCE order is insignificant (Sudret, 2008; Al-Bittar and Soubra, 2014a). Therefore, the GSA based on a SPCE of 2nd order helps to reduce the input dimension by selecting the significant variables of the input space that are used thereafter to create an accurate metamodel with a higher SPCE order. The efficiency of this reduction technique is vanished when the contributions of all the input variables to the output model response are almost the same (Li et al., 2016).

On the other hand, the dimension reduction of high dimensional problems could be achieved by another approach, the sliced inverse regression (SIR) (Li, 1991). This approach belongs to the family of dimension reduction approaches, based on the idea that most or all of the interesting feature of model

responses could be captured with least dimension formed by few linear combinations of original input variables. The reduced input dimension is called the effective dimension reduction (EDR) space. SIR is used to find the EDR through an inverse regression relation which regress the component of the original d-dimensional input vector $x = \{x^{(i)};\ i = 1 \dots d\}$ against the model response y. The dimension reduction is achieved when this new set of linear combinations on a *k*-dimensional subspace (*k*<*d*) is able to catch the essential feature of y. As a result, the *d*-dimensional input vector is projected into a *k*-dimensional subspace (*k*<*d*). More details about this efficient reduction technique and their successful applications could be found in many research papers (Li, 1991; Yeh et al., 2009; Li et al., 2016; Pan and Dias, 2017c; Xu and Wang, 2019).

4.3.4 The combination of SIR and A-bSPCE: SIR/A-bSPCE procedure

In this chapter, the reliability analysis of geosynthetic reinforced soil retaining wall is performed using a hybrid approach that combines the reduction technique SIR and the metamodeling method A-bSPCE and this approach is called SIR/A-bSPCE. The procedure of performing a reliability analysis by using the SIR/A-bSPCE is presented by a flowchart in Figure 4-1.

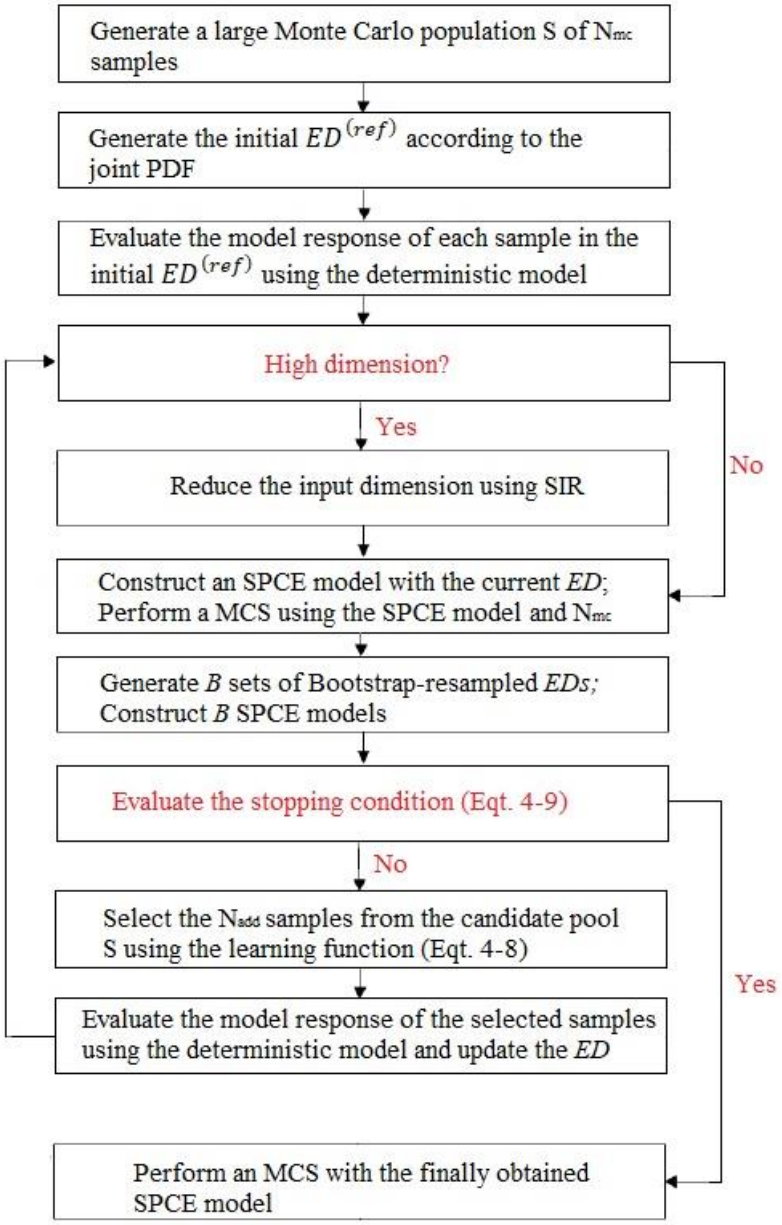

Figure 4-1 Flowchart for the reliability analysis performed by the SIR/A-bSPCE

The idea of this method is that the SIR technique is applied in order to reduce the dimension of the original input vector. Once the low-dimension subspace is available, a metamodel is constructed using the adaptive SPCE.

In this chapter, the following parameters are considered: the samples number for MCS $N_{mc} = 5 \times 10^6$, the initial size of the experimental design $ED^{(ref)}$ is equal to the initial dimension of the input vector, the number of the bootstrap SPCE models $B = 50$, the target accuracy $\varepsilon_{P_f} = 0.15$ and the samples number to be added to the ED after each iteration $N_{add} = 2$.

4.4 Probabilistic analysis of Geosynthetic Reinforced Soil Retaining Walls

This section aims to perform a probabilistic internal seismic stability analysis on the geosynthetic reinforced soil retaining walls in spatially random soils using the SIR/A-bSPCE method. The spatial variability of the soil shear strength parameters is modeled using two random fields. The Karhunen-Loève expansion method (K-L expansion) is used for the random fields generation. The deterministic calculations of the safety factors are obtained using the deterministic model presented in chapter 3, based on the upper bound theorem of limit analysis combined with the discretization technique. This latter is used to generate the rotational failure mechanism and allows the implementation of the pseudo-dynamic approach to represent the earthquake loading. The same performance function G used for the reliability analysis in the previous chapter, is considered here.

4.4.1 Presentation of the geosynthetic reinforced soil retaining wall model

The geosynthetic reinforced soil wall model considered in this chapter is the same presented in the previous chapter and it is shown in Figure 4-2. All the parameters except the soil strength parameters φ and c are taken as deterministic in order to focus on the soil variability effects. It is a vertical wall of height $H = 6m$. The backfill is reinforced with 10 geogrids layers with constant length L_r=1.2H, vertical spacing S_v=60cm and a tensile resistance strength T_u=28.7 kN/m. The soil unit weight γ is equal to 18 kN/m^3. The other parameters are as follows: k_h=0.15, λ=0.5, f=1.2, T=0.3 s, t_0=0 s, V_s=150 m/s, V_P=280.5 m/s, $\delta\theta$=0.1^o where λ=k_v/k_h.

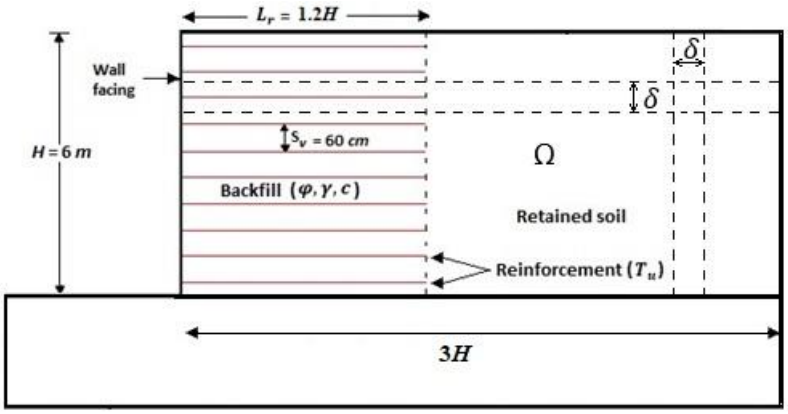

Figure 4-2 Reinforced soil retaining wall model and the random field domain

Two cross-correlated lognormal random fields are used to model the spatial variability of the soil shear strength parameters φ and c bounded by a domain Ω. Table 4-1 summarizes the mean and coefficient of variation values for soil friction angle and soil cohesion. As mentioned previously, φ and c are assumed to share an identical autocorrelation function in the soil region Ω. In other words, both random fields have the same autocorrelation distances l_x and l_y. However, anisotropic random fields are

assumed ($i.e. l_x \neq ly$) in this study since the soil is rarely isotropic in reality due to the geological soil formation process. Generally, the autocorrelation distance in the vertical direction l_y is much shorter than the one in the horizontal direction l_x (Fenton and Griffiths, 2003; Al-Bittar and Soubra, 2013; Pan and Dias, 2017b). Many literature research suggested that the autocorrelation distance l_x in the horizontal direction is usually between 10 and $40m$, while l_y ranges between 1 and $3m$ in the vertical direction (El-Ramly et al., 2003; Jiang et al., 2015; Guo et al., 2019b). In this chapter, these values ranges of l_x and l_y are adopted and the influence of the different values of the autocorrelation length on the structure reliability results is investigated and discussed. For the realization of the random field, the domain Ω is discretized into rectangular elements. The grid size is taken equal to $\delta = 0.5m$ in both directions which can ensure a sufficient accuracy of the generated random fields (Der Kiureghian and Ke, 1988; Li and Der Kiureghian, 1993).

Table 4-1 Statistics and distribution of the soil strength parameters.

Random field	Mean	COV (%)	Distribution type
$\boldsymbol{\varphi}$ (°)	28	20	Lognormal
$\boldsymbol{c}$ ($\boldsymbol{kPa}$)	5	40	Lognormal

4.4.2 Selection of the truncated order M in a K-L expansion

The approximate random process is defined by truncating the series expansion to a finite number of terms S. The truncation term number M is determined by the calculation of the truncation error estimate ε given in Eq. 4-4 with a target accuracy. In this chapter, M is determined so that ε is lower than 5%. Figure 4-3 presents the error estimate ε against the truncation term number M for the case of $l_x = 40m$ and $l_y = 3m$. A K-L term M equal to 50 is found sufficient to ensure the prescribed accuracy.

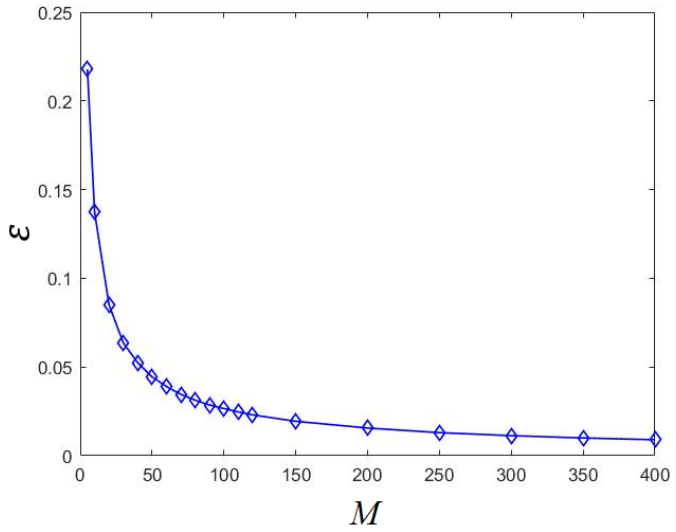

Figure 4-3 Truncation error of the random field ($l_x = 40m$, $l_y = 3m$)

Table 4-2 presents the truncation term numbers M for different values of autocorrelation distances considered in this chapter for the prescribed error. It is clear that M increases when the heterogeneity of the soil medium increases. The total number of the random variables involved in the probabilistic analysis is equal to $2M$, since two random fields are considered.

Table 4-2 Truncation term number M for different cases of autocorrelation distances

l_x (m)	ly (m)	M
10	3	140
20	3	80
30	3	60
40	3	50
40	1	130
40	1.5	90
40	2	70
40	2.5	60

4.4.3 Results and discussions

The aim of this section is to investigate the influence of the spatial variability of the two random fields and the correlation between them on the PDF of the safety factor FoS and the failure probability of the geosynthetic reinforced soil retaining wall model. Concerning the spatial variability of the random field, it is related to the autocorrelation distances and the coefficient of variation COV. The effect of the autocorrelation distances and the COV are studied apart. It is worth noting that the deterministic calculation using the mean values of the two random fields gives a safety factor $FoS \cong 1.5$.

4.4.3.1 Effect of the autocorrelation distance

The autocorrelation structure of the random field is defined by the autocorrelation distance, since the importance of this parameter. To investigate its influence, different values of the autocorrelation distances are tested within the ranges defined previously. For the horizontal autocorrelation distance l_x, it varies between 10 and $40m$, and for the vertical one l_y between 1 and $3m$. The values of the COV of the soil cohesion and of the soil friction angle are considered here constants and equals to the values presented in Table 4-1. The cross-correlation coefficient between the two random fields is not considered in all these section calculations.

Figures 4-4 and 4-5 provide the PDFs of the reinforced soil retaining wall model safety factor for different values of the autocorrelation distances. Figure 4-4 shows the influence of the horizontal autocorrelation distance l_x while Figure 4-5 shows the influence of the vertical autocorrelation distance l_y. The case of random variables is also presented in these figures, where both soil strength parameters are modeled using random variables i.e. equivalent to the case $l_x = l_y = \infty$.

It can be shown from Figure 4-4 that the PDF of the wall safety factor becomes taller and narrower when decreasing l_x. This means that the variability of the FoS decreases when increasing the backfill soil heterogeneity. The PDF of the random variables case is the widest and the shortest among all the PDFs, i.e. the more spread-out variability of the structure FoS. The same observations are noted in Figure 4-5 where increasing l_y results in shorter and wider PDF. When increasing the autocorrelation distance (l_x or l_y), the corresponding PDF gets closer to the PDF of the random variables case. This observation was also reported by many researchers in the reliability analysis of strip footings (Al-Bittar and Soubra, 2014b), tunnel stability (Pan and Dias, 2017b) and embankment dam (Guo et al., 2019a). This can be explained by the fact that when the autocorrelation distance increases, the random variables resulting from the random field discretization, becomes more correlated. Then, it means that the variation of the values of the soil strength parameters is low within the soil region Ω. Consequently, the variability of the soil strength parameters within Ω decreases in one realization. The extreme case is for the infinite values of autocorrelation distances which corresponds to the random variables approach, where the soil strength parameters are considered constants in one simulation. It can be concluded that when the autocorrelation distance increases, there is a change in the global average of the strength parameter random fields from one realization to another. On the other hand, when the autocorrelation distance decreases and tends to zero, the heterogeneity of the soil region increases. Then, in one realization of the random fields, the soil shear strength parameters vary significantly from one discretized element to another due to the soil heterogeneity. However, the global average of the soil strength parameters will be close to the fields means values due to the large number of high and small values in the discretized elements. As a result, the variability from one simulation to another is less in this case.

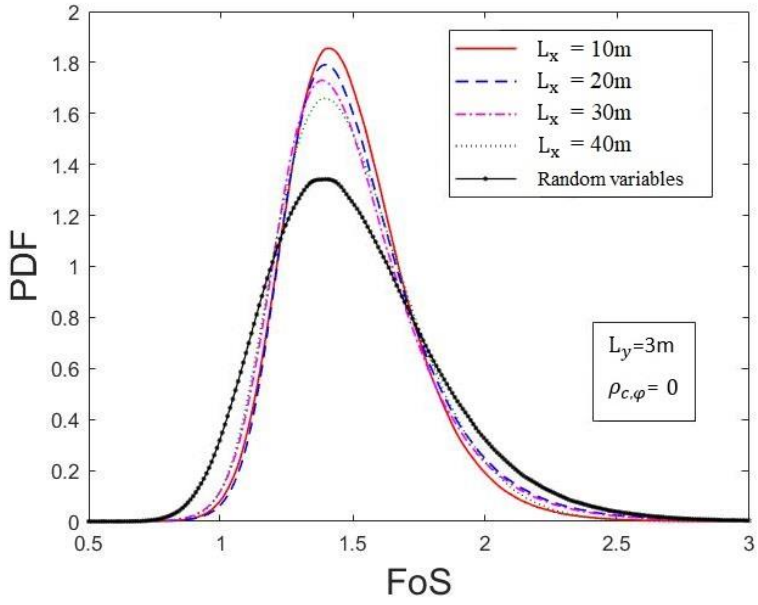

Figure 4-4 Influence of the horizontal autocorrelation distance on the PDF of the safety factor

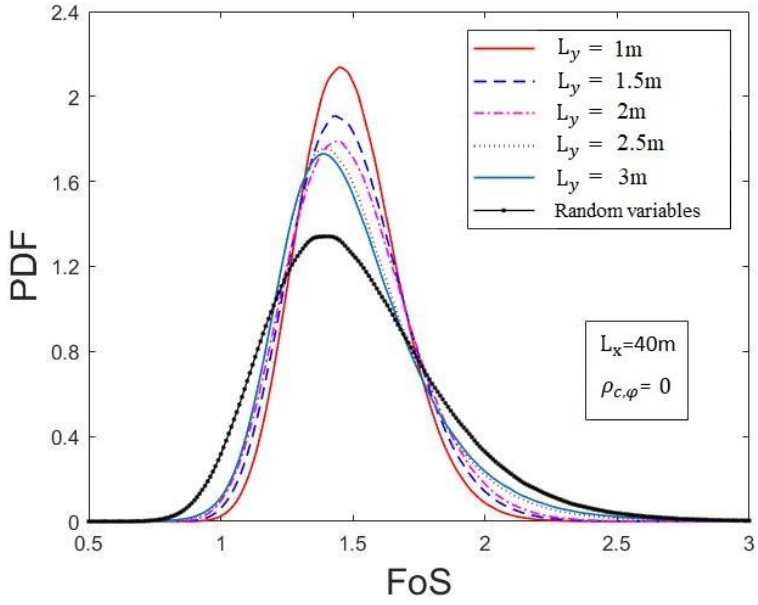

Figure 4-5 Influence of the vertical autocorrelation distance on the PDF of the safety factor

Table 4-3 shows the impact of the autocorrelation distances on the failure probability of the reinforced soil retaining wall model and on the FoS first two statistical moments. It is observed that the probability of failure increases as the autocorrelation distance increases. This is justified by the global average of the soil strength parameters in case of a strong heterogeneity, which will be close to the random fields mean values. For a vertical autcorrelation distance l_y= $3m$, when the horizontal autocorrelation distance increases from 10 to $40m$, the failure probability incraeses from 4.210× 10^{-3} to 7.114× 10^{-3}. For l_x = $40m$, when l_y increases from 1 to $3m$, the failure probability increases from 0.804× 10^{-3} to 7.114×

10^{-3}. Therefore, the variability of the failure probability is more sensitive to the change of the vertical autocorrelation distance. Additionally, it can be concluded that an underestimation of the autocorrelation distances provides lower estimation of the real failure probability and therefore unsafe design. These conclusions were also reported by Jiang et al. (2015) in the slope stability reliability analysis and by Pan and Dias (2017b) in the probabilistic evaluation of tunnel face stability in spatially variable soils. It is important to note that the case of random variables approach, leads to a much greater failure probability than all the random fields cases with a failure probability value equal to 24.738× 10^{-3}. This implies that modeling the soil strength parameters using random variables leads to a much safer and conservative design, but may not be economical. Concerning the the FoS first two statistical moments, the safety factor mean value remains almost constant with the variation of the autocorrelation distances while the standard deviation increases with the autocorrelation distances and therefore, a wider PDF is obtained with greater autocorrelation distances.

Table 4-3 Influence of the autocorrelation distance on the reliability results

Autocorrelation distance (m)	$\boldsymbol{P_f}$	$\boldsymbol{\mu_{FoS}}$	$\boldsymbol{\sigma_{FoS}}$
$\boldsymbol{l_x = 10, l_y = 3}$	4.210× 10^{-3}	1.4946	0.237
$\boldsymbol{l_x = 20, l_y = 3}$	4.855× 10^{-3}	1.499	0.268
$\boldsymbol{l_x = 30, l_y = 3}$	6.369× 10^{-3}	1.494	0.27
$\boldsymbol{l_x = 40, l_y = 3}$	7.114× 10^{-3}	1.499	0.271
Random variables: $\boldsymbol{l_x = \infty, l_y = \infty}$	24.738×10^{-3}	1.512	0.326
$\boldsymbol{l_x = 40, l_y = 1}$	0.804×10^{-3}	1.486	0.189
$\boldsymbol{l_x = 40, l_y = 1.5}$	2.384×10^{-3}	1.488	0.213
$\boldsymbol{l_x = 40, l_y = 2}$	4.341×10^{-3}	1.489	0.228
$\boldsymbol{l_x = 40, l_y = 2.5}$	5.743×10^{-3}	1.492	0.255
$\boldsymbol{l_x = 40, l_y = 3}$	7.114×10^{-3}	1.499	0.271

4.4.3.2 Effect of the cross-correlation

As noted in the section 3.2.5 in chapter 3, a negative correlation is reported between the soil strength parameters in most previous literature studies (Lumb, 1970; Yucemen et al., 1973; Hata et al., 2012). However, a positive correlation is reported in some rare cases. For instance, Wolff (1985) reported a correlation coefficient equal to 0.25 for consolidated-undrained tests (CU). Consequently, seven cross-correlation coefficients ranging from -0.6 to 0.6 are considered here to investigate the effects of cross-correlation coefficient between the random fields of the soil strength parameters (c and φ). The results are provided for autocorrelation distances l_x= 40m and l_y= 3m and coefficients of variation COV_φ=20% and COV_c=40%. The results for random variables approach are also provided.

The PDFs of reinforced soil wall model safety factor are only presented for four values of cross-correlation $\rho_{c,\varphi}$ for the sake of clarity. As a result, eight different PDFs are ploted in Figure 4-6, four PDFs related to the random fields approach and four to the random variables one. Figure 4-6 shows that the PDF curves become shorter and wider when increasing the cross-correlation $\rho_{c,\varphi}$ between the two random fields. In other words, the variability of the wall safety factor increases when the correlation between the two random fields increases. A negative cross-correlation decreases the variability while a positive one increases it. This is justified by the fact that a negative cross-correlation between the soil strength parameters random fields means that the increase of one of these parameters implies a decrease in the other one. As a result, the total shear strength slightly varies and therefore, this leads to a reduction on the variability of the reinforced soil wall safety factor. Similar observations are made on the effect of the cross-correlation coefficient on the PDF of the safety factor in case of random variables approach. In addition, the PDFs obtained in this section confirm a conclusion of the previous section, that the PDFs for the random variables approach are always more spread out compared to those obtained for the random fields approach.

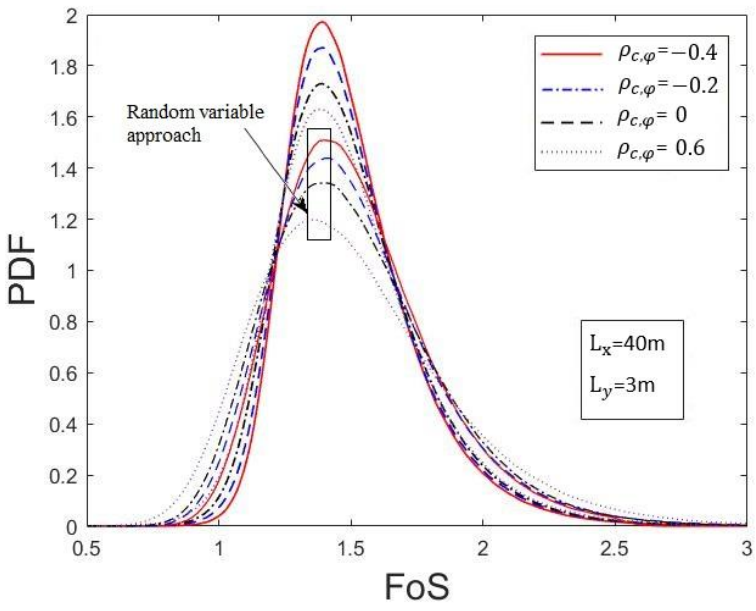

Figure 4-6 Influence of the cross-correlation coefficients on the PDF of the safety factor

Figure 4-7 presents the failure probability versus the cross-correlation coefficients for both random fields and random variables approaches. The failure probability of the reinforced soil retaining wall model increases with the increase of the cross correlation. For the random variables approach, for a cross-correlation equal to -0.6, the failure probability is 4.24×10^{-3}. This value increases to 46.50×10^{-3} when the cross-correlation increases to 0.6. For the random fields approach, for a cross-correlation equal to -0.6, the failure probability is 0.55×10^{-3}. It increases to 15.98×10^{-3} for a cross-correlation equal to 0.6. This is also because an assumption of negative cross-correlation implies that an increase of

the cohesion values is associated with a decrease of the soil friction values and vice-versa. Thus, the variability of the total shear strength and consequently of the reinforced soil wall safety factor is reduced. As a conclusion, neglecting the cross-correlation between the soil strength parameters leads to safer design of the reinforced soil retaining walls, except for the rarely case of positive correlation coefficient, where neglecting this correlation leads to unsafe design. This conclusion was also reported in many works (Mollon et al., 2009a-2009b; Guo et al., 2019a). A comparison between the random variables approach and the random fields one clearly shows that the former overestimates the reinforced soil wall model failure probability and therefore, neglecting the spatial variability of the soil strength parameters leads to a conservative design but not economical.

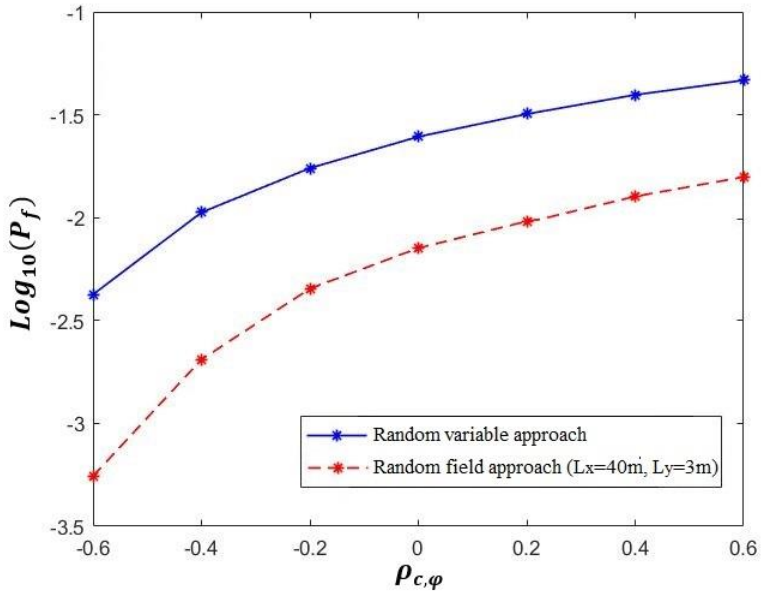

Figure 4-7 Influence of the cross-correlation coefficients on the failure probability

Table 4-4 gives summaries of all the simulations results obtained for different values of cross-correlation coefficient between the soil cohesion and the soil friction angle for both random fields and random variables approaches cases, in terms of failure probability and the first two moments of FoS. It should be mentioned that the mean value of the reinforced soil wall safety factor slightly decreases when the correlation between the two random fields increases from -0.6 to 0.6, contrary to the standard deviations that increases with the cross-correlation coefficient increase.

Table 4-4 Influence of the cross-correlation between the random fields on the reliability results

$\rho_{c,\varphi}$	P_f	μ_{FoS}	σ_{FoS}
Random fields			
-0.6	0.55×10^{-3}	1.504	0.228
-0.4	2.05×10^{-3}	1.501	0.248
-0.2	4.52×10^{-3}	1.501	0.261

0	7.11×10^{-3}	1.499	0.271
0.2	9.60×10^{-3}	1.498	0.273
0.4	12.85×10^{-3}	1.495	0.282
0.6	15.98×10^{-3}	1.492	0.288
Random variables			
-0.6	4.24×10^{-3}	1.517	0.283
-0.4	10.61×10^{-3}	1.516	0.285
-0.2	17.4×10^{-3}	1.51	0.316
0	24.74×10^{-3}	1.512	0.326
0.2	31.88×10^{-3}	1.516	0.347
0.4	39.52×10^{-3}	1.519	0.363
0.6	46.50×10^{-3}	1.517	0.376

4.4.3.3 Effect of the COV

The spatial variability of the random field is related to the autocorrelation distances and the coefficient of variation COV. This section aims to study the effect of the coefficient of variation (COV) of the friction angle φ and soil cohesion c random fields. In the previous simulations, in order to show the effects of the autocorrelation distance and the cross-correlation between the random fields, COV_φ and COV_c are fixed 20% and 40% as shown in Table 4-1. Different values of the coefficient of variation (COV) of the friction angle φ and soil cohesion c are proposed in the literature. For the soil friction angle, the COV ranges essentially between 2 and 20% (Phoon and Kulhawy, 1999; Chalermyanont and Benson, 2004; Luo et al., 2016; Javankhoshdel and Bathurst, 2017). For the soil cohesion, the value of the COV could reach 50% (Phoon and Kulhawy, 1999; Sivakumar Babu and Singh, 2011; Javankhoshdel and Bathurst, 2017; Javankhoshdel et al., 2019). In order to discuss the influence of the coefficient of variation on the reliability results, different values of COV_c and COV_φ were considered. The results are provided for autocorrelation distances l_x= 40m and l_y= 3m and the cross-correlation coefficient between the two random fields is not considered and is taken equal to zero in all calculations of this section.

Figure 4-8 presents the PDFs of the reinforced soil retaining wall model safety factor for four different values of COV_c. The coefficient of variation of the soil friction angle COV_φ is taken equal to 20%. It can be observed that when COV_c increases, the PDF of the wall safety factor becomes shorter and wider, which indicates that the variability of the safety factor increases with the increase of the coefficient of variation of the soil cohesion random field COV_c. On the other hand, Figure 4-9 presents the PDFs of the reinforced soil retaining wall model safety factor for four different values of COV_φ for a coefficient of variation of the soil cohesion COV_c equal to 40%. Similar to the former case, when COV_φ increases, the PDF of the wall safety factor becomes shorter and wider, which indicates that the variability of the safety factor increases with the increase of COV_φ. The impact of COV_φ on the PDFs shape is clearly greater than the impact of COV_c. The increase of the safety factor variability with the increase of the random fields coefficients of variation is more significant for the soil friction angle parameter. These

observations are logic since for the case of COV_φ=COV_c=0, the calculation is deterministic, i.e. the safety factor is constant and equal 1.5. Consequently, when the coefficients of variation decrease, the PDFs tends to approach the case of deterministic calculation, a vertical line with a safety factor equal to 1.5.

Concerning the random variables approach cases, it can be observed that the coefficients of variation of the two random variables have the same influence on the PDFs shapes by obtaining taller and narrower ones in case of lower coefficients of variations COV_φ and COV_c. In addition, the comparison between the random fields approach and the random variables one, gives similar results with the previous section by obtaining once again more spread out PDFs in case of random variables approach.

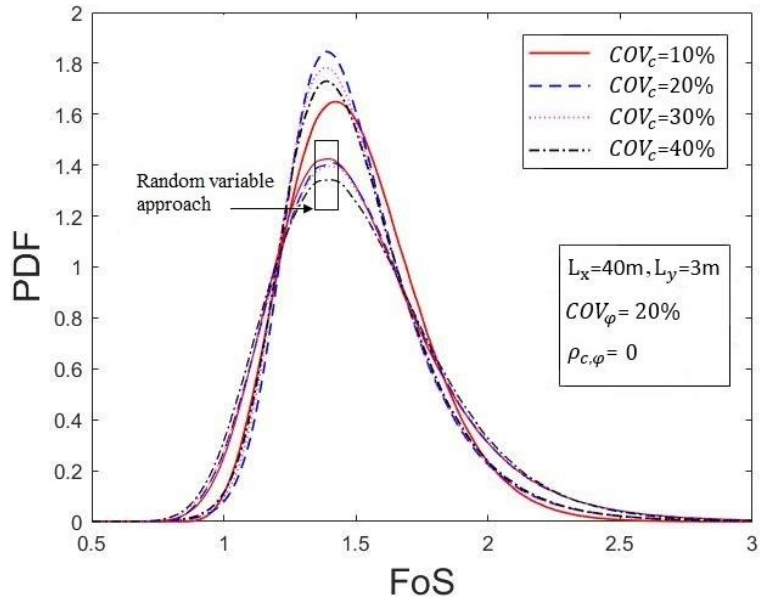

Figure 4-8 Influence of the coefficient of variation of cohesion COV_c on the PDF of the safety factor

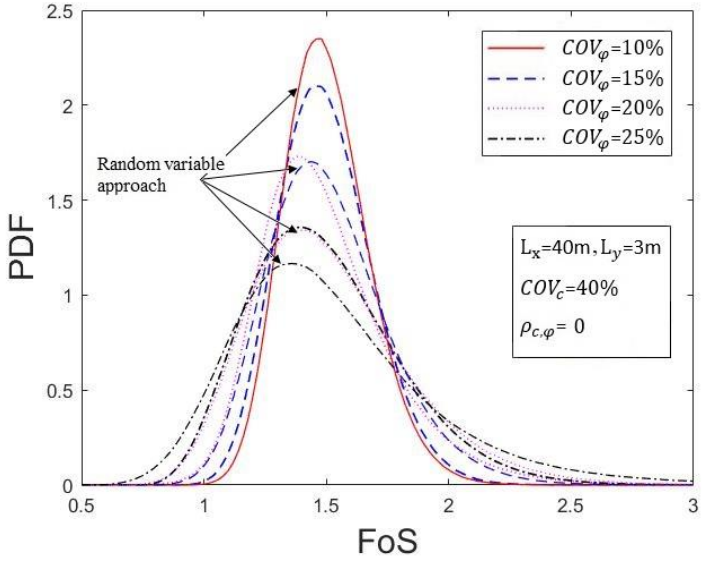

Figure 4-9 Influence of the coefficient of variation of soil friction angle COV_φ on the PDF of the safety factor

Figure 4-10 presents the failure probability of the Geosynthetic reinforced soil retaining wall model versus COV_c and COV_φ. It can be observed that the failure probability increases progressively with the increase of the coefficient of variation of random fields. The rate of increase is more important for the soil friction angle case. For COV_c=10%, the failure probability is equal to 4.117×10^{-3}, this value increases to 7.114×10^{-3} for COV_c=40%. On the other hand, the failure probability is equal to 6×10^{-6} for COV_φ=10%, this value reaches 26.5×10^{-3} for COV_φ=25%. Figure 4-10 presents also the case of random variables approach. The impact of the coefficient of variation on the failure probability in this approach is similar to that observed with the random fields approach. In addition, it is shown that the random variables approach always results in a greater failure probability of the reinforced soil wall model.

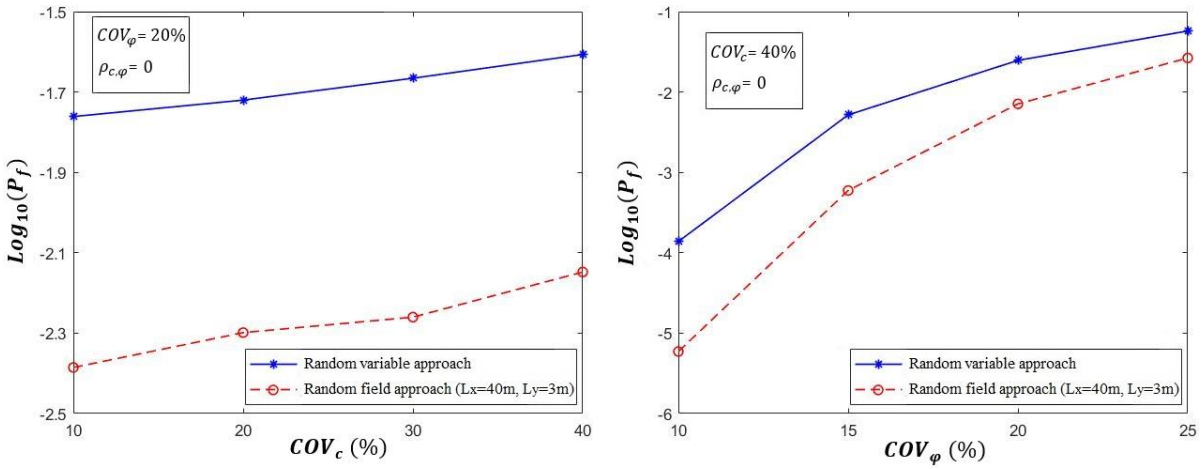

Figure 4-10 Influence of the coefficient of variation COV on the failure probability

Table 4-5 presents for all the coefficient of variation configurations, the failure probability of the wall and the first two statistical moments of the safety factor. It can be observed that the variation of the safety factor mean value is insignificant, while the standard deviation increases when increasing the COV.

Table 4-5 Influence of the coefficient of variation of the random fields on the reliability results

	P_f		μ_{FoS}		σ_{FoS}	
	RF	RV	RF	RV	RF	RV
COV_c=10% COV_φ=20%	4.117×10^{-3}	17.335×10^{-3}	1.499	1.517	0.249	0.323

$\boldsymbol{COV_c}$=20% $\boldsymbol{COV_\varphi}$=20%	5.027×10^{-3}	19.048×10^{-3}	1.503	1.518	0.264	0.325
$\boldsymbol{COV_c}$=30% $\boldsymbol{COV_\varphi}$=20%	5.493×10^{-3}	21.593×10^{-3}	1.498	1.518	0.266	0.326
$\boldsymbol{COV_c}$=40% $\boldsymbol{COV_\varphi}$=20%	7.114×10^{-3}	24.738×10^{-3}	1.499	1.512	0.271	0.326
$\boldsymbol{COV_c}$=40% $\boldsymbol{COV_\varphi}$=10%	0.6×10^{-5}	0.138×10^{-3}	1.496	1.503	0.1017	0.1745
$\boldsymbol{COV_c}$=40% $\boldsymbol{COV_\varphi}$=15%	0.595×10^{-3}	5.194×10^{-3}	1.498	1.509	0.1918	0.245
$\boldsymbol{COV_c}$=40% $\boldsymbol{COV_\varphi}$=20%	7.114×10^{-3}	24.738×10^{-3}	1.499	1.512	0.271	0.326
$\boldsymbol{COV_c}$=40% $\boldsymbol{COV_\varphi}$=25%	26.5×10^{-3}	57.415×10^{-3}	1.492	1.529	0.304	0.425

4.5 Conclusion

This chapter aims to perform a probabilistic analysis on a Geosynthetic reinforced soil retaining wall considering a random fields approach to consider the soil spatial variability of the backfill zone. The computation of the deterministic safety factor is based on the upper bound theorem of limit analysis. A rotational log-spiral failure mechanism is assumed. This latter is generated point-by-point through the discretization technique developed by Mollon et al. (2011) so that the seismic loading could be represented through the pseudo-dynamic approach. SIR/A-bSPCE is the reliability method considered to carry out the probabilistic analysis, aiming to alleviate the total computational burden. The soil cohesion and the friction angle are modelled as two anisotropic lognormal random fields. The Karhunen-Loève expansion method (K-L expansion) is employed for the random field discretization. The dimension reduction technique SIR is first applied to reduce the original high-dimensional input space. Then, an active learning sparse polynomial chaos expansion (A-bSPCE) is used to construct a metamodel in the reduced subspace. Finally, a MCS is performed using this metamodel. Different levels of spatial variability and cross-correlation are considered to investigate the influences of the autocorrelation distance, cross-correlation between the soil strength parameters and coefficient of variation of these two random fields on the probability density functions (PDFs) of the structure safety factor and on the failure probabilities. The following conclusions can be drawn:

The autocorrelation distance has a significant effect on the reinforced soil retaining wall reliability. Concerning the probability density function, the variability of the FoS decreases when increasing the backfill soil heterogeneity. On the other hand, it is observed that the failure probability increases with the autocorrelation distance increase. The variability of the failure probability is more sensitive to the change of the vertical autocorrelation distance.

The cross-correlation between the soil strength parameters has a significant influence on the probability density function as well as on the failure probability. The response variability decreases for a negative cross-correlation. In addition, the failure probability of the reinforced soil retaining wall decreases for negative cross-correlation coefficients. As a conclusion, neglecting the cross-correlation between the soil strength parameters leads to safer designs of the reinforced soil retaining walls.

The variability of the safety factor increases with the increase of the coefficient of variation of random fields. However, the impact of COV_{φ} on the PDFs shape and the safety factor variability is more significant than the COV_c one. Additionally, the failure probability increases with the coefficient of variation increase of random fields. The rate of increase is more important for the soil friction angle case.

A comparison between the random fields approach and the random variables one, shows that the PDFs for the latter are always more spread out compared to those obtained using the former approach. Accounting the soil spatial variabilities in the backfill soil provide less dispersive safety factors. The random variables approach leads to a much greater failure probability. This implies that neglecting the soil spatial variabilities leads to conservative results, ensuring safer design but uneconomical in some cases.

General conclusions

The aim of this study is to investigate the seismic internal stability of geosynthetic reinforced soil retaining walls in the context of deterministic and probabilistic analyses. First, a deterministic model is developed to evaluate the reinforcement strength required to maintain the stability of reinforced soil retaining walls under seismic conditions and to determine their safety factors. The kinematical approach of limit analysis is adopted in this context, to provide rigorous lower bounds for the required reinforcement strength or an upper bound of the wall safety factor. This approach is combined with the discretization technique proposed by (Mollon et al., 2011) in order to generate a rotational log-spiral mechanism point-by-point, which allows the possibility of presenting the seismic loading with a pseudo-dynamic approach and considers the soil heterogeneity. Then, the developed deterministic model is used in a probabilistic analysis framework. Advanced reliability methods are used to perform the probabilistic analysis using the random variables and random fields approach. The former is simpler and faster than the latter and was adopted in the first stage. Sparse polynomial chaos expansion (SPCE) is used to carry out the probabilistic analysis in this stage. The soil shear strength parameters, seismic loading and reinforcement strength parameters are modeled using random variables. In the second stage of the probabilistic analysis, a random fields approach is adopted in order to model the soil spatial variability neglected in the first stage. The random field discretization leads to a high dimensional problem. Therefore, an active learning sparse polynomial chaos expansion (A-bSPCE) combined with the sliced inverse regression reduction technique, is used at this stage to deal with the high dimensional problem.

This thesis manuscript presents a literature review on the reinforced soil retaining walls, the deterministic methods to design and assess the stability of these structures. For the probabilistic analysis, the sources of uncertainties, the reliability concept and the methods commonly used in geotechnical engineering are detailed. Two main parts are then proposed.

The first one, which is composed of chapter 2, is devoted to develop a deterministic model to evaluate the reinforcement strength required to maintain the geosynthetic reinforced wall stability. This model is based on the discretization-based kinematic theorem, proposed by Mollon et al. (2011). It is based on the combination of the upper bound theorem of limit analysis and the discretization technique to generate the failure mechanism of the reinforced soil retaining walls. The discretization technique allows to present the seismic loading with the pseudo-dynamic approach and to consider the soil heterogeneity which is not possible using the conventional limit analysis method; The proposed approach was firstly validated using the results of the conventional kinematic approach of limit analysis available in the literature (Michalowski, 1998a). Dry soils are considered in a first step. The cases of homogeneous as well as non-homogeneous and layered soils are investigated. The effects of key parameters on the required reinforcement strength were investigated using both the pseudo-static and the pseudo-dynamic approach. The crack-formation as a part of the failure mechanism as well as the case of pre-existing

crack were also considered. Then, the case of homogeneous and heterogeneous saturated soils is considered. The effect of pore water within the backfill soil is investigated together with a possible crack opening in cohesive soils. Finally, at the end of this part, the seismic internal stability analysis of geosynthetic reinforced unsaturated soil retaining walls is presented. Several empirical formulas for the estimation of the unsaturated soils shear strength were adopted.

The following conclusions are made in this part:

- The required normalized reinforcement strength decreases with the increase of the reinforcement length until a limit value above which, there is no benefit of the length increase,
- The required normalized reinforcement strength is highly dependent on the soil properties. It decreases when increasing the soil friction angle and the cohesion, and their importance is more significant for higher values of horizontal seismic coefficient k_h,
- From the analysis, the effects of the horizontal seismic coefficient k_h on the required reinforcement strength is also evident. Increasing k_h leads to an increase in the required reinforcement strength, and this is more pronounced for lower friction angle values,
- For nonhomogeneous backfills, the soil friction angle distribution has an important effect on the required normalized reinforcement. More the soil friction angle exhibits variation, greater are the reinforcement forces required to maintain the structure stability. The effect of a variation of the soil cohesion has a lower effect on the required reinforcement force than the soil friction angle variation one,
- The presence of a crack leads to an increase of the required reinforcement strength to ensure the stability of the reinforced earth wall, hence it is important to take into account of the cracks when the reinforced soils are cohesive ones,
- The required normalized reinforcement strength obtained when using the pseudo-dynamic approach is generally larger than the one obtained using the pseudo-static approach. For a range of values of the amplification factor f close to 1, the opposite occurs. Therefore, for a safety design, engineers must check the reinforcement using the two approaches for a soil class characterized by a low amplification factor. Otherwise, they should use the pseudo-dynamic approach to obtain a safe design,
- More the water table is deep, less is the required reinforcement strength for the reinforced earth wall. This is generally more pronounced when the matric suction in the unsaturated zone is greater. Therefore, it is important to carefully estimate the water table level and to account for a possible variation of this level due to the weather or other possible reasons,
- A comparison is presented for the two cases of fully unsaturated and fully saturated backfill soils. The results show a large reduction in the required reinforcement strength from saturated conditions to fully unsaturated conditions. Hence the importance of considering unsaturated soil properties instead of a saturated one can deal with economic benefits,

- The required reinforcement strength is greater when considering a linear increased matric suction distribution than in the case of a uniform one,
- The soil types represented by different SWCC models have a major influence on the required reinforcement strength for the wall stability. In addition, the increase of the soil matric suction decreases the required reinforcement strength except for the case of fine-grained soils where the required reinforcement strength remains the same.

The second part (which is composed of chapters 3 and 4), presents a reliability-based analysis of the seismic internal stability of geosynthetic reinforced soil retaining walls using random variables and random fields approach. The deterministic computation of the structure safety factor is based on the developed deterministic model to ensure rigorous results and to represent the seismic loading by the pseudo-dynamic approach. The strength reduction method is employed to calculate the safety factor. Chapter 3 constitutes the first stage of this part. The input uncertain parameters are modeled using random variables including the soil shear strength parameters, characteristics of seismic loading and reinforcement strength parameters. Sparse Polynomial Chaos Expansion (SPCE) in combination with the Monte Carlo Simulation is used to perform the probabilistic analysis. The effects of the correlation coefficients, the distributions types and the coefficient of variation of the input parameters on PDFs of the Geosynthetic reinforced soil wall safety factor FoS, mean and standard deviation of the FoS and system failure probability, were investigated. The contribution of each input variable to the FoS variance is also obtained by computing the Kucherenko sensitivity indices. The random variables approach is simpler and faster than the random fields one. However, it cannot model the soil spatial variability, which is not realistic since the soil properties changes in both the vertical and horizontal directions. In the second stage of this part (chapter 4), the effect of the soil spatial variability is investigated. The random fields approach is adopted in order to model the soil spatial variability. The random field discretization leads to a high dimensional problem. Therefore, an active learning sparse polynomial chaos expansion (A-bSPCE) combined with the sliced inverse regression reduction technique, is used to deal with this problem. Only the soil shear strength parameters are modelled as random fields to focus on the effect of the soil spatial variability on the reliability results. The Karhunen-Loève expansion method (K-L expansion) is employed for the random field discretization. The effects of the spatial variability and the cross-correlation between the random fields are investigated.

The main findings of the first stage of the probabilistic analysis part can be summarized as follows:

- The correlation between the soil parameters impacts the PDFs shape of the safety factor FoS. Considering the correlation between the soil parameters gives taller and narrower curves and smaller failure probabilities. The PDFs of the FoS are positively skewed for all cases of independent and correlated variables. The distribution is highly skewed in the case of independent variables and the skewness decreases with the increase of correlated variables. Neglecting some correlation structures

between the soil parameters ensure a conservative design. With respect to the sensitivity analysis, the correlation between the soil parameters have a significant influence on the Kucherenko indices,

- The normal distribution of random variables increases the failure probability, mean value and standard deviation of the reinforced soil wall safety factor FoS. The normal distribution appears to lead to a slightly shorter and wider PDF curve than the lognormal distribution one. With respect to the sensitivity analysis, the two distribution types of random variables give almost similar Kucherenko sensitivity indices for each variable,
- For the two distribution types, the Kucherenko sensitivity analysis helps to identify significant input parameters and shows that the soil friction angle and the horizontal seismic coefficient are the most important parameters in the reinforced soil retaining wall analysis. On the other hand, the soil unit weight has the lowest impact on the FoS variability,
- The failure probability decreased dramatically when the safety factor FoS increased from 1 to 1.4. For the same deterministic safety factor of the reinforced soil retaining wall and the same degree of uncertainty involved in the probabilistic calculations for the input random variables, the failure probability increased progressively with β, the angle formed by the wall with the horizontal. This result reflects the advantage of a probabilistic approach over a deterministic one since two systems that have the same deterministic safety factor present different failures probability in the framework of probabilistic analysis,
- The variability associated with the backfill soil friction angle plays a vital role in the design of the reinforced soil retaining wall and therefore, it is important to carefully specify the statistical parameters of this random variable through measurement data or laboratory test results.

The main findings of the second stage of this part:

- The autocorrelation distance has a significant effect on the reinforced soil retaining wall reliability. Concerning the probability density function, the variability of the FoS decreases when increasing the backfill soil heterogeneity. On the other hand, it is observed that the probability of failure increases with the autocorrelation distance increase and that the variability of the failure probability is more sensitive to the change of the vertical autocorrelation distance,
- The cross-correlation between the soil strength parameters has a significant influence on the probability density function as well as on the failure probability. The response variability decreases for a negative cross-correlation. In addition, the failure probability of the reinforced soil retaining wall model decreases for negative cross-correlation coefficients. As a conclusion, neglecting the cross-correlation between the soil strength parameters leads to safer design of the reinforced soil retaining walls,
- The variability of the safety factor increases with the coefficient of variation increase of random fields. However, the impact of COV_{φ} on the PDFs shape and the safety factor variability is more significant than the impact of COV_c. Additionally, the failure probability increased with the

coefficient of variation increase of the random fields. The rate of increase is more important for the soil friction angle case,

- A comparison between the random fields approach and the random variables one, shows that the PDFs for the later are always more spread out. Accounting for the soil spatial variabilities in the backfill soil provide less dispersive wall safety factors. The random variables approach leads to a much greater failure probability. This implies that neglecting the soil spatial variabilities leads to conservative results, ensuring safer design but uneconomical in some cases.

Perspectives

The failure of geosynthetic reinforced soil retaining structures involves three-dimensional mechanisms. In this research work, a two-dimensional analysis is considered. It will then be interesting to develop a 3D limit analysis model that will allow to better understand the seismic behavior of this type of structures, and to evaluate the efficiency of 2D models.

The study of the behavior of this type of structures will be investigated with a sophisticated three-dimensional numerical model. In this approach, advanced constitutive models for the soil and structures, and the soil-structure interface will be integrated. Numerical modeling has several advantages over limit analysis as it allows not only to focus on the failure of structures but also on their deformations. This will allow to focus on the serviceability limit state which is often the more important state to be verified.

References

AASHTO, 1996. Standard Specifications for Highway Bridges, Sixteenth. ed. American Association of State Highway and Transportation Officials, Washington, D.C., USA.

Abd, A.H., Utili, S., 2017a. Design of geosynthetic-reinforced slopes in cohesive backfills. Geotext. Geomembranes 45, 627–641. https://doi.org/10.1016/j.geotexmem.2017.08.004

Abd, A.H., Utili, S., 2017b. Geosynthetic-Reinforced Slopes in Cohesive Soils Subject to Seismic Action. Procedia Eng. 189, 898–907. https://doi.org/10.1016/j.proeng.2017.05.140

Abdul-Kader, E.H., Soubra, A.-H., Al-Bittar, T., 2019. Probabilistic analysis of strip footings based on enhanced Kriging metamodeling. Int. J. Numer. Anal. Methods Geomech. 43, 2667–2686.

Ahmadabadi, M., Ghanbari, A., 2009. New procedure for active earth pressure calculation in retaining walls with reinforced cohesive-frictional backfill. Geotext. Geomembranes 27, 456–463. https://doi.org/10.1016/j.geotexmem.2009.06.004

Ahmadi, H., Bezuijen, A., 2018. Full-scale mechanically stabilized earth (MSE) walls under strip footing load. Geotext. Geomembranes 46, 297–311. https://doi.org/10.1016/j.geotexmem.2017.12.002

Akhlaghi, T., Nikkar, A., 2014. Numerical analyses of dynamic response of geosynthetic-reinforced soil retaining wall. Geosystem Eng. 17, 142–149. https://doi.org/10.1080/12269328.2014.931259

Al-Bittar, T., Ahmed, A., Soubra, A.-H., Thajeel, J., 2017. Probabilistic Analysis of Strip Footings Resting on Spatially Varying Soils Using Importance Sampling and Kriging Metamodeling. Geotech. Spec. Publ. 440–449. https://doi.org/10.1061/9780784480717.042

Al-Bittar, T., Soubra, A.-H., 2014a. Efficient sparse polynomial chaos expansion methodology for the probabilistic analysis of computationally-expensive deterministic models. Int. J. Numer. Anal. Methods Geomech. 38, 1211–1230. https://doi.org/10.1002/nag.2251

Al-Bittar, T., Soubra, A.-H., 2014b. Probabilistic analysis of strip footings resting on spatially varying soils and subjected to vertical or inclined loads. J. Geotech. Geoenvironmental Eng. 140. https://doi.org/10.1061/(ASCE)GT.1943-5606.0001046

Al-Bittar, T., Soubra, A.-H., 2013. Bearing capacity of strip footings on spatially random soils using sparse polynomial chaos expansion. Int. J. Numer. Anal. Methods Geomech. 37, 2039–2060. https://doi.org/10.1002/nag.2120

Al-Bittar, T., Soubra, A.-H., Thajeel, J., 2018. Kriging-based reliability analysis of strip footings resting on spatially varying soils. J. Geotech. Geoenvironmental Eng. 144. https://doi.org/10.1061/(ASCE)GT.1943-5606.0001958

Alhajj Chehade, H., Dias, D., Sadek, M., Hage Chehade, F., Jenck, O., 2019a. Seismic internal stability assessment of geosynthetic reinforced earth retaining wall in cohesive soil using limit analysis, in: MATEC Web of Conferences. https://doi.org/10.1051/matecconf/201928102008

Alhajj Chehade, H., Dias, D., Sadek, M., Jenck, O., Hage Chehade, F., 2021. Pseudo-static Analysis of Reinforced Earth Retaining Walls. Acta Geotech. 2. https://doi.org/10.1007/s11440-021-01148-2

Alhajj Chehade, H., Dias, D., Sadek, M., Jenck, O., Hage Chehade, F., 2020. Upper bound seismic limit analysis of geosynthetic-reinforced unsaturated soil walls. Geotext. Geomembranes. https://doi.org/10.1016/j.geotexmem.2020.02.001

Alhajj Chehade, H., Dias, D., Sadek, M., Jenck, O., Hage Chehade, F., 2019b. Seismic analysis of geosynthetic-reinforced retaining wall in cohesive soils. Geotext. Geomembranes 47, 315–326. https://doi.org/10.1016/j.geotexmem.2019.02.003

Alhajj Chehade, H., Dias, D., Sadek, M., Jenck, O., Hage Chehade, F., 2019c. Seismic internal stability of reinforced earth retaining walls in saturated soils, in: 2nd Conference of the Arabian Journal of Geosciences (CAJG).

Alhajj Chehade, H., Sadek, M., Dias, D., Hage Chehade, F., Orianne, J., 2019d. Optimization of sensors locations in internal stability analysis of Geosynthetic-reinforced earth retaining walls, in: MATEC Web of

Conferences, SUS -Lille. Lille, p. 03001. https://doi.org/10.1051/matecconf/201929503001

Allen, T., Christopher, B., Elias, V., DeMaggio, J., 2001. Development of the simplified method for internal stability design of mechanically stabilized earth walls. Washington, DC.

Allen, T.M., Bathurst, R.J., 2014a. Performance of an 11 m high block-faced Geogrid wall designed using the K-stiffness method. Can. Geotech. J. 51, 16–29.

Allen, T.M., Bathurst, R.J., 2014b. Design and Performance of 6.3-m-High, Block-Faced Geogrid Wall Designed Using K-Stiffness Method. J. Geotech. Geoenvironmental Eng. 140.

Allen, T.M., Bathurst, R.J., Holtz, R.D., Lee, W.F., Walters, D., 2004. New Method for Prediction of Loads in Steel Reinforced Soil Walls. J. Geotech. Geoenvironmental Eng. 130, 1109–1120. https://doi.org/10.1061/(ASCE)1090-0241(2004)130

Allen, T.M., Bathurst, R.J., Holtz, R.D., Walters, D., Le, W.F., 2003. A new working stress method for prediction of reinforcement loads in geosynthetic walls. Can. Geotech. J. 40, 976–994. https://doi.org/10.1139/T03-051

Armour, T.A., Bickford, J., Pfister, T., 2004. Repair of failing MSE railroad bridge abutment, in: GeoSupport Conference 2004. Orlando, Florida, United States. https://doi.org/10.1061/40713(2004)53

Au, S.K., Beck, J.L., 2001. Estimation of small failure probabilities in high dimensions by subset simulation. Probabilistic Eng. Mech. 16, 263–277. https://doi.org/10.1016/S0266-8920(01)00019-4

Ausilio, E., Conte, E., Dente, G., 2000. Seismic stability analysis of reinforced slopes. Soil Dyn. Earthq. Eng. 19, 159–172. https://doi.org/10.1016/S0267-7261(00)00005-1

Baecher, D.G.B., Christian, J.T., 2005. Reliability and statistics in geotechnical engineering.

Baker, R., 1981. Tensile srength, tension cracks, and stability of slopes. Soils Found. 21, 1–17. https://doi.org/10.3208/sandf1972.21.2_1

Baker, R., Leshchinsky, D., 2003. Spatial distribution of safety factors: Cohesive vertical cut. Int. J. Numer. Anal. Methods Geomech. 27, 1057–1078. https://doi.org/10.1002/nag.312

Baker, R., Leshchinsky, D., 2001. Spatial distribution of safety factors. J. Geotech. Geoenvironmental Eng. 127, 135–145. https://doi.org/10.1061/(ASCE)1090-0241(2001)127:2(135)

Bao, C., Gong, B., Zhan, L., 1998. Properties of unsaturated soils and slope stability of expansive soils, in: Proceedings of the Second International Conference on Unsaturated Soils (UNSAT 98). Beijing, pp. 71–98.

Basha, B.M., Sivakumar Babu, G.L., 2012. Target reliability-based optimisation for internal seismic stability of reinforced soil structures. Géotechnique 62, 55–68. https://doi.org/10.1680/geot.8.p.076

Basha, B.M., Sivakumar Babu, G.L., 2011. Seismic reliability assessment of internal stability of reinforced soil walls using the pseudo-dynamic method. Geosynth. Int. 18, 221–241. https://doi.org/10.1680/gein.2011.18.5.221

Basha, B.M., Sivakumar Babu, G.L., 2010. Reliability assessment of internal stability of reinforced soil structures: A pseudo-dynamic approach. Soil Dyn. Earthq. Eng. 30, 336–353. https://doi.org/10.1016/j.soildyn.2009.12.007

Basha, B.M., Sivakumar Babu, G.L., 2009. Seismic reliability assessment of external stability of reinforced soil walls using pseudo-dynamic method. Geosynth. Int. 16, 197–215. https://doi.org/10.1680/gein.2009.16.3.197

Bathurst, R.J., 2019. A simple and rigorous approach for probabilistic internal stability analysis and design of reinforced soil walls, in: Eighth International Conference on Case Histories in Geotechnical Engineering. Philadelphia, Pennsylvania, pp. 203–211. https://doi.org/10.1061/9780784482087.018

Bathurst, R.J., Allen, T.M., Lin, P., Bozorgzadeh, N., 2019a. LRFD Calibration of Internal Limit States for Geogrid MSE Walls. J. Geotech. Geoenvironmental Eng. 145.

Bathurst, R.J., Allen, T.M., Nowak, A.S., 2008a. Calibration concepts for load and resistance factor design (LRFD) of reinforced soil walls. Can. Geotech. J. 45, 137761392.

Bathurst, R.J., Huang, B., Allen, T.M., 2011. Analysis of installation damage tests for LRFD calibration of reinforced soil structures. Geotext. Geomembranes 29, 323–334.

Bathurst, R.J., Huang, B.Q., Allen, T.M., 2012. Interpretation of laboratory creep testing for reliability-based analysis and load and resistance factor design (LRFD) calibration. Geosynth. Int. 19, 39–53. https://doi.org/10.1680/gein.2012.19.1.39

Bathurst, R.J., Lin, P., Allen, T.M., 2019b. Reliability-based design of internal limit states for mechanically stabilized earth walls using geosynthetic reinforcement. Can. Geotech. J. 56, 774–788. https://doi.org/10.1139/cgj-2018-0074

Bathurst, R.J., Miyata, Y., 2015. Reliability-based analysis of combined installation damage and creep for the tensile rupture limit state of geogrid reinforcement in Japan. Soils Found. 55, 437–446. https://doi.org/10.1016/j.sandf.2015.02.017

Bathurst, R.J., Miyata, Y., Nernheim, A., Allen, A.M., 2008b. Refinement of K-stiffness Method for geosynthetic-reinforced soil walls. Geosynth. Int. 15, 269–295. https://doi.org/10.1680/gein.2008.15.4.269

Benjamim, C.V.S., Bueno, B.S., Zornberg, J.G., 2007. Field monitoring evaluation of geotextile-reinforced soil-retaining walls. Geosynth. Int. 14, 100–118. https://doi.org/10.1680/gein.2007.14.2.100

Bishop, A.W., Morgenstern, N.R., 1960. Stability Coefficients for Earth Slopes. Géotechnique 10, 129–153. https://doi.org/10.1680/geot.1960.10.4.129

Blatman, G., Sudret, B., 2011. Adaptive sparse polynomial chaos expansion based on least angle regression. J. Comput. Phys. 230, 2345–2367. https://doi.org/10.1016/j.jcp.2010.12.021

Blatman, G., Sudret, B., 2010a. An adaptive algorithm to build up sparse polynomial chaos expansions for stochastic finite element analysis. Probabilistic Eng. Mech. 25, 183–197. https://doi.org/10.1016/j.probengmech.2009.10.003

Blatman, G., Sudret, B., 2010b. Efficient computation of global sensitivity indices using sparse polynomial chaos expansions. Reliab. Eng. Syst. Saf. 95, 1216–1229. https://doi.org/10.1016/j.ress.2010.06.015

Blatman, G., Sudret, B., 2008. Sparse polynomial chaos expansions and adaptive stochastic finite elements using a regression approach. Comptes Rendus - Mec. 336, 518–523. https://doi.org/10.1016/j.crme.2008.02.013

Camargo, J., Velloso, R.Q., Vargas, E.J., 2016. Numerical limit analysis of three-dimensional slope stability problems in catchment areas. Acta Geotech. 11, 1369–1383. https://doi.org/10.1007/s11440-016-0459-3

CEN (European Committee for Standardization), 2004. EN 1997-1:2004: Eurocode 7 – Geotechnical Design. Brussels, Belgium.

Chalermyanont, T., Benson, C.H., 2005. Reliability-Based Design for External Stability of Mechanically Stabilized Earth Walls. Int. J. Geomech. 5, 196–205. https://doi.org/10.1061/(asce)1532-3641(2005)5:3(196)

Chalermyanont, T., Benson, C.H., 2004. Reliability-Based Design for Internal Stability of Mechanically Stabilized Earth Walls. J. Geotech. Geoenvironmental Eng. 130, 163–173. https://doi.org/10.1061/~ASCE!1090-0241~2004!130:2~163!

Chen, T.-C., Chen, R.-H., Lin, S.-S., 2000. A nonlinear homogenized model applicable to reinforced soil analysis. Geotext. Geomembranes 18, 349–366.

Chen, W.-F., 1975. Limit Analysis and Soil Plasticity. Elsevier Scientific Publishing Company, New York.

Chen, W.-F., Giger, M.W., Fang, H.Y., 1969. On the limit analysis of stability of slopes. Soils Found. 9, 23–32. https://doi.org/10.3208/sandf1960.9.4_23

Chéret, I., 2015. Henri Vidal: Inventeur et créateur de la Terre Armée. https://doi.org/10.4000/sabix.1467

Cho, S.E., 2010. Probabilistic Assessment of Slope Stability That Considers the Spatial Variability of Soil Properties. J. Geotech. Geoenvironmental Eng. 136, 975–984. https://doi.org/10.1061/(asce)gt.1943-5606.0000309

Choudhury, D., Katdare, A.D., Pain, A., 2014. New Method to Compute Seismic Active Earth Pressure on

Retaining Wall Considering Seismic Waves. Geotech. Geol. Eng. 32, 391–402. https://doi.org/10.1007/s10706-013-9721-8

Choudhury, D., Nimbalkar, S.S., 2007. Seismic rotational displacement of gravity walls by pseudo-dynamic method: Passive case. Soil Dyn. Earthq. Eng. 27, 242–249. https://doi.org/10.1016/j.soildyn.2006.06.009

Choudhury, D., Nimbalkar, S.S., 2006. Pseudo-dynamic approach of seismic active earth pressure behind retaining wall. Geotech. Geol. Eng. 24, 1103–1113. https://doi.org/10.1007/s10706-005-1134-x

Chowdhury, R.N., Zhang, S., 1991. Tension cracks and slope failure, in: Proceedings of the International Conference: Slope Stability Engineering, Developments and Applications. Thomas Telford, London, pp. 27–32. https://doi.org/10.1680/ssedaa.16606.0005

Christopher, B.R., 1993. Deformation Response and Wall Stiffness in Relation to Reinforced Soil Wall Design. Purdue University.

Christopher, B.R., Gill, S.A., Giroud, G.-P., Juran, I., MitcheLl, G.K., Schlosser, F., Dunnicliff, J., 1990. Reinforced Soil Structures, Vol. 1 Design and Construction Guidelines, FHWA Report FHWA-RD-89-043.

Christopher, B.R., Gill, S.A., Giroud, G.-P., Juran, I., Schlosser, F., Mitchell, G.K., Dunnicliff, J., 1989. Design and Construction Guidelines - Volume II, Summary of Research and Systems Information , FHWA RD 89-043. Washington, D.C., USA.

Der Kiureghian, A., Ditlevsen, O., 2009. Aleatory or Epistemic? Does It Matter? Struct. Saf. 31, 105–112.

Der Kiureghian, A., Ke, J.B., 1988. The stochastic finite element method in structural reliability. Probabilistic Eng. Mech. 3, 83–91. https://doi.org/10.1016/0266-8920(88)90019-7

Drucker, D.C., Prager, W., 1952. SOIL MECHANICS AND PLASTIC ANALYSIS OR LIMIT DESIGN. Q. Appl. Math. 10, 157–165. https://doi.org/10.1090/qam/48291

Echard, B., Gayton, N., Lemaire, M., 2011. AK-MCS: An active learning reliability method combining Kriging and Monte Carlo Simulation. Struct. Saf. 33, 145–154. https://doi.org/10.1016/j.strusafe.2011.01.002

Echard, B., Gayton, N., Lemaire, M., Relun, N., 2013. A combined Importance Sampling and Kriging reliability method for small failure probabilities with time-demanding numerical models. Reliab. Eng. Syst. Saf. 111, 232–240. https://doi.org/10.1016/j.ress.2012.10.008

El-Emam, M.M., 2018. Experimental verification of current seismic analysis methods of reinforced soil walls. Soil Dyn. Earthq. Eng. 113.

El-Emam, M.M., Bathurst, R.J., 2007. Influence of reinforcement parameters on the seismic response of reduced-scale reinforced soil retaining walls. Geotext. Geomembranes 25, 33–49. https://doi.org/10.1016/j.geotexmem.2006.09.001

El-Ramly, H., Morgenstern, N.R., Cruden, D.M., 2003. Probabilistic stability analysis of a tailings dyke on presheared clay-shale. Can. Geotech. J. 40, 192–208. https://doi.org/10.1139/t02-095

Escario, V., Sáez, J., 1986. The shear strength of partly saturated soils. Géotechnique 36, 453–456. https://doi.org/10.1680/geot.1986.36.3.453

Esmaili, D., Hatami, K., Miller, G.A., 2014. Influence of matric suction on geotextile reinforcement-marginal soil interface strength. Geotext. Geomembranes 42, 139–153. https://doi.org/10.1016/j.geotexmem.2014.01.005

Fenton, G.A., Griffiths, D.V., 2005. Three-Dimensional Probabilistic Foundation Settlement. J. Geotech. Geoenvironmental Eng. 131, 232–239. https://doi.org/10.1061/(ASCE)1090-0241(2005)131:2(232)

Fenton, G.A., Griffiths, D.V., 2003. Bearing-capacity prediction of spatially random c - ø soils. Can. Geotech. J. 40, 54–65. https://doi.org/10.1139/t02-086

Ferreira, F.B., Topa Gomes, A., Vieira, C.S., Lopes, M.L., 2016. Reliability analysis of geosynthetic-reinforced steep slopes. Geosynth. Int. 23, 301–315. https://doi.org/10.1680/jgein.15.00057

FHWA (Federal Highway Administration), 2011. Geotechnical Engineering Circular 03 - LRFD Seismic Analysis and Design of Transportation Geotechnical Features and Structural Foundations, FHWA-NHI-11-032. Washington D.C.

FHWA (Federal Highway Administration), 2009. Design and construction of mechanically stabilized earth walls and reinforced soil slopes–Volume I, FHWA-NHI-10-024. https://doi.org/FHWA-NHI-10-024 & FHWA-NHI-10-025

Fredlund, D.G., Morgenstern, N.R., Widger, R.A., 1978. The shear strength of unsaturated soils. Can. Geotech. J. 15, 313–321.

Fredlund, D.G., Rahardjo, H., Gan, J.K.., 1987. Non-linearity of strength envelope for unsaturated soils, in: Proceedings of the Sixth International Conference on Expansive Soils. New Delhi, pp. 49–54.

Fredlund, D.G., Xing, A., 1994. Equations for the soil-water characteristic ' curve '. Can. Geotech. J. 15, 521–532.

Fredlund, D.G., Xing, A., Fredlund, M.D., Barbour, S.L., 1996. The relationship of the unsaturated soil shear strength to the soil-water characteristic curve. Can. Geotech. J. 33, 440–448. https://doi.org/10.1139/t96-065

Gao, Y., Yang, S., Zhang, F., Leshchinsky, B., 2016. Three-dimensional reinforced slopes: Evaluation of required reinforcement strength and embedment length using limit analysis. Geotext. Geomembranes 44, 133–142. https://doi.org/10.1016/j.geotexmem.2015.07.007

Gaudio, D., Masini, L., Rampello, S., 2018. Seismic Performance of Geosynthetic-Reinforced Earth Retaining Walls Subjected to Strong Ground Motions, in: Proceedings of China-Europe Conference on Geotechnical Engineering, SSGG. Springer International Publishing, pp. 1474–1478. https://doi.org/10.1007/978-3-319-97115-5

Gladstone, R.A., Anderson, P.L., Fishman, K.L., Withiam, J.L., 2006. Durability of galvanized soil reinforcement more than 30 years of experience with mechanically stabilized earth. Transp. Res. Rec. J. Transp. Res. Board 1975, 49–59. https://doi.org/10.3141/1975-08

Griffiths, D.V., Fenton, G.A., 2004. Probabilistic Slope Stability Analysis by Finite Elements. J. Geotech. Geoenvironmental Eng. 130, 507–518. https://doi.org/10.1061/(ASCE)1090-0241(2004)130:5(507)

Gu, M., Collin, J.G., Han, J., Zhang, Z., Tanyu, B.F., Leshchinsky, D., Ling, H.I., Rimoldi, P., 2017. Numerical analysis of instrumented mechanically stabilized gabion walls with large vertical reinforcement spacing. Geotext. Geomembranes 45, 294–306. https://doi.org/10.1016/j.geotexmem.2017.04.002

Guler, E., Hamderi, M., Demirkan, M.M., 2007. Numerical analysis of reinforced soil-retaining wall structures with cohesive and granular backfills. Geosynth. Int. 14, 330–345. https://doi.org/10.1680/gein.2007.14.6.330

Guo, X., Dias, D., Carvajal, C., Peyras, L., Breul, P., 2018. Reliability analysis of embankment dam sliding stability using the sparse polynomial chaos expansion. Eng. Struct. 174, 295–307. https://doi.org/10.1016/j.engstruct.2018.07.053

Guo, X., Dias, D., Pan, Q., 2019a. Probabilistic stability analysis of an embankment dam considering soil spatial variability. Comput. Geotech. 113, 103093. https://doi.org/10.1016/j.compgeo.2019.103093

Guo, X., Du, D., Dias, D., 2019b. Reliability analysis of tunnel lining considering soil spatial variability. Eng. Struct. 196, 109332. https://doi.org/10.1016/j.engstruct.2019.109332

Hamrouni, A., Dias, D., Sbartai, B., 2017a. Probabilistic analysis of piled earth platform under concrete floor slab. Soils Found. 57, 828–839. https://doi.org/10.1016/j.sandf.2017.08.012

Hamrouni, A., Dias, D., Sbartai, B., 2017b. Reliability analysis of shallow tunnels using the response surface methodology. Undergr. Sp. 2, 246–258. https://doi.org/10.1016/j.undsp.2017.11.003

Han, J., Leshchinsky, D., 2006. General Analytical Framework for Design of Flexible Reinforced Earth Structures. J. Geotech. Geoenvironmental Eng. 132. https://doi.org/10.1061/(ASCE)1090-0241(2006)132:11(1427)

Hata, Y., Ichii, K., Tokida, K.I., 2012. A probabilistic evaluation of the size of earthquake induced slope failure for an embankment. Georisk 6, 73–88. https://doi.org/10.1080/17499518.2011.604583

He, S., Ouyang, C., Luo, Y., 2012. Seismic stability analysis of soil nail reinforced slope using kinematic approach of limit analysis. Environ. Earth Sci. 66, 319–326. https://doi.org/10.1007/s12665-011-1241-3

Hu, Y., Zhang, G., Zhang, J.-M., Lee, C.F., 2010. Centrifuge modeling of geotextile-reinforced cohesive slopes.

Geotext. Geomembranes 28, 12–22. https://doi.org/10.1016/j.geotexmem.2009.09.001

Huang, B.Q., 2010. Numerical study and load and resistance factor design (LRFD) calibration for reinforced soil retaining walls.

Huang, B.Q., Bathurst, R.J., Allen, T.M., 2012. LRFD calibration for steel strip reinforced soil walls. J. Geotech. Geoenvironmental Eng. 138, 922–933. https://doi.org/10.1061/(ASCE)GT.1943-5606.0000665

Huang, W., Leong, E.-C., Rahardjo, H., 2018. Upper-Bound Limit Analysis of Unsaturated Soil Slopes under Rainfall. J. Geotech. Geoenvironmental Eng. 144, 04018066. https://doi.org/10.1061/(asce)gt.1943-5606.0001946

Ibrahim, E., Soubra, A.-H., Mollon, G., Raphael, W., Dias, D., Reda, A., 2015. Three-dimensional face stability analysis of pressurized tunnels driven in a multilayered purely frictional medium. Tunn. Undergr. Sp. Technol. 49, 18–34. https://doi.org/10.1016/j.tust.2015.04.001

Itasca, 2011. FLAC: Fast Lagrangian Analysis of Continua.

Itasca, 2005. FLAC: Fast Lagrangian Analysis of Continua.

Javankhoshdel, S., Bathurst, R.J., 2017. Deterministic and probabilistic failure analysis of simple geosynthetic reinforced soil slopes. Geosynth. Int. 24, 14–29. https://doi.org/10.1680/jgein.16.00012

Javankhoshdel, S., Bathurst, R.J., 2014. Simplified probabilistic slope stability design charts for cohesive and cohesive-frictional (c-φ) soils. Can. Geotech. J. 51, 1033–1045. https://doi.org/10.1139/cgj-2013-0385

Javankhoshdel, S., Cami, B., Yacoub, T., Bathurst, R.J., 2019. Probabilistic analysis of a MSE wall considering spatial variability of soil properties, in: Eighth International Conference on Case Histories in Geotechnical Engineering. Philadelphia, Pennsylvania. https://doi.org/10.1061/9780784482124.020

Jiang, S.H., Li, D.Q., Cao, Z.J., Zhou, C.B., Phoon, K.K., 2015. Efficient system reliability analysis of slope stability in spatially variable soils using Monte Carlo simulation. J. Geotech. Geoenvironmental Eng. 141. https://doi.org/10.1061/(ASCE)GT.1943-5606.0001227

Kaniraj, S.R., Abdullah, H., 1993. Effects of berms and tension crack on the stability of embankments on soft soils. Soils Found. 33, 99–107. https://doi.org/10.1248/cpb.37.3229

Khalili, N., Khabbaz, M.H., 1998. A unique relationship for χ for the determination of the shear strength of unsaturated soils. Géotechnique 48, 681–687. https://doi.org/10.1680/geot.52.1.76.40832

Koerner, R.M., Koerner, G.R., 2018. An extended data base and recommendations regarding 320 failed geosynthetic reinforced mechanically stabilized earth (MSE) walls. Geotext. Geomembranes 46, 904–912. https://doi.org/10.1016/j.geotexmem.2018.07.013

Kong, S.M., Lee, J.H., Jung, H.S., Lee, Y.J., 2018. 3D numerical prediction of failure behaviour for the straight and curved parts of retaining wall according to various heights. Int. J. Geo-Engineering 9, 1–18. https://doi.org/10.1186/s40703-018-0091-1

Koseki, J., Bathurst, R.J., Guler, E., Kuwano, J., Maugeri, M., 2006. Seismic stability of reinforced soil walls. 8th Int. Conf. Geosynth. 51–77.

Kucherenko, S., Tarantola, S., Annoni, P., 2012. Estimation of global sensitivity indices for models with dependent variables. Comput. Phys. Commun. 183, 937–946. https://doi.org/10.1016/j.cpc.2011.12.020

Latha, G.M., Krishna, A.M., 2008. Seismic response of reinforced soil retaining wall models: Influence of backfill relative density. Geotext. Geomembranes 26, 335–349. https://doi.org/10.1016/j.geotexmem.2007.11.001

Latha, G.M., Santhanakumar, P., 2015. Seismic response of reduced-scale modular block and rigid faced reinforced walls through shaking table tests. Geotext. Geomembranes 43, 307–316. https://doi.org/10.1016/j.geotexmem.2015.04.008

Leshchinsky, D., Han, J., 2004. Geosynthetic Reinforced Multitiered Walls. J. Geotech. Geoenvironmental Eng. 130, 1225–1235. https://doi.org/10.1061/(ASCE)1090-0241(2004)130:12(1225)

Li, C., Der Kiureghian, A., 1993. Optimal discretization of random fields. J. Eng. Mech. 119, 1136–1154.

Li, D.Q., Jiang, S.H., Cao, Z.J., Zhou, W., Zhou, C.B., Zhang, L.M., 2015. A multiple response-surface method

for slope reliability analysis considering spatial variability of soil properties. Eng. Geol. 187, 60–72. https://doi.org/10.1016/j.enggeo.2014.12.003

Li, K.C., 1991. Sliced inverse regression for dimension reduction. J. Am. Stat. Assoc. 86, 316–327. https://doi.org/10.1080/01621459.1991.10475035

Li, W., Lin, G., Li, B., 2016. Inverse regression-based uncertainty quantification algorithms for high-dimensional models: Theory and practice. J. Comput. Phys. 321, 259–278. https://doi.org/10.1016/j.jcp.2016.05.040

Li, Z.W., Yang, X.L., 2019. Active Earth Pressure from Unsaturated Soils with Different Water Levels. Int. J. Geomech. 19, 06019013. https://doi.org/10.1061/(asce)gm.1943-5622.0001471

Ling, H.I., Leshchinsky, D., Chou, N.S., 2001. Post-earthquake investigation on several geosynthetic-reinforced soil retaining walls and slopes during the ji-ji earthquake of Taiwan. Soil Dyn. Earthq. Eng. 21, 297–313. https://doi.org/10.1016/S0267-7261(01)00011-2

Ling, H.I., Leshchinsky, D., Perry, E.B., 1997. Seismic design and performance of geosynthetic-reinforced soil structures. Geotechnique 47, 933–952.

Ling, H.I., Liu, H., Kaliakin, V.N., Leshchinsky, D., 2004. Analyzing Dynamic Behavior of Geosynthetic-Reinforced Soil Retaining Walls. J. Eng. Mech. 130, 911–920. https://doi.org/10.1061/(ASCE)0733-9399(2004)130:8(911)

Ling, H.I., Liu, H., Mohri, Y., 2005a. Parametric Studies on the Behavior of Reinforced Soil Retaining Walls under Earthquake Loading. J. Eng. Mech. 131, 1056–1065. https://doi.org/10.1061/(ASCE)0733-9399(2005)131:10(1056)

Ling, H.I., Mohri, Y., Leshchinsky, D., Burke, C., Matsushima, K., Liu, H., 2005b. Large-Scale Shaking Table Tests on Modular-Block Reinforced Soil Retaining Walls. J. Geotech. Geoenvironmental Eng. 131, 465–476. https://doi.org/10.1061/(ASCE)1090-0241(2005)131:4(465)

Ling, H.I., Yang, S., Leshchinsky, D., Liu, H., Burke, C., 2010. Finite-Element Simulations of Full-Scale Modular-Block Reinforced Soil Retaining Walls under Earthquake Loading. J. Eng. Mech. 136, 653–661. https://doi.org/10.1061/(ASCE)EM.1943-7889.0000108

Low, B.K., Phoon, K.K., 2015. Reliability-based design and its complementary role to Eurocode 7 design approach. Comput. Geotech. 65, 30–44. https://doi.org/10.1016/j.compgeo.2014.11.011

Lu, Q., Low, B.K., 2011. Probabilistic analysis of underground rock excavations using response surface method and SORM. Comput. Geotech. 38, 1008–1021.

Lumb, P., 1970. Safety factors and the probability distribution of soil strength. Can. Geotech. J. 7, 225–242. https://doi.org/10.1139/t70-032

Luo, N., Bathurst, R.J., Javankhoshdel, S., 2016. Probabilistic stability analysis of simple reinforced slopes by finite element method. Comput. Geotech. 77, 45–55. https://doi.org/10.1016/j.compgeo.2016.04.001

Maji, V.B., S., S. V., Robinson, R.G., 2016. A Simple Analysis of Reinforced Soil Using Equivalent Approach. Int. J. Geosynth. Gr. Eng. 2. https://doi.org/10.1007/s40891-016-0055-5

Mao, N., Al-Bittar, T., Soubra, A.-H., 2012. Probabilistic analysis and design of strip foundations resting on rocks obeying Hoek–Brown failure criterion. Int. J. Rock Mech. Min. Sci. 49, 45–58. https://doi.org/10.1016/j.ijrmms.2011.11.005

Marelli, S., Sudret, B., 2018. An active-learning algorithm that combines sparse polynomial chaos expansions and bootstrap for structural reliability analysis. Struct. Saf. 75, 67–74. https://doi.org/10.1016/j.strusafe.2018.06.003

Masini, L., Callisto, L., Rampello, S., 2015. An interpretation of the seismic behaviour of reinforced-earth retaining structures. Géotechnique 65, 349–358. https://doi.org/10.1680/geot.sip.15.p.001

Melchers, R.E., 1999. Structural Reliability Analysis and Prediction, 2nd Editio. ed. New York.

Michalowski, R.L., 2013. Stability assessment of slopes with cracks using limit analysis. Can. Geotech. J. 50, 1011–1021. https://doi.org/10.1139/cgj-2012-0448.

Michalowski, R.L., 2012. Cracks in slopes: Limit analysis approach to stability assessment, in: Proceedings of GeoCongress. Oakland, Calif., pp. 442–450. https://doi.org/10.1061/9780784412121.046.

Michalowski, R.L., 1998a. Soil reinforcement for seismic design of geotechnical structures. Comput. Geotech. 23, 1–17. https://doi.org/10.1016/S0266-352X(98)00016-0

Michalowski, R.L., 1998b. limit analysis in stability calculations of reinforced soil structures 16, 311–331.

Michalowski, R.L., 1997. Stability of Uniformly Reinforced Slopes. J. Geotech. Geoenvironmental Eng. 123, 546–556. https://doi.org/10.1061/(ASCE)1090-0241(1999)125:1(81)

Michalowski, R.L., Zhao, A., 1995. Continuum versus structural approach to stability of reinforced soil. J. Geotech. Eng. 121, 152–162.

Molinaro, A.M., Simon, R., Pfeiffer, R.M., 2005. Prediction error estimation: a comparison of resampling methods. Bioinformatics 21, 3301–3307.

Mollon, G., Dias, D., Soubra, A.-H., 2011. Rotational failure mechanisms for the face stability analysis of tunnels driven by a pressurized shield. Int. J. Numer. Anal. Methods Geomech. 35, 1363–1388.

Mollon, G., Dias, D., Soubra, A.-H., 2009a. Probabilistic Analysis of Circular Tunnels in Homogeneous Soil Using Response Surface Methodology. J. Geotech. Geoenvironmental Eng. 135, 1314–1325. https://doi.org/10.1061/(ASCE)GT.1943-5606.0000060

Mollon, G., Dias, D., Soubra, A.-H., 2009b. Probabilistic analysis and design of circular tunnels against face stability. Int. J. Geomech. 9, 237–249. https://doi.org/10.1061/(ASCE)1532-3641(2009)9:6(237)

Moroto, N., Hasegawa, A., 1990. Anisotropic elastic stress formulae applicable to reinforced earth. Soils Found. 30, 172–178.

NF P 94-270, ., 2009. Calcul géotechnique ; Ouvrages de soutènement ; Remblais renforcés et massifs en sol cloué.

Nimbalkar, S.S., Choudhury, D., Mandal, J.N., 2006. Seismic stability of reinforced-soil wall by pseudo-dynamic method. Geosynth. Int. 13, 111–119. https://doi.org/10.1680/gein.2006.13.3.111

Noorzad, R., Mirmoradi, S.H., 2010. Laboratory evaluation of the behavior of a geotextile reinforced clay. Geotext. Geomembranes 28, 386–392. https://doi.org/10.1016/j.geotexmem.2009.12.002

Nouri, H., Fakher, A., Jones, C.J.F.P., 2006. Development of Horizontal Slice Method for seismic stability analysis of reinforced slopes and walls. Geotext. Geomembranes 24, 175–187. https://doi.org/10.1016/j.geotexmem.2005.11.004

Pain, A., Choudhury, D., Bhattacharyya, S.K., 2017. Effect of dynamic soil properties and frequency content of harmonic excitation on the internal stability of reinforced soil retaining structure. Geotext. Geomembranes 45, 471–486. https://doi.org/10.1016/j.geotexmem.2017.07.003

Pan, Q., Dias, D., 2017a. An efficient reliability method combining adaptive Support Vector Machine and Monte Carlo Simulation. Struct. Saf. 67, 85–95. https://doi.org/10.1016/j.strusafe.2017.04.006

Pan, Q., Dias, D., 2017b. Probabilistic evaluation of tunnel face stability in spatially random soils using sparse polynomial chaos expansion with global sensitivity analysis. Acta Geotech. 12, 1415–1429. https://doi.org/10.1007/s11440-017-0541-5

Pan, Q., Dias, D., 2017c. Sliced inverse regression-based sparse polynomial chaos expansions for reliability analysis in high dimensions. Reliab. Eng. Syst. Saf. 167, 484–493. https://doi.org/10.1016/j.ress.2017.06.026

Pan, Q., Dias, D., 2017d. Safety factor assessment of a tunnel face reinforced by horizontal dowels. Eng. Struct. 142, 56–66. https://doi.org/10.1016/j.engstruct.2017.03.056

Pan, Q., Dias, D., 2015. Face Stability Analysis for a Shield-Driven Tunnel in Anisotropic and Nonhomogeneous Soils by the Kinematical Approach. Int. J. Geomech. 16, 04015076. https://doi.org/10.1061/(ASCE)GM.1943-5622.0000569

Pan, Q., Jiang, Y.J., Dias, D., 2017. Probabilistic Stability Analysis of a Three-Dimensional Rock Slope Characterized by the Hoek-Brown Failure Criterion. J. Comput. Civ. Eng. 31, 1–10.

https://doi.org/10.1061/(ASCE)CP.1943-5487.0000692

Parker, C., Simon, A., Thorne, C.R., 2008. The effects of variability in bank material properties on riverbank stability: Goodwin Creek, Mississippi. Geomorphology 101, 533–543. https://doi.org/10.1016/j.geomorph.2008.02.007

Passe, P., 2000. Mechanically Stabilized Earth (MSE) Wall Inspector's Handbook. Tallahassee, Florida.

Patra, C.R., Basudhar, P.K., 2005. Optimum design of nailed soil slopes. Geotech. Geol. Eng. 23, 273–296. https://doi.org/10.1007/s10706-004-2146-7

Phoon, K.K., 2017. Role of reliability calculations in geotechnical design. Georisk 11, 4–21. https://doi.org/10.1080/17499518.2016.1265653

Phoon, K.K., 2004. Towards reliability-based design for geotechnical engineering. Spec. Lect. Korean Geotech. Soc.

Phoon, K.K., Ching, J., 2014. Risk and Reliability in Geotechnical Engineering. CRC Press, Boca Raton.

Phoon, K.K., Kulhawy, F.H., 1999. Characterization of geotechnical variability. Can. Geotech. J. 36, 612–624. https://doi.org/10.1139/t99-038

Phoon, K.K., Kulhawy, F.H., Grigoriu, M.D., 2003. Development of a Reliability-Based Design Framework for Transmission Line Structure Foundations. J. Geotech. Geoenvironmental Eng. 129, 798–806. https://doi.org/10.1061/(ASCE)1090-0241(2003)129:9(798)

Porbaha, A., Goodings, D., 1996. Centrifuge modeling of geotextile-reinforced cohesive soil retaining walls. J. Geotech. Eng. 122, 840–848. https://doi.org/10.1061/(ASCE)0733-9410(1996)122:10(840)

Portelinha, F.H.M., Bueno, B.S., 2012. Performance of geotextile reinforced soil wall in unsaturated poorly draining backfill soil conditions, in: 5th European Geosynthetics Congress. Valencia, pp. 455–459.

Portelinha, F.H.M., Bueno, B.S., Zornberg, J.G., 2013. Performance of nonwoven geotextile-reinforced walls under wetting conditions : laboratory and field investigations. Geosynth. Int. 20, 90–104. https://doi.org/10.1680/gein.13.00004

Portelinha, F.H.M., Zornberg, J.G., Pimentel, V., 2014. Field performance of retaining walls reinforced with woven and nonwoven geotextiles. Geosynth. Int. 21, 270–284. https://doi.org/10.1680/gein.14.00014

Qin, C.-B., Chian, S.C., 2018. Bearing capacity analysis of a saturated non-uniform soil slope with discretization-based kinematic analysis. Comput. Geotech. 96, 246–257. https://doi.org/10.1016/j.compgeo.2017.11.003

Qin, C.-B., Chian, S.C., 2017. Kinematic analysis of seismic slope stability with a discretisation technique and pseudo-dynamic approach: a new perspective. Géotechnique 68, 492–503. https://doi.org/10.1680/jgeot.16.P.200

Ren, F., Huang, Q., Wang, G., 2020. Shaking table tests on reinforced soil retaining walls subjected to the combined effects of rainfall and earthquakes. Eng. Geol. 267, 105475. https://doi.org/10.1016/j.enggeo.2020.105475

Riccio, M., Ehrlich, M., Dias, D., 2014. Field monitoring and analyses of the response of a block-faced geogrid wall using fine-grained tropical soils. Geotext. Geomembranes 42, 127–138. https://doi.org/10.1016/j.geotexmem.2014.01.006

Richardson, G.N., Lee, K.L., Fong, A.C., Feger, D.L., 1977. Seismic Testing of Reinforced Earth Walls. J. Geotech. Eng. 103, 1–17.

Sabermahani, M., Ghalandarzadeh, A., Fakher, A., 2009. Experimental study on seismic deformation modes of reinforced-soil walls. Geotext. Geomembranes 27, 121–136. https://doi.org/10.1016/j.geotexmem.2008.09.009

Sampaco, C.L., 1996. Behavior of welded wire mesh reinforced soil walls from field evaluation and finite element simulation. Utah State University, Logan, Utah.

Sayed, S., Dodagoudar, G.R., Rajagopal, K., 2008. Reliability analysis of reinforced soil walls under static and seismic forces. Geosynth. Int. 15, 246–257. https://doi.org/10.1680/gein.2008.15.4.246

Schlosser, F., Hoteit, N., Pierce, D., 1993. Expérimentation en vraie grandeur d'un mur Freyssisol-Websol en sol renforcé, in: Symposium International Sur Le Renforcement Des Sols. Expérimentation Des Années 1980, ENPC. Paris, pp. 299–320.

Sivakumar Babu, G.L., Singh, V.P., 2011. Reliability-based load and resistance factors for soil-nail walls. Can. Geotech. J. 48, 915–930. https://doi.org/10.1139/t11-005

Sivakumar Babu, G.L., Srivastava, A., 2007. Reliability analysis of allowable pressure on shallow foundation using response surface method. Comput. Geotech. 34, 187–194. https://doi.org/10.1016/j.compgeo.2006.11.002

Soletanche Freyssinet, ., 2014. www.terre-armee.fr [WWW Document]. Terre Armée - Orig.

Soletanche Freyssinet, ., 2013. www.terre-armee.fr [WWW Document]. GeoMega La Solut. toralement synthétique.

Song, S., Lu, Z., Qiao, H., 2009. Subset simulation for structural reliability sensitivity analysis. Reliab. Eng. Syst. Saf. 94, 658–665. https://doi.org/10.1016/j.ress.2008.07.006

Soubra, A.-H., Al-Bittar, T., Thajeel, J., Ahmed, A., 2019. Probabilistic analysis of strip footings resting on spatially varying soils using kriging metamodeling and importance sampling. Comput. Geotech. 114. https://doi.org/10.1016/j.compgeo.2019.103107

Spencer, E., 1968. Effect of tension on the stability of embakments. J. Soil Mech. Found. Div 94, 1159–1173.

Spencer, E., 1967. Embankments Assuming Parallel Inter-Slice Forces. Géotechnique 17(1), 11–26.

Steedman, R.S., Zeng, X., 1990. The influence of phase on the calculation of pseudo-static earth pressure on a retaining wall. Géotechnique 40, 103–112. https://doi.org/10.1680/geot.1990.40.1.103

Stuedlein, A.W., Allen, T.M., Holtz, R.D., Christopher, B.R., 2012. Assessment of Reinforcement Strains in Very Tall Mechanically Stabilized Earth Walls. J. Geotech. Geoenvironmental Eng. 138, 345–356. https://doi.org/10.1061/(asce)gt.1943-5606.0000586

Sudret, B., 2008. Global sensitivity analysis using polynomial chaos expansions. Reliab. Eng. Syst. Saf. 93, 964–979. https://doi.org/10.1016/j.ress.2007.04.002

Sun, Z., Li, J., Pan, Q., Dias, D., Li, S., Hou, C., 2018. Discrete Kinematic Mechanism for Nonhomogeneous Slopes and Its Application. Int. J. Geomech. 18, 04018171. https://doi.org/10.1061/(asce)gm.1943-5622.0001303

Terzaghi, K., 1950. Mechanism of Landslides, in: Application of Geology to Engineering Practice. Geological Society of America. https://doi.org/10.1130/Berkey.1950.83

Terzaghi, K., 1943. Theoretical Soil Mechanics. Wiley and Sons, New York. https://doi.org/10.1002/9780470172766

Utili, S., 2013. Investigation by limit analysis on the stability of slopes with cracks. Géotechnique 63, 140–154. https://doi.org/10.1680/geot.11.P.068

Utili, S., Abd, A.H., 2016. On the stability of fissured slopes subject to seismic action. Int. J. Numer. Anal. Methods Geomech. 40, 785–806. https://doi.org/10.1002/nag.2498

Vahedifard, F., Mortezaei, K., Leshchinsky, B.A., Leshchinsky, D., Lu, N., 2016. Role of suction stress on service state behavior of geosynthetic-reinforced soil structures. Transp. Geotech. 8, 45–56. https://doi.org/10.1016/j.trgeo.2016.02.002

Vanapalli, S.K., Fredlund, D.G., Pufahl, D.E., Clifton, A.W., 1996. Model for the prediction of shear strength with respect to soil suction. Can. Geotech. J. 33, 379–392. https://doi.org/10.1139/t96-060

Vilar, O.M., 2006. A simplified procedure to estimate the shear strength envelope of unsaturated soils. Can. Geotech. J. 43, 1088–1095. https://doi.org/10.1139/t06-055

Viratjandr, C., Michalowski, R.L., 2006. Limit analysis of submerged slopes subjected to water drawdown. Can. Geotech. J. 43, 802–814. https://doi.org/10.1139/T06-042

Vivas, C.B., Calatrava, D., 2016. Application of Soil Reinforced Structures as Urban Transportation System

solutions, in: Conference of the Transportation Association of Canada Toronto. Toronto, Canada.

Wang, L., Zhang, G., Zhang, J.-M., 2011. Centrifuge model tests of geotextile-reinforced soil embankments during an earthquake. Geotext. Geomembranes 29, 222–232. https://doi.org/10.1016/j.geotexmem.2010.11.002

Wang, Y., Aladejare, A.E., 2015. Selection of site-specific regression model for characterization of uniaxial compressive strength of rock. Int. J. Rock Mech. Min. Sci. 75, 73–81. https://doi.org/10.1016/j.ijrmms.2015.01.008

Wang, Y., Cao, Z., 2013. Probabilistic characterization of Young's modulus of soil using equivalent samples. Eng. Geol. 159, 106–118. https://doi.org/10.1016/j.enggeo.2013.03.017

Wang, Y., Cao, Z., Li, D., 2016. Bayesian perspective on geotechnical variability and site characterization. Eng. Geol. 203, 117–125. https://doi.org/10.1016/j.enggeo.2015.08.017

Wolff, T.F., 1985. ANALYSIS AND DESIGN OF EMBANKMENT DAM SLOPES: A PROBABILISTIC APPROACH. Purdue University.

Wu, T.H., 1991. Predicting performance of the Denver walls: general report, in: Proceedings of the International Symposium on Geosynthetic-Reinforced Soil Retaining Walls. Denver, Colorado, USA, pp. 3–20.

Xiu, D., Em Karniadakis, G., 2003. The Wiener-Askey polynomial chaos for stochastic differential equations. SIAM J. Sci. Comput. 24, 619–644. https://doi.org/10.1137/S1064827501387826

Xu, J., Wang, D., 2019. Structural reliability analysis based on polynomial chaos, Voronoi cells and dimension reduction technique. Reliab. Eng. Syst. Saf. 185, 329–340. https://doi.org/10.1016/j.ress.2019.01.001

Xu, J.S., Yang, X.L., 2018. Three-dimensional stability analysis of slope in unsaturated soils considering strength nonlinearity under water drawdown. Eng. Geol. 237, 102–115. https://doi.org/10.1016/j.enggeo.2018.02.010

Yang, K.-H., Nguyen, T.S., Li, Y.-H., Leshchinsky, B., 2019. Performance and Design of Reinforced Slopes Considering Regional Hydrological Conditions. Geosynth. Int. 1–77. https://doi.org/10.1680/jgein.19.00031

Yang, X.L., Chen, J.H., 2019. Factor of Safety of Geosynthetic-Reinforced Slope in Unsaturated Soils. Int. J. Geomech. 19, 04019041. https://doi.org/10.1061/(asce)gm.1943-5622.0001399

Yao, C., Yang, X., 2017. Limit Analysis of Unsaturated Soil Slope Stability Considering Intermediate Principal Stress and Strength Nonlinearity. Geotech. Geol. Eng. 35, 2053–2063. https://doi.org/10.1007/s10706-017-0226-8

Yeh, Y.R., Huang, S.Y., Lee, Y.J., 2009. Nonlinear dimension reduction with kernel sliced inverse regression. IEEE Trans. Knowl. Data Eng. 21, 1590–1603. https://doi.org/10.1109/TKDE.2008.232

Youssef Abdel Massih, D.S., Soubra, A.-H., 2008. Reliability-Based Analysis of Strip Footings Using Response Surface Methodology. Int. J. Geomech. 8, 134–143. https://doi.org/10.1061/_ASCE_1532-3641_2008_8:2_134

Youssef Abdel Massih, D.S., Soubra, A.-H., Low, B.K., 2008. Reliability-Based Analysis and Design of Strip Footings against Bearing Capacity Failure. J. Geotech. Geoenvironmental Eng. 134, 917–928. https://doi.org/10.1061/_ASCE_1090-0241_2008_134:7_917

Yu, Y., Bathurst, R.J., 2017. Probabilistic assessment of reinforced soil wall performance using response surface method. Geosynth. Int. 24, 524–542. https://doi.org/10.1680/jgein.17.00019

Yu, Y., Bathurst, R.J., Allen, T.M., 2017. Numerical modelling of two full-scale reinforced soil wrapped-face walls. Geotext. Geomembranes 45, 237–249. https://doi.org/10.1016/j.geotexmem.2017.02.004

Yucemen, M.S., Tang, W.H., Ang, A.H.-S., 1973. A probabilistic study of safety and design of earth slopes, Civil Engineering Studies, Structural Research Series 402. Urbana.

Zevgolis, I.E., Bourdeau, P.L., 2017. Reliability and redundancy of the internal stability of reinforced soil walls. Comput. Geotech. 84, 152–163. https://doi.org/10.1016/j.compgeo.2016.11.022

Zhang, F., Leshchinsky, D., Gao, Y., Leshchinsky, B., 2014. Required unfactored strength of geosynthetics in reinforced 3D slopes. Geotext. Geomembranes 42, 576–585.

https://doi.org/10.1016/j.geotexmem.2014.10.006

Zhang, L.L., Fredlund, D.G., Fredlund, M.D., Wilson, G.W., 2014. Modeling the unsaturated soil zone in slope stability analysis. Can. Geotech. J. 51, 1384–1398. https://doi.org/10.1139/cgj-2013-0394

Zhao, H.-B., 2008. Slope reliability analysis using a support vector machine. Comput. Geotech. 35, 459–467.

Zhao, L.H., Cheng, X., Zhang, Y., Li, L., Li, D.J., 2016. Stability analysis of seismic slopes with cracks. Comput. Geotech. 77, 77–90. https://doi.org/10.1016/j.compgeo.2016.04.007

Zhou, Y., Chen, F., Wang, X., 2018. Seismic Active Earth Pressure for Inclined Rigid Retaining Walls Considering Rotation of the Principal Stresses with Pseudo-Dynamic Method. Int. J. Geomech. ASCE 18, 1–9. https://doi.org/10.1061/(ASCE)GM.1943-5622.0001198